

**JAERI-M**  
**85-029**

**A MAIN STEAM LINE BREAK EXPERIMENT  
AT ROSA III-RUN 953  
(100% BREAK WITH AN HPCS FAILURE)**

March 1985

Masahiro KAWAJI, Mitsuhiro SUZUKI, Hideo NAKAMURA,  
Kanji TASAKA, Yoshinari ANODA, Hiroshige KUMAMARU,  
Taisuke YONOMOTO, Hideo MURATA and Masayoshi SHIBA

JAERI-M レポートは、日本原子力研究所が不定期に公刊している研究報告書です。

入手の問合わせは、日本原子力研究所技術情報部情報資料課（〒319-11茨城県那珂郡東海村）  
あて、お申しこしください。なお、このほかに財団法人原子力弘済会資料センター（〒319-11茨城  
県那珂郡東海村日本原子力研究所内）で複写による実費頒布をおこなっております。

JAERI-M reports are issued irregularly.

Inquiries about availability of the reports should be addressed to Information Division, Department  
of Technical Information, Japan Atomic Energy Research Institute, Tokai-mura, Naka-gun,  
Ibaraki-ken 319-11, Japan.

© Japan Atomic Energy Research Institute, 1985

---

編集兼発行 日本原子力研究所  
印 刷 日立高速印刷株式会社

A MAIN STEAM LINE BREAK EXPERIMENT AT ROSA III - RUN 953  
(100% BREAK WITH AN HPCS FAILURE)

Masahiro KAWAJI, Mitsuhiro SUZUKI, Hideo NAKAMURA,  
Kanji TASAKA, Yoshinari ANODA, Hiroshige KUMAMARU,  
Taisuke YONOMOTO, Hideo MURATA and Masayoshi SHIBA

Department of Nuclear Safety Research,  
Tokai Research Establishment, JAERI

( Received January 31, 1985 )

This report presents the experimental results of RUN 953, a 100% Main Steam Line (MSL) break experiment performed at the ROSA-III test facility. The ROSA-III facility is a volumetrically scaled (1/424) system of a BWR/6 used for integral BWR LOCA simulation experiments. RUN 953 is one of several MSL break tests with a 100% break located upstream of the main steam isolation valve (MSIV), and performed to investigate the effect of an HPCS failure on the system behavior. This test is characterized, just as in a reference MSL break test, RUN 952, by a relatively slower depressurization of the system due to a break flow of high mass quality in comparison with the recirculation line break tests. Continuous flashing of the fluid in the pressure vessel was observed and a decrease in the pressure vessel coolant level eventually led to the uncovering of the entire core at about 200 s after break. After the water level in the downcomer dropped to the L1 level, LPCS and LPCI were activated at 281 s and the core recovered quickly thereafter. The peak cladding temperature reached was 1004 K, which is 252 K higher than that obtained in RUN 952, a reference MSL break test with HPCS actuation logic. This test has demonstrated the importance of HPCS actuation in achieving early core recovery during an MSL break LOCA.

Keywords: BWR, LOCA, ECCS, Integral Test, ROSA-III Program, Core Recovery, Main Steam Line Break, PCT, Flashing, Failure

R O S A - Ⅲ主蒸気ライン破断実験 - R U N 9 5 3

(H P C S 故障を仮定した 1 0 0 % 破断)

日本原子力研究所東海研究所安全工学部  
川路 正裕・鈴木 光弘・中村 秀夫・田坂 完二  
安濃田良成・熊丸 博滋・与能本泰介・村田 秀男  
斯波 正誼

(1985年1月31日受理)

本報は ROSA-Ⅲ実験装置を用いて行った主蒸気管ライン (MSL) 100 % 破断実験, R U N 953 の実験結果について述べたものである。ROSA-Ⅲ装置はBWR/6 を体積比で1/424に縮尺模擬した総合 L O C A 実験装置である。R U N 953 は主蒸気管ライン破断実験シリーズの一環として ECCS の単一故障の影響を調べるために HPCS 故障を仮定して行ったものである。R U N 953 では主蒸気管ライン破断実験の標準ケース, R U N 952, の場合と同じく高クオリティーの破断流が生じ、システムの圧力降下は再循環ライン破断実験に比べてやや緩かであり、減圧沸騰も長く続いた。そして HPCS 故障のため炉心水位の低下が続き、破断後約 200 秒で炉心全体が露出した。その後ダウンカマー水位が L 1 レベルまで低下したことにより、破断後 281 秒で L P C S と L P C I が起動したため炉心は水位が回復しクエンチされた。しかし R U N 953 で得られた P C T は 1 0 0 4 K であり、HPCS が作動した標準ケース, R U N 952, の P C T より 2 5 2 K 高く、主蒸気管ライン破断 L O C A 時の炉心冷却に及ぼす HPCS の重要性が明らかとなった。

## TABLE OF CONTENTS

1. Introduction.....	1
2. ROSA-III Test Facility.....	3
3. Instrumentation.....	14
4. Test Conditions and Procedure.....	43
5. Data Processing.....	52
6. Discussion of Test Results.....	166
7. Effect of HPCS failure on MSL Break LOCA.....	177
8. Concluding Remarks.....	186
Acknowledgement.....	188
References.....	188

## 目 次

1. 序 .....	1
2. ROSA - III 試験装置 .....	3
3. 計 測 .....	14
4. 実験条件と実験方法 .....	43
5. 実験データ処理 .....	52
6. 実験結果及び考察 .....	166
7. 主蒸気管ライン破断 L O C A に於ける H P C S 故障の影響 .....	177
8. 結 び .....	186
謝 辞 .....	188
参考文献 .....	188

**ABBREVIATIONS**

ADS	Automatic Depressurization System
AT	Air Tank
AV	Air Actuation Valve
(2)B	(2) inches pipe of Schedule 80
BN	Boron Nitride
BWR	Boiling Water Reactor
CA	Chromel-Alumel
CCFL	Counter Current Flow Limiting
CHV	Check Valve
CP	Conductivity Probe
CV	Control Valve
CWT	Cooling Water Tank
D	Differential Pressure
d	Diameter
DF	Density of Fluid
DL(+100)	Elevation (+100 mm) from the bottom of PV
ECCS	Emergency Core Cooling System
ESF	Engineered Safety Features
EX	Heat Exchanger
F	Flow Rate
Fig.	Figure
FS	Full Scale
FW	Feedwater
FWLF	Feedwater Line Flashing
FWP	Feedwater Pump
FWT	Feedwater Tank
HPCS	High Pressure Core Spray
HPCSP	High Pressure Core Spray Pump
HPCST	High Pressure Core Spary Tank

HPWP	High Pressure Water Pump
ID	Inner diameter
INC 600	Inconel 600
JP	Jet Pump
K	Kelvin
kg	Kilogram
kPa	Kilopascal
kW	Kilowatt
L	Liter
LB	Liquid Level in Channel Box
LBWR	Large Boiling Water Reactor
LL	Liquid Level
LOCA	Loss-of-Coolant Accident
LOCE	Loss-of-Coolant Experiment
LP	Lower Plenum
LPCI	Low Pressure Coolant Injection
LPCIP	Low Pressure Coolant Injection Pump
LPCIT	Low Pressure Coolant Injection Tank
LPCS	Low Pressure Core Spray
LPCSP	Low Pressure Core Spary Pump
LPCST	Low Pressure Core Spary Tank
LPF	Lower Plenum Flashing
LTP	Lower Tie Plate
M	Momentum Flux
m	Meter
mm	Milimeter
MLHR	Maximum Linear Heat Rate
MPa	Megapascal
MRP	Main Recirculation Pump
MSIV	Main Steam Isolation Valve
MSL	Main Steam Line

MW	<b>Megawatt</b>
N	<b>Rotation Speed</b>
OR	<b>Orifice</b>
P	<b>Pressure</b>
	<b>Power</b>
PCT	<b>Peak Cladding Temperature</b>
PV	<b>Pressure Vessel</b>
PWT	<b>Pure Water Tank</b>
QOBV	<b>Quick Opening Blowdown Valve</b>
QSV	<b>Quick Shut-off Valve</b>
RCN	<b>Rapid Condenser</b>
ROSA	<b>Rig of Safety Assessment</b>
rpm	<b>Revolution per Minute</b>
S	<b>Signal</b>
s	<b>Second</b>
Sch	<b>Schedule</b>
SUS	<b>Stainless Steel</b>
T	<b>Temperature</b>
T/C	<b>Thermocouple</b>
TC	<b>Temperature of Fluid</b>
TF	<b>Temperature of Fuel</b>
TS	<b>Temperature of Structure Material</b>
UTP	<b>Upper Tie Plate</b>
V	<b>Valve</b>
VF	<b>Void Fraction</b>
W	<b>Watt</b>
WL	<b>Water Level</b>
WSP	<b>Water Supply Pump</b>

LIST OF TABLES

- Table 2.1 Primary characteristics of ROSA-III and BWR/6
- Table 3.1 ROSA-III instrumentation summary list
- Table 3.2 Measurement list for RUN 953
- Table 3.3 Core instrumentation map
- Table 4.1 Test conditions of RUN 953
- Table 4.2 Characteristics of steam discharge line valves
- Table 4.3 Control sequence for steam discharge line valves  
in RUN 953
- Table 5.1 Sequence of events in RUN 953
- Table 5.2 Maximum cladding temperature distribution in the  
core
- Table 7.1 Test conditions and major events in RUN 953 and  
RUN 952

LIST OF FIGURES

- Fig. 2.1 Schematic diagram of ROSA-III test facility
- Fig. 2.2 Internal structure of pressure vessel of ROSA-III
- Fig. 2.3 ROSA-III piping schematic
- Fig. 2.4 Pressure vessel internals arrangement
- Fig. 2.5 Simulated fuel rod of ROSA-III
- Fig. 2.6 Axial power distribution of heater rod
- Fig. 2.7 Radial power distribution of core
- Fig. 2.8 Piping layout of recirculation loops and jet pumps

- Fig. 3.1 Instrumentation location of ROSA-III test facility
- Fig. 3.2 Instrumentation location in pressure vessel
- Fig. 3.3 Upper plenum instrumentation
- Fig. 3.4 Lower plenum instrumentation
- Fig. 3.5 Core instrumentation (cf. Table 3.3)
- Fig. 3.6 Upper tieplate instrumentations
- Fig. 3.7 Beam directions of three-beam gamma densitometer
- Fig. 3.8 Beam directions of two-beam gamma densitometer
- Fig. 3.9 Arrangement and location of drag disks
- Fig. 3.10 Location of two-phase flow measurement spool pieces

- Fig. 4.1 Break orifice details
- Fig. 4.2 Normalized power transient for ROSA-III test
- Fig. 4.3 Main steam line schematic
- Fig. 4.4 Feedwater line schematic
- Fig. 4.5 Feedwater line between valve AV-112 and pressure vessel

- Fig. 5.1 Pressure in PV (pressure vessel)
- Fig. 5.2 Pressure in recirc. line (jet pump)
- Fig. 5.3 Pressure near MRP-1 and MRP-2 (main recirculation pump)
- Fig. 5.4 Pressure at break
- Fig. 5.5 Pressure in JP outlet spool
- Fig. 5.6 Differential pressure between lower plenum and upper plenum
- Fig. 5.7 Differential pressure between upper plenum and steam dome
- Fig. 5.8 DC (downcomer) head
- Fig. 5.9 Differential pressure between PV bottom and top
- Fig. 5.10 Differential pressure between JP-1,2 discharge and

suction

Fig. 5.11 Differential pressure between JP-1,2 drive and suction

Fig. 5.12 Differential pressure between JP-3,4 discharge and suction

Fig. 5.13 Differential pressure between JP-3,4 drive and suction

Fig. 5.14 Differential pressure between MRP delivery and suction

Fig. 5.15 Differential pressure between downcomer bottom and MRP suction

Fig. 5.16 Differential pressure between MRP delivery and JP-1,2 drive

Fig. 5.17 Differential pressure between downcomer middle and JP-1,2 suction

Fig. 5.18 Differential pressure between JP-1,2 discharge and lower plenum

Fig. 5.19 Differential pressure between downcomer bottom and break

Fig. 5.20 Differential pressure between MRP dilivery and JP-3,4 drive

Fig. 5.21 Differential pressure between downcomer middle and JP-3,4 suction

Fig. 5.22 Differential pressure between JP-3,4 discharge and confluence

Fig. 5.23 Differential pressure between JP-3,4 confluence and LP

Fig. 5.24 Differential pressure between lower plenum and downcomer middle

Fig. 5.25 Differential pressure between lower plenum and downcomer bottom

Fig. 5.26 Differential pressure between downcomer bottom and downcomer middle

- Fig. 5.27 Differential pressure between downcomer middle and steam dome
- Fig. 5.28 Differential pressure between lp bottom and lp middle
- Fig. 5.29 Differential pressure across channel inlet orifice A
- Fig. 5.30 Differential pressure across channel inlet orifice B
- Fig. 5.31 Differential pressure across channel inlet orifice C
- Fig. 5.32 Differential pressure across channel inlet orifice D
- Fig. 5.33 Differential pressure across bypass hole
- Fig. 5.34 Liquid levels in ECCS tanks
- Fig. 5.35 Liquid levels in upper and lower downcomer
- Fig. 5.36 Mass flow rate in MSL
- Fig. 5.37 ECC injection flow rate
- Fig. 5.38 Feedwater flow rate
- Fig. 5.39 JP-1,2 discharge flow rate
- Fig. 5.40 JP-3,4 discharge flow rate
- Fig. 5.41 MRP flow rate
- Fig. 5.42 Diff. pressure across orifice F-1 in MSL
- Fig. 5.43 Diff. pressure across orifice F-2 in MSL
- Fig. 5.44 Diff. pressure across orifice F-3 in MSL
- Fig. 5.45 Diff. pressure across venturi F-17 in JP1
- Fig. 5.46 Diff. pressure across venturi F-18 in JP2
- Fig. 5.47 Diff. pressure across orifice F-19 in JP3
- Fig. 5.48 Diff. pressure across orifice F-20 in JP4
- Fig. 5.49 Diff. pressure across orifice F-21 in JP3
- Fig. 5.50 Diff. pressure across orifice F-22 in JP4
- Fig. 5.51 Diff. pressure across venturi F-27 in MRP-1
- Fig. 5.52 Diff. pressure across venturi F-28 in MRP-2
- Fig. 5.53 Electric core power
- Fig. 5.54 MRP revolution

- Fig. 5.55 Valve operation signals  
Fig. 5.56 ECCS operation signals  
Fig. 5.57 MRP operation signals  
Fig. 5.58 Fluid density at JP-1,2 outlet, beam A  
Fig. 5.59 Fluid density at JP-1,2 outlet, beam B  
Fig. 5.60 Fluid density at JP-1,2 outlet, beam C  
Fig. 5.61 Fluid density at JP-3,4 outlet, beam A  
Fig. 5.62 Fluid density at JP-3,4 outlet, beam B  
Fig. 5.63 Fluid density at JP-3,4 outlet, beam C  
Fig. 5.64 Fluid density at break, beam A  
Fig. 5.65 Fluid density at break, beam B  
Fig. 5.66 Momentum flux at JP-1,2 outlet  
Fig. 5.67 Momentum flux at JP-3,4 outlet  
Fig. 5.68 Momentum flux at break spool piece (high range)  
Fig. 5.69 Fluid temperatures in lower plenum and upper plenum  
Fig. 5.70 Fluid temperatures in steam dome and MSL  
Fig. 5.71 Fluid temperatures in downcomer  
Fig. 5.72 Fluid temperatures in recirculation loop A  
Fig. 5.73 Fluid temperatures in recirculation loop B  
Fig. 5.74 Fluid temperatures at JP-1,2 outlet  
Fig. 5.75 Fluid temperatures at JP-3,4 outlet  
Fig. 5.76 Fluid temperature upstream of break  
Fig. 5.77 Feedwater temperature  
Fig. 5.78 Fluid temperatures at break orifice  
Fig. 5.79 JP diffuser wall temperature  
Fig. 5.80 PV feedwater fluid temperature  
Fig. 5.81 Discharged steam temperature  
Fig. 5.82 Surface temperatures of fuel rod A11  
Fig. 5.83 Surface temperatures of fuel rod A12

- Fig. 5.84 Surface temperatures of fuel rod A13
- Fig. 5.85 Surface temperatures of fuel rod A22
- Fig. 5.86 Surface temperatures of fuel rod A33
- Fig. 5.87 Surface temperatures of fuel rod A77
- Fig. 5.88 Surface temperatures of fuel rod A87
- Fig. 5.89 Surface temperatures of fuel rod A88
- Fig. 5.90 Surface temperatures of fuel rod B11
- Fig. 5.91 Surface temperatures of fuel rod B22
- Fig. 5.92 Surface temperatures of fuel rod B77
- Fig. 5.93 Surface temperatures of fuel rod C11
- Fig. 5.94 Surface temperatures of fuel rod C13
- Fig. 5.95 Surface temperatures of fuel rod C22
- Fig. 5.96 Surface temperatures of fuel rod C33
- Fig. 5.97 Surface temperatures of fuel rod C77
- Fig. 5.98 Surface temperatures of fuel rod D22
- Fig. 5.99 Surface temperatures of water rod simulator A45
- Fig. 5.100 Surface temperatures of water rod simulator C45
- Fig. 5.101 Outer surface temperatures of channel Box A
- Fig. 5.102 Surface temperature of fuel rods A17,A28,A31,A57 at position 4
- Fig. 5.103 Surface temperature of fuel rods A68,A71,A73,B13 at position 4
- Fig. 5.104 Surface temperature of fuel rod A84 at position 1
- Fig. 5.105 Surface temperatures of fuel rods D11,D13,D77,D86 at position 4
- Fig. 5.106 Surface temperatures of fuel rods A11,A12,A13,A87,A88 at position 1
- Fig. 5.107 Surface temperatures of fuel rods A11,A12,A13,A87,A88 at position 2

Fig. 5.108 Surface temperatures of fuel rods A11,A12,A13,A87,A88 at position 3

Fig. 5.109 Surface temperatures of fuel rods A11,A12,A13,A87,A88 at position 4

Fig. 5.110 Surface temperatures of fuel rods A11,A12,A13,A87,A88 at position 5

Fig. 5.111 Surface temperatures of fuel rods A11,A12,A13,A87,A88 at position 6

Fig. 5.112 Surface temperatures of fuel rods A11,A12,A13,A87,A88 at position 7

Fig. 5.113 Surface temperatures of fuel rods A22,B22,C22,D22 at position 1

Fig. 5.114 Surface temperatures of fuel rods A22,B22,C22,D22 at position 2

Fig. 5.115 Surface temperatures of fuel rods A22,B22,C22,D22 at position 3

Fig. 5.116 Surface temperatures of fuel rods A22,B22,C22,D22 at position 4

Fig. 5.117 Surface temperatures of fuel rods A22,B22,C22,D22 at position 5

Fig. 5.118 Surface temperatures of fuel rods A22,B22,C22,D22 at position 6

Fig. 5.119 Surface temperatures of fuel rods A22,B22,C22,D22 at position 7

Fig. 5.120 Surface temperatures of fuel rods A77,B77,C77 at position 1

Fig. 5.121 Surface temperatures of fuel rods A77,B77,C77 at position 2

Fig. 5.122 Surface temperatures of fuel rods A77,B77,C77 at

position 3

Fig. 5.123 Surface temperatures of fuel rods A77,B77,C77,d77 at position 4

Fig. 5.124 Surface temperatures of fuel rods A77,C77 at position 5

Fig. 5.125 Surface temperatures of fuel rods A77,B77,C77 at position 6

Fig. 5.126 Surface temperatures of fuel rods B77,C77 at position 7

Fig. 5.127 Fluid temperatures at channel inlet

Fig. 5.128 Fluid temperatures at channel A outlet

Fig. 5.129 Fluid temperatures at channel C outlet

Fig. 5.130 Fluid temperatures above UTP of channel A, opening 1 and 4

Fig. 5.131 Fluid temperatures above UTP of channel A, opening 10

Fig. 5.132 Fluid temperatures below UTP of channel A, opening 1 and 4

Fig. 5.133 Fluid temperatures below UTP of channel A, opening 10

Fig. 5.134 Fluid temperatures across UTP in channel A, opening 1

Fig. 5.135 Fluid temperatures across UTP in channel A, opening 4

Fig. 5.136 Fluid temperatures across UTP in channel A, opening 10

Fig. 5.137 Fluid temperatures above UTP of channel C, opening 1 and 4

Fig. 5.138 Fluid temperatures above UTP of channel C, opening 10

Fig. 5.139 Fluid temperatures below UTP of channel C, opening 1 and 4

Fig. 5.140 Fluid temperatures below UTP of channel C, opening 10

Fig. 5.141 Fluid temperatures across UTP in channel C, opening 1

Fig. 5.142 Fluid temperatures across UTP in channel C, opening 4

Fig. 5.143 Fluid temperatures across UTP in channel C, opening 10

Fig. 5.144 Outer surface temperatures of channel Box A

Fig. 5.145 Fluid temperature in lower plenum, center

Fig. 5.146 Liquid level signals in channel Box A, location A2

- Fig. 5.147 Liquid level signals in channel Box B
- Fig. 5.148 Liquid level signals in channel Box C
- Fig. 5.149 Liquid level signals in channel A outlet, location A2
- Fig. 5.150 Liquid level signals in channel A outlet, center
- Fig. 5.151 Liquid level signals in channel C outlet, location C1
- Fig. 5.152 Liquid level signals in channel C outlet, center
- Fig. 5.153 Liquid level signals in channel A inlet
- Fig. 5.154 Liquid level signals in channel C inlet
- Fig. 5.155 Liquid level signals in lower plenum, north
- Fig. 5.156 Liquid level signals in guide tube, north
- Fig. 5.157 Liquid level signals in downcomer, D side
- Fig. 5.158 Liquid level in core and downcomer
- Fig. 5.159 Dryout and quench front transients in channel A
- Fig. 5.160 Dryout and quench front transients in channels A,  
B,C and D
- Fig. 5.161 Average density at JP-1,2 outlet
- Fig. 5.162 Average density at JP-3,4 outlet
- Fig. 5.163 Average density at break
- Fig. 5.164 Flow rate at break (based on high range drag disk data)
- Fig. 5.165 Steam discharge flow rate through MSL
- Fig. 5.166 Flow rate at channel A inlet
- Fig. 5.167 Flow rate at channel B inlet
- Fig. 5.168 Flow rate at channel C inlet
- Fig. 5.169 Flow rate at channel D inlet
- Fig. 5.170 Flow rate at bypass hole
- Fig. 5.171 Total channel inlet flow rate
- Fig. 5.172 Flow rate at JP-1,2 outlet (pos. flow)
- Fig. 5.173 Flow rate at JP-3,4 outlet (pos. flow)
- Fig. 5.174 Flow rate at JP-3,4 outlet (neg. flow)

Fig. 5.175 Total JP outlet flow rate (pos. flow)

Fig. 5.176 Collapsed liquid level in downcomer

Fig. 5.177 Collapsed liquid level inside core shroud

Fig. 5.178 Fluid inventory in downcomer

Fig. 5.179 Fluid inventory inside core shroud

Fig. 5.180 Total fluid inventory in pressure vessel

Fig. 7.1 Lower plenum pressure transients in RUN 953 and RUN 952

Fig. 7.2 Differential pressure across core

Fig. 7.3 ECCS flow rates

Fig. 7.4 Core mass inventory

Fig. 7.5 Collapsed liquid level in upper and lower downcomer

Fig. 7.6 Mass inventory in downcomer

Fig. 7.7 Steam flow rate in the Main Steam Line

Fig. 7.8 Comparison of surface temperatures at position 1 of  
fuel rod A22

Fig. 7.9 Comparison of surface temperatures at position 4 of  
fuel rod A22

Fig. 7.10 Comparison of surface temperatures at position 6 of  
fuel rod A22

Fig. 7.11 Comparison of peak cladding temperatures

## 1. Introduction

The Rig of Safety Assessment (ROSA)-III program was initiated in 1976 to study the thermal-hydraulic behavior of a Boiling Water Reactor (BWR) during a postulated Loss of Coolant Accident (LOCA) with the Emergency Core Cooling System (ECCS) actuation and to provide the data base necessary for evaluation of computer codes developed for reactor safety analysis. The ROSA-III test facility, which was completed in 1978, consists of a volumetrically scaled (1/424) primary system of a 3800 MW BWR/6-251 with an electrically heated core, a break simulator and a scaled ECCS<sup>(1)</sup>.

Special emphasis has been placed on the following objectives in the ROSA-III program :

- (1) To provide the system data required for improvement and evaluation of analytical methods currently used to predict the LOCA response of large BWRs. In particular, the performance of Engineered Safety Features (ESFs), with an emphasis on ECCSs, and the quantitative margins of safety inherent in performance of the ESFs are of primary interest.
- (2) To identify and investigate any unexpected event(s) or threshold(s) in the response of either the plant or the ESFs and to develop analytical techniques that adequately describe and account for such unexpected behavior.

The information acquired from Loss of Coolant Experiments (LOCEs) is thus used for evaluation and development of LOCA analytical methods and assessment of the ESFs in response to a LOCA.

RUN 953 was conducted on July 23, 1982 to simulate a 100% Main Steam Line (MSL) break LOCA with an assumption of an HPCS failure.

The specific objectives of this test were as follows :

- (1) To acquire test data on a 100% MSL break LOCA with an HPCS failure logic, and
- (2) To determine the effect of a partial ECCS failure on the system response for an MSL break LOCA.

In this report, all of the data obtained in RUN 953 are presented and discussed, including the processed data such as mass inventory in the pressure vessel. The data from this test are then compared with the results of a similar 100% MSL break test, RUN 952, in which only the HPCS was activated<sup>(6)</sup>. Some important parameters describing the system response from both experiments are compared to determine the effect of a partial ECCS failure on the MSL break LOCA.

## 2. ROSA-III Test Facility

The ROSA-III test facility is a volumetrically scaled (1/424) BWR system with an electrically heated core designed to study the response of the primary system, the core and the ECCS during a postulated LOCA. The test facility is instrumented to measure and record various thermal-hydraulic parameters during the test. Details of the instrumentation are described in section 3.

The test facility consists of four subsystems. These subsystems are : (a) pressure vessel, (b) steam line and feedwater line, (c) recirculation loops and (d) ECCS. Figures 2.1 through 2.3 illustrate the configuration of the test facility including the pressure vessel internals and piping schematics. Table 2.1 compares the major dimensions of the ROSA-III test facility with the corresponding dimensions of the reference BWR.

The ROSA-III pressure vessel includes various components simulating the internal structures of the reactor vessel in the BWR system as shown in Fig. 2.4. The interior of the vessel is divided into the core, lower plenum, upper plenum, downcomer annulus, steam separator, steam dome and steam dryer. The core consists of four model fuel assemblies of half length and a control rod simulator. Each fuel assembly contains 62 heater rods (Fig. 2.5) and 2 water rods spaced in a 8 x 8 square array and supported by spacers and upper and lower tie plates. The heater rod is heated electrically with chopped cosine power distribution along the axis as shown in Fig. 2.6. The effective heated length is 1880 mm, one half of the active length of a BWR fuel rod. The electric power supplied to the model fuel assembly A is 1.4 times larger than the power supplied to each of the other assemblies, B, C and D. The heater rods in each assembly are divided into three groups in terms of heat generation rate as shown in Fig. 2.7.

The relative power generation rate of a heater rod in each group is 1.1, 1.0, and 0.875 respectively. The orifice plates are inserted at the core inlet to control the core inlet flow<sup>(1)</sup>.

The steam line and the feedwater line simulate those of a BWR. The steam line of the ROSA III system has three branches as shown in Fig. 4.3. The first branch is initially closed by a valve AV-165 and used for the simulation of steam line break by opening the valve AV-165. The steam discharge flow after break is limited by the break orifice OR-5 with 31.0 mm I.D. shown in Fig. 4.1 located in the first branch and is led to the outdoor pool through the break unit B where a gamma densitometer and a drag disk are installed to measure the break flow. The break unit A was not used in RUN 953 and the quick shutoff valve between the two break units was also closed. The inner diameter of the orifice in the break unit B was 49.5 mm.

The second branch is the Automatic Depressurization Line which was not used in RUN 953. The third branch is used for controlling the steady state system pressure and the steam is used partially for heating-up the feedwater. Immediately after the break initiation, the third branch is shut off by closing the main steam isolation valve (MSIV), AV-168, so that the steam is discharged only through the first branch simulating the break. A control valve is installed in the steam line to control the steam dome pressure at steady state before the initiation of tests. The steam line has a branch in which the Automatic Depressurization System (ADS) is installed. The operation of valves in the steam line is described in sec. 4. The feedwater is supplied from the feedwater tank (FWT) through the feedwater line and the sparger below the steam separator.

Figure 2.8 shows the recirculation line consisting of two loops. Each loop is furnished with a pump and two jet pumps. The jet pumps are installed outside the pressure vessel to simulate the relative volume and height with respect to the core. The ROSA-III test facility is furnished

with all types of ECCS which are available in the BWR system, i.e., High Pressure Core Spray (HPCS), Low Pressure Core Spray (LPCS), Low Pressure Coolant Injection (LPCI), and Automatic Depressurization System (ADS). The HPCS and LPCS provide the cooling water from the top of the core. The LPCI injects the cooling water into the core bypass. Each ECCS consists of a pump, a tank, piping, and a control and measurement system. Reference (1) provides more detailed information on the ROSA-III facility.

Table 2.1 Primary Characteristics of ROSA-III and BWR/6

	BWR*	ROSA-III	BWR/ROSA-III
Number of Recirc. Loops	2	2	1
Number of Jet Pumps	24	4	6
Number of Separators	251	1	251
Number of Fuel Assemblies	848	4	212
Active Fuel Length (m)	3.76	1.88	2
Total Volume (m <sup>3</sup> )	621	1.42	437
Power (MW)	3,800	4.40	864
Pressure (MPa)	7.23	7.23	1
Core Flow (kg/s)	$1.54 \times 10^4$	36.4	424
Recirculation Flow (l/s)	2,970	7.01	424
Feedwater Flow (kg/s)	2,060	4.86	424
Feedwater Temp. (K)	489	489	1

\* BWR/6-251

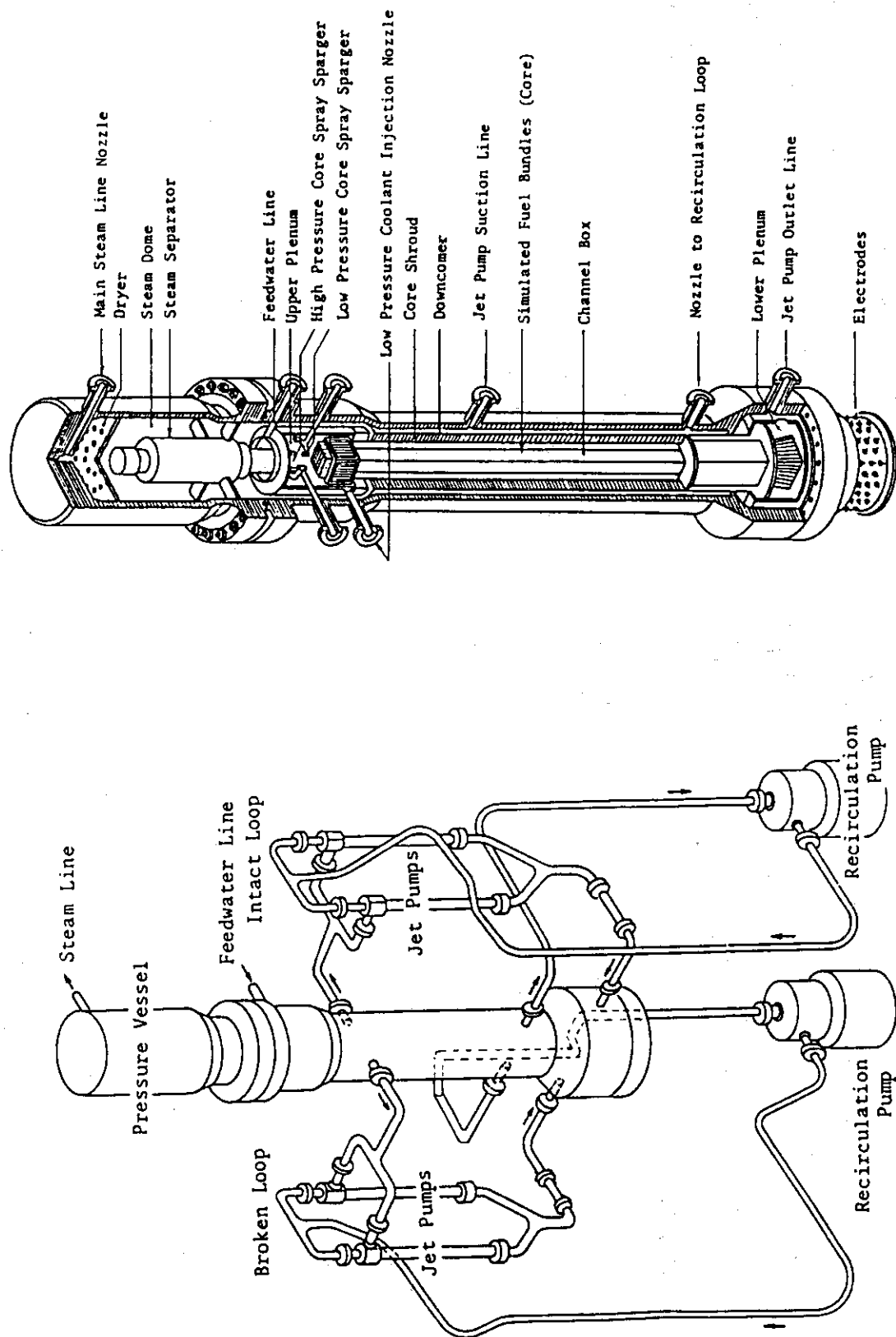


Fig. 2.1

Schematic Diagram of ROSA-III Test Facility

Internal Structure of Pressure Vessel of ROSA-III

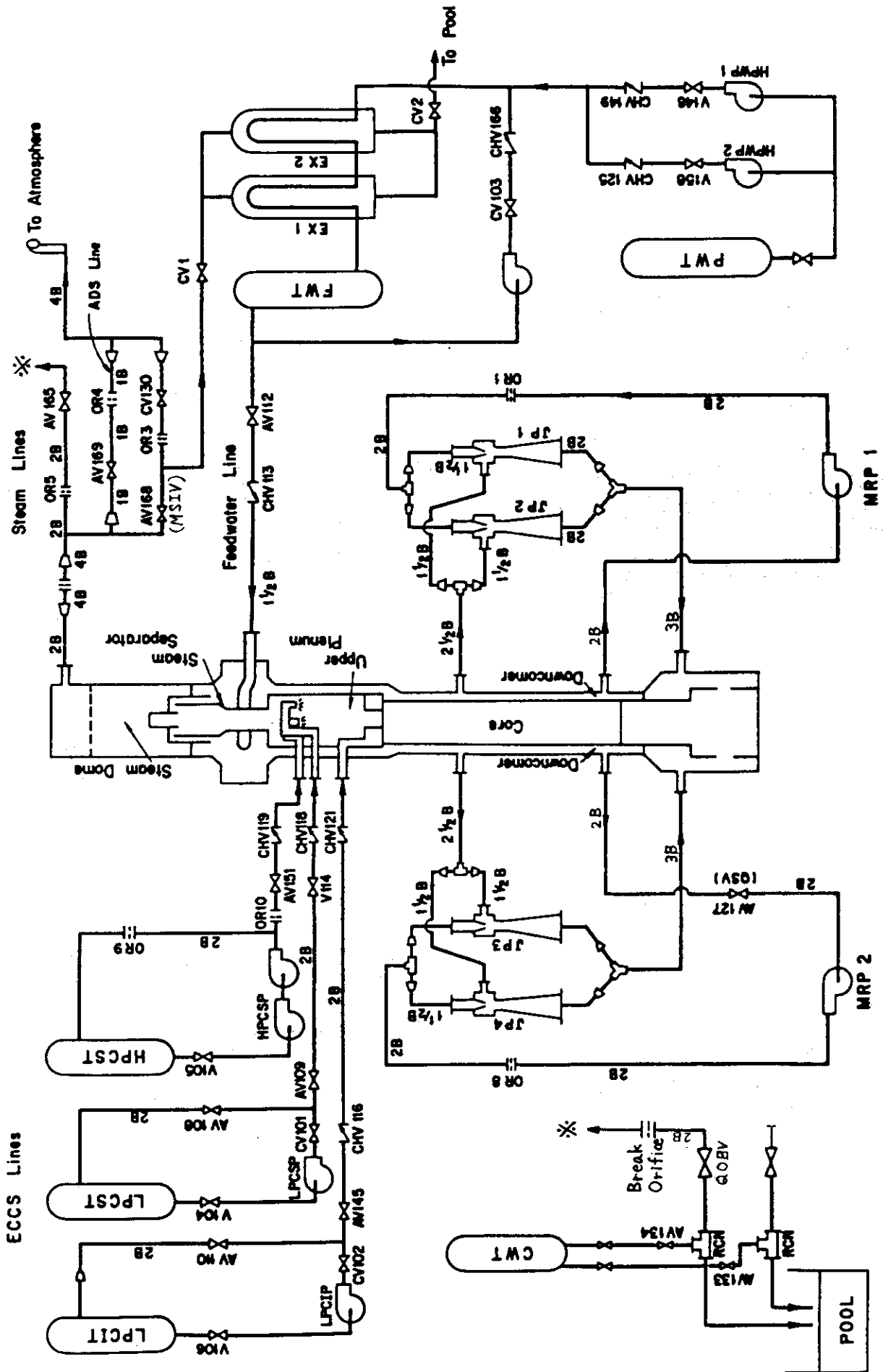


Fig. 2.3 ROSA-III Piping Schematic

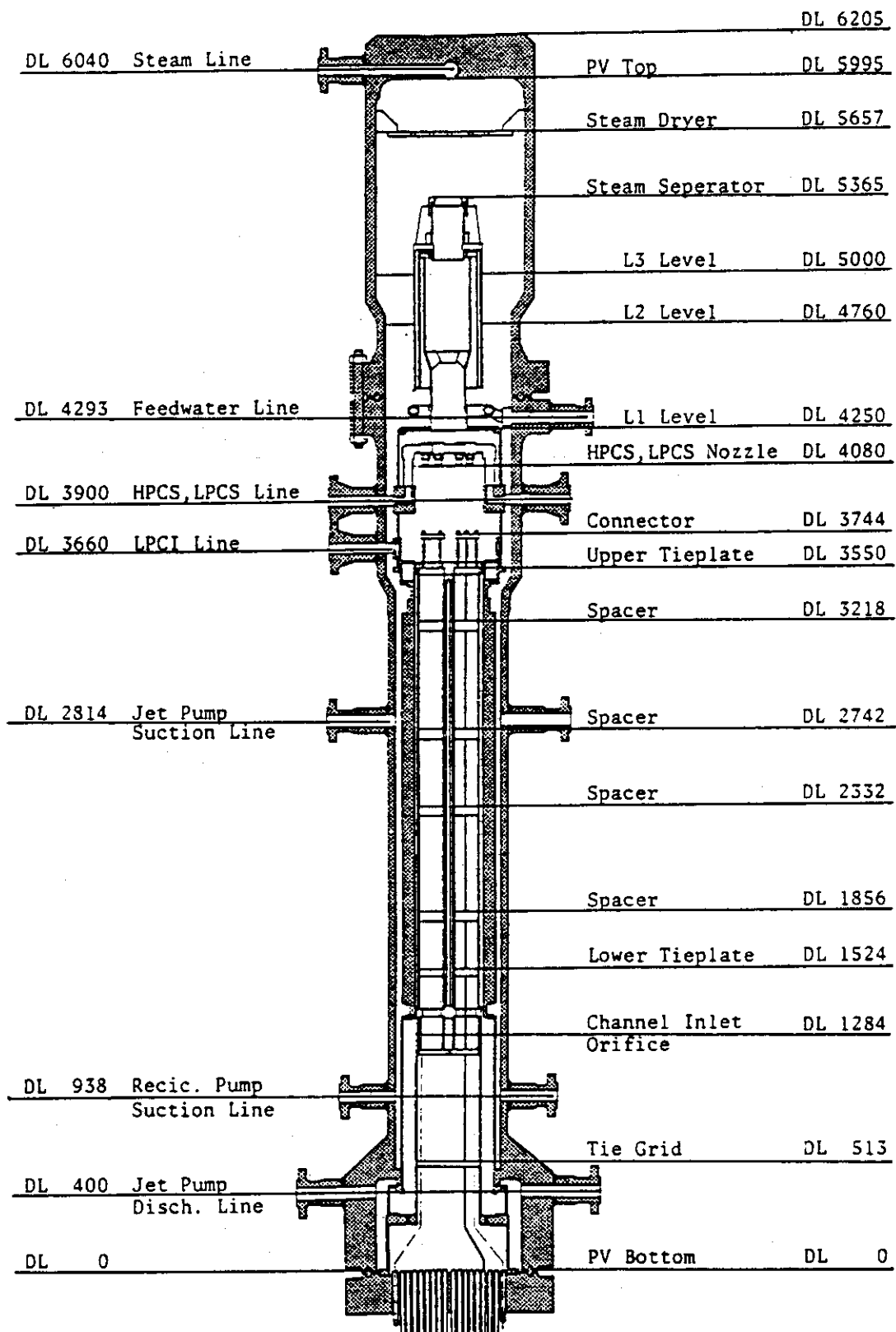


Fig. 2.4 Pressure Vessel Internals Arrangement

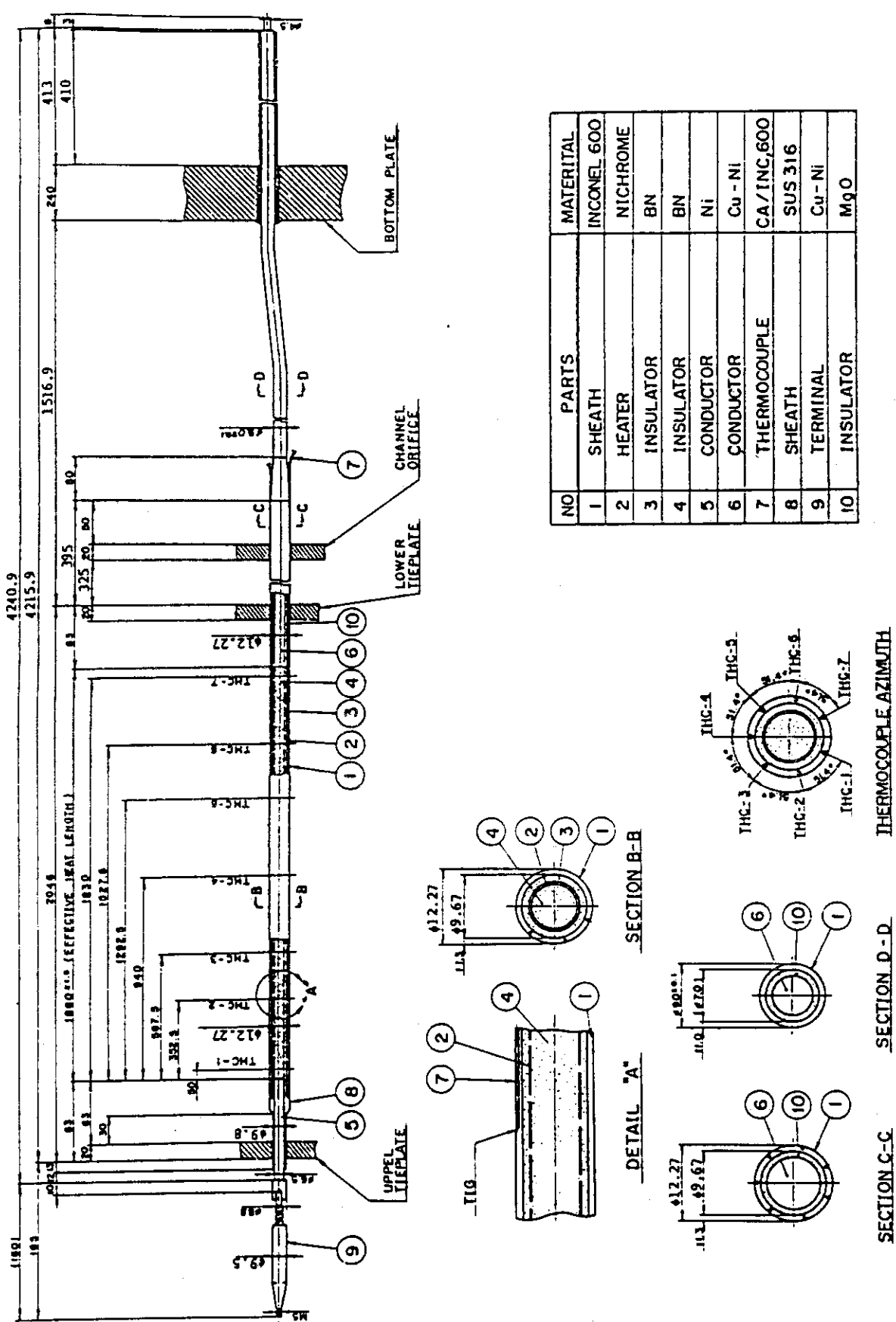
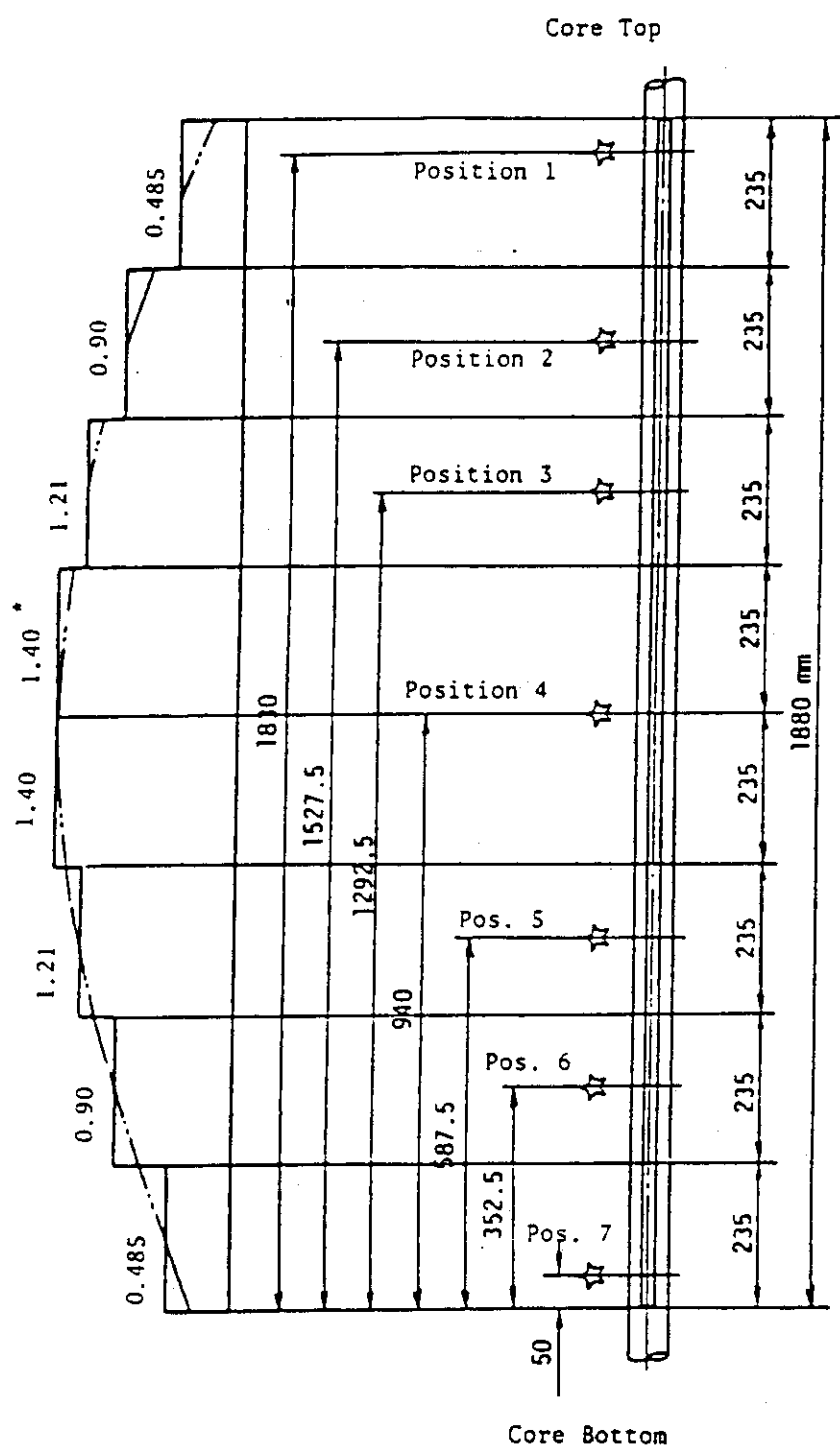
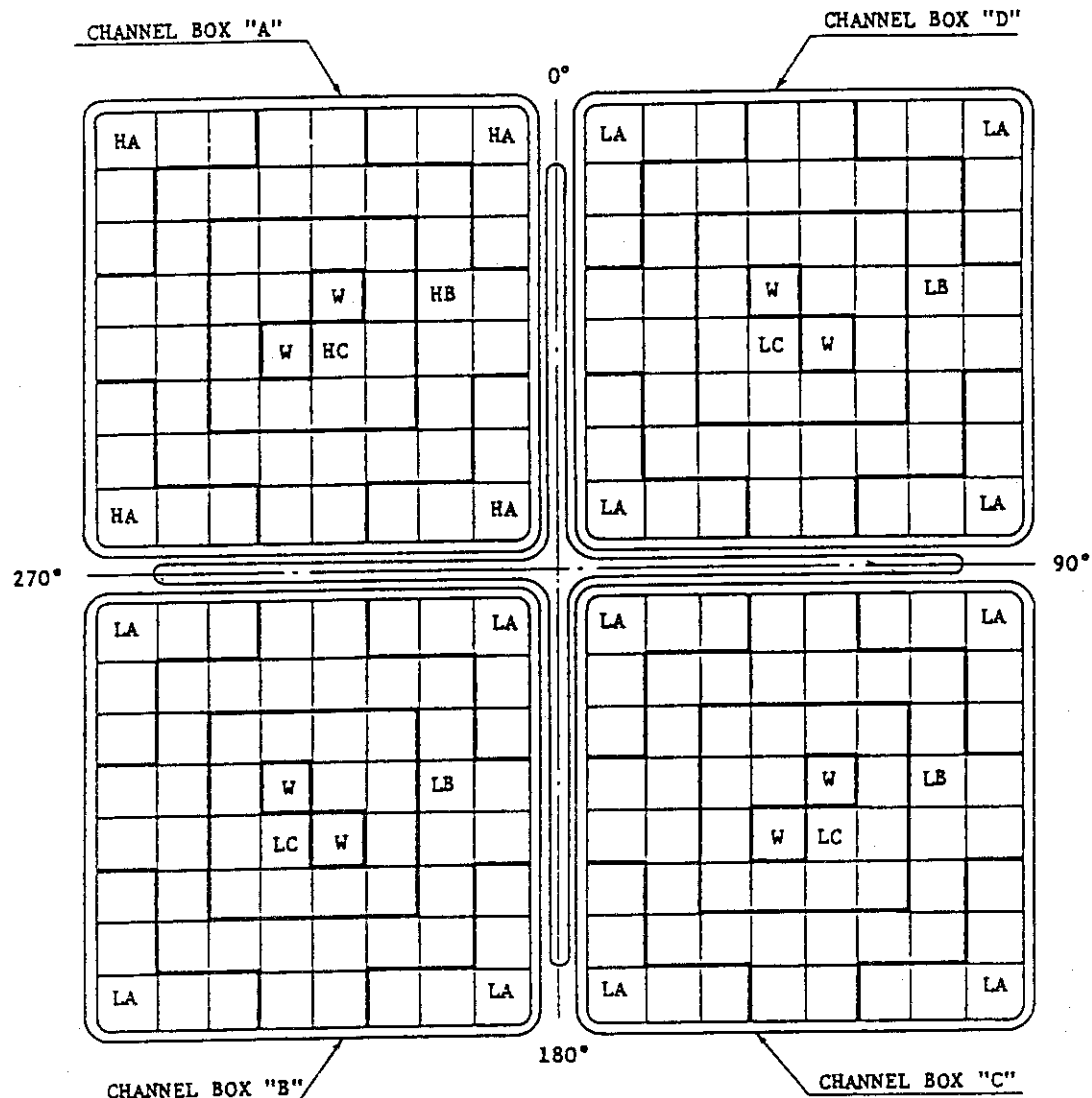


Fig. 2.5 Simulated Fuel Rod of ROSA-III



☆ indicates position of thermocouple. \* Axial Peaking Factor

Fig.2.6 Axial Power Distribution of Heater Rod



Region	HA	HB	HC	LA	LB	LC	W
Linear Heat Rate (kW/m)	18.5	16.81	14.41	13.21	12.01	10.29	0.0
Local peaking factor	1.1	1.0	0.875	1.1	1.0	0.875	0.0
No. of Rods	20	28	14	60	84	42	8

\* note : Radial peaking factor is 1.4

Fig. 2.7 Radial Power Distribution of Core

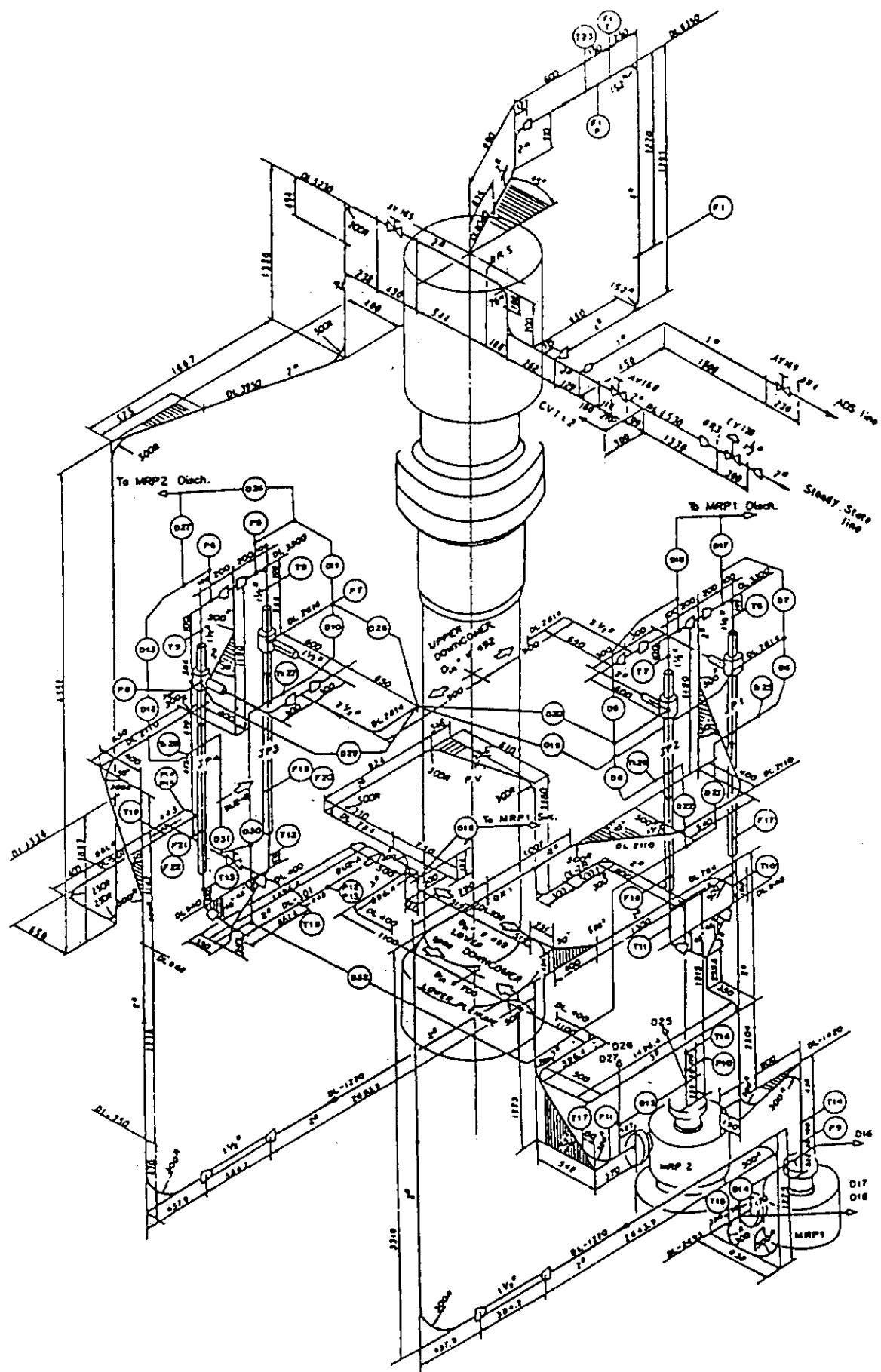


Fig. 2.8 Piping layout of recirculation loops and jet pumps

### 3. Instrumentation

The instrumentation for the ROSA-III facility has been designed to provide thermal-hydraulic data for a simulated BWR LOCA. The data obtained from the experiments are used for the assessment of analytical computer codes. Table 3.1 summarizes the instrumentation used in RUN 953.

Tables 3.2 and 3.3 show the measurement list and the core instrumentation list, respectively. Instrument locations are shown in Fig. 3.1 through Fig. 3.6.

Typical parameters measured in the ROSA-III facility are pressure, differential pressure, flow rate, electric power, pump speed, fluid and metal temperatures, collapsed liquid level, two-phase mixture level, coolant density, on-off type signals and so on.

Pressure and differential pressure transducers are two-wire, direct-current type which convert diaphragm displacement to electric capacitance. The pressure lead lines are either the standard single, cylindrical pipes used in conjunction with condensate pots, or dual concentric cylinders capable of circulating the cooling water to prevent flashing of the fluid.

The flow rate is measured either by an orifice or a venturi type flow meter depending on the fluid condition and measurement location.

The temperatures of the fluid, structural materials and the cladding of fuel rods are measured with sheathed chromel-alumel (C/A) thermocouples of 1.6mm or 0.5 mm diameter.

Liquid level is measured by either differential pressure transducers described above or needle type electrical conduction probes (CP) developed specially for the ROSA-III program. These probes are distributed in the pressure vessel to detect the presence of water or vapor at different heights.

The electric power supplied to the simulated fuel rods is controlled to

follow the predetermined decay curve and measured by a fast response electric power meter.

Pump speed is measured by a pulse generator integral to the pump. On-off signals indicating the valve positions selected, core power decay and pump coastdown initiation and so on are also detected and recorded.

Fluid density in the pipe is measured by means of multi-beam gamma densitometers. Preliminary studies indicated that a three-beam densitometer should be used to determine the flow regime. Figures 3.7 and 3.8 show the beam directions of the three-beam and two-beam gamma densitometers, respectively. The gamma-ray source is  $^{137}\text{Cs}$  and the detector is a water cooled NaI(Tl) scintillation counter.

Momentum flux is measured by a drag disk shown in Fig. 3.9. The combination of signals from a drag disk and a gamma densitometer is used to determine the two-phase flow rate as shown in Fig. 3.10.

The data acquisition system ( DATAC 2000B, Iwasaki Tsushinki Co. ) scans all of the 700 instrument channels at a rate of up to 30 Hz. The data recorded on magnetic tapes are processed by the FACOM M380/200 computer system after the experiment. More detailed information on the instrumentation and the data processing procedure is available in reference (2).

Table 3.1 ROSA-III Instrumentation Summary List

ITEM	SENSOR	NUMBER	NOTE
Pressure	Pressure Transducer	20	
Differential Pressure	DP Cell	60	PV and Loop 44 Level Measurement 5 Flow Meter 11
Fluid Temperature	CA Thermocouple	85	Primary Loop 35 DTT 4 Tie Rod 14 Upper Plenum 10 Lower Plenum 10 Tie Plate 12 Bypass 0
Fuel Rod Temperature	CA Thermocouple	133	
Slab Surface Temperature	CA Thermocouple	7	Core Barrel 0 Pressure Vessel 0 Channel Box 7 Shroud Support 0
Slab Inner Temperature	CA Thermocouple	0	JP Diffuser 0 PV Wall 0
Volumetric Flow Rate	Turbine Flow Meter Venturi Flow Meter Orifice Flow Meter	3 4 6	ECCS Loop 3 Primary Loop 10
Mass Flow Rate	Turbine Flow Meter Orifice Flow Meter	4 3	Recirculation Loop 4 Main Steam Line 3
Liquid Level	Conductivity Probe Capacitance Probe	56 0	
Density	Gamma Densitometer	10	2 Beam GD 2 3 Beam GD 2
Momentum Flux	Drag Disk	7	JP Spool Piece 2 Break Spool Piece 4 Break Orifice 1
Signal	ON/OFF Switch	14	
Pump Speed	Revolution Counter	2	
Electric Core Power	VA Meter	2	
TOTAL		416	

Table 3.2 Measurement List for RUN 953

Ch.	Item	Symbol	ID.	Location	Fig.No.	Range	Unit	Accuracy
1	Press.	P-	1	PA	Fig.5. 1	0-100	-	1.08%FS
2	Press.	P-	2	PA	Fig.5. 1	0-100	-	1.08%FS
3	Press.	P-	3	PA	Fig.5. 1,5. 4	0-100	-	1.08%FS
4	Press.	P-	4	PA	Fig.5. 1	0-100	-	1.08%FS
5	Press.	P-	5	PA	Fig.5. 1	0-100	-	1.08%FS
6	Press.	P-	6	PA	Fig.5. 2	0-100	-	1.08%FS
7	Press.	P-	7	PA	Fig.5. 2	0-100	-	1.08%FS
8	Press.	P-	8	PA	Fig.5. 2	0-100	-	1.08%FS
9	Press.	P-	9	PA	Fig.5. 3	0-100	-	1.08%FS
10	Press.	P-	10	PA	Fig.5. 3	0-100	-	1.08%FS
11	Press.	P-	11	PA	Fig.5. 3	0-100	-	1.08%FS
12	Press.	P-	12	PA	Not Measured	0-100	-	1.08%FS
13	Press.	P-	13	PA	Not Used	0-100	-	1.08%FS
14	Press.	P-	14	PA	Fig.5. 4	0-100	-	1.08%FS
15	Press.	P-	15	PA	Fig.5. 4	0-100	-	1.08%FS
16	Press.	P-	16	PA	Failure	0-100	-	1.08%FS
17	Press.	P-	17	PA	Fig.5. 5	0-100	-	1.08%FS
18	Press.	P-	18	PA	Fig.5. 5	0-100	-	1.08%FS
19	Press.	P-	19	PA	Not Used	0-100	-	1.08%FS
20	Press.	P-	20	PA	Fig.5. 4	0-100	-	1.08%FS
21	Diff.P.	D-	1	PD	Fig.5. 6	-50.0	-	0.63%FS
22	Diff.P.	D-	2	PD	Upper Pl.-Steam Dome	-10.0	-	0.63%FS
23	Diff.P.	D-	3	PD	Lower Plenum Head	90.0	-	0.63%FS
24	Diff.P.	D-	4	PD	Downcomer Head	0.0	-	0.63%FS
25	Diff.P.	D-	5	PD	PV Bottom-Top	-100.	-	0.63%FS
26	Diff.P.	D-	6	PD	JP-1 Disch.-Suction	-100.	-	0.63%FS
27	Diff.P.	D-	7	PD	JP-1 Drive -Suction	0.0	-	0.63%FS
28	Diff.P.	D-	8	PD	JP-2 Disch.-Suction	-100.	-	0.63%FS
29	Diff.P.	D-	9	PD	JP-2 Drive -Suction	0.0	-	0.63%FS
30	Diff.P.	D-	10	PD	JP-3 Disch.-Suction	-100.	-	0.63%FS
31	Diff.P.	D-	11	PD	JP-3 Drive -Suction	-4.00	-	0.63%FS
32	Diff.P.	D-	12	PD	JP-4 Disch.-Suction	-100.	-	0.63%FS
33	Diff.P.	D-	13	PD	JP-4 Drive -Suction	-4.00	-	0.63%FS
34	Diff.P.	D-	14	PD	MRP-1 Deliv.-JP2 Drive	-0.100	-	0.63%FS
35	Diff.P.	D-	15	PD	MRP-2 Deliv.-JP1 Suction	-0.100	-	0.63%FS
36	Diff.P.	D-	16	PD	DC Bottom-MRP-1 Suc.	-50.0	-	0.63%FS
37	Diff.P.	D-	17	PD	MRP1 Deliv.-JP1 Drive	0.0	-	0.63%FS
38	Diff.P.	D-	18	PD	MRP1 Deliv.-JP2 Drive	0.0	-	0.63%FS
39	Diff.P.	D-	19	PD	DC Middle-JP1 Suction	0.0	-	0.63%FS
40	Diff.P.	D-	20	PD	DC Middle-JP2 Suction	0.0	-	0.63%FS
41	Diff.P.	D-	21	PD	JP1 Disch.-Lower Pl.	-100.	-	0.63%FS
42	Diff.P.	D-	22	PD	JP2 Disch.-Lower Pl.	-100.	-	0.63%FS
43	Diff.P.	D-	23	PD	DC Bottom-Break B	0.0	-	0.63%FS
44	Diff.P.	D-	24	PD	Break B - Break A	0.0	-	0.63%FS
45	Diff.P.	D-	25	PD	Break A - MRP2 Suction	-500.	-	0.63%FS
46	Diff.P.	D-	26	PD	MRP2 Deliv.-JP3 Drive	-500.	-	0.63%FS
47	Diff.P.	D-	27	PD	MRP2 Deliv.-JP4 Drive	-500.	-	0.63%FS
48	Diff.P.	D-	28	PD	DC Middle-JP3 Suction	-250.	-	0.63%FS
49	Diff.P.	D-	29	PD	DC Middle-JP4 Suction	-250.	-	0.63%FS
50	Diff.P.	D-	30	PD	JP3 Disch.-Confluence	-100.	-	0.63%FS

Table 3.2 Measurement List for RUN 953 (Continued)

Ch.	Item	Symbol	ID.	Location	Fig.No.	Range	Unit	Accuracy
51	Diff.P.	D-31	PD	JP4 Disch.-Confluence	Fig.5-22	-100.	-	0.63%FS
52	Diff.P.	D-32	PD	Confluence -Lower Pl.	Fig.5-23	-50.0	-	0.63%FS
53	Diff.P.	D-33	PD	Lower Pl.-DC Middle	Fig.5-24	-250.	-	0.63%FS
54	Diff.P.	D-34	PD	Lower Pl.-DC Bottom	Fig.5-25	-250.	-	0.63%FS
55	Diff.P.	D-35	PD	DC Bottom-DC Middle	Fig.5-26	-50.0	-	0.63%FS
56	Diff.P.	D-36	PD	DC Middle-Stream Dome	Fig.5-27	-50.0	-	0.63%FS
57	Diff.P.	D-37	PD	Lower Pl.-MidUpper PL	Not Measured	0.0	-	0.63%FS
58	Diff.P.	D-38	PD	Lower Pl.-Bottom-middle	Fig.5-28	Not Used	-20.0	0.63%FS
59	Diff.P.	D-39	PD	Upper PL-Head	Fig.5-29	-50.0	-	0.63%FS
60	Diff.P.	D-40	PD	Channel Orifice A	Fig.5-30	-50.0	-	0.63%FS
61	Diff.P.	D-41	PD	Channel Orifice B	Fig.5-31	-25.0	-	0.63%FS
62	Diff.P.	D-42	PD	Channel Orifice C	Fig.5-32	-50.0	-	0.63%FS
63	Diff.P.	D-43	PD	Channel Orifice D	Fig.5-33	-100.	-	0.63%FS
64	Diff.P.	D-44	PD	Bypass Hole	Fig.5-34	0.0	-	0.63%FS
65	Level	WL-1	LM	HPCS Tank	Fig.5-34	0.0	-	1.00%FS
66	Level	WL-2	LM	LPCS Tank	Fig.5-34	0.0	-	2.30
67	Level	WL-3	LM	LPCI Tank	Fig.5-34	0.0	-	1.00%FS
68	Level	WL-4	LM	Pressure Vessel	Fig.5-35	3.90	-	6.04
69	Level	WL-5	LM	Downcomer	Fig.5-35	0.938	-	3.90
70	Mass.F.	F-1	FM	Steam Line (Low Range)	Not Measured	0.0	-	1.3
71	Mass.F.	F-2	FM	Steam Line (High Range)	Fig.5-36	0.0	-	3.00
72	Mass.F.	F-3	FM	Steam Line (High-High)	Fig.5-36	0.0	-	14.3
73	Vol.F.	F-7	FV	HPCS (Upper Plenum)	Fig.5-37	0.0	-	0.250E-02 m <sup>3</sup> /s
74	Vol.F.	F-9	FV	LPCS (Upper Plenum)	Fig.5-37	0.0	-	0.250E-02 m <sup>3</sup> /s
75	Vol.F.	F-11	FV	LPCI (Core Bypass)	Fig.5-37	0.0	-	0.830E-02 m <sup>3</sup> /s
76	Vol.F.	F-15	FV	Feedwater	Fig.5-38	0.0	-	0.100E-01 m <sup>3</sup> /s
77	Vol.F.	F-16	FV	HPWP Suction	Not Measured	0.0	-	0.420E-02 m <sup>3</sup> /s
78	Vol.F.	F-17	FV	JP1 Discharge	Fig.5-39	0.0	-	0.170E-01 m <sup>3</sup> /s
79	Vol.F.	F-18	FV	JP2 Discharge	Fig.5-39	0.0	-	0.170E-01 m <sup>3</sup> /s
80	Vol.F.	F-19	FV	JP3 Disch. Positive	Fig.5-40	0.0	-	0.170E-01 m <sup>3</sup> /s
81	Vol.F.	F-20	FV	JP3 Disch. Negative	Not Measured	0.0	-	0.170E-02 m <sup>3</sup> /s
82	Vol.F.	F-21	FV	JP4 Disch. Positive	Fig.5-40	0.0	-	0.170E-01 m <sup>3</sup> /s
83	Vol.F.	F-22	FV	JP4 Disch. Negative	Not Measured	0.0	-	0.500E-02 m <sup>3</sup> /s
84	Mass.F.	F-23	FM	JP1.2 Outlet Spool	Not Measured	0.0	-	0.92%FS
85	Mass.F.	F-24	FM	JP3.4 Outlet Spool	Not Measured	0.0	-	0.92%FS
86	Mass.F.	F-25	FM	Break A Spool Piece	Not Measured	0.0	-	0.92%FS
87	Mass.F.	F-26	FM	Break B Spool Piece	Not Measured	0.0	-	0.92%FS
88	Vol.F.	F-27	FV	MRP-1	Fig.5-41	0.0	-	0.120E-01 m <sup>3</sup> /s
89	Vol.F.	F-28	FV	MRP-2	Fig.5-41	0.0	-	0.120E-01 m <sup>3</sup> /s
90	Diff.P.	D-F1	PD	F1 Orifice	Fig.5-42	0.0	-	4.90
91	Diff.P.	D-F2	PD	F2 Orifice	Fig.5-43	0.0	-	34.9
92	Diff.P.	D-F3	PD	F3 Orifice	Fig.5-44	0.0	-	800.
93	Diff.P.	D-F17	PD	F17 Venturi	Fig.5-45	0.0	-	98.1
94	Diff.P.	D-F18	PD	F18 Venturi	Fig.5-46	0.0	-	98.1
95	Diff.P.	D-F19	PD	F19 Orifice	Fig.5-47	0.0	-	147.
96	Diff.P.	D-F20	PD	F20 Orifice	Fig.5-48	0.0	-	13.2
97	Diff.P.	D-F21	PD	F21 Orifice	Fig.5-49	0.0	-	147.
98	Diff.P.	D-F22	PD	F22 Orifice	Fig.5-50	0.0	-	13.2
99	Diff.P.	D-F27	PD	F27 Venturi	Fig.5-51	0.0	-	200.
100	Diff.P.	D-F28	PD	F28 Venturi	Fig.5-52	0.0	-	200.

Table 3.2 Measurement List for RUN 953 (Continued)

Ch.	Item	Symbol	ID.	Location	Fig.No.	Range	Unit	Accuracy
101	Power Power	W- 1 W- 2	WE WE	101 102	2100 KW Power Supply 3150 KW Power Supply	Fig.5.53 Fig.5.53 Not Used	0.0 0.0	- 0.210E+04 KW 0.315E+04 KW
103	Rev. Rev.	N- 1 N- 2	SR SR	104 105	MRP-1 Revolution MRP-2 Revolution	Fig.5.54 Fig.5.54 Fig.5.55	0.0 0.0	- 0.500E+04 RPM 0.500E+04 RPM
104	Signal	S- 1	EV	106	Break Signal A	Fig.5.55	-	1.00%FS
105	Signal	S- 2	EV	107	Break Signal B	Fig.5.55	-	1.00%FS
106	Signal	S- 3	EV	108	QSV Signal	Fig.5.55	-	1.00%FS
107	Signal	S- 4	EV	109	HPCS Valve	Fig.5.56	-	1.00%FS
108	Signal	S- 5	EV	110	LPCS Valve	Fig.5.56	-	1.00%FS
109	Signal	S- 6	EV	111	LPCI Valve	Fig.5.56	-	1.00%FS
110	Signal	S- 7	EV	112	Feedwater Control	Fig.5.55	-	1.00%FS
111	Signal	S- 8	EV	113	MSIV Signal	Fig.5.55	-	1.00%FS
112	Signal	S- 9	EV	114	Steam Line Valve	Fig.5.55	-	1.00%FS
113	Signal	S- 10	EV	115	ADS Valve	Fig.5.56	-	1.00%FS
114	Signal	S- 11	EV	116	MRP-1 Power OFF	Fig.5.57	-	1.00%FS
115	Signal	S- 12	EV	117	MRP-2 Power OFF	Fig.5.57	-	1.00%FS
116	Signal	S- 13	EV	118	MRP-1 Rev. Direction	Fig.5.57	-	1.00%FS
117	Signal	S- 14	EV	119	MRP-2 Rev. Direction	Fig.5.57	-	1.00%FS
118	Density	DF- 1	DE	120	JP1/2 Outlet Beam A	Fig.5.58	0.0	-
119	Density	DF- 2	DE	121	JP1/2 Outlet Beam B	Fig.5.59	0.0	-
120	Density	DF- 3	DE	122	JP1/2 Outlet Beam C	Fig.5.60	0.0	-
121	Density	DF- 4	DE	123	JP3/4 Outlet Beam A	Fig.5.61	0.0	-
122	Density	DF- 5	DE	124	JP3/4 Outlet Beam B	Fig.5.62	0.0	-
123	Density	DF- 6	DE	125	JP3/4 Outlet Beam C	Fig.5.63	0.0	-
124	Density	DF- 7	DE	126	Break A Beam A	Not Measured	0.0	-
125	Density	DF- 8	DE	127	Break A Beam B	Not Measured	0.0	-
126	Density	DF- 9	DE	128	Break B Beam A	Fig.5.64	0.0	-
127	Density	DF- 10	DE	129	Break B Beam B	Fig.5.65	0.0	-
128	Mo.Flux	M- 1	MF	130	JP1/2 Outlet Spool	Fig.5.66	0.0	-
129	Mo.Flux	M- 2	MF	131	JP3/4 Outlet Spool	Fig.5.67	0.0	-
130	Mo.Flux	M- 3	MF	132	Break A (Low Range)	Not Used	0.0	-
131	Mo.Flux	M- 4	MF	133	Break B (Low Range)	Not Measured	0.0	-
132	Mo.Flux	M- 5	MF	134	Break A (High Range)	Not Used	0.0	-
133	Mo.Flux	M- 6	MF	135	Break B (High Range)	Fig.5.68	0.0	-
134	Mo.Flux	M- 7	MF	136	Break Orifice	Not Measured	0.0	-
135	Fluid T.	T- 1	TE	138	Lower Plenum	Fig.5.69	273.	-
136	Fluid T.	T- 2	TE	139	Upper Plenum	Fig.5.69	273.	-
137	Fluid T.	T- 3	TE	140	Steam Dome	Fig.5.70	673.	-
138	Fluid T.	T- 4	TE	141	Upper Downcomer	Fig.5.71	673.	-
139	Fluid T.	T- 5	TE	142	Lower Downcomer	Fig.5.71	673.	-
140	Fluid T.	T- 6	TE	143	JP-1 Drive	Fig.5.72	673.	-
141	Fluid T.	T- 7	TE	144	JP-2 Drive	Fig.5.72	673.	-
142	Fluid T.	T- 8	TE	145	JP-3 Drive	Fig.5.73	673.	-
143	Fluid T.	T- 9	TE	146	JP-4 Drive	Fig.5.73	673.	-
144	Fluid T.	T- 10	TE	147	JP-1 Discharge	Fig.5.74	673.	-
145	Fluid T.	T- 11	TE	148	JP-2 Discharge	Fig.5.74	673.	-
146	Fluid T.	T- 12	TE	149	JP-3 Discharge	Fig.5.75	673.	-
147	Fluid T.	T- 13	TE	150	JP-4 Discharge	Fig.5.75	673.	-

Table 3.2 Measurement List for RUN 953 (Continued)

Ch.	Item	Symbol	ID.	Location	Fig.No.	Range	Unit	Accuracy
151	Fluid T.	T-14	TE 151	MRP-1 Suction	Fig.5.72	273.	-	0.64%FS
152	Fluid T.	T-15	TE 152	MRP-1 Delivery	Fig.5.72	273.	-	0.64%FS
153	Fluid T.	T-16	TE 153	MRP-2 Suction	Fig.5.73	273.	-	0.64%FS
154	Fluid T.	T-17	TE 154	MRP-2 Delivery	Fig.5.73	273.	-	0.64%FS
155	Fluid T.	T-18	TE 155	Break A Upstream	Not Used	273.	-	0.64%FS
156	Fluid T.	T-19	TE 156	Break B Upstream	Fig.5.76	273.	-	0.64%FS
157	Fluid T.	T-20	TE 157	RCN A Condensed Water	Not Used	273.	-	0.64%FS
158	Fluid T.	T-21	TE 158	RCN B Condensed Water	Not Used	273.	-	0.64%FS
159	Fluid T.	T-22	TE 159	Discharged Steam	Fig.5.70	273.	-	0.64%FS
160	Fluid T.	T-24	TE 160	JP-1,2 Outlet Spool	Not Measured	273.	-	0.64%FS
161	Fluid T.	T-25	TE 161	JP-3,4 Outlet Spool	Not Measured	273.	-	0.64%FS
162	Fluid T.	T-26	TE 162	Break A Spool Piece	Not Used	273.	-	0.64%FS
163	Fluid T.	T-27	TE 163	Break B Spool Piece	Not measured	273.	-	0.64%FS
164	Fluid T.	T-28	TE 164	Feedwater	Fig.5.77	273.	-	0.64%FS
165	Fluid T.	T-29	TE 165	Break Orifice Top	Fig.5.78	273.	-	0.64%FS
166	Fluid T.	T-30	TE 166	Break Orifice Bottom	Fig.5.78	273.	-	0.64%FS
167	Fluid T.	T-31	TE 167	Break A Downst. Drag	Not Measured	273.	-	0.64%FS
168	Fluid T.	T-32	TE 168	Break B Downst. Drag	Not Measured	273.	-	0.64%FS
169	Fluid T.	T-33	TE 169	Break A Upst. of Drag	Not Measured	273.	-	0.64%FS
170	Fluid T.	T-34	TE 170	Break B Upst. of Drag	Not Measured	273.	-	0.64%FS
171	Slab T.	TS-1	TE 171	JP-1 Diffuser Wall	Fig.5.79	273.	-	0.64%FS
172	Slab T.	TS-2	TE 172	JP-2 Diffuser Wall	Fig.5.79	273.	-	0.64%FS
173	Slab T.	TS-3	TE 173	JP-3 Diffuser Wall	Fig.5.79	273.	-	0.64%FS
174	Slab T.	TS-4	TE 174	JP-4 Diffuser Wall	Fig.5.79	273.	-	0.64%FS
175	Fluid T.	T-35	TE 175	Feedwater 2	Fig.5.80	273.	-	0.64%FS
176	Fluid T.	T-36	TE 176	Discharged Steam	Fig.5.81	273.	-	0.64%FS
177	Slab T.	TS-13	TE 177	Filler Block C Pos.1	Not Measured	273.	-	0.64%FS
178	Slab T.	TS-14	TE 178	Filler Block C Pos.2	Not Measured	273.	-	0.64%FS
179	Slab T.	TS-15	TE 179	Filler Block C Pos.3	Not Measured	273.	-	0.64%FS
180	Slab T.	TS-16	TE 180	Filler Block C Pos.4	Not Measured	273.	-	0.64%FS
181	Slab T.	TS-17	TE 181	Filler Block C Pos.5	Not Measured	273.	-	0.64%FS
182	Slab T.	TS-18	TE 182	Filler Block C Pos.6	Not Measured	273.	-	0.64%FS
183	Slab T.	TS-19	TE 183	Filler Block A Pos.1	Not Measured	273.	-	0.64%FS
184	Slab T.	TS-20	TE 184	Filler Block A Pos.2	Not Measured	273.	-	0.64%FS
185	Slab T.	TS-21	TE 185	Filler Block A Pos.3	Not Measured	273.	-	0.64%FS
186	Slab T.	TS-22	TE 186	Filler Block A Pos.4	Not Measured	273.	-	0.64%FS
187	Slab T.	TS-23	TE 187	Filler Block A Pos.5	Not Measured	273.	-	0.64%FS
188	Slab T.	TS-24	TE 188	Filler Block A Pos.6	Not Measured	273.	-	0.64%FS
189	Slab T.	TS-25	TE 189	JP-1 Diffuser Wall	Not Measured	273.	-	0.64%FS
190	Slab T.	TS-26	TE 190	JP-2 Diffuser Wall	Not Measured	273.	-	0.64%FS
191	Slab T.	TS-27	TE 191	JP-3 Diffuser Wall	Not Measured	273.	-	0.64%FS
192	Slab T.	TS-28	TE 192	JP-4 Diffuser Wall	Not Measured	273.	-	0.64%FS
193	Slab T.	TS-29	TE 193	PV Wall Inside 1-1	Not Measured	273.	-	0.64%FS
194	Slab T.	TS-30	TE 194	PV Inner Surface 1-2	Not Measured	273.	-	0.64%FS
195	Slab T.	TS-31	TE 195	PV Inner Surface 1-3	Not Measured	273.	-	0.64%FS
196	Slab T.	TS-32	TE 196	PV Wall Inside 2	Not Measured	273.	-	0.64%FS
197	Slab T.	TS-33	TE 197	PV Wall Inside 3	Not Measured	273.	-	0.64%FS
198	Slab T.	TS-34	TE 198	PV Wall Inside 4	Not Measured	273.	-	0.64%FS
199	Slab T.	TS-35	TE 199	L.P. Inner Surface	Not Measured	273.	-	0.64%FS
200	Slab T.	TS-36	TE 200	L.P. Wall Inside	Not Measured	273.	-	0.64%FS

Table 3.2 Measurement List for RUN 953 (Continued)

Ch.	Item	Symbol	ID.	Location	Fig.No.	Range	Unit	Accuracy
201	Temp.	TF-	1	TE	201	A11 Fuel Rod Pos.1	Fig.5.82, 106	0.147E+04 K
202	Temp.	TF-	2	TE	202	A11 Fuel Rod Pos.2	Fig.5.82, 107	0.147E+04 K
203	Temp.	TF-	3	TE	203	A11 Fuel Rod Pos.3	Fig.5.82, 108	0.147E+04 K
204	Temp.	TF-	4	TE	204	A11 Fuel Rod Pos.4	Fig.5.82, 109	0.147E+04 K
205	Temp.	TF-	5	TE	205	A11 Fuel Rod Pos.5	Fig.5.82, 110	0.147E+04 K
206	Temp.	TF-	6	TE	206	A11 Fuel Rod Pos.6	Fig.5.82, 111	0.147E+04 K
207	Temp.	TF-	7	TE	207	A11 Fuel Rod Pos.7	Fig.5.82, 112	0.147E+04 K
208	Temp.	TF-	8	TE	208	A12 Fuel Rod Pos.1	Fig.5.83, 106	0.147E+04 K
209	Temp.	TF-	9	TE	209	A12 Fuel Rod Pos.2	Fig.5.83, 107	0.147E+04 K
210	Temp.	TF-	10	TE	210	A12 Fuel Rod Pos.3	Fig.5.83, 108	0.147E+04 K
211	Temp.	TF-	11	TE	211	A12 Fuel Rod Pos.4	Fig.5.83, 109	0.147E+04 K
212	Temp.	TF-	12	TE	212	A12 Fuel Rod Pos.5	Fig.5.83, 110	0.147E+04 K
213	Temp.	TF-	13	TE	213	A12 Fuel Rod Pos.6	Fig.5.83, 111	0.147E+04 K
214	Temp.	TF-	14	TE	214	A12 Fuel Rod Pos.7	Fig.5.83, 112	0.147E+04 K
215	Temp.	TF-	15	TE	215	A13 Fuel Rod Pos.1	Fig.5.84, 106	0.147E+04 K
216	Temp.	TF-	16	TE	216	A13 Fuel Rod Pos.2	Fig.5.84, 107	0.147E+04 K
217	Temp.	TF-	17	TE	217	A13 Fuel Rod Pos.3	Fig.5.84, 108	0.147E+04 K
218	Temp.	TF-	18	TE	218	A13 Fuel Rod Pos.4	Fig.5.84, 109	0.147E+04 K
219	Temp.	TF-	19	TE	219	A13 Fuel Rod Pos.5	Fig.5.84, 110	0.147E+04 K
220	Temp.	TF-	20	TE	220	A13 Fuel Rod Pos.6	Fig.5.84, 111	0.147E+04 K
221	Temp.	TF-	21	TE	221	A13 Fuel Rod Pos.7	Fig.5.84, 112	0.147E+04 K
222	Temp.	TF-	22	TE	222	A14 Fuel Rod Pos.1	Not Measured	0.147E+04 K
223	Temp.	TF-	23	TE	223	A14 Fuel Rod Pos.2	Not Measured	0.147E+04 K
224	Temp.	TF-	24	TE	224	A14 Fuel Rod Pos.3	Not Measured	0.147E+04 K
225	Temp.	TF-	25	TE	225	A14 Fuel Rod Pos.4	Not Measured	0.147E+04 K
226	Temp.	TF-	26	TE	226	A14 Fuel Rod Pos.5	Not Measured	0.147E+04 K
227	Temp.	TF-	27	TE	227	A14 Fuel Rod Pos.6	Not Measured	0.147E+04 K
228	Temp.	TF-	28	TE	228	A14 Fuel Rod Pos.7	Not Measured	0.147E+04 K
229	Temp.	TF-	29	TE	229	A15 Fuel Rod Pos.1	Not Measured	0.147E+04 K
230	Temp.	TF-	30	TE	230	A15 Fuel Rod Pos.4	Not Measured	0.147E+04 K
231	Temp.	TF-	31	TE	231	A17 Fuel Rod Pos.1	Not Measured	0.147E+04 K
232	Temp.	TF-	32	TE	232	A17 Fuel Rod Pos.4	Fig.5.102	0.147E+04 K
233	Temp.	TF-	33	TE	233	A22 Fuel Rod Pos.1	Fig.5.85, 113	0.147E+04 K
234	Temp.	TF-	34	TE	234	A22 Fuel Rod Pos.2	Fig.5.85, 114	0.147E+04 K
235	Temp.	TF-	35	TE	235	A22 Fuel Rod Pos.3	Fig.5.85, 115	0.147E+04 K
236	Temp.	TF-	36	TE	236	A22 Fuel Rod Pos.4	Fig.5.85, 116	0.147E+04 K
237	Temp.	TF-	37	TE	237	A22 Fuel Rod Pos.5	Fig.5.85, 117	0.147E+04 K
238	Temp.	TF-	38	TE	238	A22 Fuel Rod Pos.6	Fig.5.85, 118	0.147E+04 K
239	Temp.	TF-	39	TE	239	A22 Fuel Rod Pos.7	Fig.5.85, 119	0.147E+04 K
240	Temp.	TF-	40	TE	240	A24 Fuel Rod Pos.1	Failure	0.147E+04 K
241	Temp.	TF-	41	TE	241	A24 Fuel Rod Pos.2	Not Measured	0.147E+04 K
242	Temp.	TF-	42	TE	242	A24 Fuel Rod Pos.3	Not Measured	0.147E+04 K
243	Temp.	TF-	43	TE	243	A24 Fuel Rod Pos.4	Not Measured	0.147E+04 K
244	Temp.	TF-	44	TE	244	A24 Fuel Rod Pos.5	Not Measured	0.147E+04 K
245	Temp.	TF-	45	TE	245	A24 Fuel Rod Pos.6	Not Measured	0.147E+04 K
246	Temp.	TF-	46	TE	246	A24 Fuel Rod Pos.7	Not Measured	0.147E+04 K
247	Temp.	TF-	47	TE	247	A26 Fuel Rod Pos.1	Not Measured	0.147E+04 K
248	Temp.	TF-	48	TE	248	A26 Fuel Rod Pos.2	Not Measured	0.147E+04 K
249	Temp.	TF-	49	TE	249	A28 Fuel Rod Pos.1	Failure	0.125E+04 K
250	Temp.	TF-	50	TE	250	A28 Fuel Rod Pos.4	Fig.5.102	0.125E+04 K

Table 3.2 Measurement List for RUN 953 (Continued)

Ch.	Item	Symbol	ID.	Location	Fig. No.	Range	Unit	Accuracy
251	Temp.	TF-	51	TE 251	A31 Fuel Rod Pos.1	Failure	0.125E+04	K 0.64%FS
252	Temp.	TF-	52	TE 252	A31 Fuel Rod Pos.4	Fig. 5.102	0.125E+04	K 0.64%FS
253	Temp.	TF-	53	TE 253	A33 Fuel Rod Pos.1	Fig. 5.86	0.125E+04	K 0.64%FS
254	Temp.	TF-	54	TE 254	A33 Fuel Rod Pos.2	Fig. 5.86	0.125E+04	K 0.64%FS
255	Temp.	TF-	55	TE 255	A33 Fuel Rod Pos.3	Fig. 5.86	0.125E+04	K 0.64%FS
256	Temp.	TF-	56	TE 256	A33 Fuel Rod Pos.4	Fig. 5.86	0.125E+04	K 0.64%FS
257	Temp.	TF-	57	TE 257	A33 Fuel Rod Pos.5	Fig. 5.86	0.125E+04	K 0.64%FS
258	Temp.	TF-	58	TE 258	A33 Fuel Rod Pos.6	Fig. 5.86	0.125E+04	K 0.64%FS
259	Temp.	TF-	59	TE 259	A33 Fuel Rod Pos.7	Fig. 5.86	0.125E+04	K 0.64%FS
260	Temp.	TF-	60	TE 260	A34 Fuel Rod Pos.1	Not Measured	0.125E+04	K 0.64%FS
261	Temp.	TF-	61	TE 261	A34 Fuel Rod Pos.2	Failure	0.125E+04	K 0.64%FS
262	Temp.	TF-	62	TE 262	A34 Fuel Rod Pos.3	Not Measured	0.125E+04	K 0.64%FS
263	Temp.	TF-	63	TE 263	A34 Fuel Rod Pos.4	Not Measured	0.125E+04	K 0.64%FS
264	Temp.	TF-	64	TE 264	A34 Fuel Rod Pos.5	Not Measured	0.125E+04	K 0.64%FS
265	Temp.	TF-	65	TE 265	A34 Fuel Rod Pos.6	Not Measured	0.125E+04	K 0.64%FS
266	Temp.	TF-	66	TE 266	A34 Fuel Rod Pos.7	Not Measured	0.125E+04	K 0.64%FS
267	Temp.	TF-	67	TE 267	A37 Fuel Rod Pos.1	Not Measured	0.125E+04	K 0.64%FS
268	Temp.	TF-	68	TE 268	A37 Fuel Rod Pos.4	Not Measured	0.125E+04	K 0.64%FS
269	Temp.	TF-	69	TE 269	A42 Fuel Rod Pos.1	Not Measured	0.125E+04	K 0.64%FS
270	Temp.	TF-	70	TE 270	A42 Fuel Rod Pos.4	Failure	0.125E+04	K 0.64%FS
271	Temp.	TF-	71	TE 271	A44 Fuel Rod Pos.1	Not Measured	0.125E+04	K 0.64%FS
272	Temp.	TF-	72	TE 272	A44 Fuel Rod Pos.2	Not Measured	0.125E+04	K 0.64%FS
273	Temp.	TF-	73	TE 273	A44 Fuel Rod Pos.3	Not Measured	0.125E+04	K 0.64%FS
274	Temp.	TF-	74	TE 274	A44 Fuel Rod Pos.4	Not Measured	0.125E+04	K 0.64%FS
275	Temp.	TF-	75	TE 275	A44 Fuel Rod Pos.5	Not Measured	0.125E+04	K 0.64%FS
276	Temp.	TF-	76	TE 276	A44 Fuel Rod Pos.6	Not Measured	0.125E+04	K 0.64%FS
277	Temp.	TF-	77	TE 277	A44 Fuel Rod Pos.7	Not Measured	0.125E+04	K 0.64%FS
278	Temp.	TF-	78	TE 278	A48 Fuel Rod Pos.1	Not Measured	0.125E+04	K 0.64%FS
279	Temp.	TF-	79	TE 279	A48 Fuel Rod Pos.4	Not Measured	0.125E+04	K 0.64%FS
280	Temp.	TF-	80	TE 280	A51 Fuel Rod Pos.1	Not Measured	0.125E+04	K 0.64%FS
281	Temp.	TF-	81	TE 281	A51 Fuel Rod Pos.4	Not Measured	0.125E+04	K 0.64%FS
282	Temp.	TF-	82	TE 282	A53 Fuel Rod Pos.1	Not Measured	0.125E+04	K 0.64%FS
283	Temp.	TF-	83	TE 283	A53 Fuel Rod Pos.4	Not Measured	0.125E+04	K 0.64%FS
284	Temp.	TF-	84	TE 284	A57 Fuel Rod Pos.1	Not Measured	0.125E+04	K 0.64%FS
285	Temp.	TF-	85	TE 285	A57 Fuel Rod Pos.4	Fig. 5.102	0.125E+04	K 0.64%FS
286	Temp.	TF-	86	TE 286	A62 Fuel Rod Pos.1	Not Measured	0.125E+04	K 0.64%FS
287	Temp.	TF-	87	TE 287	A62 Fuel Rod Pos.4	Not Measured	0.125E+04	K 0.64%FS
288	Temp.	TF-	88	TE 288	A66 Fuel Rod Pos.1	Not Measured	0.125E+04	K 0.64%FS
289	Temp.	TF-	89	TE 289	A66 Fuel Rod Pos.4	Failure	0.125E+04	K 0.64%FS
290	Temp.	TF-	90	TE 290	A68 Fuel Rod Pos.1	Not Measured	0.125E+04	K 0.64%FS
291	Temp.	TF-	91	TE 291	A68 Fuel Rod Pos.4	Fig. 5.103	0.125E+04	K 0.64%FS
292	Temp.	TF-	92	TE 292	A71 Fuel Rod Pos.1	Not Measured	0.125E+04	K 0.64%FS
293	Temp.	TF-	93	TE 293	A71 Fuel Rod Pos.4	Fig. 5.103	0.125E+04	K 0.64%FS
294	Temp.	TF-	94	TE 294	A73 Fuel Rod Pos.1	Not Measured	0.125E+04	K 0.64%FS
295	Temp.	TF-	95	TE 295	A73 Fuel Rod Pos.4	Fig. 5.103	0.125E+04	K 0.64%FS
296	Temp.	TF-	96	TE 296	A75 Fuel Rod Pos.1	Not Measured	0.125E+04	K 0.64%FS
297	Temp.	TF-	97	TE 297	A75 Fuel Rod Pos.4	Not Measured	0.125E+04	K 0.64%FS
298	Temp.	TF-	98	TE 298	A77 Fuel Rod Pos.1	Fig. 5.87, 120	0.125E+04	K 0.64%FS
299	Temp.	TF-	99	TE 299	A77 Fuel Rod Pos.2	Fig. 5.87, 121	0.125E+04	K 0.64%FS
300	Temp.	TF-100	TE 300		A77 Fuel Rod Pos.3	Fig. 5.87, 122	0.125E+04	K 0.64%FS

Table 3.2 Measurement List for RUN 953 (Continued)

Ch.	Item	Symbol	ID.	Location	Fig.No.	Range	Unit	Accuracy
301	Temp.	TF-101	TE 301	A77 Fuel Rod Pos.4	Fig.5.87, 123	273.	0.125E+04 K	0.64%FS
302	Temp.	TF-102	TE 302	A77 Fuel Rod Pos.5	Fig.5.87, 124	273.	0.125E+04 K	0.64%FS
303	Temp.	TF-103	TE 303	A77 Fuel Rod Pos.6	Fig.5.87, 125	273.	0.125E+04 K	0.64%FS
304	Temp.	TF-104	TE 304	A77 Fuel Rod Pos.7	Failure	273.	0.125E+04 K	0.64%FS
305	Temp.	TF-105	TE 305	A82 Fuel Rod Pos.1	Not Measured	273.	0.125E+04 K	0.64%FS
306	Temp.	TF-106	TE 306	A82 Fuel Rod Pos.4	Failure	273.	0.125E+04 K	0.64%FS
307	Temp.	TF-107	TE 307	A84 Fuel Rod Pos.1	Fig.5.104	273.	0.125E+04 K	0.64%FS
308	Temp.	TF-108	TE 308	A84 Fuel Rod Pos.4	Fig.5.104	273.	0.125E+04 K	0.64%FS
309	Temp.	TF-109	TE 309	A85 Fuel Rod Pos.1	Not Measured	273.	0.125E+04 K	0.64%FS
310	Temp.	TF-110	TE 310	A85 Fuel Rod Pos.2	Failure	273.	0.125E+04 K	0.64%FS
311	Temp.	TF-111	TE 311	A85 Fuel Rod Pos.3	Failure	273.	0.125E+04 K	0.64%FS
312	Temp.	TF-112	TE 312	A85 Fuel Rod Pos.4	Not Measured	273.	0.125E+04 K	0.64%FS
313	Temp.	TF-113	TE 313	A85 Fuel Rod Pos.5	Not Measured	273.	0.125E+04 K	0.64%FS
314	Temp.	TF-114	TE 314	A85 Fuel Rod Pos.6	Not Measured	273.	0.125E+04 K	0.64%FS
315	Temp.	TF-115	TE 315	A85 Fuel Rod Pos.7	Not Measured	273.	0.125E+04 K	0.64%FS
316	Temp.	TF-116	TE 316	A87 Fuel Rod Pos.1	Fig.5.88, 106	273.	0.125E+04 K	0.64%FS
317	Temp.	TF-117	TE 317	A87 Fuel Rod Pos.2	Fig.5.88, 107	273.	0.125E+04 K	0.64%FS
318	Temp.	TF-118	TE 318	A87 Fuel Rod Pos.3	Fig.5.88, 108	273.	0.125E+04 K	0.64%FS
319	Temp.	TF-119	TE 319	A87 Fuel Rod Pos.4	Fig.5.88, 109	273.	0.125E+04 K	0.64%FS
320	Temp.	TF-120	TE 320	A87 Fuel Rod Pos.5	Fig.5.88, 110	273.	0.125E+04 K	0.64%FS
321	Temp.	TF-121	TE 321	A87 Fuel Rod Pos.6	Fig.5.88, 111	273.	0.125E+04 K	0.64%FS
322	Temp.	TF-122	TE 322	A87 Fuel Rod Pos.7	Fig.5.88, 112	273.	0.125E+04 K	0.64%FS
323	Temp.	TF-123	TE 323	A88 Fuel Rod Pos.1	Fig.5.89, 106	273.	0.125E+04 K	0.64%FS
324	Temp.	TF-124	TE 324	A88 Fuel Rod Pos.2	Fig.5.89, 107	273.	0.125E+04 K	0.64%FS
325	Temp.	TF-125	TE 325	A88 Fuel Rod Pos.3	Fig.5.89, 108	273.	0.125E+04 K	0.64%FS
326	Temp.	TF-126	TE 326	A88 Fuel Rod Pos.4	Fig.5.89, 109	273.	0.125E+04 K	0.64%FS
327	Temp.	TF-127	TE 327	A88 Fuel Rod Pos.5	Fig.5.89, 110	273.	0.125E+04 K	0.64%FS
328	Temp.	TF-128	TE 328	A88 Fuel Rod Pos.6	Fig.5.89, 111	273.	0.125E+04 K	0.64%FS
329	Temp.	TF-129	TE 329	A88 Fuel Rod Pos.7	Fig.5.89, 112	273.	0.125E+04 K	0.64%FS
330	Temp.	TF-130	TE 330	B11 Fuel Rod Pos.1	Fig.5.90	273.	0.125E+04 K	0.64%FS
331	Temp.	TF-131	TE 331	B11 Fuel Rod Pos.2	Fig.5.90	273.	0.125E+04 K	0.64%FS
332	Temp.	TF-132	TE 332	B11 Fuel Rod Pos.3	Fig.5.90	273.	0.125E+04 K	0.64%FS
333	Temp.	TF-133	TE 333	B11 Fuel Rod Pos.4	Fig.5.90	273.	0.125E+04 K	0.64%FS
334	Temp.	TF-134	TE 334	B11 Fuel Rod Pos.5	Fig.5.90	273.	0.125E+04 K	0.64%FS
335	Temp.	TF-135	TE 335	B11 Fuel Rod Pos.6	Fig.5.90	273.	0.125E+04 K	0.64%FS
336	Temp.	TF-136	TE 336	B11 Fuel Rod Pos.7	Failure	273.	0.125E+04 K	0.64%FS
337	Temp.	TF-137	TE 337	B13 Fuel Rod Pos.4	Fig.5.103	273.	0.125E+04 K	0.64%FS
338	Temp.	TF-138	TE 338	B22 Fuel Rod Pos.1	Fig.5.91, 113	273.	0.125E+04 K	0.64%FS
339	Temp.	TF-139	TE 339	B22 Fuel Rod Pos.2	Fig.5.91, 114	273.	0.125E+04 K	0.64%FS
340	Temp.	TF-140	TE 340	B22 Fuel Rod Pos.3	Fig.5.91, 115	273.	0.125E+04 K	0.64%FS
341	Temp.	TF-141	TE 341	B22 Fuel Rod Pos.4	Fig.5.91, 116	273.	0.125E+04 K	0.64%FS
342	Temp.	TF-142	TE 342	B22 Fuel Rod Pos.5	Fig.5.91, 117	273.	0.125E+04 K	0.64%FS
343	Temp.	TF-143	TE 343	B22 Fuel Rod Pos.6	Fig.5.91, 118	273.	0.125E+04 K	0.64%FS
344	Temp.	TF-144	TE 344	B22 Fuel Rod Pos.7	Fig.5.91, 119	273.	0.125E+04 K	0.64%FS
345	Temp.	TF-145	TE 345	B31 Fuel Rod Pos.4	Not Measured	273.	0.125E+04 K	0.64%FS
346	Temp.	TF-146	TE 346	B33 Fuel Rod Pos.4	Not Measured	273.	0.125E+04 K	0.64%FS
347	Temp.	TF-147	TE 347	B51 Fuel Rod Pos.4	Not Measured	273.	0.125E+04 K	0.64%FS
348	Temp.	TF-148	TE 348	B53 Fuel Rod Pos.4	Not Measured	273.	0.125E+04 K	0.64%FS
349	Temp.	TF-149	TE 349	B66 Fuel Rod Pos.4	Not Measured	273.	0.125E+04 K	0.64%FS
350	Temp.	TF-150	TE 350	B77 fuel Rod Pos.1	Fig.5.92, 120	273.	0.125E+04 K	0.64%FS

Table 3.2 Measurement List for RUN 953 (Continued)

Ch.	Item	Symbol	ID.	Location	Fig.No.	Range	Unit	Accuracy
351	Temp.	TF-151	TE 351	B77 Fuel Rod Pos.-2	Fig.5.92, 121	273.	-	0.64%FS
352	Temp.	TF-152	TE 352	B77 Fuel Rod Pos.3	Fig.5.92, 122	273.	-	0.64%FS
353	Temp.	TF-153	TE 353	B77 Fuel Rod Pos.4	Fig.5.92, 123	273.	-	0.64%FS
354	Temp.	TF-154	TE 354	B77 Fuel Rod Pos.5	Failure	273.	-	0.64%FS
355	Temp.	TF-155	TE 355	B77 Fuel Rod Pos.6	Fig.5.92, 125	273.	-	0.64%FS
356	Temp.	TF-156	TE 356	B77 Fuel Rod Pos.7	Fig.5.92, 126	273.	-	0.64%FS
357	Temp.	TF-157	TE 357	B86 Fuel Rod Pos.4	Failure	273.	-	0.64%FS
358	Temp.	TF-158	TE 358	C11 Fuel Rod Pos.1	Fig.5.93	273.	-	0.64%FS
359	Temp.	TF-159	TE 359	C11 Fuel Rod Pos.2	Fig.5.93	273.	-	0.64%FS
360	Temp.	TF-160	TE 360	C11 Fuel Rod Pos.3	Fig.5.93	273.	-	0.64%FS
361	Temp.	TF-161	TE 361	C11 Fuel Rod Pos.4	Fig.5.93	273.	-	0.64%FS
362	Temp.	TF-162	TE 362	C11 Fuel Rod Pos.5	Fig.5.93	273.	-	0.64%FS
363	Temp.	TF-163	TE 363	C11 Fuel Rod Pos.6	Fig.5.93	273.	-	0.64%FS
364	Temp.	TF-164	TE 364	C11 Fuel Rod Pos.7	Fig.5.93	273.	-	0.64%FS
365	Temp.	TF-165	TE 365	C13 Fuel Rod Pos.1	Fig.5.94	273.	-	0.64%FS
366	Temp.	TF-166	TE 366	C13 Fuel Rod Pos.2	Fig.5.94	273.	-	0.64%FS
367	Temp.	TF-167	TE 367	C13 Fuel Rod Pos.3	Fig.5.94	273.	-	0.64%FS
368	Temp.	TF-168	TE 368	C13 Fuel Rod Pos.4	Fig.5.94	273.	-	0.64%FS
369	Temp.	TF-169	TE 369	C13 Fuel Rod Pos.5	Fig.5.94	273.	-	0.64%FS
370	Temp.	TF-170	TE 370	C13 Fuel Rod Pos.6	Fig.5.94	273.	-	0.64%FS
371	Temp.	TF-171	TE 371	C13 Fuel Rod Pos.7	Fig.5.94	273.	-	0.64%FS
372	Temp.	TF-172	TE 372	C15 Fuel Rod Pos.4	Not Measured	273.	-	0.64%FS
373	Temp.	TF-173	TE 373	C22 Fuel Rod Pos.1	Fig.5.95, 113	273.	-	0.64%FS
374	Temp.	TF-174	TE 374	C22 Fuel Rod Pos.2	Fig.5.95, 114	273.	-	0.64%FS
375	Temp.	TF-175	TE 375	C22 Fuel Rod Pos.3	Fig.5.95, 115	273.	-	0.64%FS
376	Temp.	TF-176	TE 376	C22 Fuel Rod Pos.4	Fig.5.95, 116	273.	-	0.64%FS
377	Temp.	TF-177	TE 377	C22 Fuel Rod Pos.5	Fig.5.95, 117	273.	-	0.64%FS
378	Temp.	TF-178	TE 378	C22 Fuel Rod Pos.6	Fig.5.95, 118	273.	-	0.64%FS
379	Temp.	TF-179	TE 379	C22 Fuel Rod Pos.7	Fig.5.95, 119	273.	-	0.64%FS
380	Temp.	TF-180	TE 380	C31 Fuel Rod Pos.4	Not Measured	273.	-	0.64%FS
381	Temp.	TF-181	TE 381	C33 Fuel Rod Pos.1	Fig.5.96	273.	-	0.64%FS
382	Temp.	TF-182	TE 382	C33 Fuel Rod Pos.2	Fig.5.96	273.	-	0.64%FS
383	Temp.	TF-183	TE 383	C33 Fuel Rod Pos.3	Fig.5.96	273.	-	0.64%FS
384	Temp.	TF-184	TE 384	C33 Fuel Rod Pos.4	Fig.5.96	273.	-	0.64%FS
385	Temp.	TF-185	TE 385	C33 Fuel Rod Pos.5	Fig.5.96	273.	-	0.64%FS
386	Temp.	TF-186	TE 386	C33 Fuel Rod Pos.6	Fig.5.96	273.	-	0.64%FS
387	Temp.	TF-187	TE 387	C33 Fuel Rod Pos.7	Fig.5.96	273.	-	0.64%FS
388	Temp.	TF-188	TE 388	C35 Fuel Rod Pos.4	Not Measured	273.	-	0.64%FS
389	Temp.	TF-189	TE 389	C66 Fuel Rod Pos.4	Not Measured	273.	-	0.64%FS
390	Temp.	TF-190	TE 390	C68 Fuel Rod Pos.4	Not Measured	273.	-	0.64%FS
391	Temp.	TF-191	TE 391	C77 Fuel Rod Pos.1	Fig.5.97, 120	273.	-	0.64%FS
392	Temp.	TF-192	TE 392	C77 Fuel Rod Pos.2	Fig.5.97, 121	273.	-	0.64%FS
393	Temp.	TF-193	TE 393	C77 Fuel Rod Pos.3	Fig.5.97, 122	273.	-	0.64%FS
394	Temp.	TF-194	TE 394	C77 Fuel Rod Pos.4	Fig.5.97, 123	273.	-	0.64%FS
395	Temp.	TF-195	TE 395	C77 Fuel Rod Pos.5	Fig.5.97, 124	273.	-	0.64%FS
396	Temp.	TF-196	TE 396	C77 Fuel Rod Pos.6	Fig.5.97, 125	273.	-	0.64%FS
397	Temp.	TF-197	TE 397	C77 Fuel Rod Pos.7	Fig.5.97, 126	273.	-	0.64%FS
398	Temp.	TF-198	TE 398	D11 Fuel Rod Pos.4	Fig.5.105	273.	-	0.64%FS
399	Temp.	TF-199	TE 399	D13 Fuel Rod Pos.4	Fig.5.105	273.	-	0.64%FS
400	Temp.	TF-200	TE 400	D22 Fuel Rod Pos.1	Fig.5.98, 113	273.	-	0.64%FS

Table 3.2 Measurement List for RUN 953 (Continued)

Ch.	Item	Symbol	ID.	Location	Fig.No.	Range	Unit	Accuracy
401	Temp.	TF-201	TE 401	D22 Fuel Rod Pos.2	Fig.5.98, 114	-	0.125E+04 K	0.64%FS
402	Temp.	TF-202	TE 402	D22 Fuel Rod Pos.3	Fig.5.98,	273.	0.125E+04 K	0.64%FS
403	Temp.	TF-203	TE 403	D22 Fuel Rod Pos.4	Fig.5.98,	273.	0.125E+04 K	0.64%FS
404	Temp.	TF-204	TE 404	D22 Fuel Rod Pos.5	Fig.5.98,	273.	0.125E+04 K	0.64%FS
405	Temp.	TF-205	TE 405	D22 Fuel Rod Pos.6	Fig.5.98,	273.	0.125E+04 K	0.64%FS
406	Temp.	TF-206	TE 406	D22 Fuel Rod Pos.7	Fig.5.98,	273.	0.125E+04 K	0.64%FS
407	Temp.	TF-207	TE 407	D31 Fuel Rod Pos.4	Not Measured	273.	0.125E+04 K	0.64%FS
408	Temp.	TF-208	TE 408	D33 Fuel Rod Pos.4	Not Measured	273.	0.125E+04 K	0.64%FS
409	Temp.	TF-209	TE 409	D51 Fuel Rod Pos.4	Not Measured	273.	0.125E+04 K	0.64%FS
410	Temp.	TF-210	TE 410	D53 Fuel Rod Pos.4	Not Measured	273.	0.125E+04 K	0.64%FS
411	Temp.	TF-211	TE 411	D66 Fuel Rod Pos.4	Not Measured	273.	0.125E+04 K	0.64%FS
412	Temp.	TF-212	TE 412	D77 Fuel Rod Pos.4	Fig.5.105	273.	0.125E+04 K	0.64%FS
413	Temp.	TF-213	TE 413	D86 Fuel Rod Pos.4	Fig.5.105	273.	0.125E+04 K	0.64%FS
414	Fluid T.	TW-1	TE 414	A45 Tie Rod Pos.1	Fig.5.99	273.	0.125E+04 K	0.64%FS
415	Fluid T.	TW-2	TE 415	A45 Tie Rod Pos.2	Fig.5.99	273.	0.125E+04 K	0.64%FS
416	Fluid T.	TW-3	TE 416	A45 Tie Rod Pos.3	Fig.5.99	273.	0.125E+04 K	0.64%FS
417	Fluid T.	TW-4	TE 417	A45 Tie Rod Pos.4	Fig.5.99	273.	0.125E+04 K	0.64%FS
418	Fluid T.	TW-5	TE 418	A45 Tie Rod Pos.5	Fig.5.99	273.	0.125E+04 K	0.64%FS
419	Fluid T.	TW-6	TE 419	A45 Tie Rod Pos.6	Fig.5.99	273.	0.125E+04 K	0.64%FS
420	Fluid T.	TW-7	TE 420	A45 Tie Rod Pos.7	Fig.5.99	273.	0.125E+04 K	0.64%FS
421	Fluid T.	TW-8	TE 421	B45 Tie Rod Pos.1	Not Measured	273.	0.125E+04 K	0.64%FS
422	Fluid T.	TW-9	TE 422	B45 Tie Rod Pos.2	Not Measured	273.	0.125E+04 K	0.64%FS
423	Fluid T.	TW-10	TE 423	B45 Tie Rod Pos.3	Not Measured	273.	0.125E+04 K	0.64%FS
424	Fluid T.	TW-11	TE 424	B45 Tie Rod Pos.4	Not Measured	273.	0.125E+04 K	0.64%FS
425	Fluid T.	TW-12	TE 425	B45 Tie Rod Pos.5	Not Measured	273.	0.125E+04 K	0.64%FS
426	Fluid T.	TW-13	TE 426	B45 Tie Rod Pos.6	Not Measured	273.	0.125E+04 K	0.64%FS
427	Fluid T.	TW-14	TE 427	B45 Tie Rod Pos.7	Not Measured	273.	0.125E+04 K	0.64%FS
428	Fluid T.	TW-15	TE 428	C45 Tie Rod Pos.1	Fig.5.100	273.	0.125E+04 K	0.64%FS
429	Fluid T.	TW-16	TE 429	C45 Tie Rod Pos.2	Fig.5.100	273.	0.125E+04 K	0.64%FS
430	Fluid T.	TW-17	TE 430	C45 Tie Rod Pos.3	Fig.5.100	273.	0.125E+04 K	0.64%FS
431	Fluid T.	TW-18	TE 431	C45 Tie Rod Pos.4	Fig.5.100	273.	0.125E+04 K	0.64%FS
432	Fluid T.	TW-19	TE 432	C45 Tie Rod Pos.5	Fig.5.100	273.	0.125E+04 K	0.64%FS
433	Fluid T.	TW-20	TE 433	C45 Tie Rod Pos.6	Fig.5.100	273.	0.125E+04 K	0.64%FS
434	Fluid T.	TW-21	TE 434	C45 Tie Rod Pos.7	Fig.5.100	273.	0.125E+04 K	0.64%FS
435	Fluid T.	TW-22	TE 435	D45 Tie Rod Pos.1	Not Measured	273.	0.125E+04 K	0.64%FS
436	Fluid T.	TW-23	TE 436	D45 Tie Rod Pos.2	Not Measured	273.	0.125E+04 K	0.64%FS
437	Fluid T.	TW-24	TE 437	D45 Tie Rod Pos.3	Not Measured	273.	0.125E+04 K	0.64%FS
438	Fluid T.	TW-25	TE 438	D45 Tie Rod Pos.4	Not Measured	273.	0.125E+04 K	0.64%FS
439	Fluid T.	TW-26	TE 439	D45 Tie Rod Pos.5	Not Measured	273.	0.125E+04 K	0.64%FS
440	Fluid T.	TW-27	TE 440	D45 Tie Rod Pos.6	Not Measured	273.	0.125E+04 K	0.64%FS
441	Fluid T.	TW-28	TE 441	D45 Tie Rod Pos.7	Not Measured	273.	0.125E+04 K	0.64%FS
442	Fluid T.	TC-1	TE 442	Channel Box A Inlet	Fig.5.127	273.	0.125E+04 K	0.64%FS
443	Fluid T.	TC-2	TE 443	Channel Box B Inlet	Fig.5.127	273.	0.125E+04 K	0.64%FS
444	Fluid T.	TC-3	TE 444	Channel Box C Inlet	Fig.5.127	273.	0.125E+04 K	0.64%FS
445	Fluid T.	TC-4	TE 445	Channel Box D Inlet	Fig.5.127	273.	0.125E+04 K	0.64%FS
446	Fluid T.	TC-5	TE 446	Channel Box Outlet A-1	Fig.5.128	273.	0.125E+04 K	0.64%FS
447	Fluid T.	TC-6	TE 447	Channel Box Outlet A-2	Fig.5.128	273.	0.125E+04 K	0.64%FS
448	Fluid T.	TC-7	TE 448	Channel Box Outlet A-3	Fig.5.128	273.	0.125E+04 K	0.64%FS
449	Fluid T.	TC-8	TE 449	Channel Box Outlet A-4	Fig.5.128	273.	0.125E+04 K	0.64%FS
450	Fluid T.	TC-9	TE 450	Channel Box Outlet A-5	Fig.5.128	273.	0.125E+04 K	0.64%FS

Table 3.2 Measurement List for RUN 953 (Continued)

Ch.	Item	Symbol	ID.	Location	Fig. No.	Range	Unit	Accuracy
451	Fluid T.	TC-10	TE	451	Channel Box Outlet C-1	273.	-	0.64%FS
452	Fluid T.	TC-11	TE	452	Channel Box Outlet C-2	273.	-	0.64%FS
453	Fluid T.	TC-12	TE	453	Channel Box Outlet C-3	273.	-	0.64%FS
454	Fluid T.	TC-13	TE	454	Channel Box Outlet C-4	273.	-	0.64%FS
455	Fluid T.	TC-14	TE	455	Channel Box Outlet C-6	273.	-	0.64%FS
456	Fluid T.	TG-1	TE	456	Upper Tieplate A Up-1	Fig.5.130, 134	-	0.64%FS
457	Fluid T.	TG-2	TE	457	Upper Tieplate A Up-2	Not Measured	273.	0.64%FS
458	Fluid T.	TG-3	TE	458	Upper Tieplate A Up-3	Not Measured	273.	0.64%FS
459	Fluid T.	TG-4	TE	459	Upper Tieplate A Up-4	Fig.5.130, 135	-	0.64%FS
460	Fluid T.	TG-5	TE	460	Upper Tieplate A Up-5	Not Measured	273.	0.64%FS
461	Fluid T.	TG-6	TE	461	Upper Tieplate A Up-6	Not Measured	273.	0.64%FS
462	Fluid T.	TG-7	TE	462	Upper Tieplate A Up-7	Not Measured	273.	0.64%FS
463	Fluid T.	TG-8	TE	463	Upper Tieplate A Up-8	Not Measured	273.	0.64%FS
464	Fluid T.	TG-9	TE	464	Upper Tieplate A Up-9	Not Measured	273.	0.64%FS
465	Fluid T.	TG-10	TE	465	Upper Tieplate A Up-10	Fig.5.131, 136	-	0.64%FS
466	Fluid T.	TG-11	TE	466	Upper Tieplate A Lo-1	Fig.5.132, 134	-	0.64%FS
467	Fluid T.	TG-12	TE	467	Upper Tieplate A Lo-2	Not Measured	273.	0.64%FS
468	Fluid T.	TG-13	TE	468	Upper Tieplate A Lo-3	Not Measured	273.	0.64%FS
469	Fluid T.	TG-14	TE	469	Upper Tieplate A Lo-4	Fig.5.132, 135	-	0.64%FS
470	Fluid T.	TG-15	TE	470	Upper Tieplate A Lo-5	Not Measured	273.	0.64%FS
471	Fluid T.	TG-16	TE	471	Upper Tieplate A Lo-6	Not Measured	273.	0.64%FS
472	Fluid T.	TG-17	TE	472	Upper Tieplate A Lo-7	Not Measured	273.	0.64%FS
473	Fluid T.	TG-18	TE	473	Upper Tieplate A Lo-8	Not Measured	273.	0.64%FS
474	Fluid T.	TG-19	TE	474	Upper Tieplate A Lo-9	Not Measured	273.	0.64%FS
475	Fluid T.	TG-20	TE	475	Upper Tieplate A Lo-10	Fig.5.133, 136	-	0.64%FS
476	Fluid T.	TG-21	TE	476	Upper Tieplate C Up-1	Fig.5.137, 141	-	0.64%FS
477	Fluid T.	TG-22	TE	477	Upper Tieplate C Up-2	Not Measured	273.	0.64%FS
478	Fluid T.	TG-23	TE	478	Upper Tieplate C Up-3	Not Measured	273.	0.64%FS
479	Fluid T.	TG-24	TE	479	Upper Tieplate C Up-4	Fig.5.137, 142	-	0.64%FS
480	Fluid T.	TG-25	TE	480	Upper Tieplate C Up-5	Not Measured	273.	0.64%FS
481	Fluid T.	TG-26	TE	481	Upper Tieplate C Up-6	Not Measured	273.	0.64%FS
482	Fluid T.	TG-27	TE	482	Upper Tieplate C Up-7	Not Measured	273.	0.64%FS
483	Fluid T.	TG-28	TE	483	Upper Tieplate C Up-8	Not Measured	273.	0.64%FS
484	Fluid T.	TG-29	TE	484	Upper Tieplate C Up-9	Not Measured	273.	0.64%FS
485	Fluid T.	TG-30	TE	485	Upper Tieplate C Up-10	Fig.5.138, 143	-	0.64%FS
486	Fluid T.	TG-31	TE	486	Upper Tieplate C Lo-1	Fig.5.139, 141	-	0.64%FS
487	Fluid T.	TG-32	TE	487	Upper Tieplate C Lo-2	Not Measured	273.	0.64%FS
488	Fluid T.	TG-33	TE	488	Upper Tieplate C Lo-3	Not Measured	273.	0.64%FS
489	Fluid T.	TG-34	TE	489	Upper Tieplate C Lo-4	Fig.5.139, 142	-	0.64%FS
490	Fluid T.	TG-35	TE	490	Upper Tieplate C Lo-5	Not Measured	273.	0.64%FS
491	Fluid T.	TG-36	TE	491	Upper Tieplate C Lo-6	Not Measured	273.	0.64%FS
492	Fluid T.	TG-37	TE	492	Upper Tieplate C Lo-7	Not Measured	273.	0.64%FS
493	Fluid T.	TG-38	TE	493	Upper Tieplate C Lo-8	Not Measured	273.	0.64%FS
494	Fluid T.	TG-39	TE	494	Upper Tieplate C Lo-9	Not Measured	273.	0.64%FS
495	Fluid T.	TG-40	TE	495	Upper Tieplate C Lo-10	Fig.5.140, 143	-	0.64%FS
496	Slab T.	TB-1	TE	496	C.B. A1 Inner Pos-1	Not Measured	273.	0.64%FS
497	Slab T.	TB-2	TE	497	C.B. A1 Inner Pos-2	Not Measured	273.	0.64%FS
498	Slab T.	TB-3	TE	498	C.B. A1 Inner Pos-3	Not Measured	273.	0.64%FS
499	Slab T.	TB-4	TE	499	C.B. A1 Inner Pos-4	Not Measured	273.	0.64%FS
500	Slab T.	TB-5	TE	500	C.B. A1 Inner Pos-5	Not Measured	273.	0.64%FS

Table 3.2 Measurement List for RUN 953 (Continued)

Ch.	Item	Symbol	ID.	Location	Fig.No.	Range	Unit	Accuracy
501	Slab T.	TB-6	TE 501	C.B. A1 Inner ,Pos.6	Not Measured	273.	-	0.64%FS
502	Slab T.	TB-7	TE 502	C.B. A1 Inner ,Pos.7	Not Measured	273.	-	0.64%FS
503	Slab T.	TB-8	TE 503	C.B. A2 Inner ,Pos.1	Not Measured	273.	-	0.64%FS
504	Slab T.	TB-9	TE 504	C.B. A2 Inner ,Pos.2	Not Measured	273.	-	0.64%FS
505	Slab T.	TB-10	TE 505	C.B. A2 Inner ,Pos.3	Not Measured	273.	-	0.64%FS
506	Slab T.	TB-11	TE 506	C.B. A2 Inner ,Pos.4	Not Measured	273.	-	0.64%FS
507	Slab T.	TB-12	TE 507	C.B. A2 Inner ,Pos.5	Not Measured	273.	-	0.64%FS
508	Slab T.	TB-13	TE 508	C.B. A2 Inner ,Pos.6	Not Measured	273.	-	0.64%FS
509	Slab T.	TB-14	TE 509	C.B. A2 Inner ,Pos.7	Not Measured	273.	-	0.64%FS
510	Slab T.	TB-15	TE 510	C.B. B Inner ,Pos.1	Not Measured	273.	-	0.64%FS
511	Slab T.	TB-16	TE 511	C.B. B Inner ,Pos.2	Not Measured	273.	-	0.64%FS
512	Slab T.	TB-17	TE 512	C.B. B Inner ,Pos.3	Not Measured	273.	-	0.64%FS
513	Slab T.	TB-18	TE 513	C.B. B Inner ,Pos.4	Not Measured	273.	-	0.64%FS
514	Slab T.	TB-19	TE 514	C.B. B Inner ,Pos.5	Not Measured	273.	-	0.64%FS
515	Slab T.	TB-20	TE 515	C.B. B Inner ,Pos.6	Not Measured	273.	-	0.64%FS
516	Slab T.	TB-21	TE 516	C.B. B Inner ,Pos.7	Not Measured	273.	-	0.64%FS
517	Slab T.	TB-22	TE 517	C.B. C Inner ,Pos.1	Not Measured	273.	-	0.64%FS
518	Slab T.	TB-23	TE 518	C.B. C Inner ,Pos.2	Not Measured	273.	-	0.64%FS
519	Slab T.	TB-24	TE 519	C.B. C Inner ,Pos.3	Not Measured	273.	-	0.64%FS
520	Slab T.	TB-25	TE 520	C.B. C Inner ,Pos.4	Not Measured	273.	-	0.64%FS
521	Slab T.	TB-26	TE 521	C.B. C Inner ,Pos.5	Not Measured	273.	-	0.64%FS
522	Slab T.	TB-27	TE 522	C.B. C Inner ,Pos.6	Not Measured	273.	-	0.64%FS
523	Slab T.	TB-28	TE 523	C.B. C Inner ,Pos.7	Not Measured	273.	-	0.64%FS
524	Slab T.	TB-29	TE 524	C.B. D Inner ,Pos.1	Not Measured	273.	-	0.64%FS
525	Slab T.	TB-30	TE 525	C.B. D Inner ,Pos.2	Not Measured	273.	-	0.64%FS
526	Slab T.	TB-31	TE 526	C.B. D Inner ,Pos.3	Not Measured	273.	-	0.64%FS
527	Slab T.	TB-32	TE 527	C.B. D Inner ,Pos.4	Not Measured	273.	-	0.64%FS
528	Slab T.	TB-33	TE 528	C.B. D Inner ,Pos.5	Not Measured	273.	-	0.64%FS
529	Slab T.	TB-34	TE 529	C.B. D Inner ,Pos.6	Not Measured	273.	-	0.64%FS
530	Slab T.	TB-35	TE 530	C.B. D Inner ,Pos.7	Not Measured	273.	-	0.64%FS
531	Slab T.	TB-36	TE 531	C.B. A Outer ,Pos.1	Fig. 5.101,144	273.	-	0.64%FS
532	Slab T.	TB-37	TE 532	C.B. A Outer ,Pos.2	Fig. 5.101,144	273.	-	0.64%FS
533	Slab T.	TB-38	TE 533	C.B. A Outer ,Pos.3	Fig. 5.101,144	273.	-	0.64%FS
534	Slab T.	TB-39	TE 534	C.B. A Outer ,Pos.4	Fig. 5.101,144	273.	-	0.64%FS
535	Slab T.	TB-40	TE 535	C.B. A Outer ,Pos.5	Fig. 5.101,144	273.	-	0.64%FS
536	Slab T.	TB-41	TE 536	C.B. A Outer ,Pos.6	Fig. 5.101,144	273.	-	0.64%FS
537	Slab T.	TB-42	TE 537	C.B. A Outer ,Pos.7	Fig. 5.101,144	273.	-	0.64%FS
538	Slab T.	TB-43	TE 538	C.B. C Outer ,Pos.1	Not Measured	273.	-	0.64%FS
539	Slab T.	TB-44	TE 539	C.B. C Outer ,Pos.2	Not Measured	273.	-	0.64%FS
540	Slab T.	TB-45	TE 540	C.B. C Outer ,Pos.3	Not Measured	273.	-	0.64%FS
541	Slab T.	TB-46	TE 541	C.B. C Outer ,Pos.4	Not Measured	273.	-	0.64%FS
542	Slab T.	TB-47	TE 542	C.B. C Outer ,Pos.5	Not Measured	273.	-	0.64%FS
543	Slab T.	TB-48	TE 543	C.B. C Outer ,Pos.6	Not Measured	273.	-	0.64%FS
544	Slab T.	TB-49	TE 544	C.B. C Outer ,Pos.7	Not Measured	273.	-	0.64%FS
545	Fluid T.	TP-1	TE 545	Lower PL. Center 1	Not Measured	273.	-	0.64%FS
546	Fluid T.	TP-2	TE 546	Lower PL. Center 2	Not Measured	273.	-	0.64%FS
547	Fluid T.	TP-3	TE 547	Lower PL. Center 3	Not Measured	273.	-	0.64%FS
548	Fluid T.	TP-4	TE 548	Lower PL. Center 4	Not Measured	273.	-	0.64%FS
549	Fluid T.	TP-5	TE 549	Lower PL. Center 5	Not Measured	273.	-	0.64%FS
550	Fluid T.	TP-6	TE 550	Lower PL. Center 7	Fig. 5.145	273.	-	0.64%FS

Table 3.2 Measurement List for RUN 953 (Continued)

Ch.	Item	Symbol	ID.	Location	Fig. No.	Range	Unit	Accuracy
551	Slab T.	TP-	7	TE	551	Lower Pl.- North	1	Not Measured
552	Slab T.	TP-	8	TE	552	Lower Pl.- North	2	Not Measured
553	Slab T.	TP-	9	TE	553	Lower Pl.- North	4	Not Measured
554	Slab T.	TP-	10	TE	554	Lower Pl.- North	6	Not Measured
555	Slab T.	TP-	11	TE	555	Lower Pl.- South	1	Not Measured
556	Slab T.	TP-	12	TE	556	Lower Pl.- South	2	Not Measured
557	Slab T.	TP-	13	TE	557	Lower Pl.- South	4	Not Measured
558	Slab T.	TP-	14	TE	558	Lower Pl.- South	6	Not Measured
559	Level	LB-	1	LM	559	C.B.Liquid Level	A1-1	Not Measured
560	Level	LB-	2	LM	560	C.B.Liquid Level	A1-2	Not Measured
561	Level	LB-	3	LM	561	C.B.Liquid Level	A1-3	Not Measured
562	Level	LB-	4	LM	562	C.B.Liquid Level	A1-4	Failure
563	Level	LB-	5	LM	563	C.B.Liquid Level	A1-5	Not Measured
564	Level	LB-	6	LM	564	C.B.Liquid Level	A1-6	Not Measured
565	Level	LB-	7	LM	565	C.B.Liquid Level	A1-7	Not Measured
566	Level	LB-	8	LM	566	C.B.Liquid Level	A2-1	Fig.5.146
567	Level	LB-	9	LM	567	C.B.Liquid Level	A2-2	Fig.5.146
568	Level	LB-	10	LM	568	C.B.Liquid Level	A2-3	Fig.5.146
569	Level	LB-	11	LM	569	C.B.Liquia Level	A2-4	Fig.5.146
570	Level	LB-	12	LM	570	C.B.Liquid Level	A2-5	Failure
571	Level	LB-	13	LM	571	C.B.Liquid Level	A2-6	Fig.5.146
572	Level	LB-	14	LM	572	C.B.Liquid Level	A2-7	Fig.5.146
573	Level	LB-	15	LM	573	C.B.Liquid Level	B-1	Fig.5.147
574	Level	LB-	16	LM	574	C.B.Liquid Level	B-2	Fig.5.147
575	Level	LB-	17	LM	575	C.B.Liquid Level	B-3	Fig.5.147
576	Level	LB-	18	LM	576	C.B.Liquid Level	B-4	Fig.5.147
577	Level	LB-	19	LM	577	C.B.Liquid Level	B-5	Fig.5.147
578	Level	LB-	20	LM	578	C.B.Liquid Level	B-6	Fig.5.147
579	Level	LB-	21	LM	579	C.B.Liquid Level	B-7	Fig.5.147
580	Level	LB-	22	LM	580	C.B.Liquid Level	C-1	Fig.5.148
581	Level	LB-	23	LM	581	C.B.Liquid Level	C-2	Fig.5.148
582	Level	LB-	24	LM	582	C.B.Liquid Level	C-3	Fig.5.148
583	Level	LB-	25	LM	583	C.B.Liquid Level	C-4	Fig.5.148
584	Level	LB-	26	LM	584	C.B.Liquid Level	C-5	Fig.5.148
585	Level	LB-	27	LM	585	C.B.Liquid Level	C-6	Fig.5.148
586	Level	LB-	28	LM	586	C.B.Liquid Level	C-7	Fig.5.148
587	Level	LB-	29	LM	587	C.B.Liquid Level	D-1	Not Measured
588	Level	LB-	30	LM	588	C.B.Liquid Level	D-2	Not Measured
589	Level	LB-	31	LM	589	C.B.Liquid Level	D-3	Not Measured
590	Level	LB-	32	LM	590	C.B.Liquid Level	D-4	Not Measured
591	Level	LB-	33	LM	591	C.B.Liquid Level	D-5	Failure
592	Level	LB-	34	LM	592	C.B.Liquid Level	D-6	Not Measured
593	Level	LB-	35	LM	593	C.B.Liquid Level	D-7	Not Measured
594	Level	LL-	1	LM	594	Ch.Box Outlet	A1-5	Failure
595	Level	LL-	2	LM	595	Ch.Box Outlet	A1-6	Failure
596	Level	LL-	3	LM	596	Ch.Box Outlet	A1-7	Fig.5.177
597	Level	LL-	4	LM	597	Ch.Box Outlet	A2-5	Fig.5.149
598	Level	LL-	5	LM	598	Ch.Box Outlet	A2-6	Fig.5.149
599	Level	LL-	6	LM	599	Ch.Box Outlet	A2-7	Failure
600	Level	LL-	7	LM	600	Ch.Box Outlet	A-1	Failure

Table 3.2 Measurement List for RUN 953 (Continued)

Ch.	Item	Symbol	ID.	Location	Fig. No.	Range	Unit	Accuracy
601	Level	LL-	8 LM	601 Ch.Box Outlet A-2	Failure			
602	Level	LL-	9 LM	602 Ch.Box Outlet A-3	Fig.5.150			
603	Level	LL-	10 LM	603 Ch.Box Outlet A-4	Fig.5.150			
604	Level	LL-	11 LM	604 Ch.Box Outlet A-6	Fig.5.150			
605	Level	LL-	12 LM	605 Ch.Box Outlet C1-S	Fig.5.151			
606	Level	LL-	13 LM	606 Ch.Box Outlet C1-6	Fig.5.151			
607	Level	LL-	14 LM	607 Ch.Box Outlet C1-7	Fig.5.151			
608	Level	LL-	15 LM	608 Ch.Box Outlet C2-5	Not Measured			
609	Level	LL-	16 LM	609 Ch.Box Outlet C2-6	Not Measured			
610	Level	LL-	17 LM	610 Ch.Box Outlet C2-7	Not Measured			
611	Level	LL-	18 LM	611 Ch.Box Outlet C-1	Fig.5.152			
612	Level	LL-	19 LM	612 Ch.Box Outlet C-2	Fig.5.152			
613	Level	LL-	20 LM	613 Ch.Box Outlet C-3	Fig.5.152			
614	Level	LL-	21 LM	614 Ch.Box Outlet C-4	Fig.5.152			
615	Level	LL-	22 LM	615 Ch.Box Outlet C-6	Fig.5.152			
616	Level	LL-	23 LM	616 Ch.Box Inlet A-1	Fig.5.153			
617	Level	LL-	24 LM	617 Ch.Box Inlet A-2	Fig.5.153			
618	Level	LL-	25 LM	618 Ch.Box Inlet B-1	Not Measured			
619	Level	LL-	26 LM	619 Ch.Box Inlet B-2	Not Measured			
620	Level	LL-	27 LM	620 Ch.Box Inlet C-1	Fig.5.154			
621	Level	LL-	28 LM	621 Ch.Box Inlet C-2	Fig.5.154			
622	Level	LL-	29 LM	622 Ch.Box Inlet D-1	Not Measured			
623	Level	LL-	30 LM	623 Ch.Box Inlet D-2	Fig.5.155			
624	Level	LL-	31 LM	624 Lower PL North 1	Fig.5.155			
625	Level	LL-	32 LM	625 Lower PL North 2	Fig.5.155			
626	Level	LL-	33 LM	626 Lower PL North 3	Fig.5.155			
627	Level	LL-	34 LM	627 Lower PL North 4	Fig.5.155			
628	Level	LL-	35 LM	628 Lower PL North 5	Fig.5.155			
629	Level	LL-	36 LM	629 Lower PL North 6	Fig.5.155			
630	Level	LL-	37 LM	630 Lower PL South 1	Not Measured			
631	Level	LL-	38 LM	631 Lower PL South 2	Not Measured			
632	Level	LL-	39 LM	632 Lower PL South 3	Not Measured			
633	Level	LL-	40 LM	633 Lower PL South 4	Not Measured			
634	Level	LL-	41 LM	634 Lower PL South 5	Not Measured			
635	Level	LL-	42 LM	635 Lower PL South 6	Not Measured			
636	Level	LL-	43 LM	636 Guide Tube North 0	Fig.5.156			
637	Level	LL-	44 LM	637 Guide Tube North 1	Fig.5.156			
638	Level	LL-	45 LM	638 Guide Tube North 3	Fig.5.156			
639	Level	LL-	46 LM	639 Guide Tube North 6	Fig.5.156			
640	Level	LL-	47 LM	640 Guide Tube South 0	Not Measured			
641	Level	LL-	48 LM	641 Guide Tube South 1	Not Measured			
642	Level	LL-	49 LM	642 Guide Tube South 3	Not Measured			
643	Level	LL-	50 LM	643 Guide Tube South 6	Not Measured			
644	Level	L-	1 LM	644 Downcomer D-Side 1	Fig.5.157			
645	Level	L-	2 LM	645 Downcomer D-Side 2	Fig.5.157			
646	Level	L-	3 LM	646 Downcomer D-Side 3	Fig.5.157			
647	Level	L-	4 LM	647 Downcomer D-Side 4	Fig.5.157			
648	Level	L-	5 LM	648 Downcomer D-Side 5	Fig.5.157			
649	Level	L-	6 LM	649 Downcomer B-Side 1	Not Measured			
650	Level	L-	7 LM	650 Downcomer B-Side 2	Not Measured			

Table 3-2 Measurement List for RUN 953 (Continued)

Ch.	Item	Symbol	ID.	Location	Fig.No.	Range	Unit	Accuracy
651	Level	L-	8	LM	651	Downcomer	B-Side	3
652	Level	L-	9	LM	652	Downcomer	B-Side	4
653	Level	L-	10	LM	653	Downcomer	B-Side	5
654	Void	VF-	1	VD	654	A54 Tie Rod Pos.1	Not Measured	0.0
655	Void	VF-	2	VD	655	A54 Tie Rod Pos.2	Not Measured	0.0
656	Void	VF-	3	VD	656	A54 Tie Rod Pos.3	Not Measured	0.0
657	Void	VF-	4	VD	657	A54 Tie Rod Pos.4	Not Measured	0.0
658	Void	VF-	5	VD	658	A54 Tie Rod Pos.5	Not Measured	0.0
659	Void	VF-	6	VD	659	A54 Tie Rod Pos.6	Not Measured	0.0
660	Void	VF-	7	VD	660	A54 Tie Rod Pos.7	Not Measured	0.0
661	Void	VF-	8	VD	661	B54 Tie Rod Pos.1	Not Measured	0.0
662	Void	VF-	9	VD	662	B54 Tie Rod Pos.2	Not Measured	0.0
663	Void	VF-	10	VD	663	B54 Tie Rod Pos.3	Not Measured	0.0
664	Void	VF-	11	VD	664	B54 Tie Rod Pos.4	Not Measured	0.0
665	Void	VF-	12	VD	665	B54 Tie Rod Pos.5	Not Measured	0.0
666	Void	VF-	13	VD	666	B54 Tie Rod Pos.6	Not Measured	0.0
667	Void	VF-	14	VD	667	B54 Tie Rod Pos.7	Not Measured	0.0
668	Void	VF-	15	VD	668	C54 Tie Rod Pos.1	Not Measured	0.0
669	Void	VF-	16	VD	669	C54 Tie Rod Pos.2	Not Measured	0.0
670	Void	VF-	17	VD	670	C54 Tie Rod Pos.3	Not Measured	0.0
671	Void	VF-	18	VD	671	C54 Tie Rod Pos.4	Not Measured	0.0
672	Void	VF-	19	VD	672	C54 Tie Rod Pos.5	Not Measured	0.0
673	Void	VF-	20	VD	673	C54 Tie Rod Pos.6	Not Measured	0.0
674	Void	VF-	21	VD	674	C54 Tie Rod Pos.7	Not Measured	0.0
675	Void	VF-	22	VD	675	D54 Tie Rod Pos.7	Not Measured	0.0
676	Void	VF-	23	VD	676	D54 Tie Rod Pos.7	Not Measured	0.0
677	Void	VF-	24	VD	677	D54 Tie Rod Pos.7	Not Measured	0.0
678	Void	VF-	25	VD	678	D54 Tie Rod Pos.7	Not Measured	0.0
679	Void	VF-	26	VD	679	D54 Tie Rod Pos.7	Not Measured	0.0
680	Void	VF-	27	VD	680	D54 Tie Rod Pos.7	Not Measured	0.0
681	Void	VF-	28	VD	681	D54 Tie Rod Pos.7	Not Measured	0.0
682	Void	VE-	1	VD	682	Channel A Outlet 1	Not Measured	0.0
683	Void	VE-	2	VD	683	Channel A Outlet 2	Not Measured	0.0
684	Void	VE-	3	VD	684	Channel A Outlet 3	Not Measured	0.0
685	Void	VE-	4	VD	685	Channel B Outlet 1	Not Measured	0.0
686	Void	VE-	5	VD	686	Channel B Outlet 2	Not Measured	0.0
687	Void	VE-	6	VD	687	Channel B Outlet 3	Not Measured	0.0
688	Void	VE-	7	VD	688	Channel C Outlet 1	Not Measured	0.0
689	Void	VE-	8	VD	689	Channel C Outlet 2	Not Measured	0.0
690	Void	VE-	9	VD	690	Channel C Outlet 3	Not Measured	0.0
691	Void	VE-	10	VD	691	Channel D Outlet 1	Not Measured	0.0
692	Void	VE-	11	VD	692	Channel D Outlet 2	Not Measured	0.0
693	Void	VE-	12	VD	693	Channel D Outlet 3	Not Measured	0.0
694	Void	VE-	13	VD	694	Lower Plenum Bottom 1	Not Measured	0.0
695	Void	VE-	14	VD	695	Lower Plenum Bottom 2	Not Measured	0.0
696	Void	VE-	15	VD	696	Lower Plenum Bottom 3	Not Measured	0.0
697	Void	VP-	1	VD	697	Lower Plenum Inlet	Not Measured	0.0
698	Void	VP-	2	VD	698	Lower Plenum Inlet	Not Measured	0.0

Table 3.3 Core Instrumentation Map

Item	Pos. DL	Core Outlet	Pos.1	Pos.2	Pos.3	Pos.4	Pos.5	Pos.6	Pos.7	Core Inlet
			Rod NO.	3660	3417	3114.5	2879.5	2527	2174.5	1939.5
Surface Temp.	A11		TF 1	TF 2	TF 3	TF 4	TF 5	TF 6	TF 7	
	A12		TF 8	TF 9	TF 10	TF 11	TF 12	TF 13	TF 14	
	A13		TF 15	TF 16	TF 17	TF 18	TF 19	TF 20	TF 21	
	A14		TF 22	TF 23	TF 24	TF 25	TF 26	TF 27	TF 28	
	A15		TF 29			TF 30				
	A17		TF 31			TF 32				
	A22		TF 33	TF 34	TF 35	TF 36	TF 37	TF 38	TF 39	
	A23		TF 40	TF 41	TF 42	TF 43	TF 44	TF 45	TF 46	
	A24		TF 47	TF 48	TF 49	TF 50	TF 51	TF 52	TF 53	
	A26		TF 54			TF 55				
	A28		TF 56			TF 57				
	A31		TF 58			TF 59				
	A33		TF 60	TF 61	TF 62	TF 63	TF 64	TF 65	TF 66	
	A34		TF 67	TF 68	TF 69	TF 70	TF 71	TF 72	TF 73	
	A35		TF 74			TF 75				
Fluid Temp.	A37		TF 76			TF 77				
	A42		TF 78			TF 79				
	A44	TC 1	TF180	TF181	TF182	TF183	TF184	TF185	TF186	TC 2
	A45		TF 80			TF 81				
	A46		TF 82			TF 83				
	A48		TF 84			TF 85				
	A51		TF 86			TF 87				
	A53		TF 88			TF 89				
	A54		TF 90							
	A57		TF 91			TF 92				
	A62		TF 93			TF 94				
	A64		TF 95			TF 96				
	A66		TF 97			TF 98				
	A68		TF 99			TF100				
	A71		TF101			TF102				
	A73		TF103			TF104				
	A75		TF105			TF106				
	A77		TF107			TF108				

Table 3.3 Core Instrumentation Map (Continued)

Item	Pos. Rod NO.	Core Outlet	Pos.1	Pos.2	Pos.3	Pos.4	Pos.5	Pos.6	Pos.7	Core Inlet
			3660	3417	3114.5	2879.5	2527	2174.5	1939.5	1637
Surface Temp.	A82		TF109			TF110				
	A84		TF111			TF112				
	A86		TF113			TF114				
	A88		TF115			TF116				
	B11					TF117				
	B13					TF118				
	B15		TF119	TF120	TF121	TF122	TF123	TF124	TF125	
	B31					TF126				
	B33					TF127				
	B35					TF128				
Fluid Temp.	B44	TC 3	TF187	TF188	TF189	TF190	TF191	TF192	TF193	TC 4
Surface Temp.	B51					TF129				
	B53					TF130				
	B85		TF131	TF132	TF133	TF134	TF135	TF136	TF137	
	C11					TF138				
	C13					TF139				
	C15					TF140				
	C31					TF141				
	C33		TF142	TF143	TF144	TF145	TF146	TF147	TF148	
	C35					TF149				
Fluid Temp.	C44	TC 5	TF194	TF195	TF196	TF197	TF198	TF199	TF200	TC 6
Surface Temp.	C51					TF150				
	C53					TF151				
	C77		TF152	TF153	TF154	TF155	TF156	TF157	TF158	
	D11					TF159				
	D13					TF160				
	D27		TF161	TF162	TF163	TF164	TF165	TF166	TF167	
	D31					TF168				
	D33					TF169				
	D35					TF170				
Fluid Temp.	D44	TC 7	TF201	TF202	TF203	TF204	TF205	TF206	TF207	TC 8
Surface Temp.	D51					TF171				
	D53					TF172				
	D88		TF173	TF174	TF175	TF176	TF177	TF178	TF179	

Table 3.3 Core Instrumentation Map (Continued)

Item	Pos. Rod NO.	Core Outlet DL	Pos.1	Pos.2	Pos.3	Pos.4	Pos.5	Pos.6	Pos.7	Core Inlet
			3660	3417	3114.5	2879.5	2527	2174.5	1939.5	1454
Void	A55		VF 1	VF 2	VF 3	VF 4	VF 5	VF 6	VF 7	
	B55		VF 8	VF 9	VF 10	VF 11	VF 12	VF 13	VF 14	
	C55		VF 15	VF 16	VF 17	VF 18	VF 19	VF 20	VF 21	
	D55		VF 22	VF 23	VF 24	VF 25	VF 26	VF 27	VF 28	
Channel Box Surface Temp.	A1*		TB 1	TB 2	TB 3	TB 4	TB 5	TB 6	TB 7	
	A2*		TB 8	TB 9	TB 10	TB 11	TB 12	TB 13	TB 14	
	B*		TB 15	TB 16	TB 17	TB 18	TB 19	TB 20	TB 21	
	C*		TB 22	TB 23	TB 24	TB 25	TB 26	TB 27	TB 28	
	D*		TB 29	TB 30	TB 31	TB 32	TB 33	TB 34	TB 35	
Liquid Level in the Channel Box	A1*		LB 1	LB 2	LB 3	LB 4	LB 5	LB 6	LB 7	
	A2*		LB 8	LB 9	LB 10	LB 11	LB 12	LB 13	LB 14	
	B*		LB 15	LB 16	LB 17	LB 18	LB 19	LB 20	LB 21	
	C*		LB 22	LB 23	LB 24	LB 25	LB 26	LB 27	LB 28	
	D*		LB 29	LB 30	LB 31	LB 32	LB 33	LB 34	LB 35	

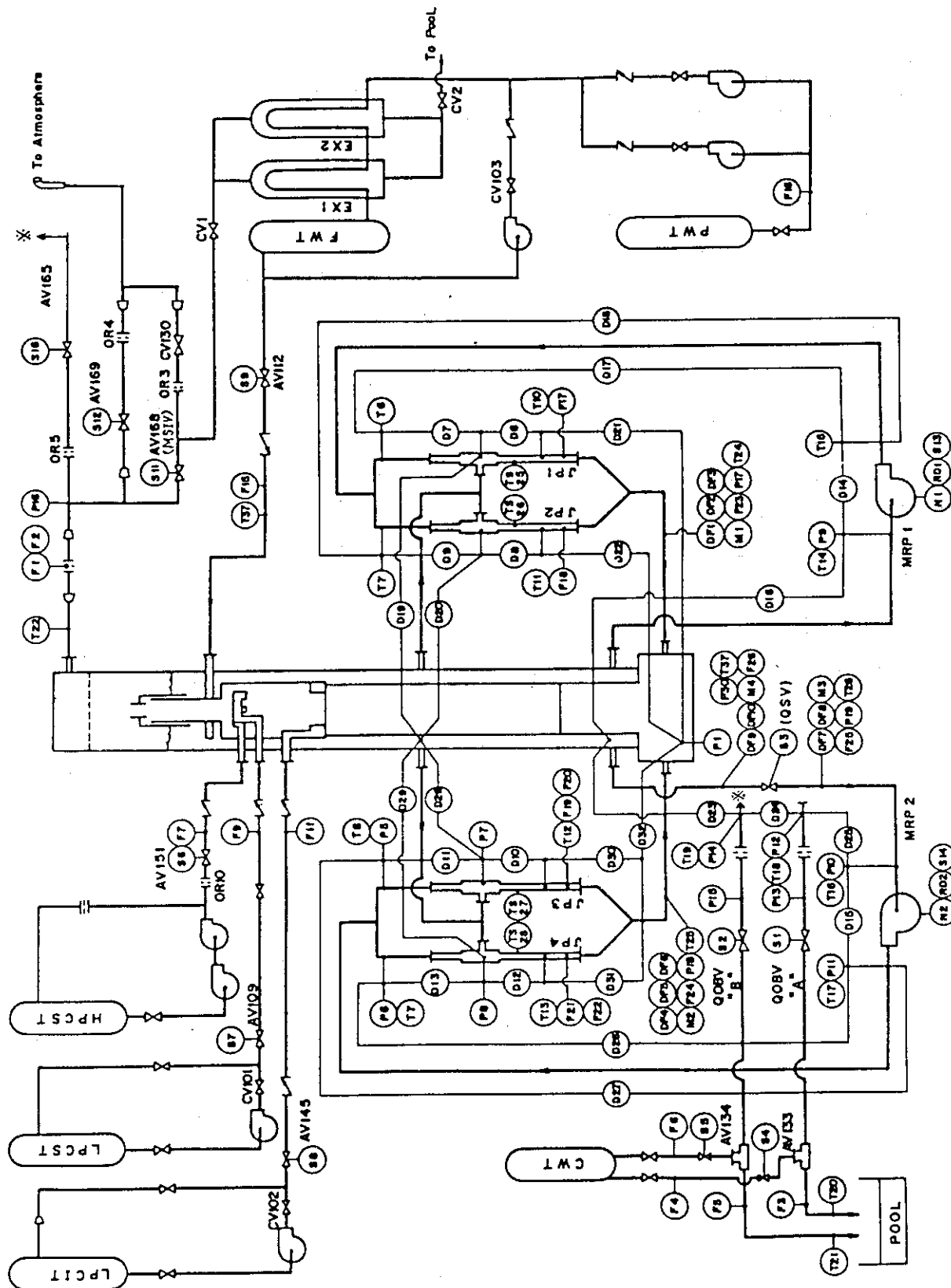


Fig. 3.1 Instrumentation Location of ROSA-III Test Facility

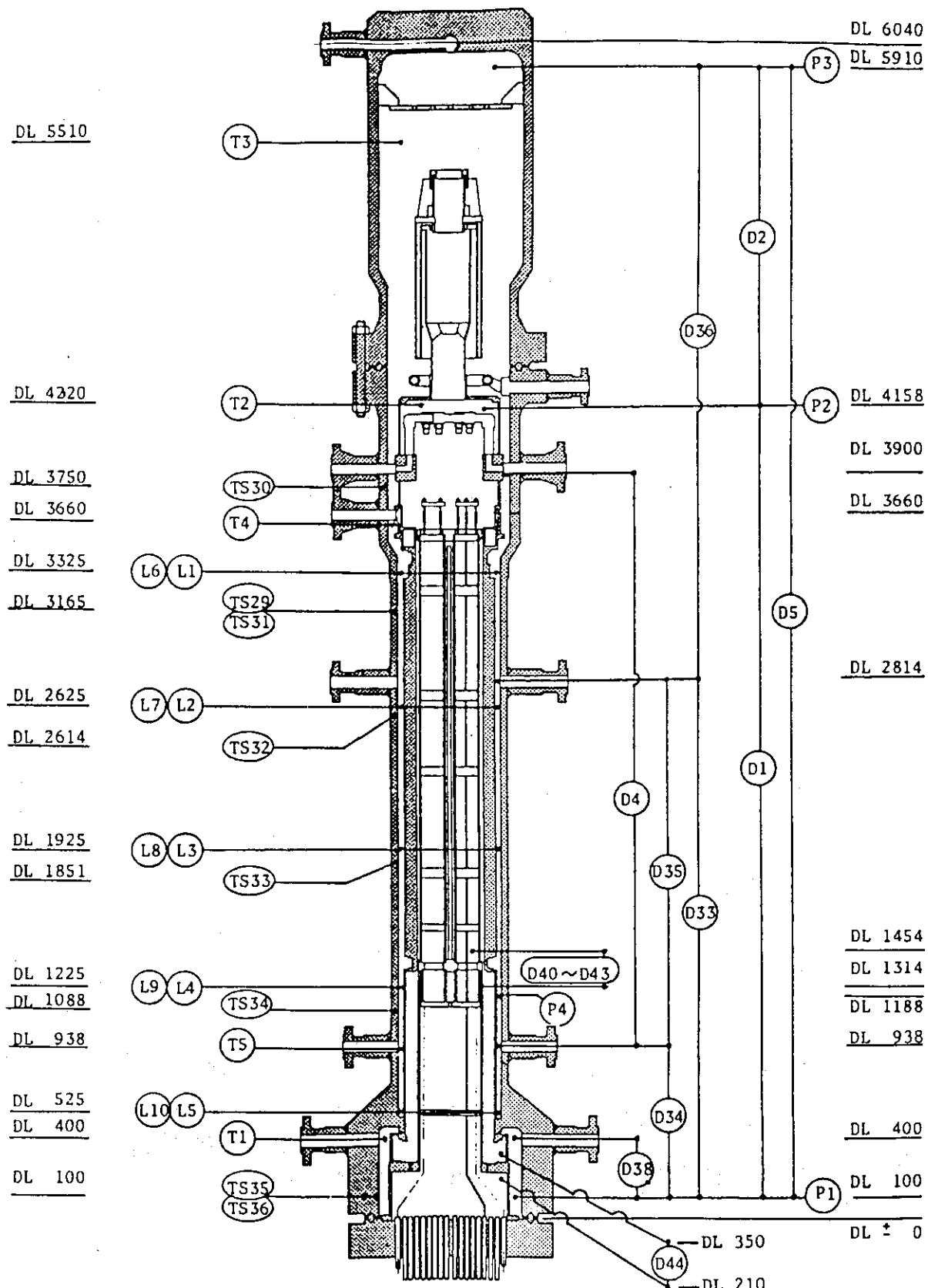


Fig. 3.2 Instrumentation Location in Pressure Vessel

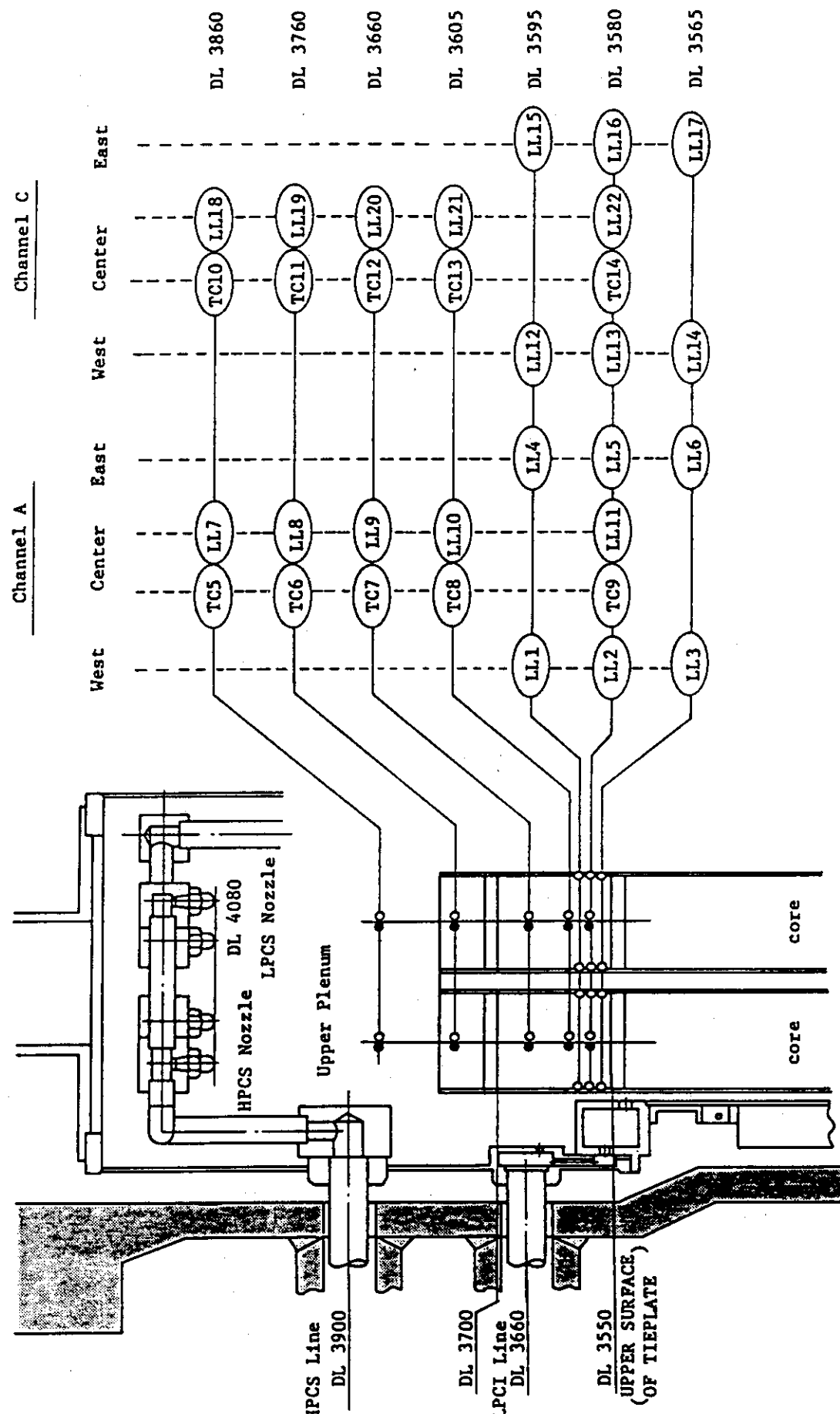


Fig. 3.3 Upper Plenum Instrumentation

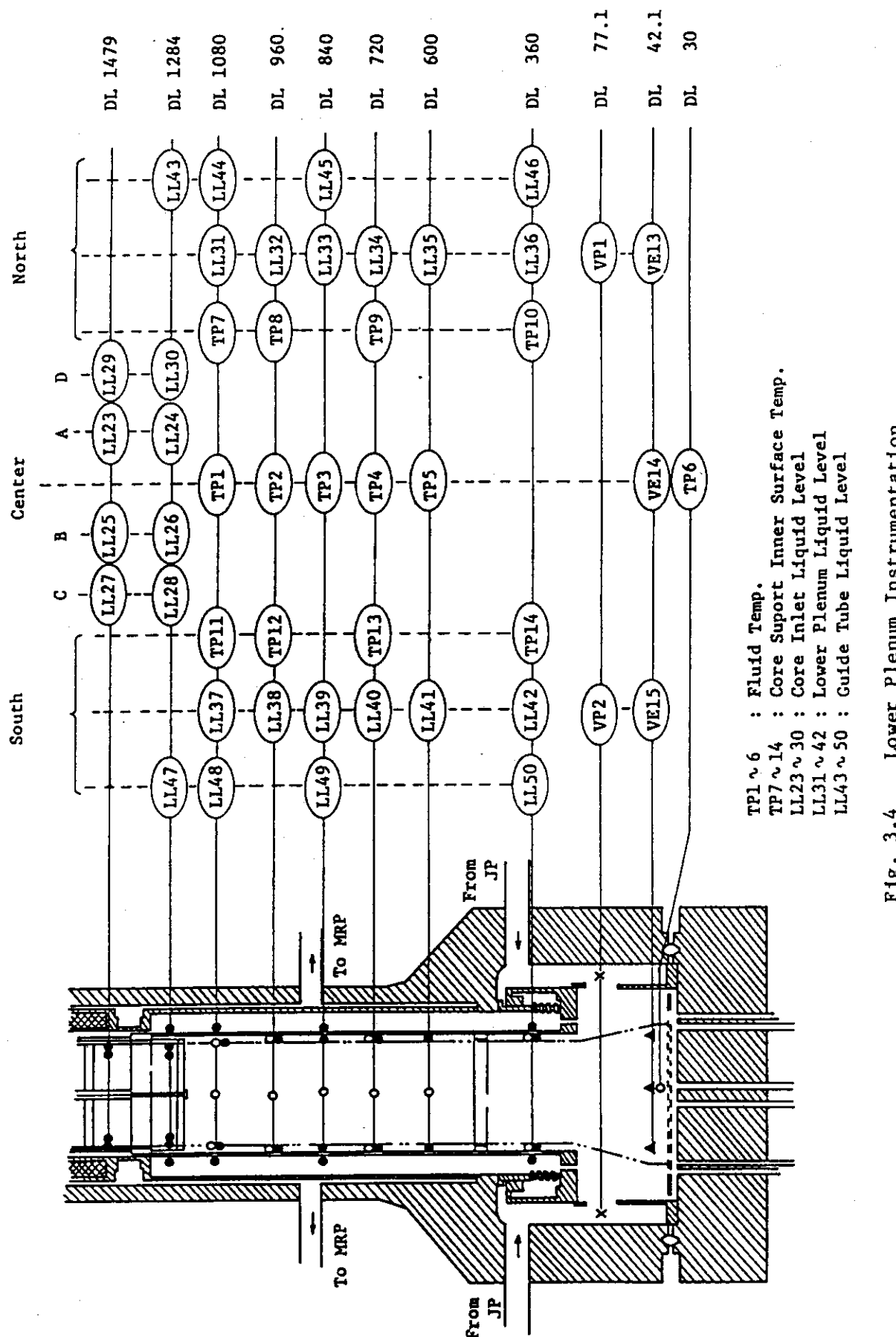
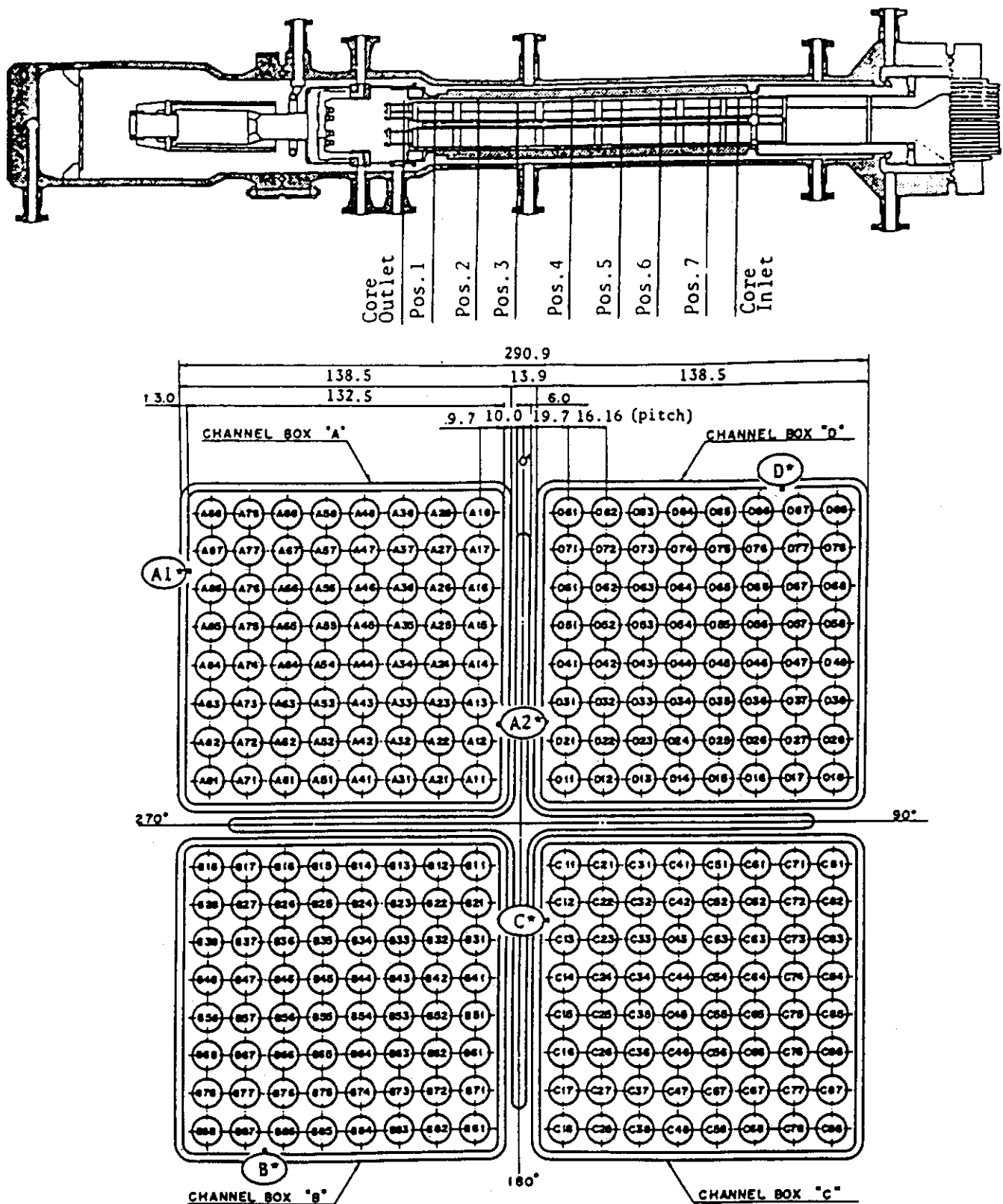


Fig. 3.4 Lower Plenum Instrumentation



Heater rod O.D. is 12.27mm

A54,B54,C54 and D54 are water rod simulators with void probes,  
O.D.= 15.01mm

A45,B45,C45 and D45 are water rod simulators with thermocouples,  
O.D.= 15.01mm

Fig. 3.5 Core Instrumentation (cf. Table 3.3)

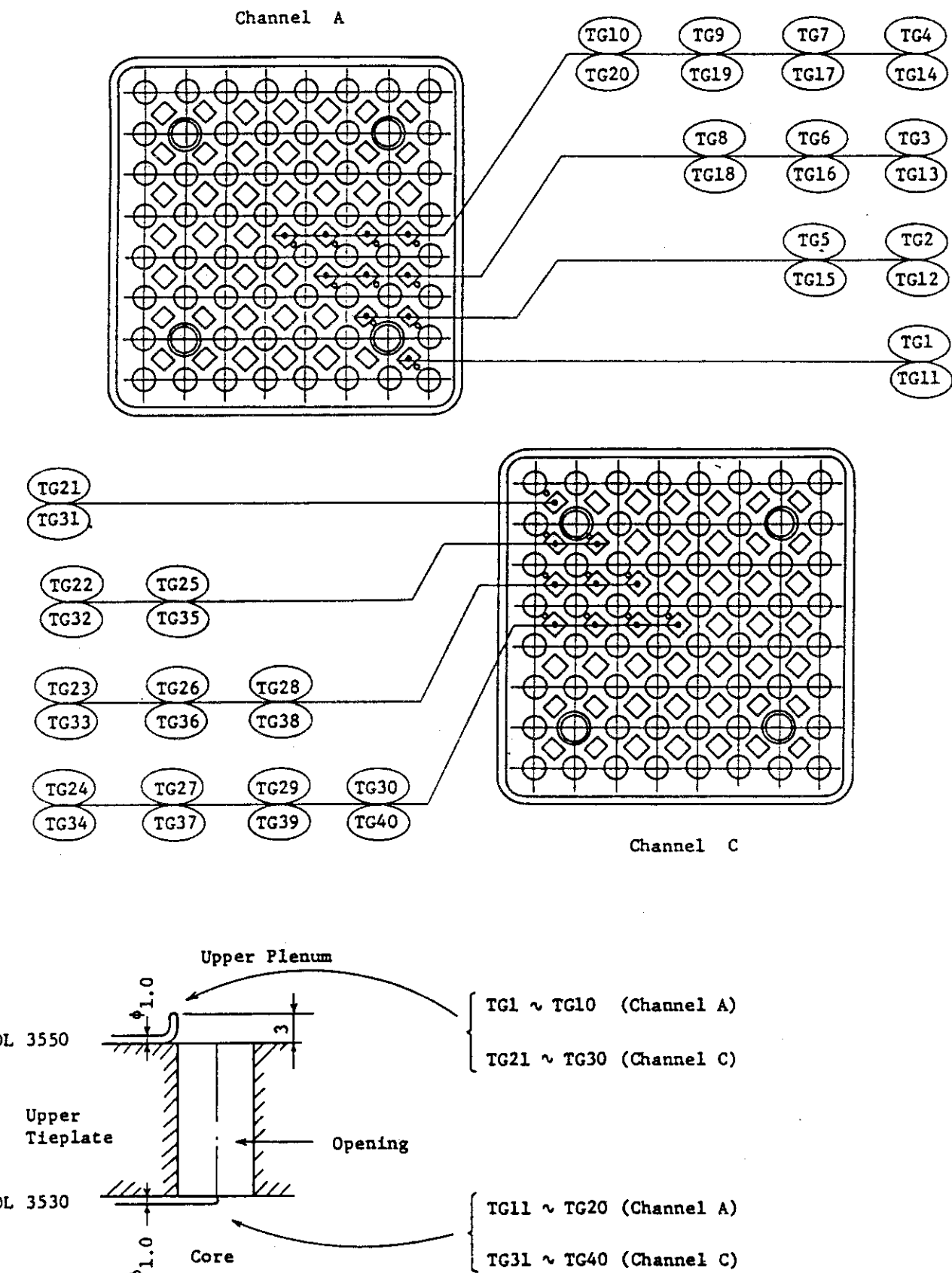


Fig. 3.6 Upper Tieplate Instrumentation

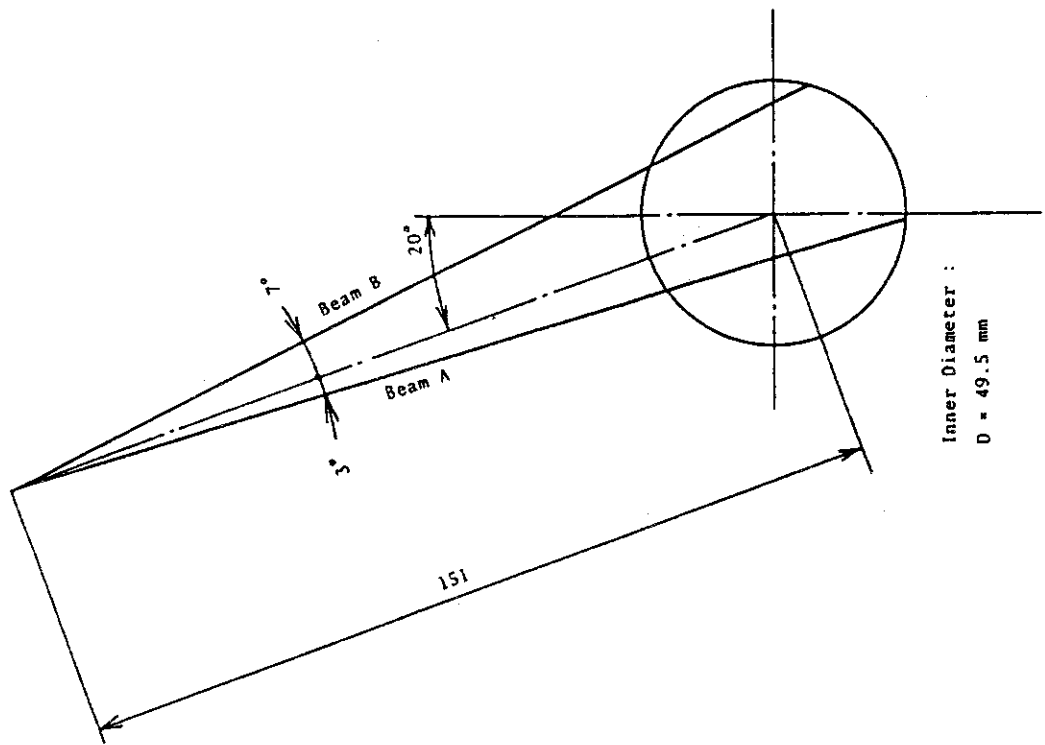


Fig. 3.8 Beam Directions of Two-Beam  
Gamma Densitometer

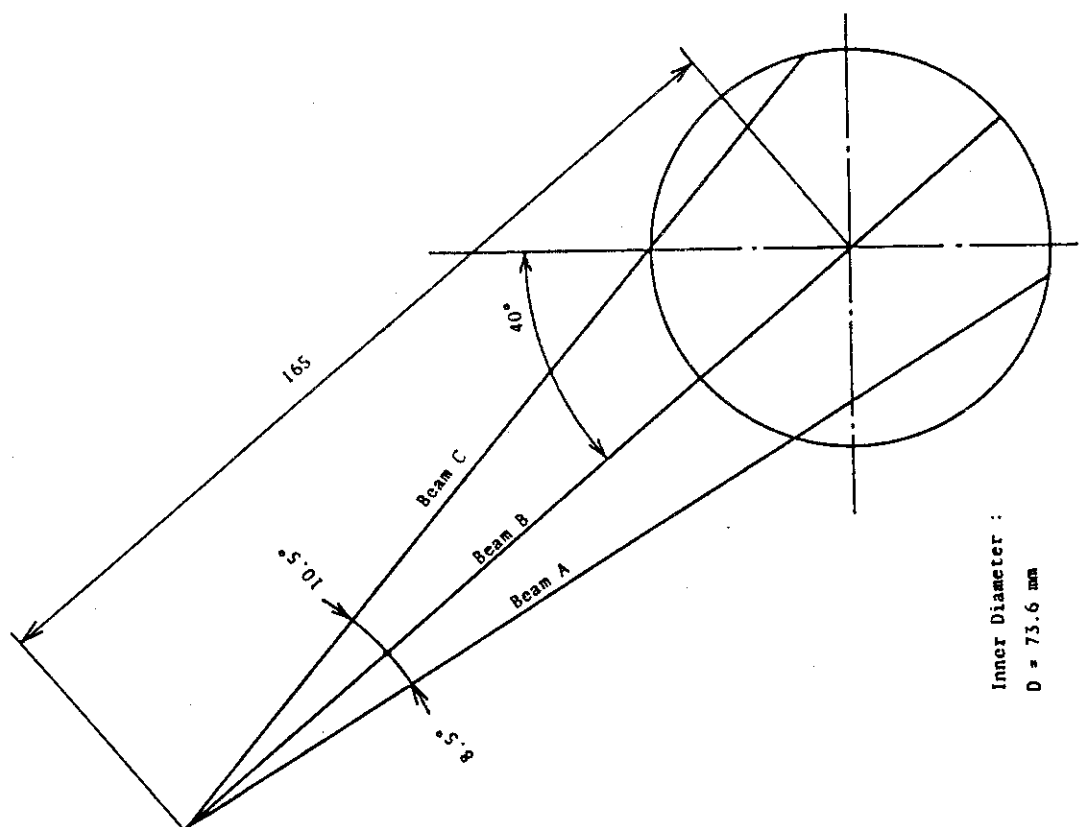


Fig. 3.7 Beam Directions of Three-Beam  
Gamma Densitometer

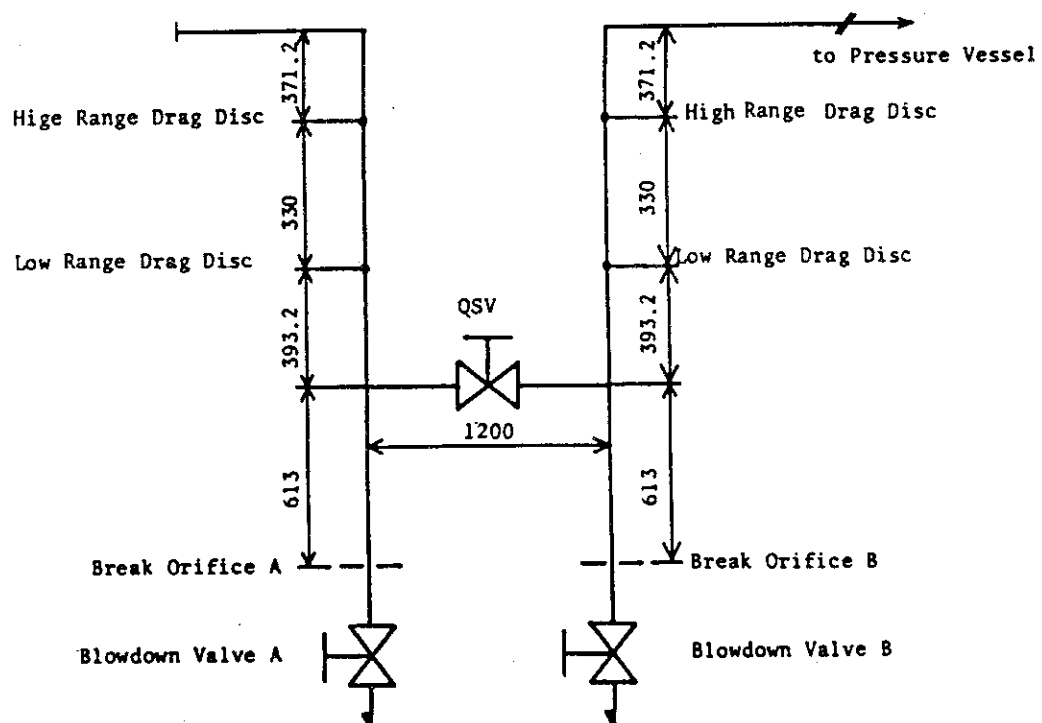
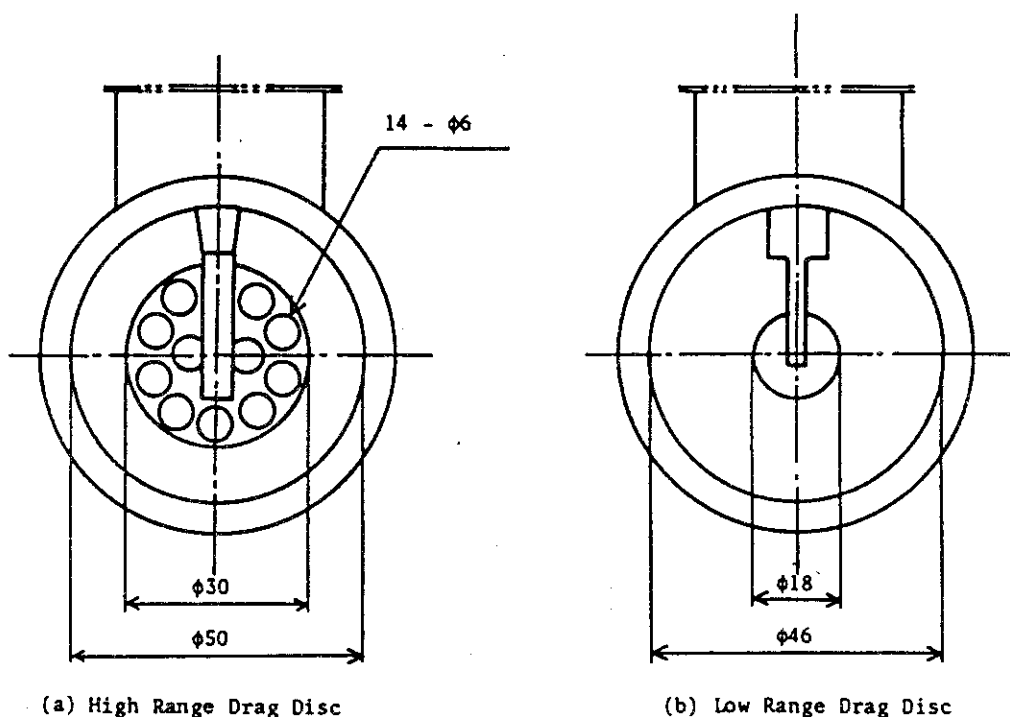
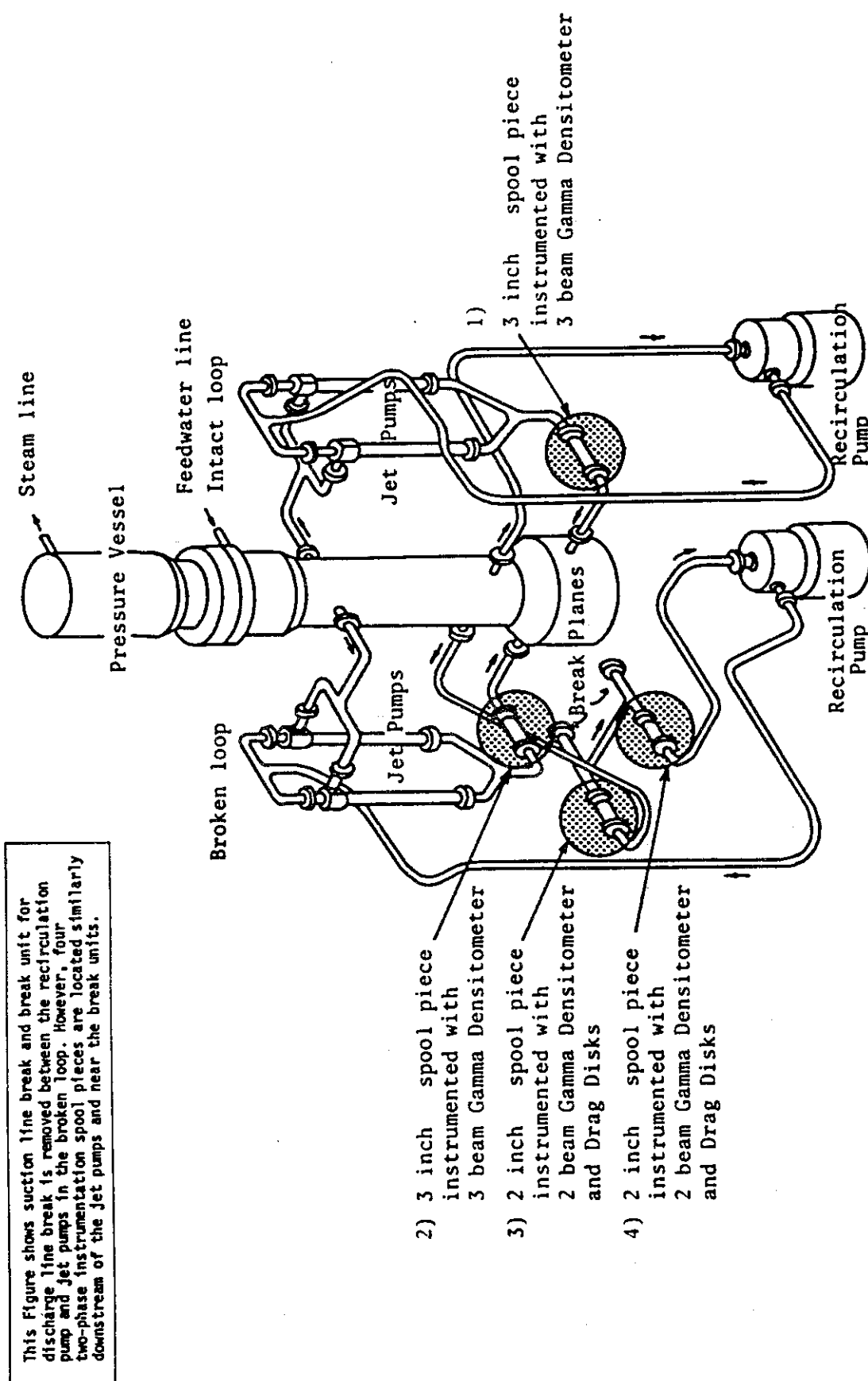


Fig. 3.9 Arrangement and Location of Drag Disks



#### 4. Test Conditions and Procedure

RUN 953 is a 100% Main Steam Line break test with a break located at the main steam line. The break area is adjusted by inserting an orifice shown in Fig. 4.1 in the main steam line. Blowdown is initiated by opening the QOBV and closing the valve AOV-168 in the steady steam flow line. The initial conditions of this test were specified as follows: the steam dome pressure of 7.35 MPa, the lower plenum temperature of 552.6 K giving the subcooling of 10.6 K, the core inlet flow rate of 16.0 kg/s, and the core heat generation rate of 3.96 MW. The quality in the upper plenum was estimated to be 12.5%. The actual conditions are summarized in Table 4.1.

To prepare for the test, makeup water (pure water) was pumped into the primary system of the test facility and electric power was supplied to the core to heat the water in the system and to achieve saturation conditions in the upper region of the pressure vessel. The core power was maintained at 3.962 MW before the break initiation, which is 44% of the steady state power of 8.96 MW necessary to achieve the same power-to-volume ratio as in a reference BWR. The core power was decreased during the transient following the break as shown in Fig. 4.2. Here, the power is kept constant for the first 9.0 seconds and reduced along the decay curve that simulates the total heat transfer rate in the core of the reference BWR (the delayed neutron fission power, the decay power of fission products and actinides and the stored heat in the nuclear fuel) neglecting the stored heat of ROSA-III heater rods<sup>(3)</sup>. The maximum linear heat rate of the peak power rod before the break initiation is 16.7 kW/m.

The schematics of the main steam line and the feedwater line are shown in Figs. 4.3 and 4.4 respectively. The main steam line of the ROSA-III has three branches: (1) steady flow branch, (2) ADS branch and (3) transient branch. Before the break initiation, CV-130 in the steady flow branch

controls the steam flow rate to maintain the steam dome pressure constant and CV-1 and CV-2 are opened to provide steam to the heat exchanger to heat the feedwater. At the break initiation, the steam flow is switched to the transient branch by opening AV-165 and closing AV-168, CV-1 and CV-2. The break flow during the MSL break test was limited by an orifice OR-5 of 31.0 mm ID (inner diameter) shown in Fig. 4.1 installed upstream of AV-165 as shown in Fig. 4.3. The ADS was not actuated in the present MSL break test and Tables 4.2 and 4.3 respectively show the characteristics and control sequence of steam discharge line valves in the present test.

The details of the feedwater line is shown in Fig. 4.5. The feedwater flow is terminated at 3.8 s after break by closing the valve AV-112 in the feedwater line. However, some feedwater remained in the piping between AV-112 and the feedwater sparger below the steam separator in the pressure vessel.

The coolant recirculation pumps are tripped to start coasting down at the time of break initiation.

The liquid level signal in the downcomer is used to actuate the ECCS in the ROSA-III MSL break tests. The downcomer water level during a steady state operation is set at the scram level L3 (5.00 meters above the bottom of the pressure vessel). When the liquid level in the downcomer falls to the L2 level (4.76m), HPCS is ordinarily actuated with a time delay of 27 s. However, in the present test, an HPCS failure has been assumed. If the liquid level further falls to the L1 level (4.25m), both LPCS and LPCI are actuated with a time delay of 40 s in the present test. The delay times given above are used in a safety analysis of the reference BWR<sup>(4)</sup>. Injection of emergency coolant by LPCS and LPCI in the reference BWR, however, occurs when the primary system pressure falls below 2.16 MPa and 1.57 MPa respectively, because of early actuation of the high containment pressure signal which activates the LPCS and LPCI pumps. This occurs despite a delay

in the lowering of the downcomer water level. Thus, the actuation of LPCS and LPCI by the L1 level signal in the present test corresponds to the failure of the containment pressure signal in the case of an MSL break LOCA of the reference BWR. The system pressures selected for actuation of LPCS and LPCI were calculated from the pump characteristics used in the safety analysis of the reference BWR(5). The test was terminated after the entire core was quenched and the top of the pressure vessel was nearly filled with water.

Table 4.1 Test conditions of the ROSA-III test RUN 953

Items	Specified Value	Measured Value
<b>Break Conditions</b>		
Location	Main Steam Line	Main Steam Line
Type	Single-ended	Single-ended
Break Orifice Diameter (mm)	31.0	31.0
Break Area Ratio (%)	100	100
Break Initiation Logic	AV165 open, AV168 close	AV165 open, AV168 close
<b>Initial Conditions</b>		
Steam Dome Pressure (MPa)	7.35	7.35
Lower Plenum Temperature (K)	552.6 (279.4°C)	552.5 (279.3°C)
Lower Plenum Subcooling (K)	10.6	10.7
Core Inlet Flow Rate (*1) (kg/s)	16.0	16.69
Core Outlet Quality (*2) (%)	13.2	12.5
Power Generation (KJ/s)	3960 (1260+2700)	3977 (1265+2712)
<b>Max. Linear Heat Rate (KJ/m.s)</b>		
Channel A { P.F.=1.0	16.65	16.72
{ P.F.=1.0	15.13	15.19
{ P.F.=0.875	13.24	13.30
Channel B,C,D { P.F.=1.1	11.89	11.94
{ P.F.=1.0	10.81	10.86
{ P.F.=0.875	9.46	9.50
Power Simulation (*3)	dh+dn+sh (Fig. 4.2)	dh+dn+sh (Fig. 5.53)
Fuel Assembly Number	4	4
Water Level in PV (m)	5.00	5.03

(\*1) Flow rate include core bypass flow, i.e., 10% of total flow.

(\*2) Average quality in the upper plenum.

(\*3) decay heat + delayed fission power + stored heat release

Table 4.1 (Cont'd)

Items		Specified Value	Measured Value
Steam Line Conditions			
Steady State Flow Rate	(kg/s)	2.08 <sup>(*5)</sup>	2.08
Transient Flow Rate	(kg/s)	—	(Fig. 5.36 & 5.165)
MSIV closure	(s)	0.0	0.0
Safety Relief Valve Set Point (MPa)		8.13	not reached
ECCS Conditions			
HPCS		not used	not used
LPCS			
Injection Location		Upper Plenum	Upper Plenum
Initiation Time	t (s)	$L_1 + 40 \leq t$	281
Initiation Pressure	p (MPa)	$2.16 \geq p$	0.65
Coolant Temperature	(K)	313 (40°C)	313 (40°C)
Injection Flow Rate	(m <sup>3</sup> /s)	$1.13 \times 10^{-3}$	(Fig. 5.37)
LPCI			
Injection Location		Top of Core Bypass	Top of Core Bypass
Initiation Time	t (s)	$L_1^{(*4)} + 40 \leq t$	281
Initiation Pressure	p (MPa)	$1.57 \geq p$	0.65
Coolant Temperature	(K)	313 (40°C)	313 (40°C)
Injection Flow Rate	(m <sup>3</sup> /s)	$3.50 \times 10^{-3}$	(Fig. 5.37)
ADS Conditions		not used	not used
Feedwater Conditions			
Temperature	(K)	489 (216°C)	489 (216°C)
Steady State Flow Rate	(kg/s)	2.08 <sup>(*5)</sup>	2.04
Valve Closure Time	(s)	2	(Fig. 5.55)

(\*4) L1 : Water level in the downcomer, 4.76 m from PV bottom

(\*5) Core power of 3.960 MW, heat input by MRPs of 0.022 MW, heat loss of 0.157 MW (at ΔT = 281 K) and no leakage flow were assumed in the calculation of flow rate at steady state.

Table 4.2 Characteristics of Steam Discharge Line Valves

Valve	Close to Open (sec)	Open to Close (sec)
AV165	0.1	-
AV168	-	0.1
AV169	not used	not used

Orifice	Diameter (mm)	Area (mm <sup>2</sup> )
OR3	18.0	254.5
OR4	not used	not used
OR5	31.0	754.8

Table 4.3 Control Sequence for Steam Discharge Line Valves

Time	t < 0 s	t = 0 s (Break)
CV-1	Open	Close (Manual)
CV-2 (see Fig.2.3)	Open	Close (Manual)
CV-130	Control to maintain steady state pressure	Close (Manual)
AV-168 (MSIV)	Open	Close
AV-165 (Transient Line)	Closed	Open

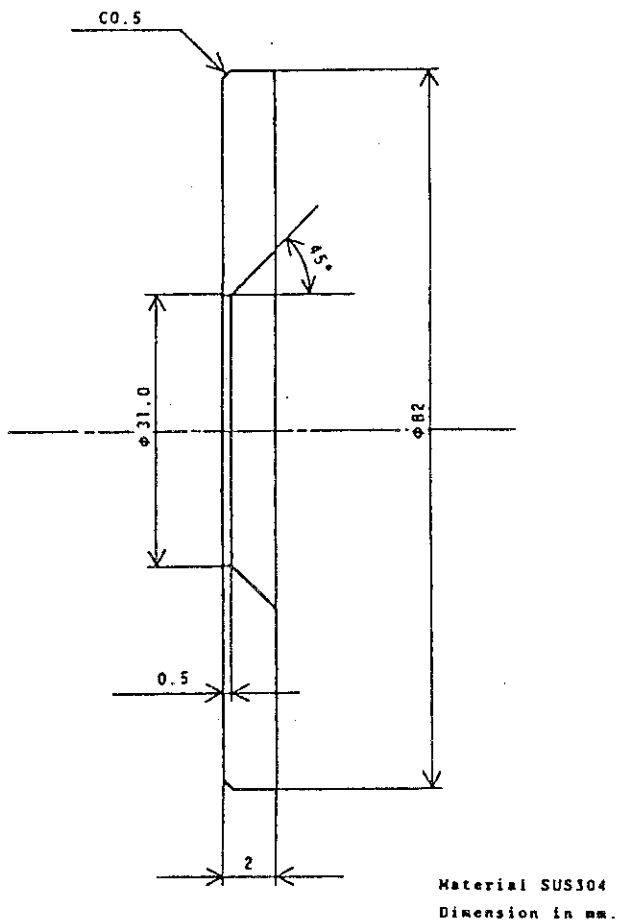


Fig. 4.1 Break Orifice Details

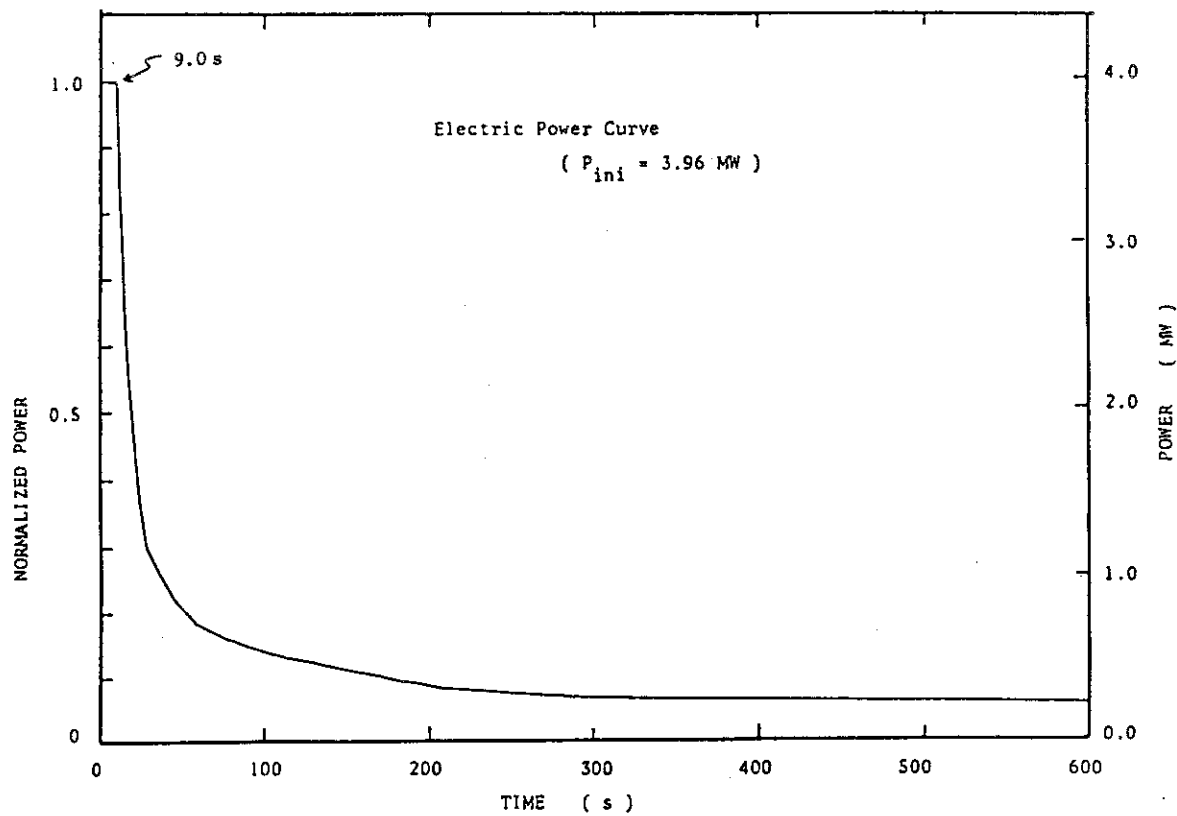


Fig. 4.2 Normalized Poewr Transient for ROSA-III Test

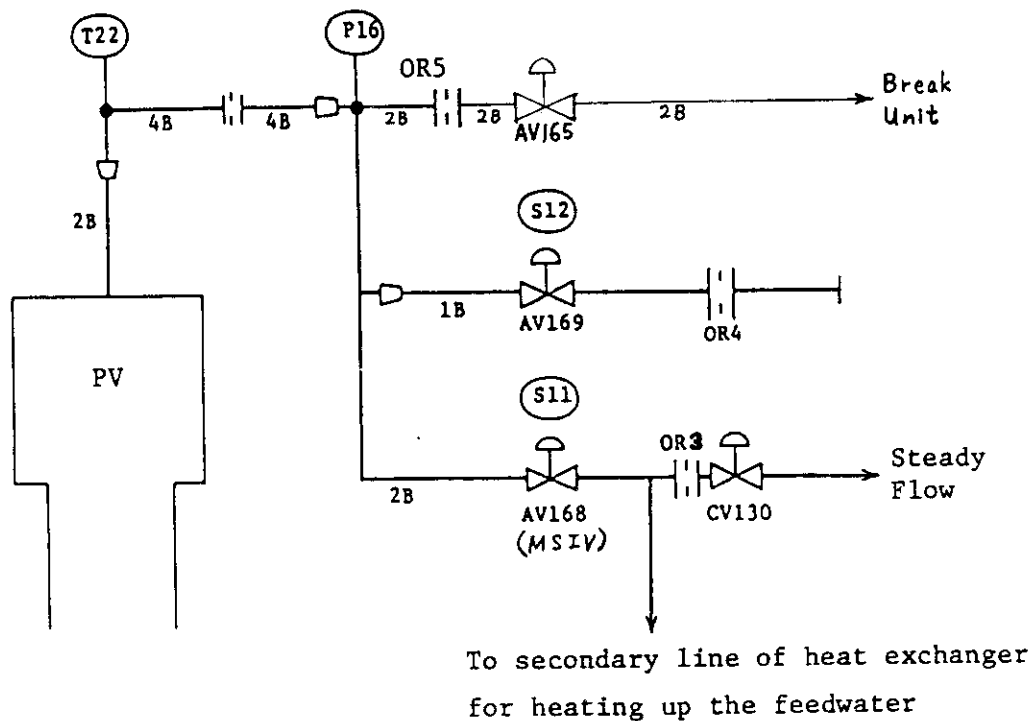


Fig. 4.3 Main Steam Line Schematic

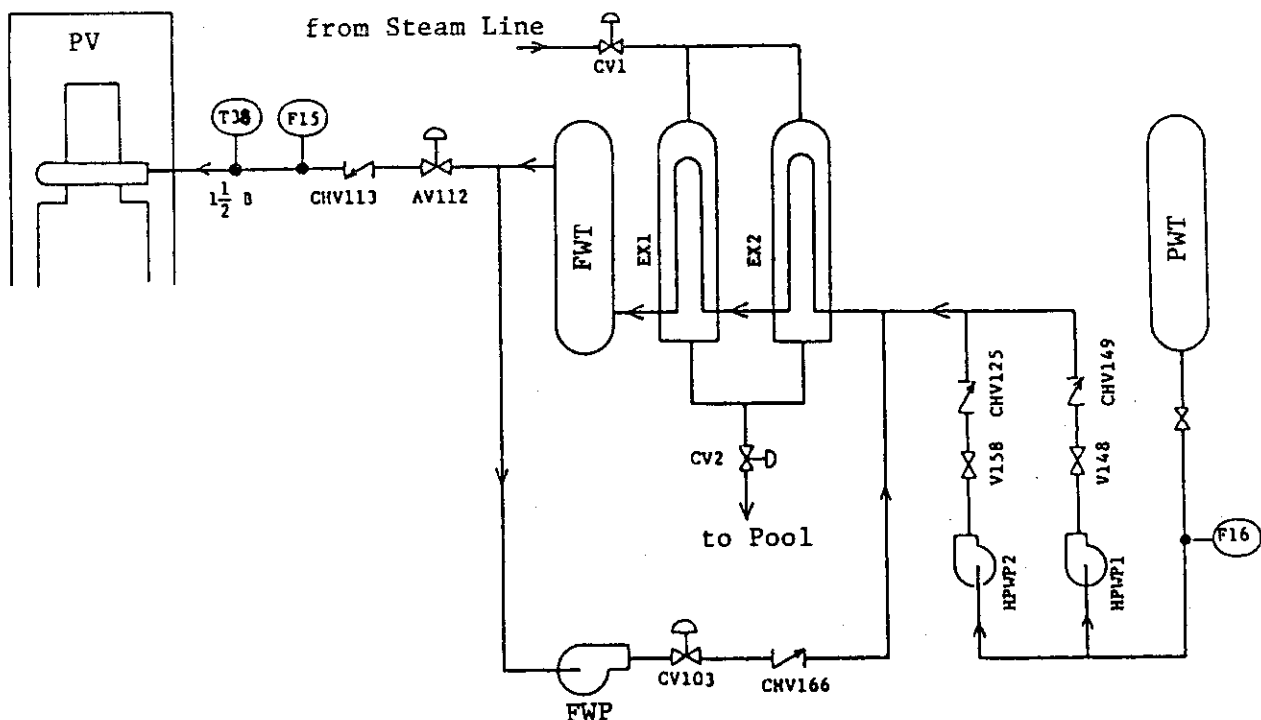


Fig. 4.4 Feedwater Line Schematic

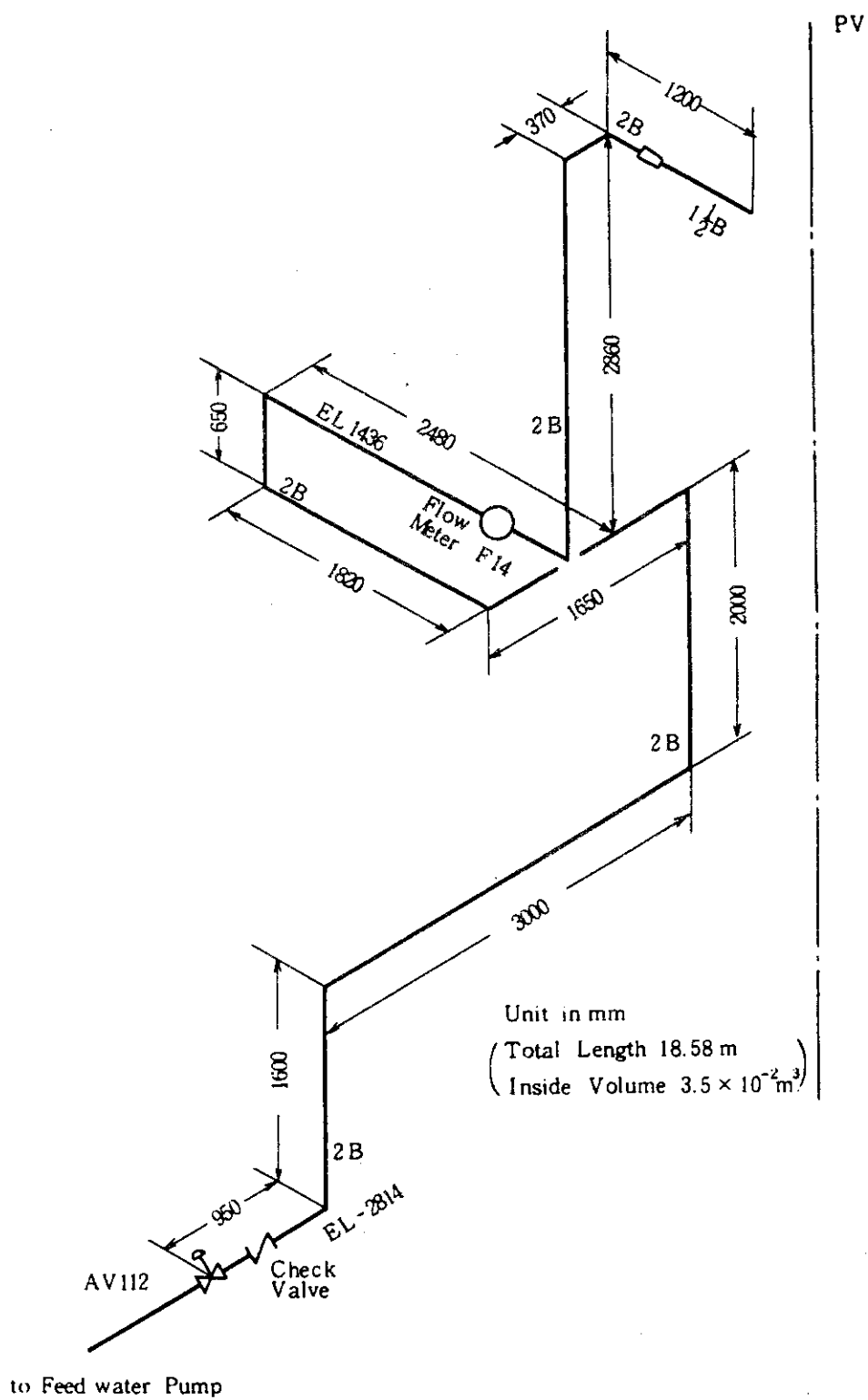


Fig. 4.5 Feedwater Line between Valve AV-112 and Pressure Vessel

## 5. Data Processing

In the present test, data acquisition with DATAC 2000B was started 121 s before the break initiation and terminated at 757 s after break. The data sampling rate was 10 Hz throughout the test. The test data were processed and a set of 1000 data points was selected for plotting. The time span and frequency of the reduced data for plotting were 460 s and 2.2 Hz, respectively.

### Measured Data

The test data from RUN 953 are shown in Fig. 5.1 through 5.157. In these figures, each measurement is identified by the channel number shown in Table 3.2. The major test sequences and events observed are summarized in Table 5.1.

Figures 5.1 through 5.5 show the pressure data obtained in the pressure vessel and in the recirculation line. Figures 5.6 through 5.33 show differential pressures measured between various locations in the pressure vessel, break unit and recirculation line. Figures 5.34 and 5.35 show the liquid levels in the pressure vessel and ECCS tanks. Figures 5.36 through 5.41 show the flow rates in MSL, ECC injection, feedwater and recirculation lines. Differential pressures measured across the orifice and venturi flow meters located in the MSL and recirculation lines are useful for checking out the flow rate instrumentation. They are shown in Figs. 5.42 through 5.52. Figure 5.53 shows the power supplied to the core from two power supplies with maximum capacities of 2100 kW and 3150 kW. The revolution speeds of the recirculation pumps are shown in Fig. 5.54. On-off signals indicating the break initiation, the status of ECCS, pump and valve operations are shown in Figs. 5.55, 5.56 and 5.57. Figures 5.58 through 5.65

show the fluid densities measured by the gamma densitometers. Figures 5.66 through 5.68 show momentum fluxes measured at jet pump outlets and break unit using drag disks. Figures 5.69 through 5.81 show the fluid temperatures at various locations in the loop. The fuel rod cladding temperatures and the surface temperatures of the water rods and the channel boxes measured at positions 1 through 7 are given in Figs. 5.82 through 5.101. Figures 5.102 through 5.126 compare the cladding temperatures of different fuel rods at the same elevation. Figures 5.127 through 5.143 show the fluid temperatures at the inlet and outlet of the channel box. The surface temperatures of the channel box and the fluid temperature in the lower plenum are shown in Figs. 5.144 and 5.145 respectively. The liquid level signals in the core, upper and lower plena, guide tube and downcomer are shown in Figs. 5.146 through 5.157. The Peak Cladding Temperature (PCT) distribution in the core is given in Table 5.2

#### Derived Data

Quantities calculated from the measured data are shown in Figs. 5.158 through 5.180.

Figure 5.158 shows the estimated mixture level in the pressure vessel obtained from the conductivity probe signals shown in Figs. 5.146 through 5.157. Figures 5.159 and 5.160 show the location of the dryout front and the quench front obtained from the fuel rod cladding temperature data.

Figures 5.161 through 5.163 show the average fluid densities at the jet pump outlet and break unit, which are calculated from the three-beam and two-beam gamma densitometer data shown in Figs. 5.58 through 5.65. The beam configurations of the gamma densitometers installed in the ROSA-III facility are shown in Figs. 3.7 and 3.8. The average density is calculated as an arithmetic mean of the chordal-average densities using the chord

length as the weighting factors.

For the three beam densitometer at the jet pump outlet spool piece, the average fluid density is calculated using the following equation.

$$\rho_{av} = 0.3221\rho_A + 0.43\rho_B + 0.2479\rho_C \quad (5.1)$$

where,

$\rho_{av}$  = average density obtained from the three-beam gamma densitometer,

$\rho_A$  = density measured by beam A (bottom),

$\rho_B$  = density measured by beam B (middle),

$\rho_C$  = density measured by beam C (top).

For the two-beam densitometer at the break spool piece,

$$\rho_{av} = 0.5863\rho_A + 0.4137\rho_B \quad (5.2)$$

where,

$\rho_{av}$  = average density obtained from the two-beam gamma densitometer,

$\rho_A$  = density measured by beam A (bottom),

$\rho_B$  = density measured by beam B (top).

Figure 5.164 shows the flow rate at the break computed from the drag disk and gamma densitometer data using the following equation.

$$G = C_D \cdot A \cdot \sqrt{\rho_{av} \cdot \rho v^2} \quad (5.3)$$

where,

$G$  = mass flow rate,

$C_D$  = drag coefficient ( $= 1.13$ ),

$A$  = flow area ( $= 1.923 \times 10^{-3} \text{ m}^2$ ),

$\rho_{av}$  = average density from gamma densitometer,

$\rho v^2$  = momentum flux from drag disk.

Figures 5.165 through 5.175 show the fluid flow rates at the main steam line, channel inlet orifices, bypass hole and jet pump outlets. These flow rates are calculated from the pressure drop measured across the orifice or venturi flow meters and the vapor or liquid density obtained from the temperature and pressure measurements. The equation used for this calculation is as follows :

$$G = C_D \cdot A \cdot \sqrt{2g \cdot \rho_l \cdot \Delta P} \quad (5.4)$$

where,

$G$  = flow rate,

$\Delta P$  = pressure drop across the orifice,

$C_D$  = discharge coefficient,

= 0.6552 ( orifice to measure the steam discharge flow rate )

= 0.4761 ( channel inlet orifice )

= 0.8032 ( bypass hole )

= 0.7383 ( orifice to measure the jet pump outlet flow rate )

= 1.1260 ( venturi tube to measure the jet pump outlet flow rate )

$A$  = flow area (  $m^2$  )

=  $2.875 \times 10^{-3}$  ( orifice to measure the steam discharge flow rate )

=  $1.521 \times 10^{-3}$  ( channel inlet orifice )

=  $1.758 \times 10^{-4}$  ( bypass hole )

=  $1.133 \times 10^{-3}$  ( orifice to measure the jet pump outlet flow rate )

=  $9.095 \times 10^{-4}$  ( venturi tube to measure the jet pump outlet flow rate )

$g$  = gravitational acceleration ( =  $9.807 \text{ m/s}^2$  ),

$\rho_l$  = density of the single-phase liquid (  $\text{kg/m}^3$  ),

Although the above calculation method is not applicable to two-phase flow conditions after the initiation of flashing in the lower plenum, the values calculated are useful in determining a trend in two-phase flow rates. Total channel inlet flow rate represents the sum of four separate channel inlet flow rates.

Figures 5.176 and 5.177 show the collapsed water levels outside and inside the core shroud, respectively. The collapsed water level is obtained from the differential pressure measurement in the pressure vessel. The differential pressure may include the friction and acceleration effects, however, these effects are considered to become negligible after completion of the recirculation pump coastdown.

Finally, Figures 5.178 through 5.180 show the fluid mass inventories in the downcomer, core shroud and pressure vessel. The fluid mass inventory is determined from the density and the volume of liquid outside and inside the core shroud as follows.

$$M = \rho_l \cdot Q \quad (5.5)$$

where,

$M$  = fluid inventory,

$\rho_l$  = liquid density estimated from the saturation temperature and/or pressure,

$Q$  = liquid volume calculated from the liquid level.

The volume  $Q$  (  $\text{m}^3$  ) outside the core shroud is given below as a function of height.

$Q = 0.0$	(	$L \leq 0.494$	)
$Q = 0.0225L - 0.0111$	(	$0.494 < L \leq 1.384$	)
$Q = 0.0697L - 0.0769$	(	$1.384 < L \leq 1.519$	)
$Q = 0.0225L - 0.0048$	(	$1.519 < L \leq 3.355$	)
$Q = 0.0801L - 0.1980$	(	$3.355 < L \leq 4.250$	)
$Q = 0.2443L - 0.8959$	(	$4.250 < L \leq 4.413$	)
$Q = 0.2611L - 0.9700$	(	$4.413 < L \leq 4.578$	)
$Q = 0.2504L - 0.9211$	(	$4.578 < L \leq 4.654$	)
$Q = 0.2375L - 0.8610$	(	$4.654 < L \leq 4.815$	)
$Q = 0.2866L - 1.0974$	(	$4.815 < L \leq 4.915$	)
$Q = 0.3396L - 1.3580$	(	$4.915 < L \leq 5.143$	)
$Q = 0.3607L - 1.4665$	(	$5.143 < L \leq 5.365$	)
$Q = 0.3848L - 1.5960$	(	$5.365 < L \leq 5.955$	)
$Q = 0.7111$	(	$5.955 < L$	)

The volume  $Q$  (  $\text{m}^3$  ) inside the core shroud is similarly given below as a function of height.

$Q = 0.0$	(	$L \leq 0.0$	)
$Q = 0.2350L$	(	$0.0 < L \leq 0.497$	)
$Q = 0.1245L + 0.0549$	(	$0.497 < L \leq 1.354$	)
$Q = 0.0698L + 0.1290$	(	$1.354 < L \leq 3.589$	)
$Q = 0.1648L - 0.2120$	(	$3.589 < L \leq 3.744$	)
$Q = 0.1963L - 0.3299$	(	$3.744 < L \leq 4.243$	)
$Q = 0.0196L + 0.4199$	(	$4.243 < L \leq 4.578$	)

$$Q = 0.0186L + 0.4244 \quad ( 4.578 < L \leq 4.654 )$$

$$Q = 0.0410L + 0.3201 \quad ( 4.654 < L \leq 5.099 )$$

$$Q = 0.0196L + 0.4292 \quad ( 5.099 < L \leq 5.365 )$$

$$Q = 0.5344 \quad ( 5.365 < L )$$

The total fluid mass inventory in the pressure vessel is given by the sum of the mass inventories inside and outside of the core shroud. The initial mass inventory before the break initiation is estimated to be at 640 kg.

Table 5.1 Test Procedure and Sequence of Events in RUN 953

Time (s)	Events and Procedure
-121	- Initiation of data recording with DATAC 2000B System
-10	- Initiation of data plotting in the figures
0.0	- Initiation of break in the Main Steam Line (BU-B open, AV-168 close, AV165 open) - MRP1 and MRP2 coast-down
1.5	- Feedwater began to stop (terminated at 3.8 s)
5.4	- Initiation of Lower Plenum flashing
9.0	- Initiation of core power decrease
29	- Initiation of top core uncovering in channel D
62	- Initiation of top core uncovering in channel A
74	- L2 level
95	- Initiation of Feedwater flashing
245	- L1 level
281	- LPCS and LPCI actuation (pressure = 0.65 MPa)
290	- PCT detected at position 3 of A22 rod
438	- Completion of core quenching at position 1 of A88 rod
450	- Termination of data plotting in figures
500	- Top of Pressure Vessel filled with water
757	- Termination of data recording

Table 5.2 Maximum Cladding Temperature Distribution in the Core

	Pos.1	Pos.2	Pos.3	Pos.4	Pos.5	Pos.6	Pos.7
A-11 rod	TE 201	TE 202	TE 203	TE 204	TE 205	TE 206	TE 207
PCT (K)	717.1	934.3	975.1	979.9	889.9	708.7	570.0
Time (s)	294.0	289.2	284.4	285.6	289.8	289.8	0.0
A-12 rod	TE 208	TE 209	TE 210	TE 211	TE 212	TE 213	TE 214
PCT (K)	762.7	934.3	978.7	964.3	862.3	690.7	565.6
Time (s)	296.4	290.4	291.0	285.6	284.4	285.0	0.0
A-13 rod	TE 215	TE 216	TE 217	TE 218	TE 219	TE 220	TE 221
PCT (K)	792.7	924.7	972.7	960.7	863.5	687.1	568.4
Time (s)	295.2	289.8	287.4	288.6	285.6	284.4	0.0
A-14 rod	TE 222	TE 223	TE 224	TE 225	TE 226	TE 227	TE 228
PCT (K)	-----	-----	-----	-----	-----	-----	-----
Time (s)	-----	-----	-----	-----	-----	-----	-----
A-15 rod	TE 229			TE 230			
PCT (K)	-----			-----			
Time (s)	-----			-----			
A-17 rod	TE 231			TE 232			
PCT (K)	-----			954.7			
Time (s)	-----			286.8			
A-22 rod	TE 233	TE 234	TE 235	TE 236	TE 237	TE 238	TE 239
PCT (K)	834.7	959.5	1003.9	957.7	867.9	683.0	560.7
Time (s)	295.8	292.2	291.6	292.2	286.2	285.6	0.0
A-24 rod	TE 240	TE 241	TE 242	TE 243	TE 244	TE 245	TE 246
PCT (K)	-----	-----	-----	-----	-----	-----	-----
Time (s)	-----	-----	-----	-----	-----	-----	-----
A-26 rod	TE 247			TE 248			
PCT (K)	-----			-----			
Time (s)	-----			-----			
A-28 rod	TE 249			TE 250			
PCT (K)	-----			960.0			
Time (s)	-----			291.0			
A-31 rod	TE 251			TE 252			
PCT (K)	-----			991.0			
Time (s)	-----			284.4			
A-33 rod	TE 253	TE 254	TE 255	TE 256	TE 257	TE 258	TE 259
PCT (K)	-----	-----	-----	-----	798.5	637.1	563.6
Time (s)	-----	-----	-----	-----	287.4	288.0	0.0
A-34 rod	TE 260	TE 261	TE 262	TE 263	TE 264	TE 265	TE 266
PCT (K)	-----	-----	-----	-----	-----	-----	-----
Time (s)	-----	-----	-----	-----	-----	-----	-----
A-37 rod	TE 267			TE 268			
PCT (K)	-----			-----			
Time (s)	-----			-----			
A-42 rod	TE 269			TE 270			
PCT (K)	-----			-----			
Time (s)	-----			-----			
A-44 rod	TE 271	TE 272	TE 273	TE 274	TE 275	TE 276	TE 277
PCT (K)	-----	-----	-----	-----	-----	-----	-----
Time (s)	-----	-----	-----	-----	-----	-----	-----

Table 5.2 Maximum Cladding Temperature Distribution in the Core (Continued)

	Pos.1	Pos.2	Pos.3	Pos.4	Pos.5	Pos.6	Pos.7
A-48 rod	TE 278			TE 279			
PCT (K)	-----			-----			
Time (s)	-----			-----			
A-51 rod	TE 280			TE 281			
PCT (K)	-----			-----			
Time (s)	-----			-----			
A-53 rod	TE 282			TE 283			
PCT (K)	-----			-----			
Time (s)	-----			-----			
A-57 rod	TE 284			TE 285			
PCT (K)	-----			948.2			
Time (s)	-----			290.4			
A-62 rod	TE 286			TE 287			
PCT (K)	-----			-----			
Time (s)	-----			-----			
A-66 rod	TE 288			TE 289			
PCT (K)	-----			-----			
Time (s)	-----			-----			
A-68 rod	TE 290			TE 291			
PCT (K)	-----			950.1			
Time (s)	-----			283.8			
A-71 rod	TE 292			TE 293			
PCT (K)	-----			998.8			
Time (s)	-----			284.4			
A-73 rod	TE 294			TE 295			
PCT (K)	-----			972.0			
Time (s)	-----			289.2			
A-75 rod	TE 296			TE 297			
PCT (K)	-----			-----			
Time (s)	-----			-----			
A-77 rod	TE 298	TE 299	TE 300	TE 301	TE 302	TE 303	TE 304
PCT (K)	809.7	931.1	973.0	945.4	839.8	674.2	553.3
Time (s)	291.0	290.4	289.8	288.6	286.2	286.2	0.0
A-82 rod	TE 305			TE 306			
PCT (K)	-----			996.9			
Time (s)	-----			285.6			
A-84 rod	TE 307			TE 308			
PCT (K)	996.9			954.9			
Time (s)	285.6			290.4			
A-85 rod	TE 309	TE 310	TE 311	TE 312	TE 313	TE 314	TE 315
PCT (K)	-----	-----	-----	-----	-----	-----	-----
Time (s)	-----	-----	-----	-----	-----	-----	-----
A-87 rod	TE 316	TE 317	TE 318	TE 319	TE 320	TE 321	TE 322
PCT (K)	776.0	913.2	963.4	954.9	855.7	696.0	564.5
Time (s)	291.0	291.0	291.0	288.0	284.4	285.6	0.0
A-88 rod	TE 323	TE 324	TE 325	TE 326	TE 327	TE 328	TE 329
PCT (K)	613.3	875.5	934.0	945.4	859.5	700.7	566.0
Time (s)	19.8	289.2	286.8	284.4	285.0	287.4	0.0

Table 5.2 Maximum Cladding Temperature Distribution in the Core (Continued)

	Pos.1	Pos.2	Pos.3	Pos.4	Pos.5	Pos.6	Pos.7
B-11 rod	TE 330	TE 331	TE 332	TE 333	TE 334	TE 335	TE 336
PCT (K)	602.8	826.6	862.3	856.7	768.5	630.5	-----
Time (s)	303.6	289.2	285.0	285.6	284.4	285.0	-----
B-13 rod				TE 337			
PCT (K)				859.5			
Time (s)				288.0			
B-22 rod	TE 338	TE 339	TE 340	TE 341	TE 342	TE 343	TE 344
PCT (K)	749.7	838.8	867.9	849.2	749.7	610.4	562.4
Time (s)	289.8	291.6	285.0	285.6	285.6	288.6	0.0
B-31 rod				TE 345			
PCT (K)				-----			
Time (s)				-----			
B-33 rod				TE 346			
PCT (K)				-----			
Time (s)				-----			
B-51 rod				TE 347			
PCT (K)				-----			
Time (s)				-----			
B-53 rod				TE 348			
PCT (K)				-----			
Time (s)				-----			
B-66 rod				TE 349			
PCT (K)				-----			
Time (s)				-----			
B-77 rod	TE 350	TE 351	TE 352	TE 353	TE 354	TE 355	TE 356
PCT (K)	727.1	853.9	884.9	866.1	-----	620.9	565.1
Time (s)	286.2	284.4	283.8	284.4	-----	287.4	0.0
B-86 rod				TE 357			
PCT (K)				-----			
Time (s)				-----			
C-11 rod	TE 358	TE 359	TE 360	TE 361	TE 362	TE 363	TE 364
PCT (K)	567.6	806.0	841.6	843.5	725.2	601.8	560.2
Time (s)	0.0	286.2	283.8	283.2	288.6	285.0	0.0
C-13 rod	TE 365	TE 366	TE 367	TE 368	TE 369	TE 370	TE 371
PCT (K)	566.2	607.6	689.3	832.3	717.7	586.4	563.8
Time (s)	64.8	312.6	296.4	285.6	285.6	288.0	0.0
C-15 rod				TE 372			
PCT (K)				-----			
Time (s)				-----			
C-22 rod	TE 373	TE 374	TE 375	TE 376	TE 377	TE 378	TE 379
PCT (K)	723.3	823.8	852.0	836.0	696.9	568.7	563.5
Time (s)	300.0	301.8	285.6	286.8	282.0	0.0	0.0
C-31 rod				TE 380			
PCT (K)				-----			
Time (s)				-----			
C-33 rod	TE 381	TE 382	TE 383	TE 384	TE 385	TE 386	TE 387
PCT (K)	716.7	791.9	809.7	783.5	651.4	564.7	561.2
Time (s)	307.2	303.6	304.2	283.8	285.0	0.0	0.0

Table 5.2 Maximum Cladding Temperature Distribution in the Core (Continued)

	Pos.1	Pos.2	Pos.3	Pos.4	Pos.5	Pos.6	Pos.7
C-35 rod				TE 388			
PCT (K)				-----			
Time (s)				-----			
C-66 rod				TE 389			
PCT (K)				-----			
Time (s)				-----			
C-68 rod				TE 390			
PCT (K)				-----			
Time (s)				-----			
C-77 rod	TE 391	TE 392	TE 393	TE 394	TE 395	TE 396	TE 397
PCT (K)	749.7	850.1	867.9	850.1	723.3	594.1	563.4
Time (s)	308.4	304.8	304.2	283.8	284.4	284.4	0.0
D-11 rod				TE 398			
PCT (K)				870.8			
Time (s)				279.6			
D-13 rod				TE 399			
PCT (K)				870.8			
Time (s)				273.0			
D-22 rod	TE 400	TE 401	TE 402	TE 403	TE 404	TE 405	TE 406
PCT (K)	756.2	855.7	881.1	869.8	752.5	615.2	563.8
Time (s)	289.2	287.4	286.8	284.4	283.8	283.8	0.0
D-31 rod				TE 407			
PCT (K)				-----			
Time (s)				-----			
D-33 rod				TE 408			
PCT (K)				-----			
Time (s)				-----			
D-51 rod				TE 409			
PCT (K)				-----			
Time (s)				-----			
D-53 rod				TE 410			
PCT (K)				-----			
Time (s)				-----			
D-66 rod				TE 411			
PCT (K)				-----			
Time (s)				-----			
D-77 rod				TE 412			
PCT (K)				856.7			
Time (s)				285.0			
D-86 rod				TE 413			
PCT (K)				863.2			
Time (s)				284.4			

Table 5.2 Maximum Cladding Temperature Distribution in the Core (Continued)

## \*\* Order of PCT \*\*

No. 1	A-22 rod	Pos. 3	PCT = 1003.9 (K)	Time = 291.6 (s)
No. 2	A-71 rod	Pos. 4	PCT = 998.8 (K)	Time = 284.4 (s)
No. 3	A-82 rod	Pos. 4	PCT = 996.9 (K)	Time = 285.6 (s)
No. 4	A-84 rod	Pos. 1	PCT = 996.9 (K)	Time = 285.6 (s)
No. 5	A-31 rod	Pos. 4	PCT = 991.0 (K)	Time = 284.4 (s)
No. 6	A-11 rod	Pos. 4	PCT = 979.9 (K)	Time = 285.6 (s)
No. 7	A-12 rod	Pos. 3	PCT = 978.7 (K)	Time = 291.0 (s)
No. 8	A-11 rod	Pos. 3	PCT = 975.1 (K)	Time = 284.4 (s)
No. 9	A-77 rod	Pos. 3	PCT = 973.0 (K)	Time = 289.8 (s)
No.10	A-13 rod	Pos. 3	PCT = 972.7 (K)	Time = 287.4 (s)

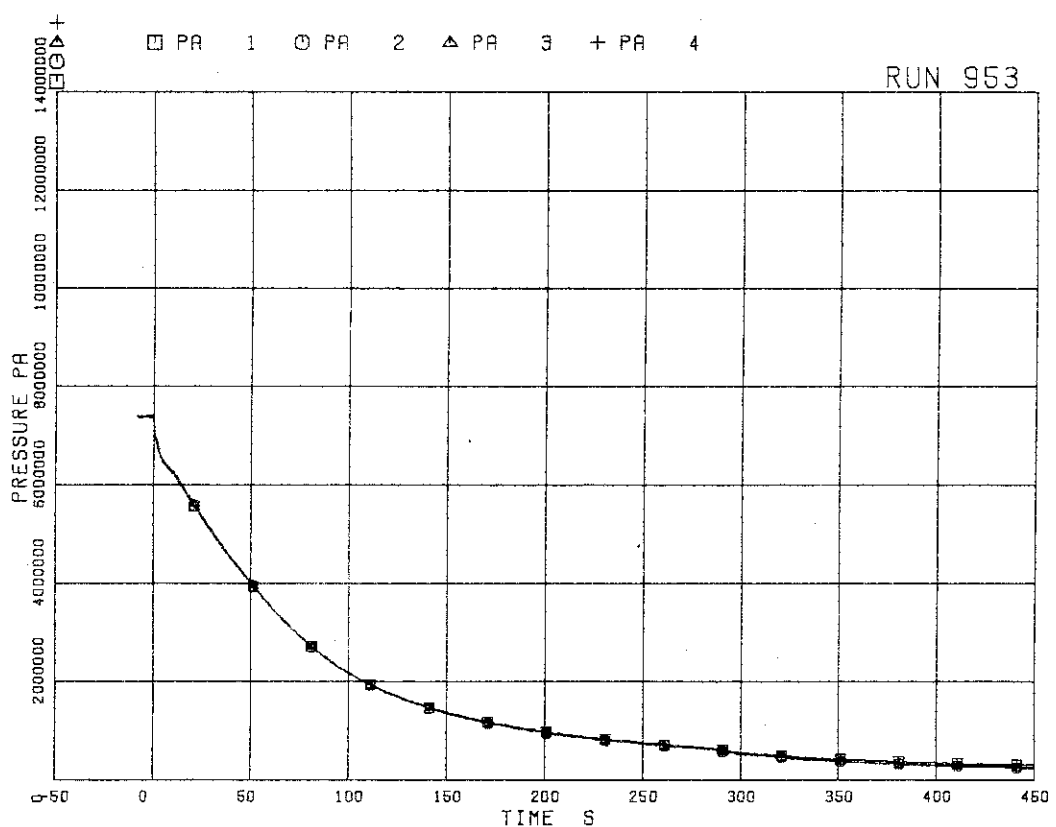


FIG.5. 1 PRESSURE IN PV (PRESSURE VESSEL)

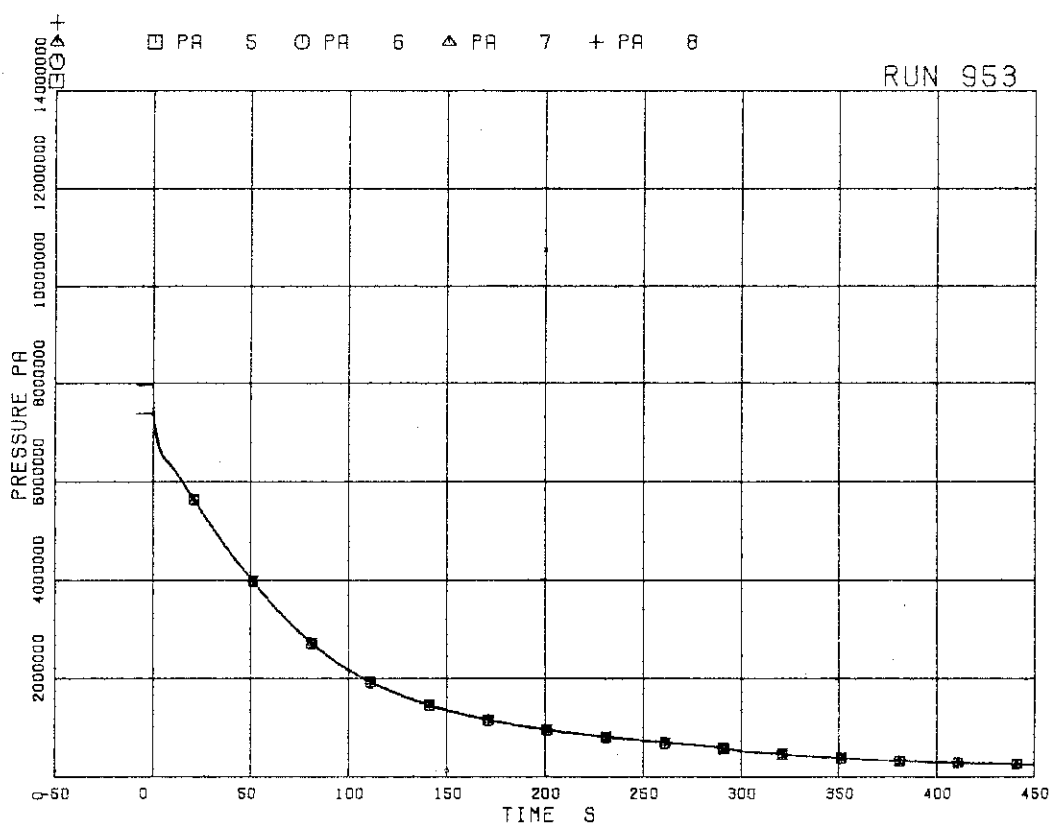


FIG.5. 2 PRESSURE IN RECIRC. LINE (JET PUMP)

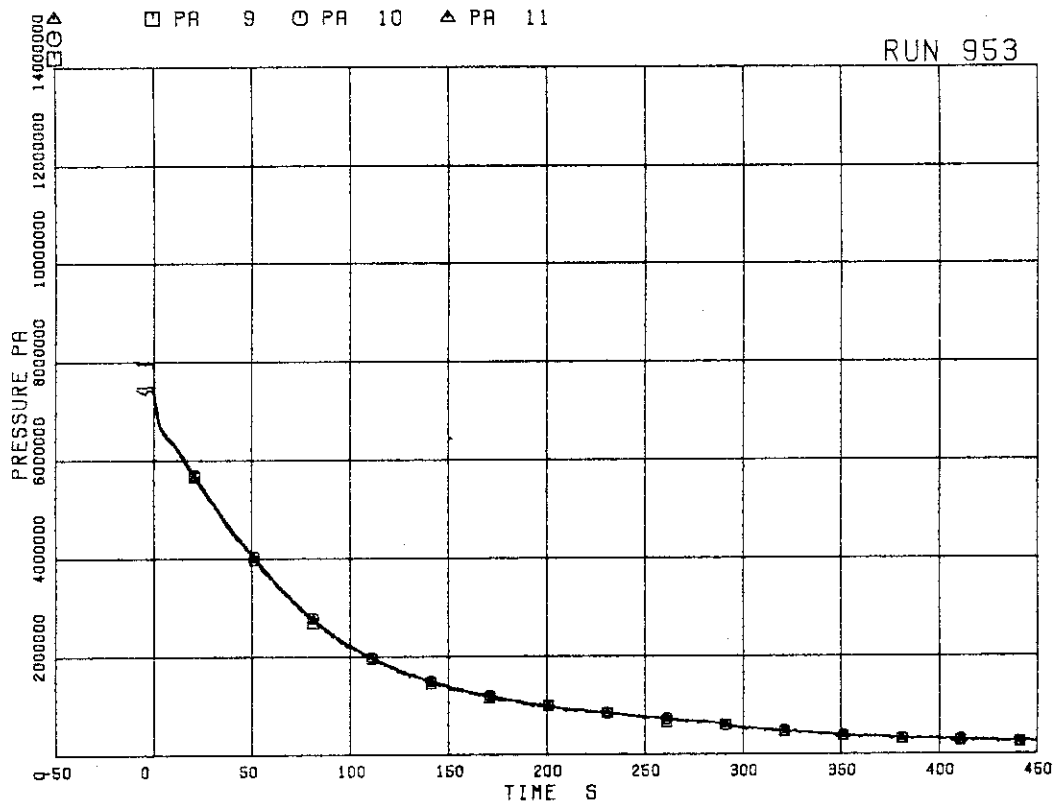


FIG. 5. 3 PRESSURE NEAR MRP-1 AND MRP-2  
(MAIN RECIRCULATION PUMP)

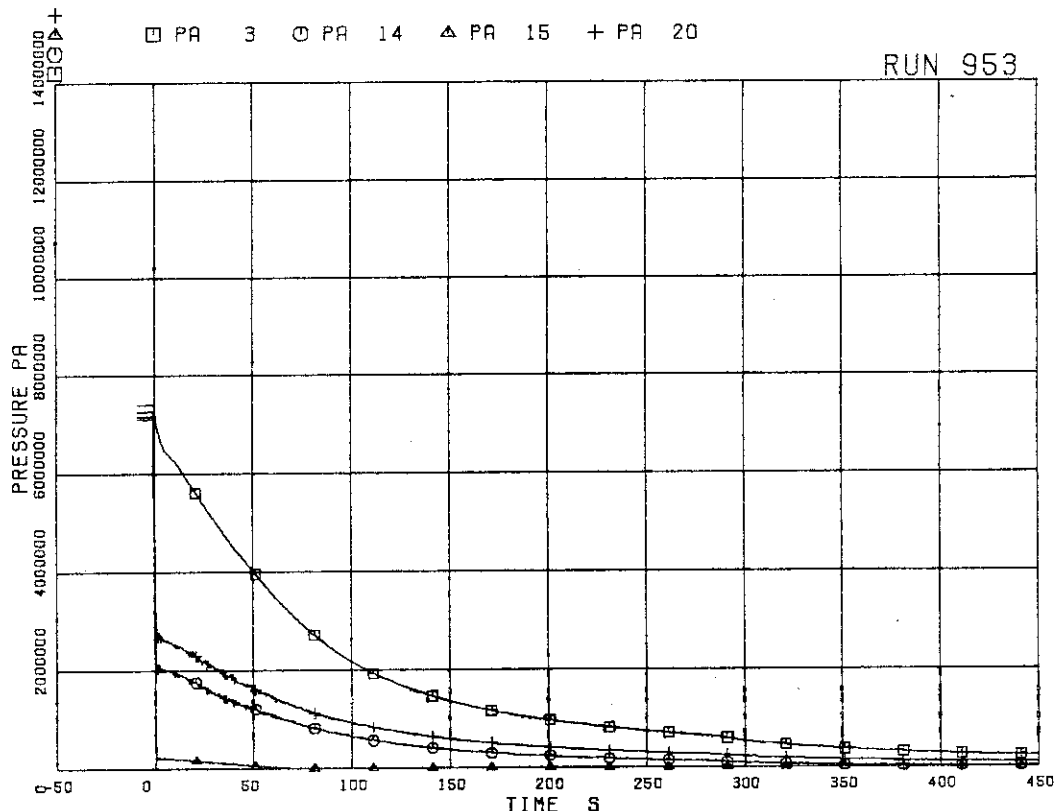


FIG. 5. 4 PRESSURE AT BREAK

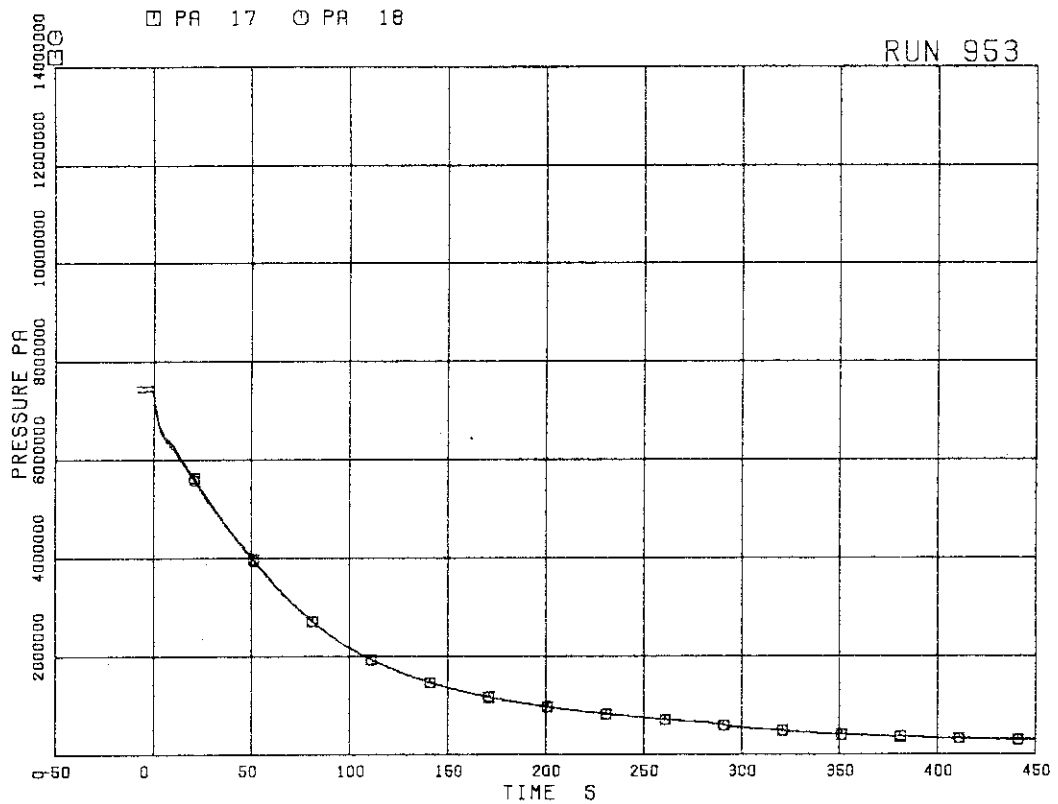


FIG. 5. 5 PRESSURE IN JP OUTLET SPOOL

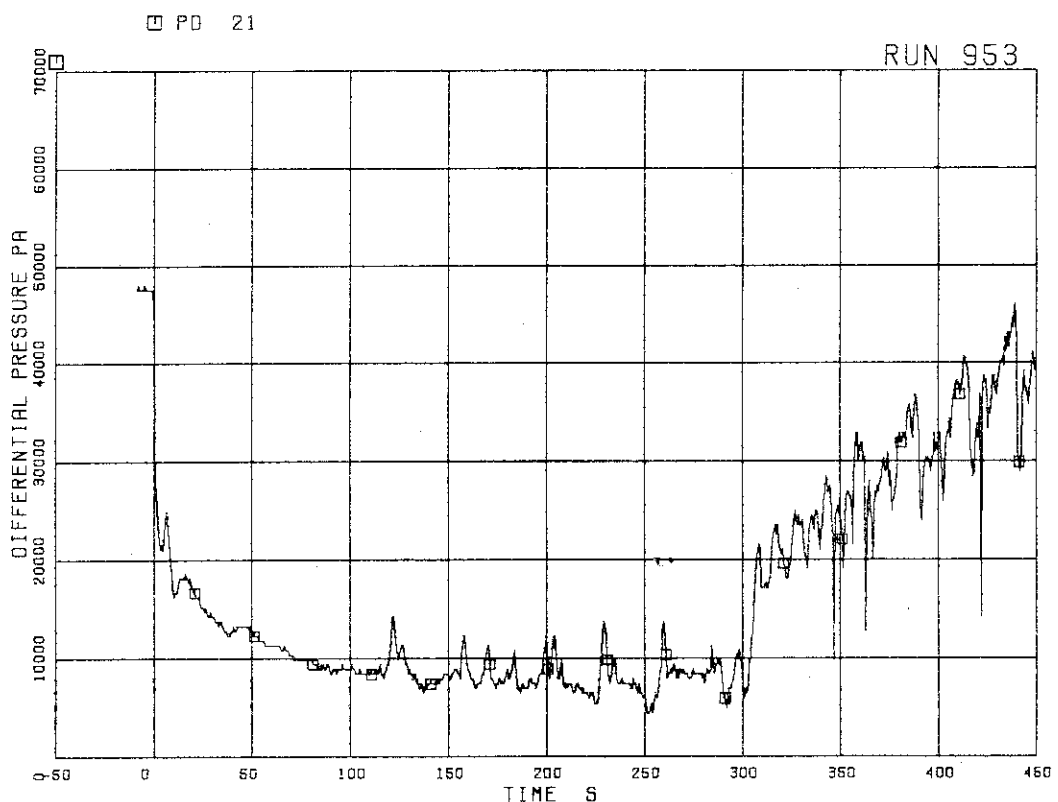


FIG. 5. 6 DIFFERENTIAL PRESSURE BETWEEN LOWER PLENUM AND UPPER PLENUM

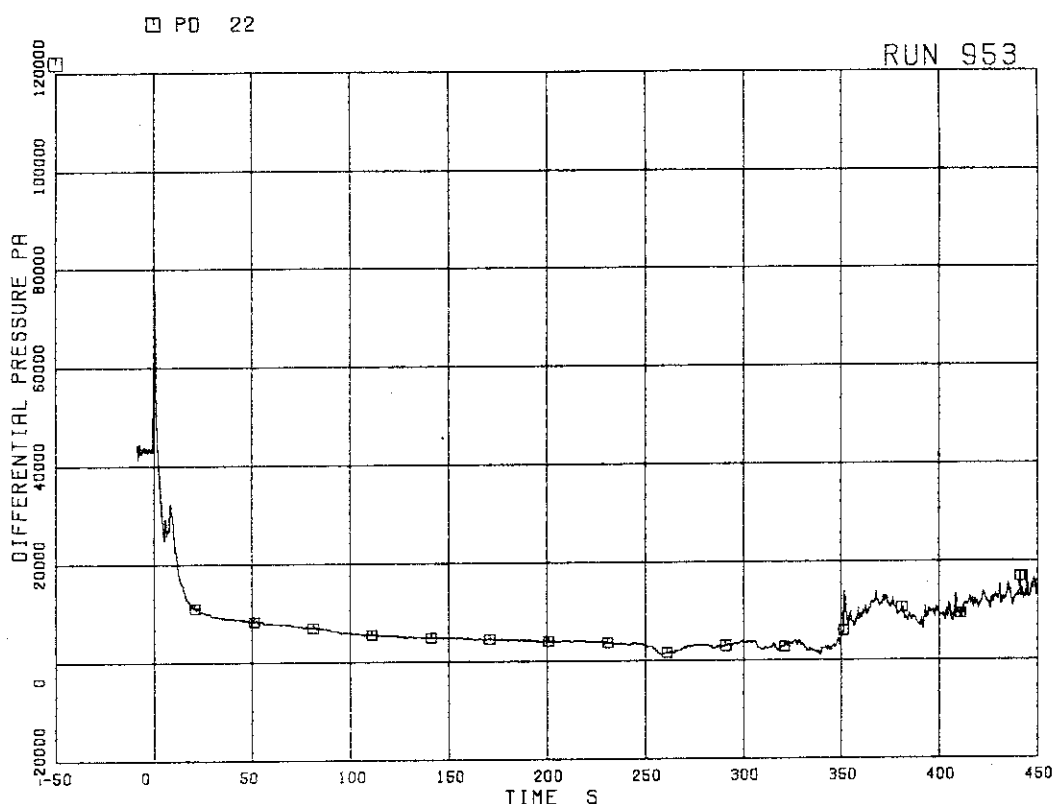


FIG. 5. 7 DIFFERENTIAL PRESSURE BETWEEN  
UPPER PLENUM AND STEAM DOME

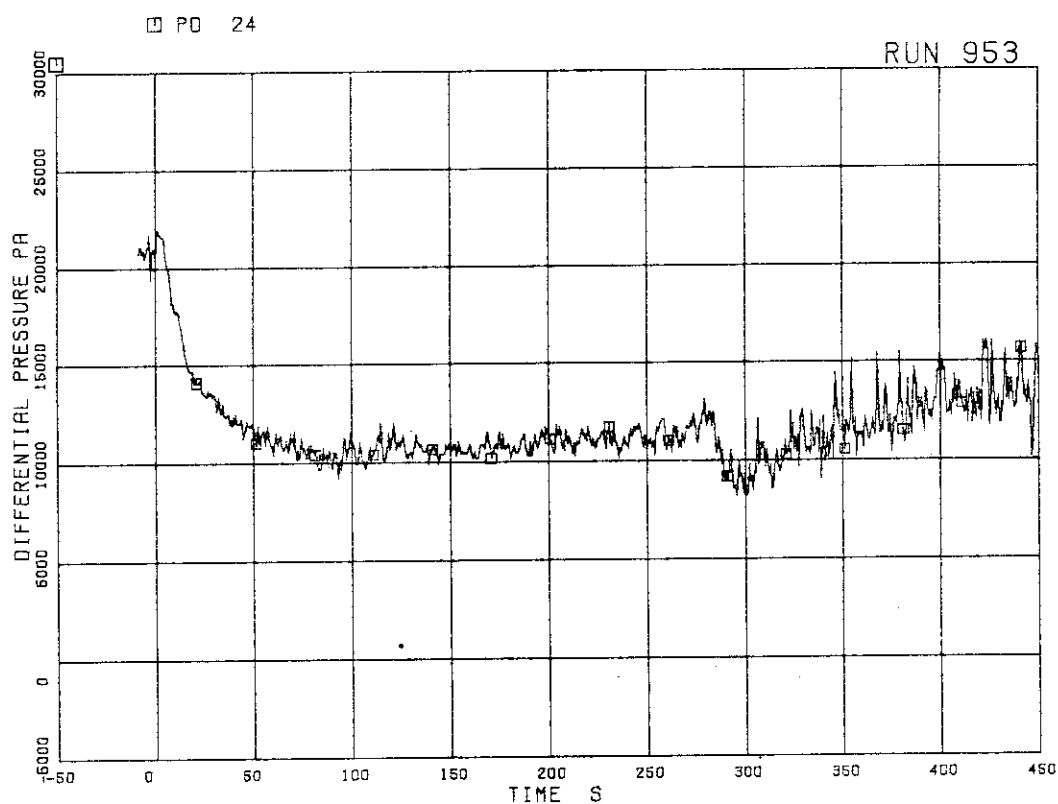
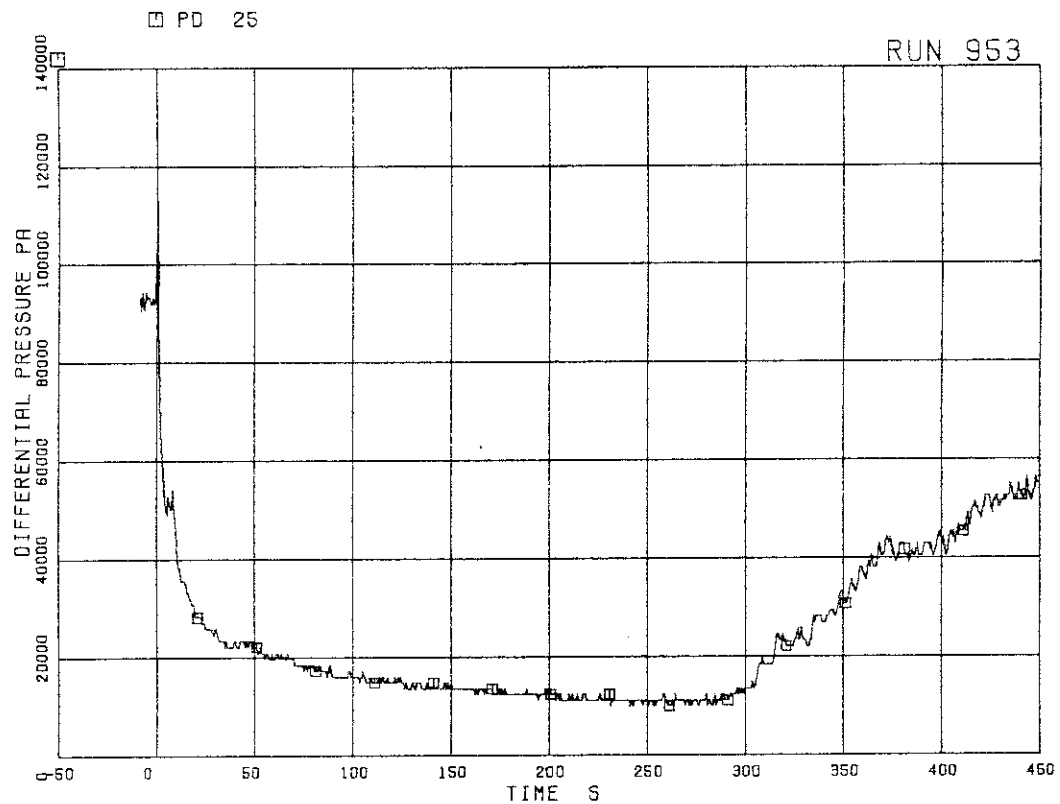
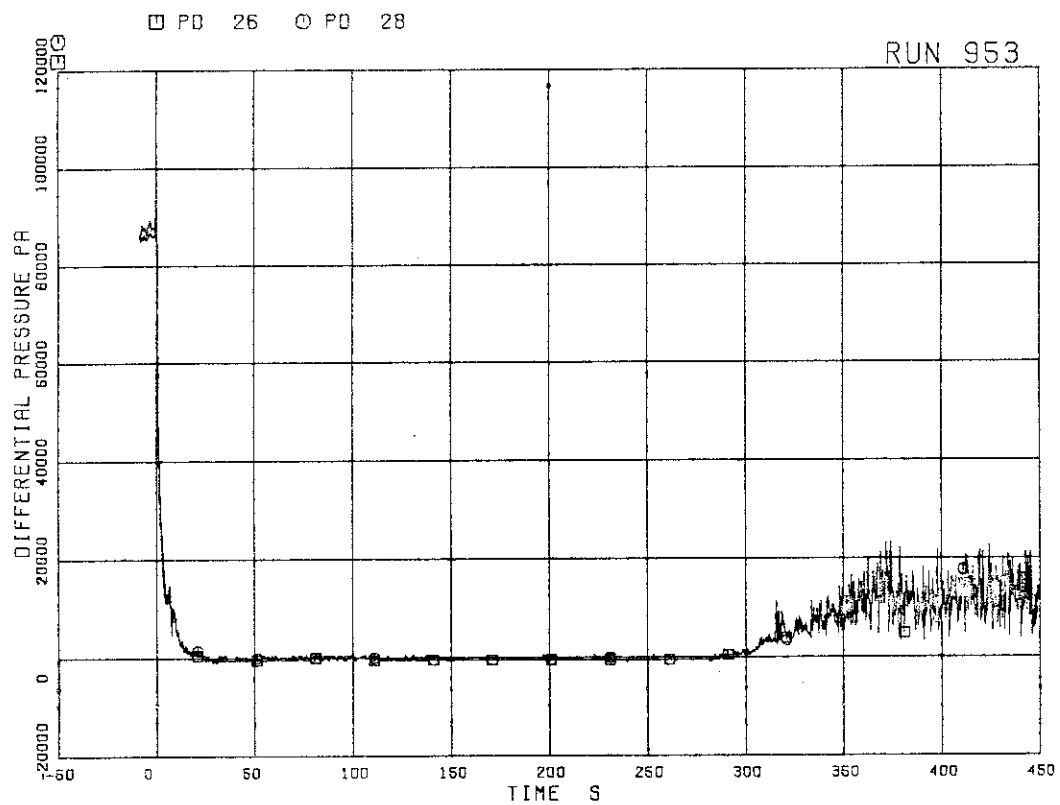


FIG. 5. 8 DC (DOWNCOMER) HEAD

FIG. 5. 9 DIFFERENTIAL PRESSURE BETWEEN  
PV BOTTOM AND TOPFIG. 5. 10 DIFFERENTIAL PRESSURE BETWEEN  
JP-1,2 DISCHARGE AND SUCTION

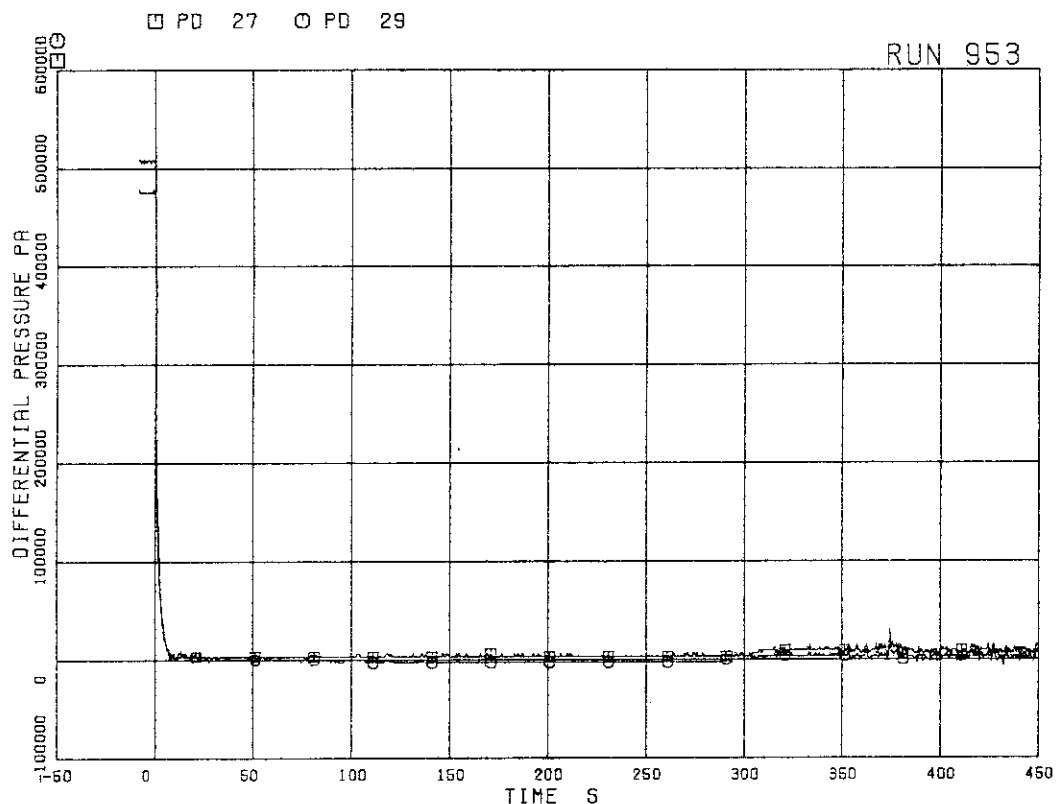


FIG. 5. 11 DIFFERENTIAL PRESSURE BETWEEN  
JP-1,2 DRIVE AND SUCTION

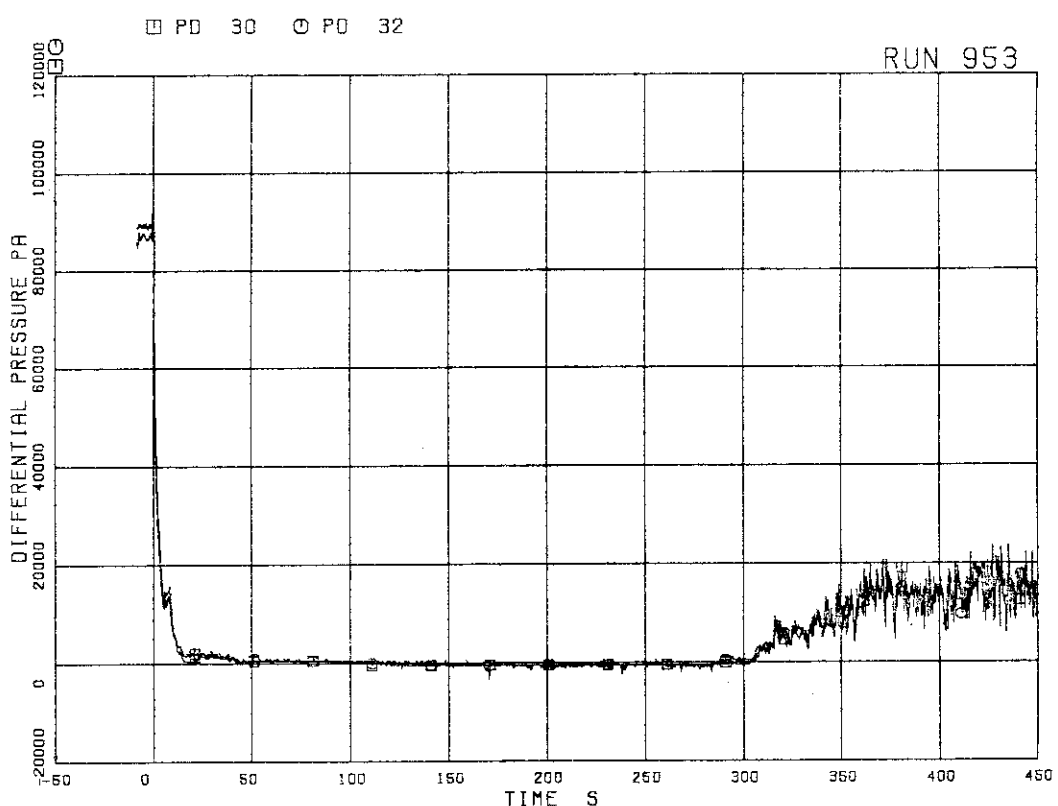


FIG. 5. 12 DIFFERENTIAL PRESSURE BETWEEN  
JP-3,4 DISCHARGE AND SUCTION

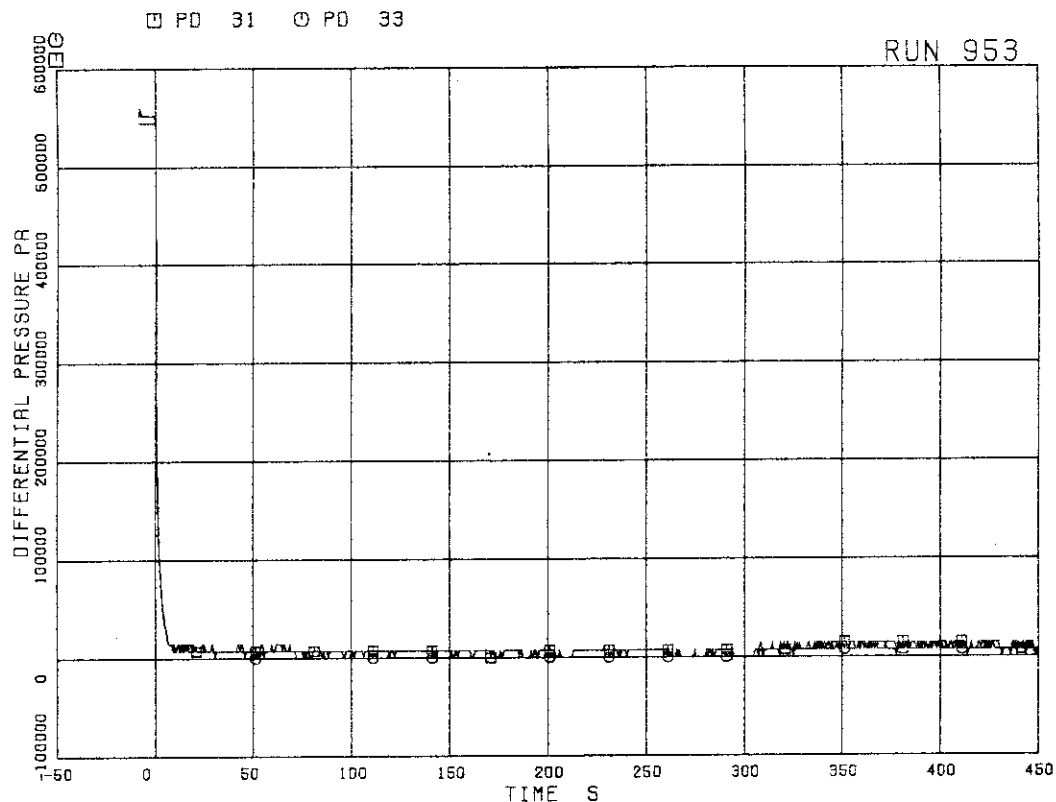


FIG. 5. 13 DIFFERENTIAL PRESSURE BETWEEN  
JP-3,4 DRIVE AND SUCTION

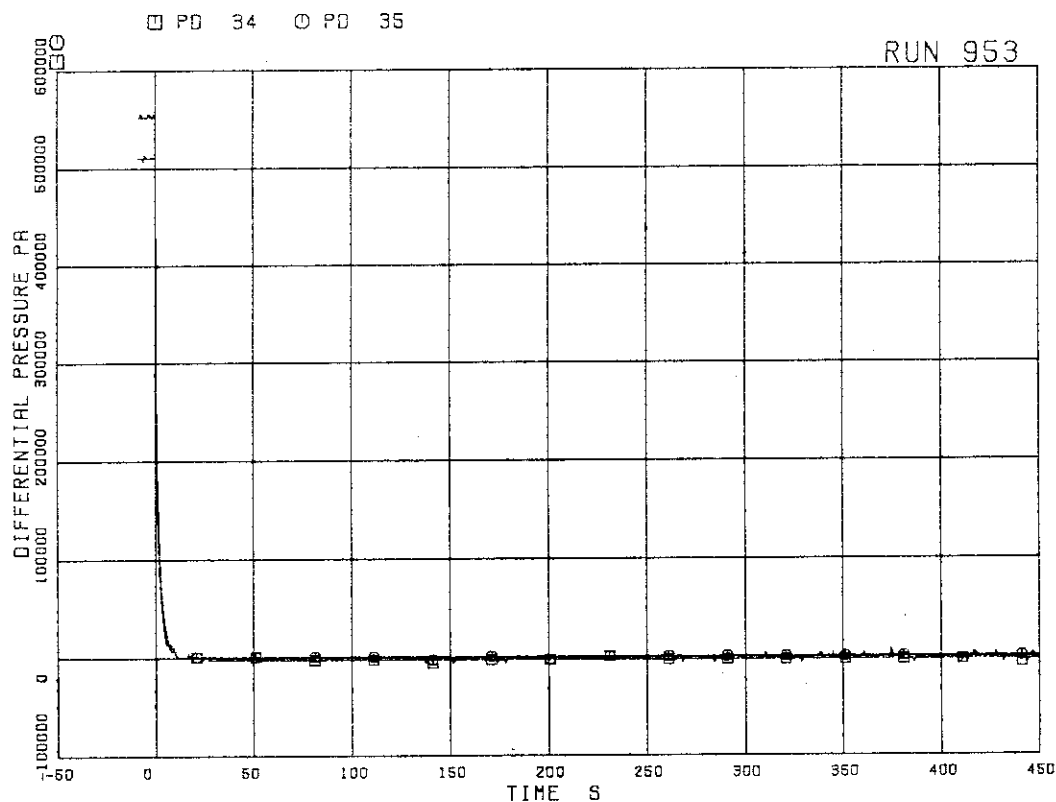


FIG. 5. 14 DIFFERENTIAL PRESSURE BETWEEN  
MRP DELIVERY AND SUCTION

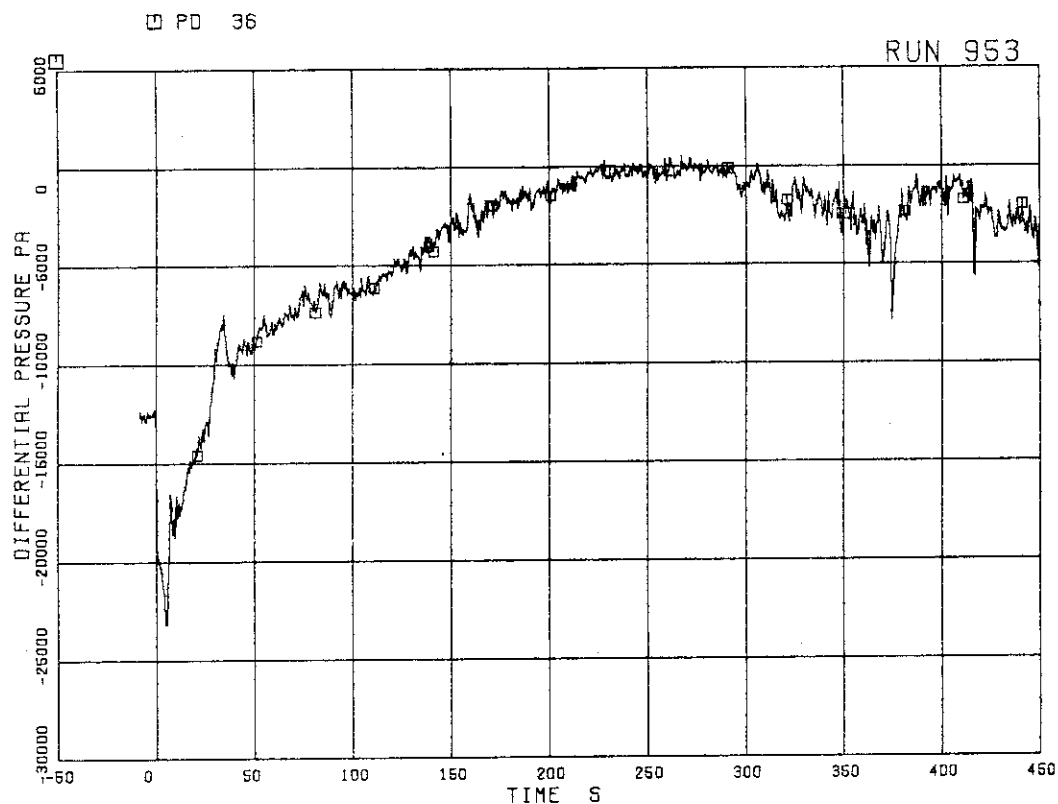


FIG. 5. 15 DIFFERENTIAL PRESSURE BETWEEN  
DOWNCOMER BOTTOM AND MRP1 SUCTION

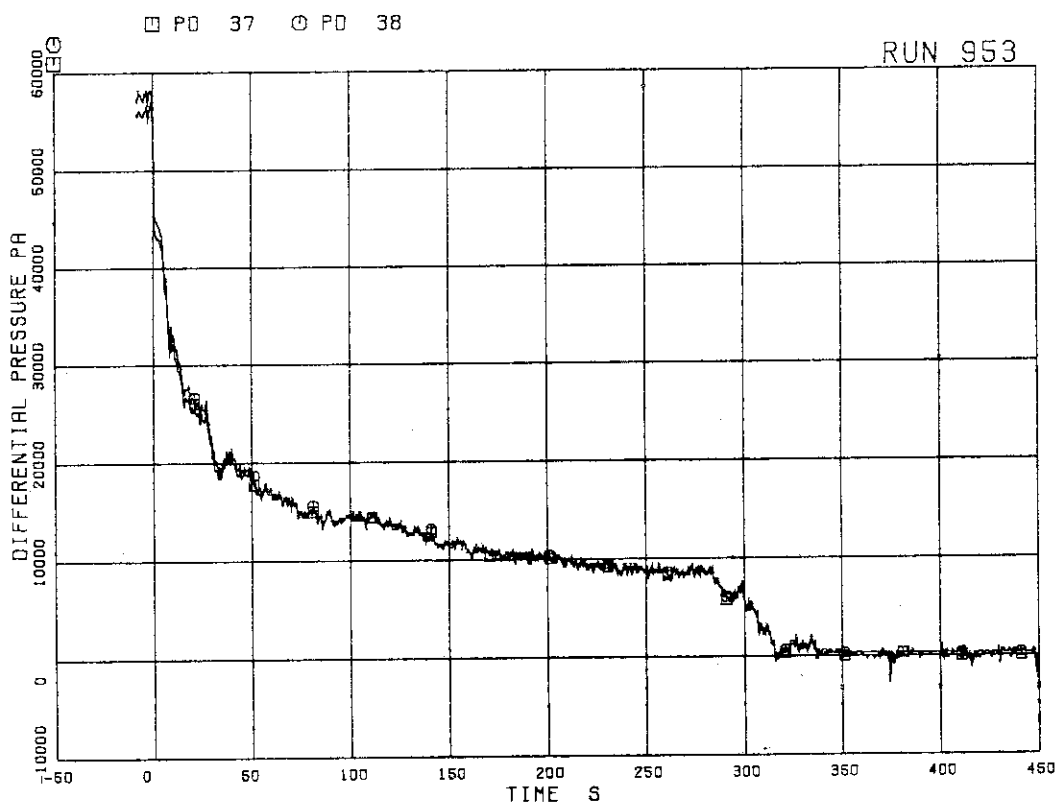


FIG. 5. 16 DIFFERENTIAL PRESSURE BETWEEN  
MRP DELIVERY AND JP-1.2 DRIVE

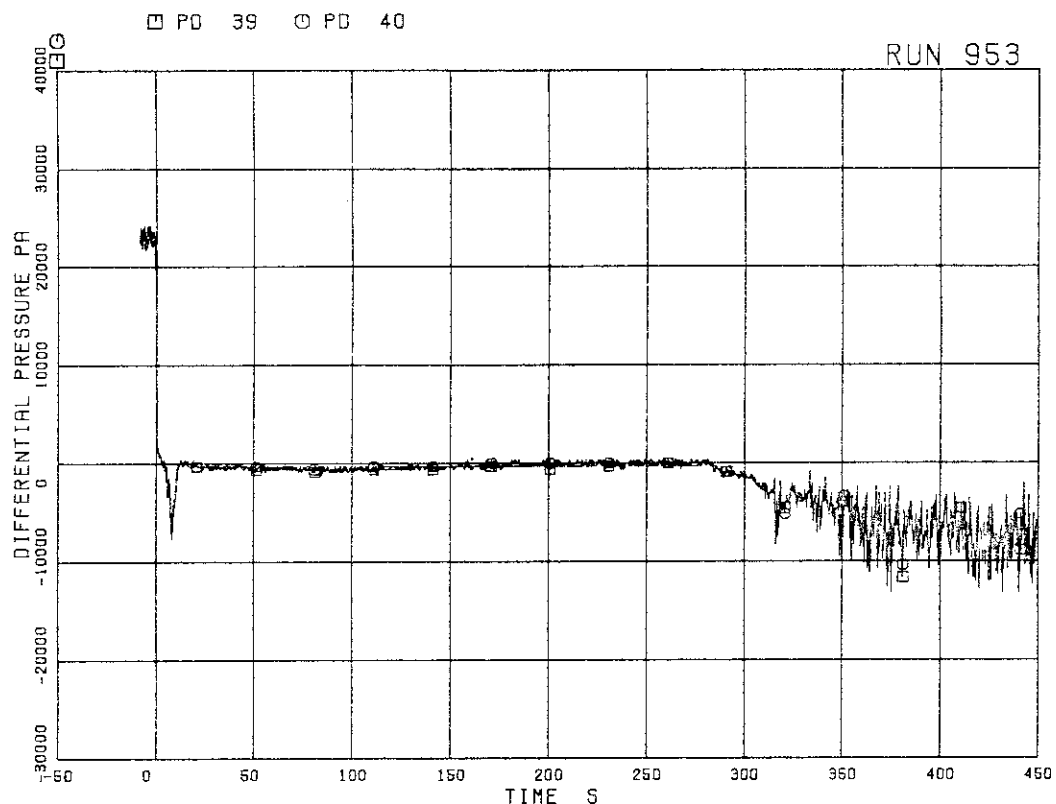


FIG. 5. 17 DIFFERENTIAL PRESSURE BETWEEN  
DOWNCOMER MIDDLE AND JP-1,2 SUCTION

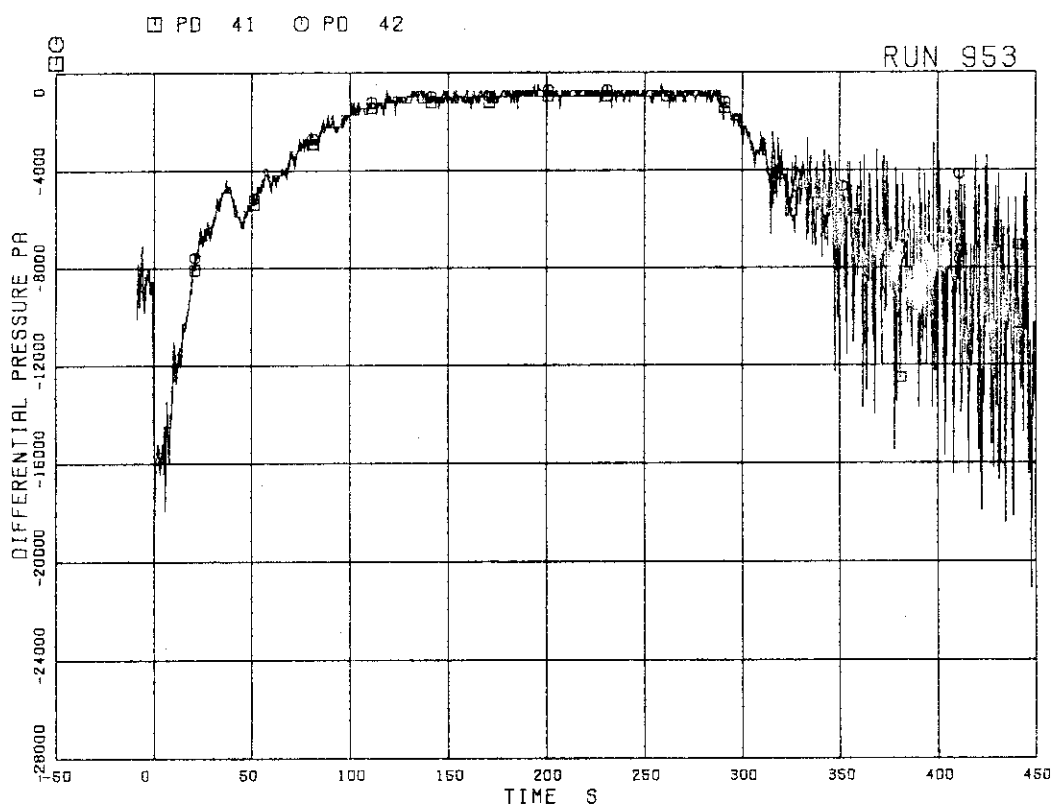


FIG. 5. 18 DIFFERENTIAL PRESSURE BETWEEN  
JP-1,2 DISCHARGE AND LOWER PLENUM

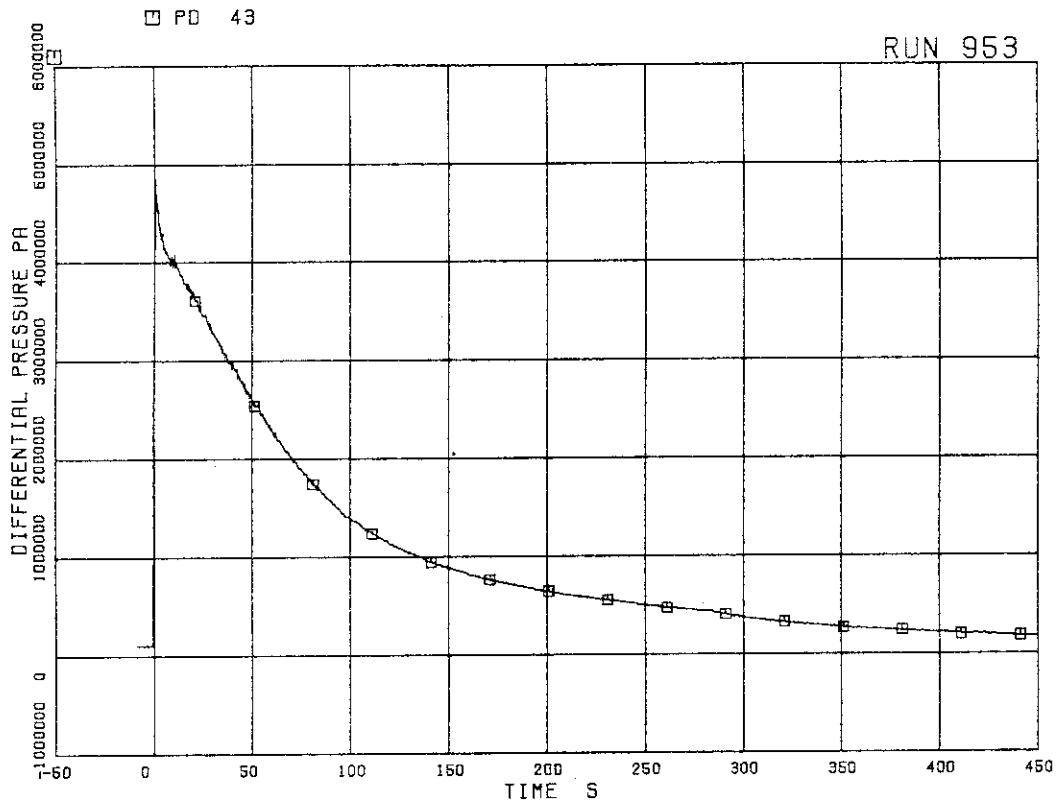


FIG. 5. 19 DIFFERENTIAL PRESSURE BETWEEN  
DOWNCOMER BOTTOM AND DOWNSTREAM OF BREAK

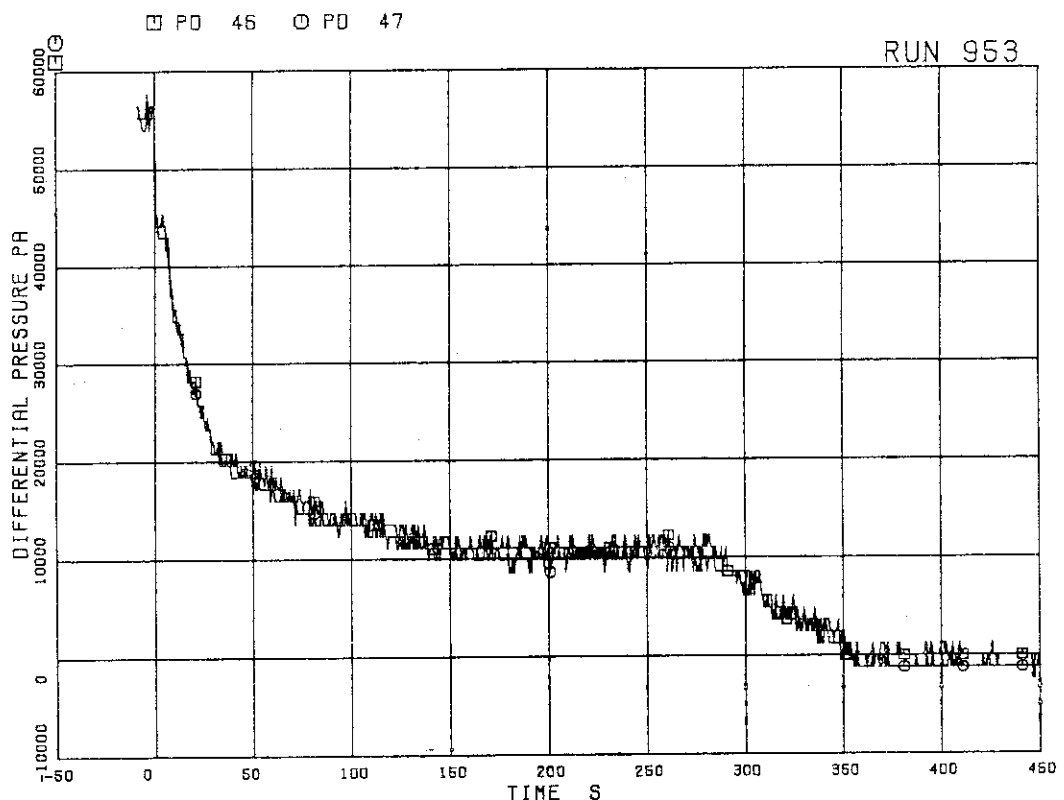


FIG. 5. 20 DIFFERENTIAL PRESSURE BETWEEN  
MRP DELIVERY AND JP-3,4 DRIVE

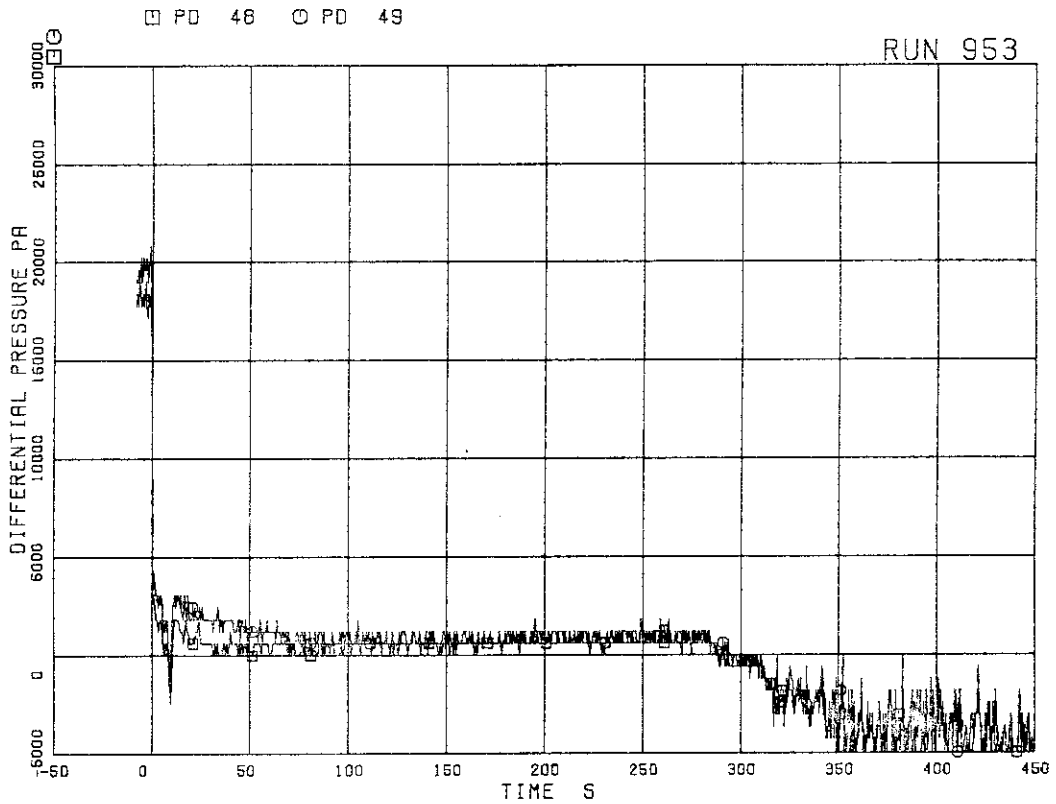


FIG. 5. 21 DIFFERENTIAL PRESSURE BETWEEN  
DOWNCOMER MIDDLE AND JP-3,4 SUCTION

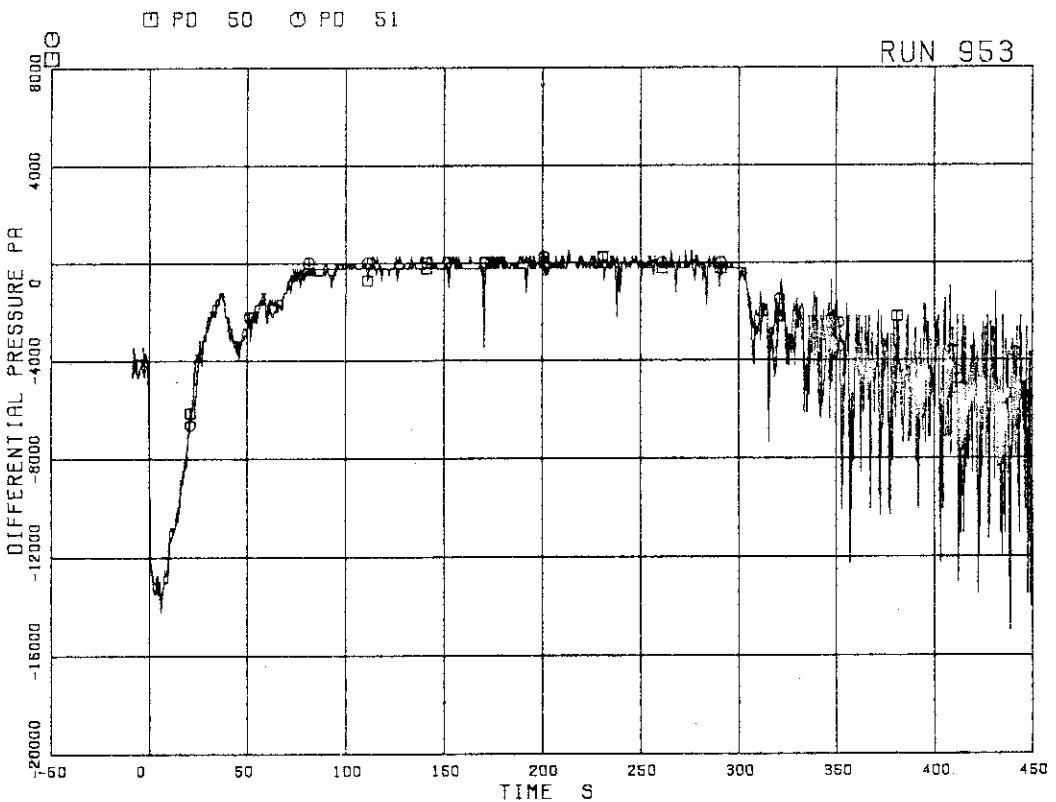
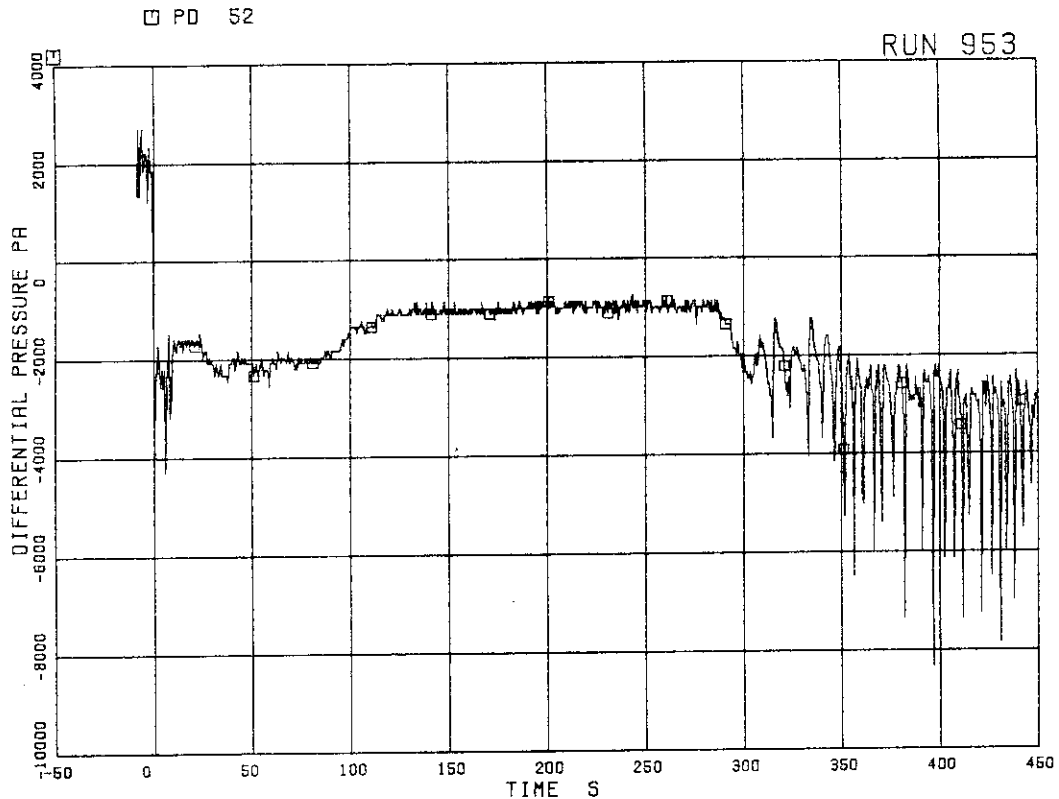
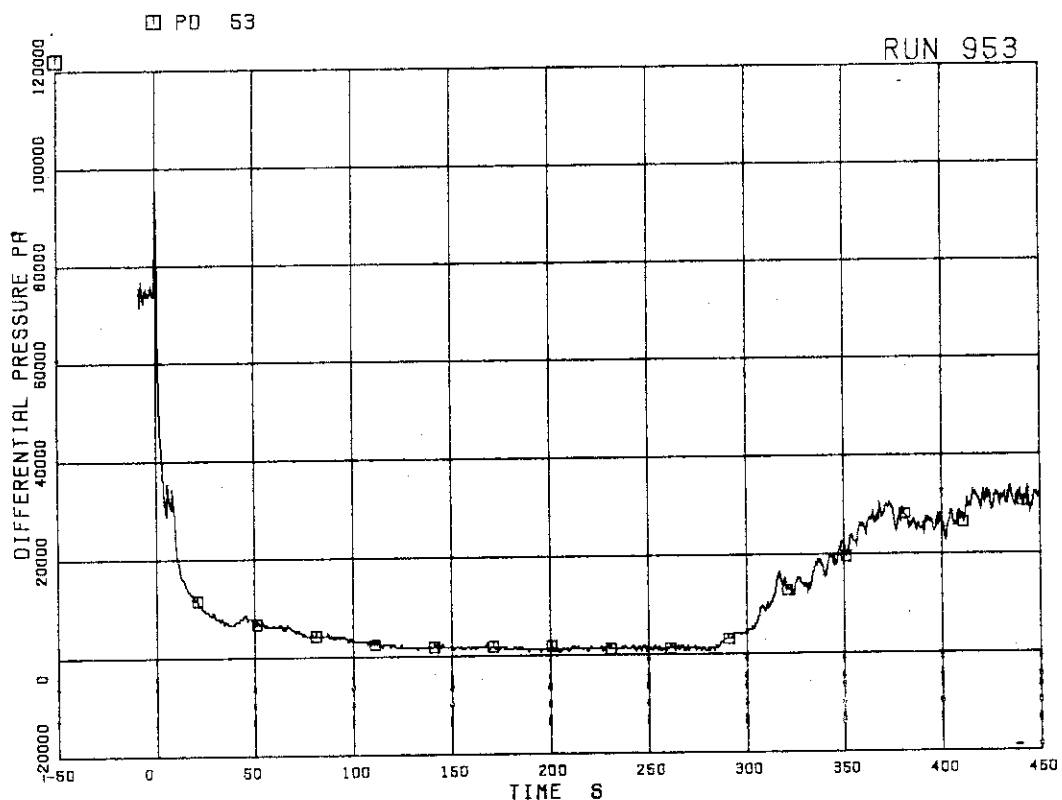


FIG. 5. 22 DIFFERENTIAL PRESSURE BETWEEN  
JP-3,4 DISCHARGE AND CONFLUENCE

FIG. 5. 23 DIFFERENTIAL PRESSURE BETWEEN  
JP-3,4 CONFLUENCE AND LPFIG. 5. 24 DIFFERENTIAL PRESSURE BETWEEN  
LOWER PLENUM AND DOWNCOMER MIDDLE

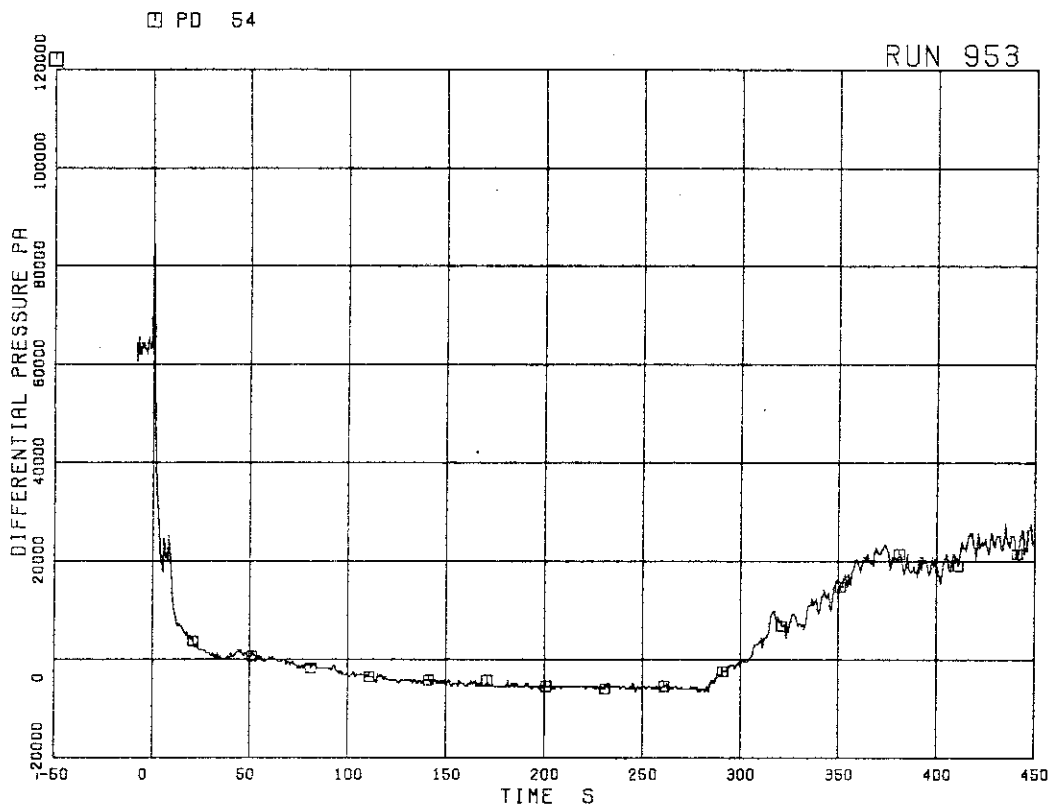


FIG. 5. 25 DIFFERENTIAL PRESSURE BETWEEN  
LOWER PLENUM AND DOWNCOMER (BOTTOM)

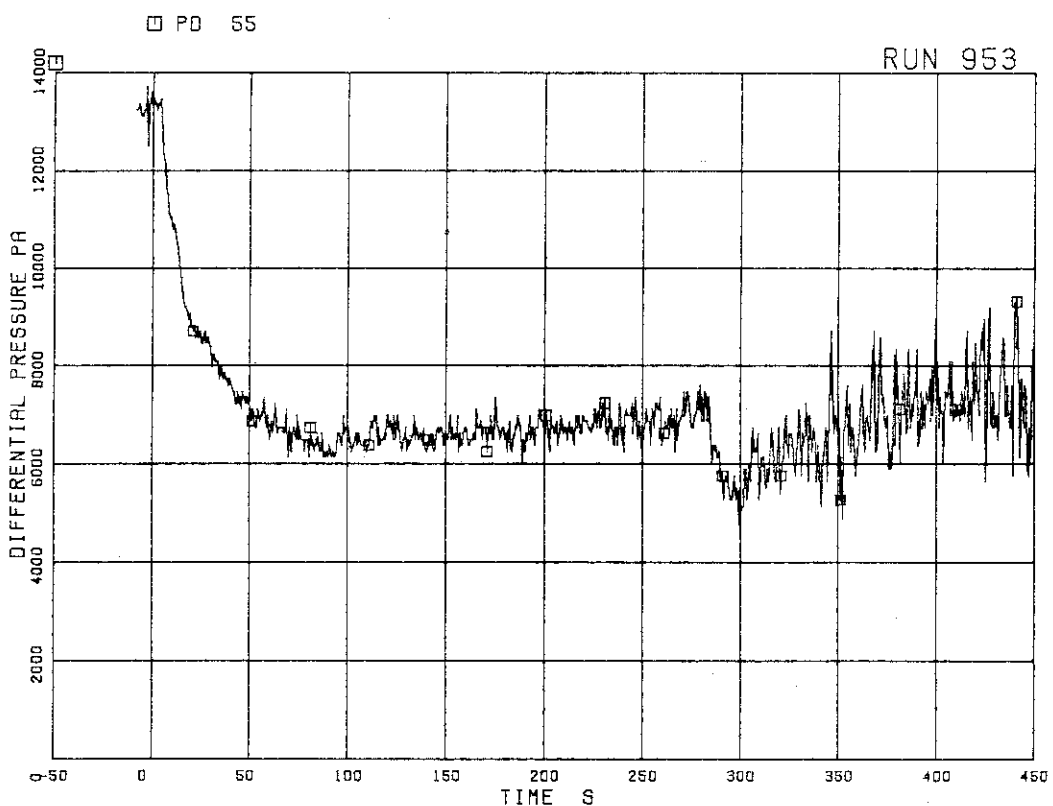
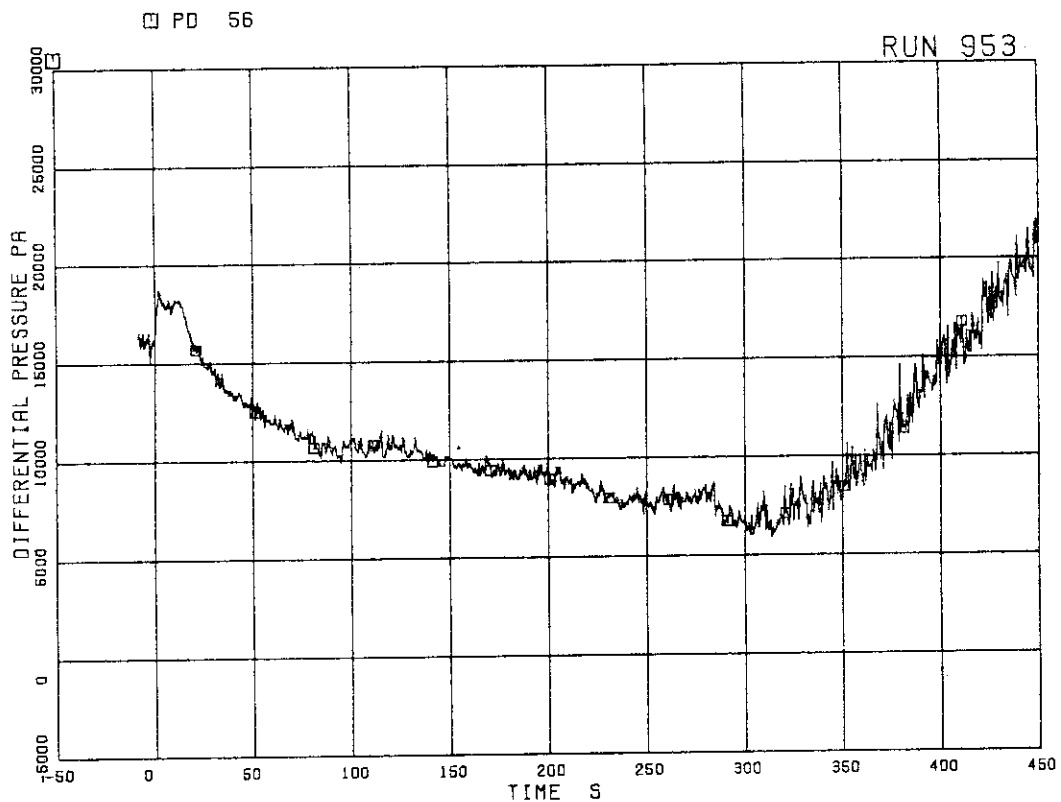
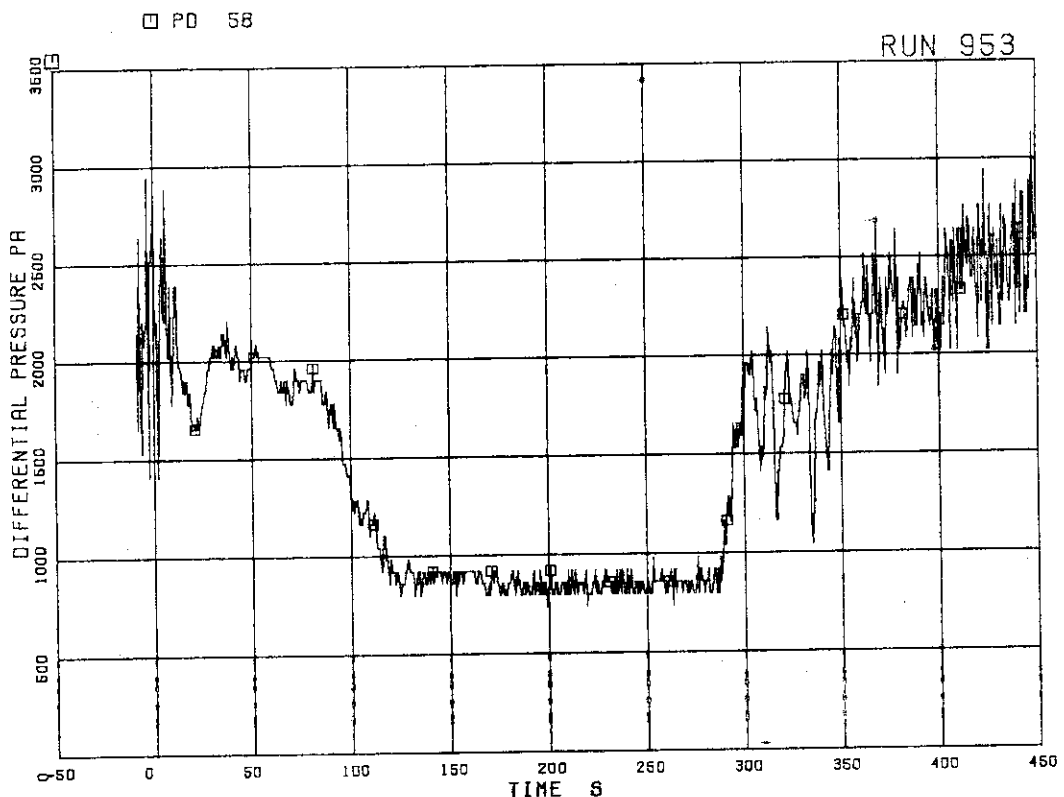


FIG. 5. 26 DIFFERENTIAL PRESSURE BETWEEN  
DOWNCOMER BOTTOM AND DOWNCOMER MIDDLE

FIG. 5. 27 DIFFERENTIAL PRESSURE BETWEEN  
DOWNCOMER MIDDLE AND STEAM DOMEFIG. 5. 28 DIFFERENTIAL PRESSURE BETWEEN  
LP BOTTOM AND LP MIDDLE

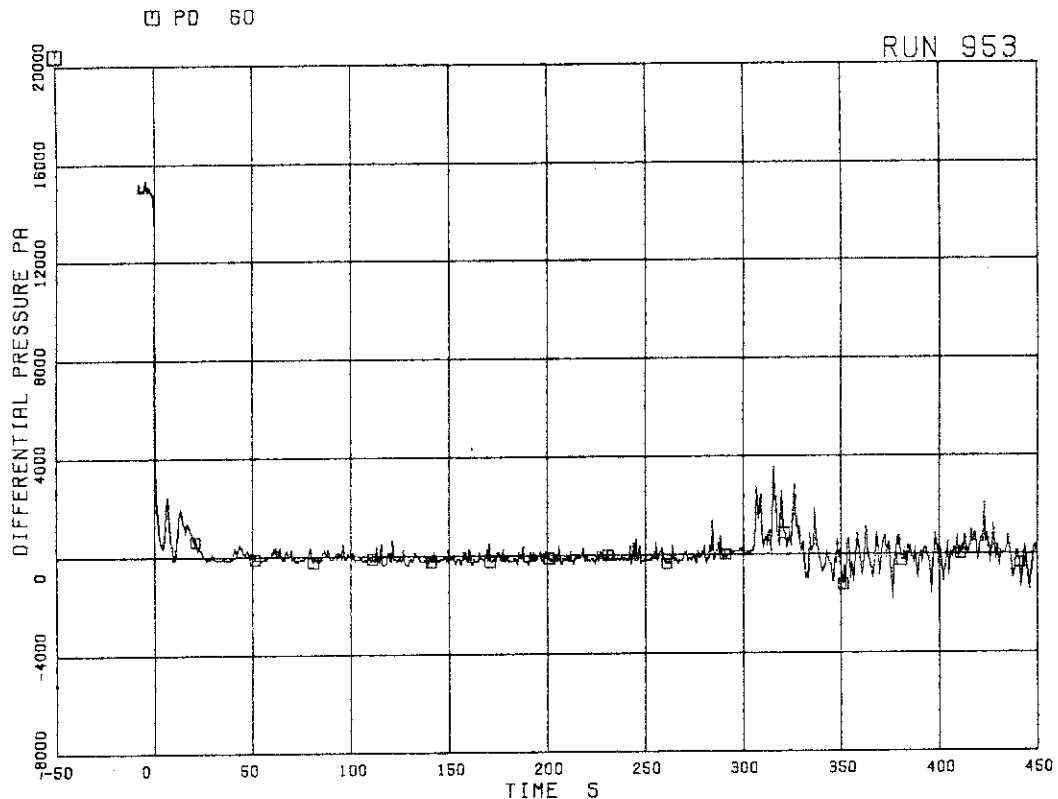


FIG. 5. 29 DIFFERENTIAL PRESSURE ACROSS  
CHANNEL INLET ORIFICE A

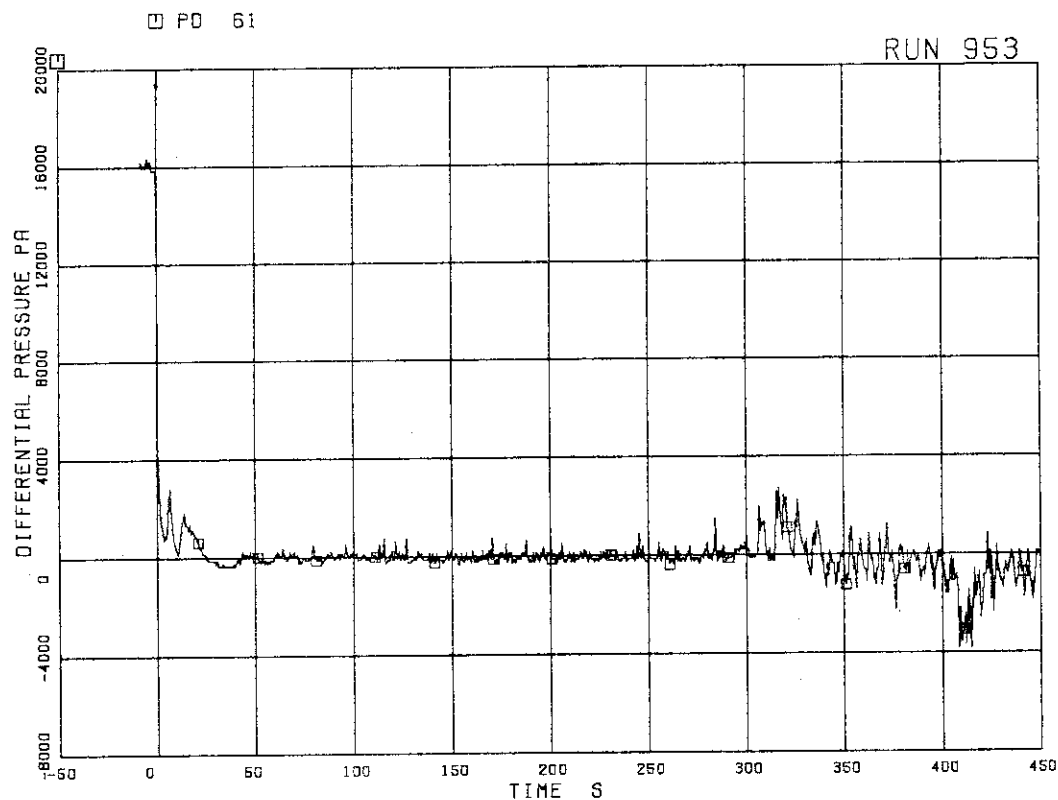


FIG. 5. 30 DIFFERENTIAL PRESSURE ACROSS  
CHANNEL INLET ORIFICE B

□ PD 62

RUN 953

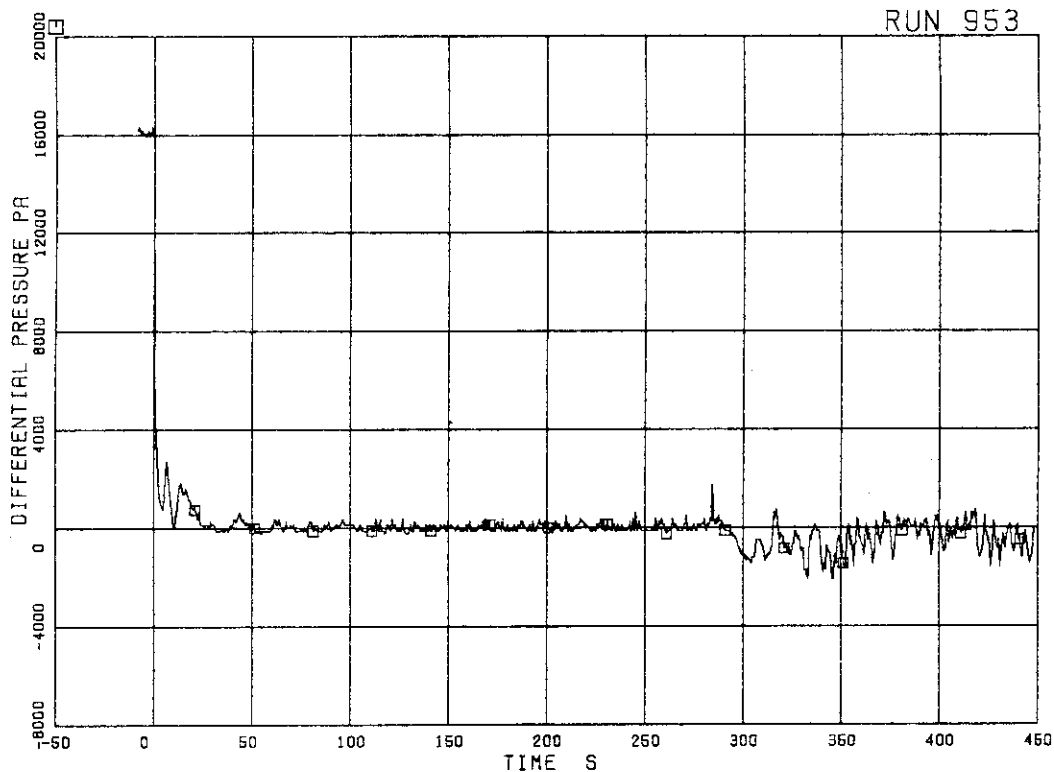


FIG. 5. 31 DIFFERENTIAL PRESSURE ACROSS CHANNEL INLET ORIFICE C

□ PD 63

RUN 953

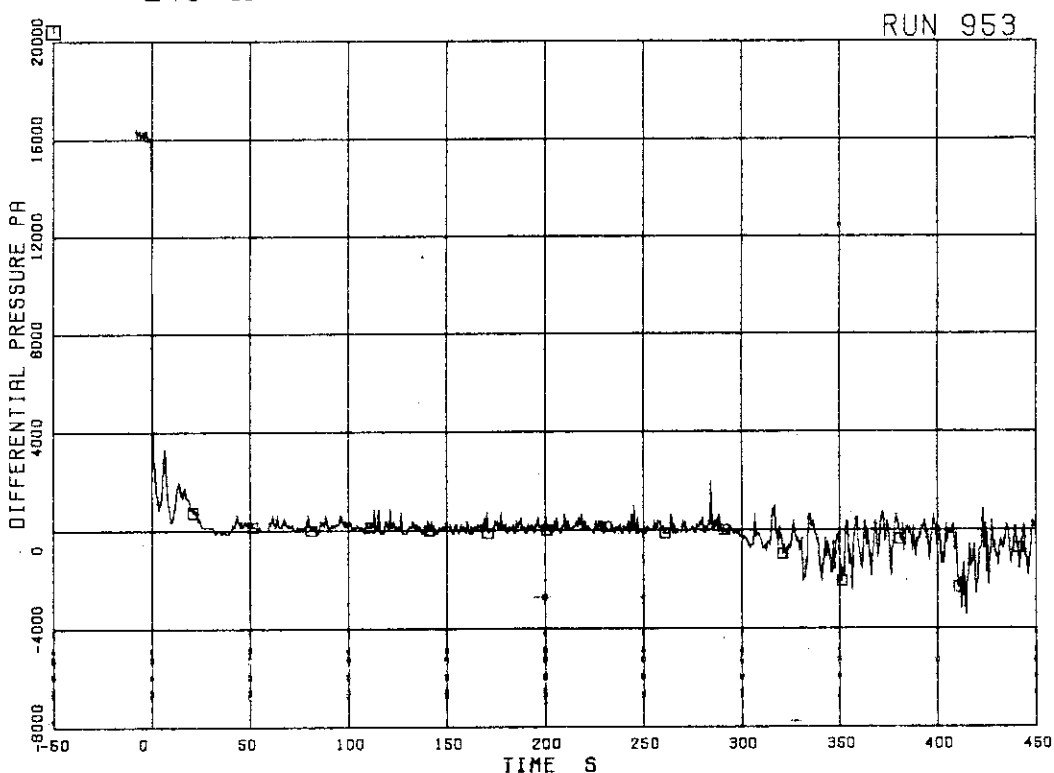


FIG. 5. 32 DIFFERENTIAL PRESSURE ACROSS CHANNEL INLET ORIFICE D

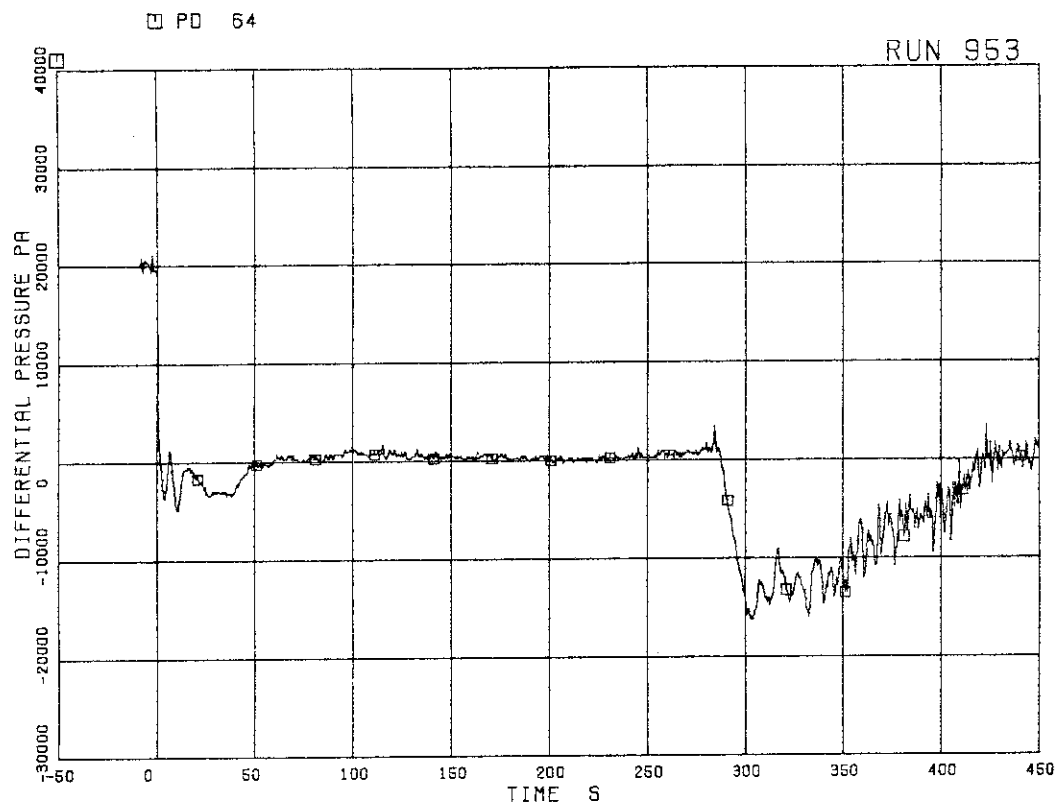


FIG. 5. 33 DIFFERENTIAL PRESSURE ACROSS BYPASS HOLE

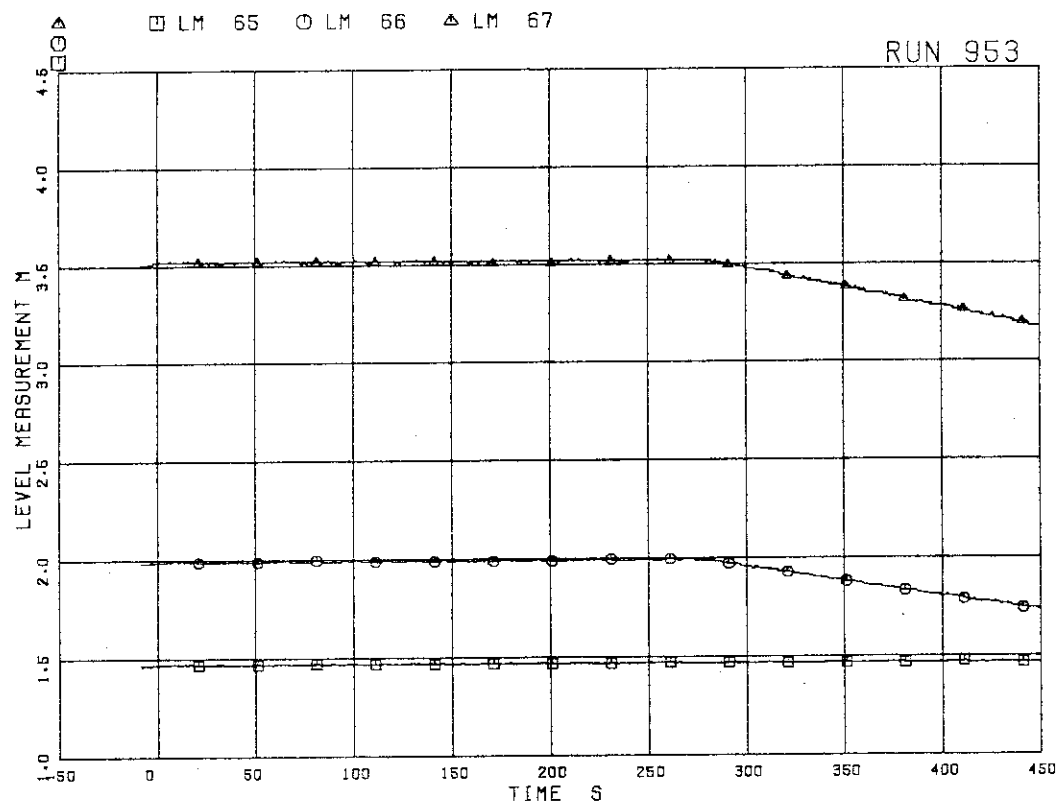


FIG. 5. 34 LIQUID LEVELS IN ECCS TANKS

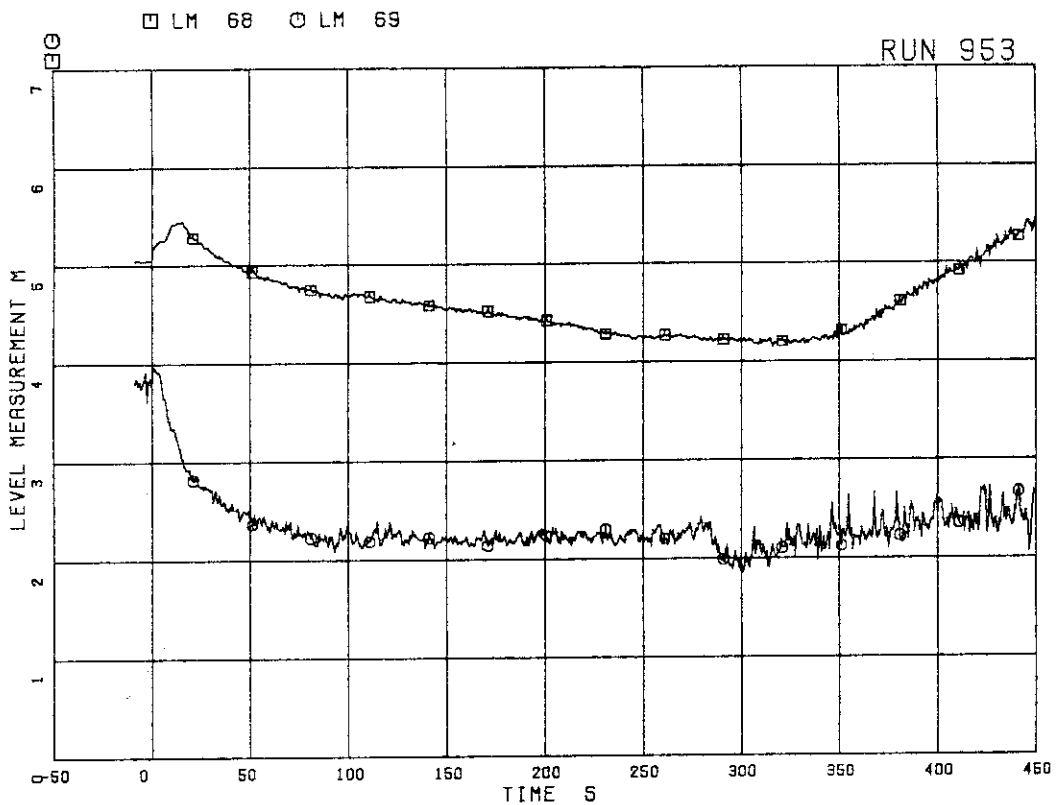


FIG. 5. 35 LIQUID LEVELS IN UPPER AND LOWER DOWNCOM

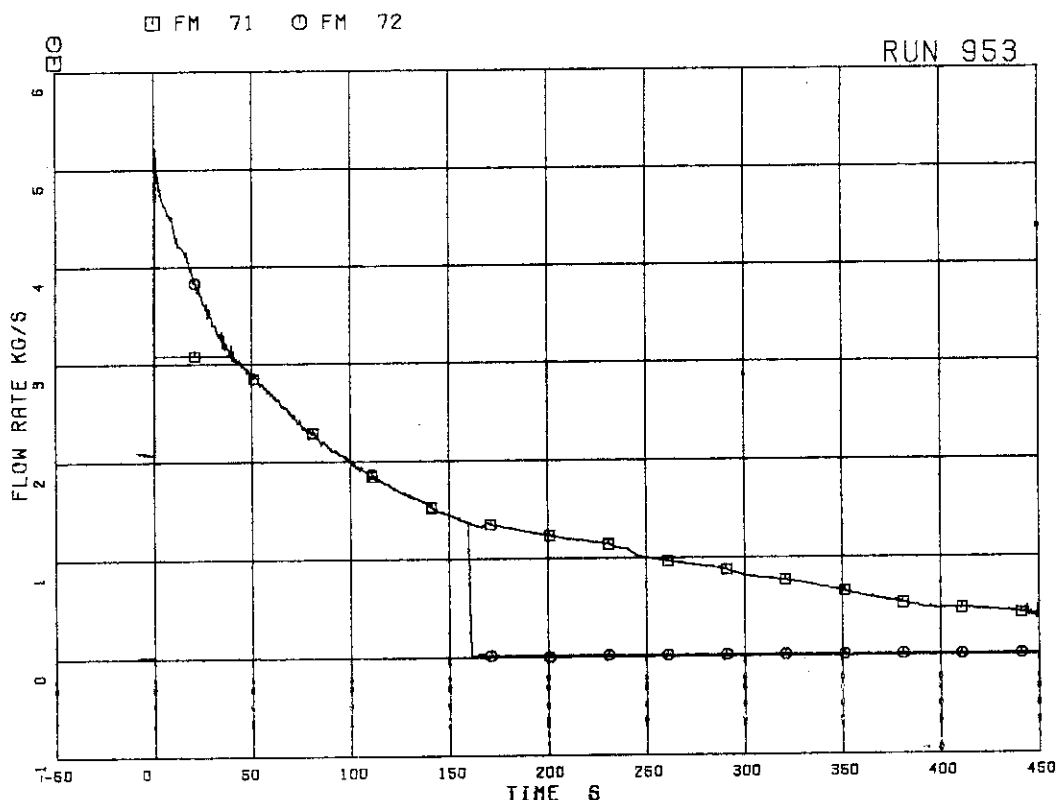


FIG. 5. 36 MASS FLOW RATE IN MSL

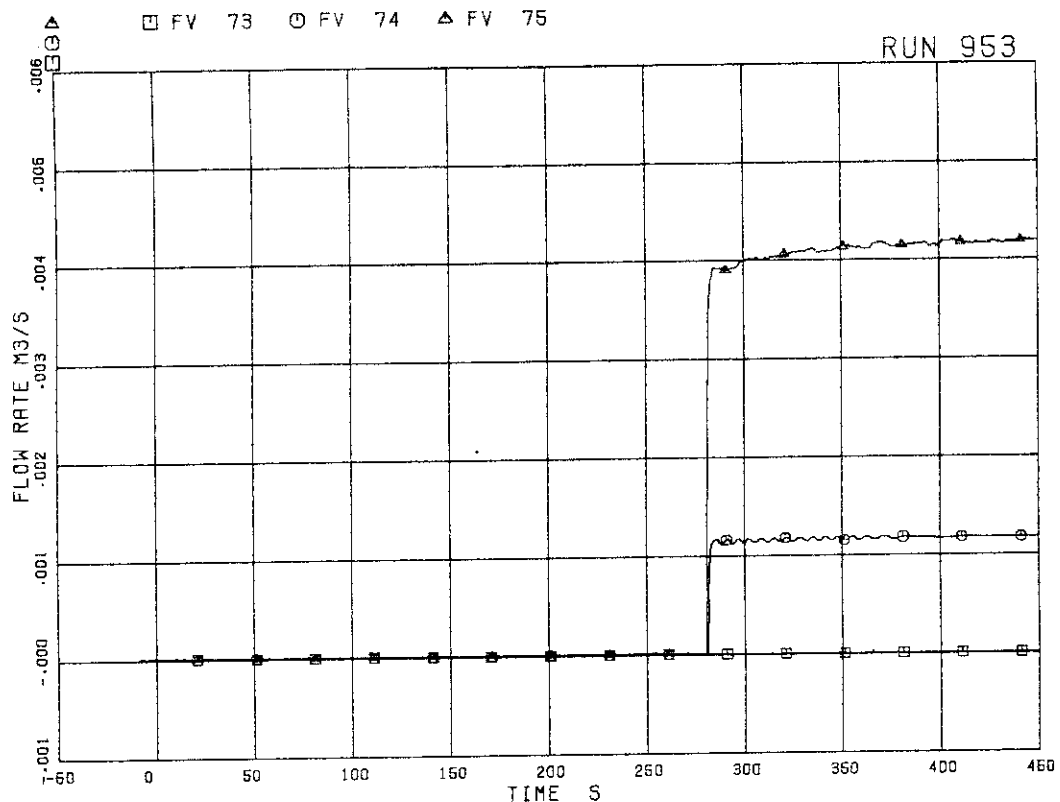


FIG. 5. 37 ECC INJECTION FLOW RATE

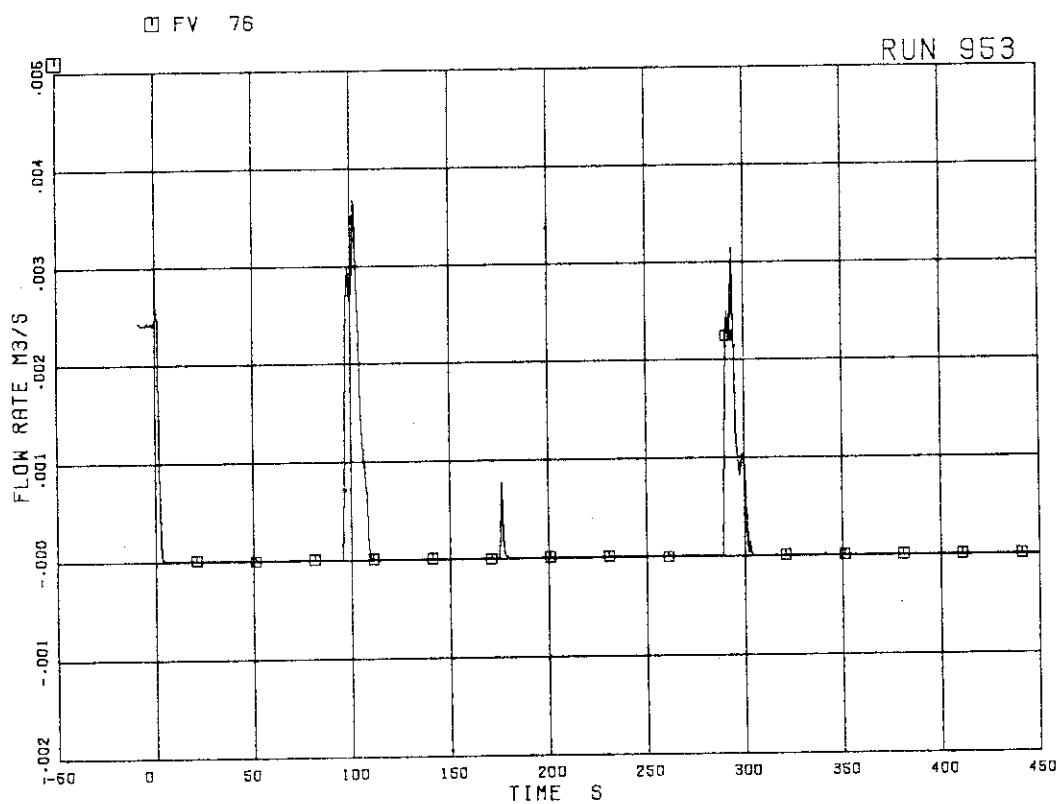


FIG. 5. 38 FEEDWATER FLOW RATE

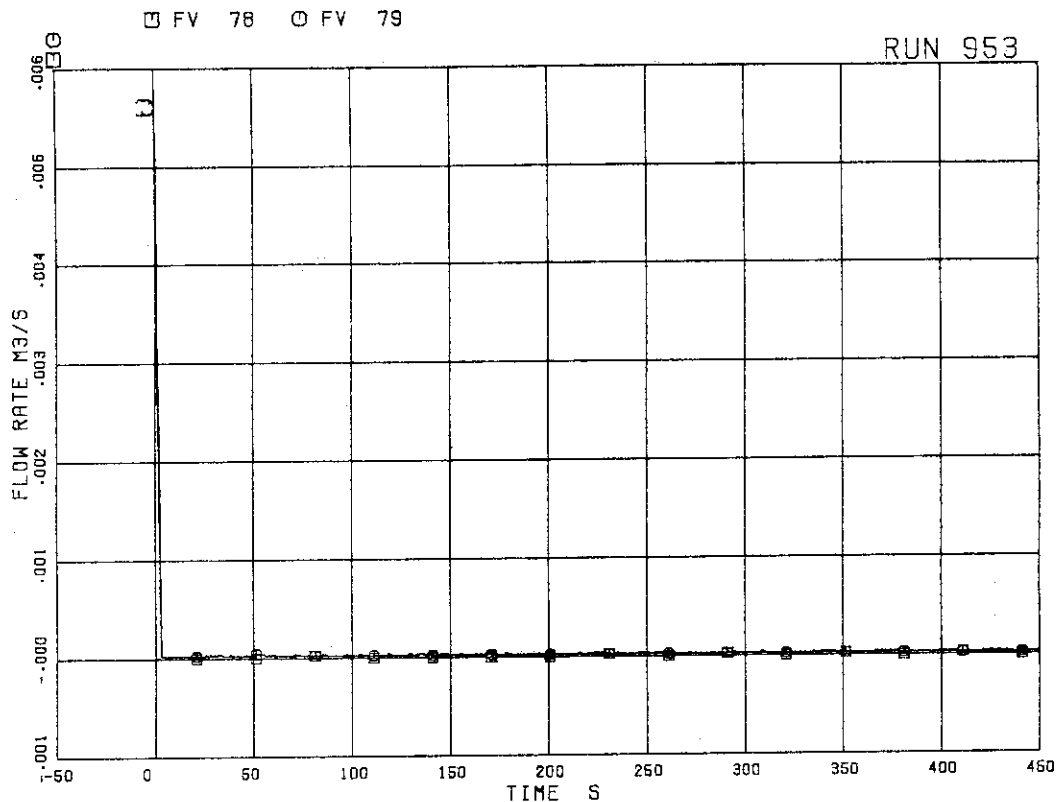


FIG. 5. 39 JP-1,2 DISCHARGE FLOW RATE

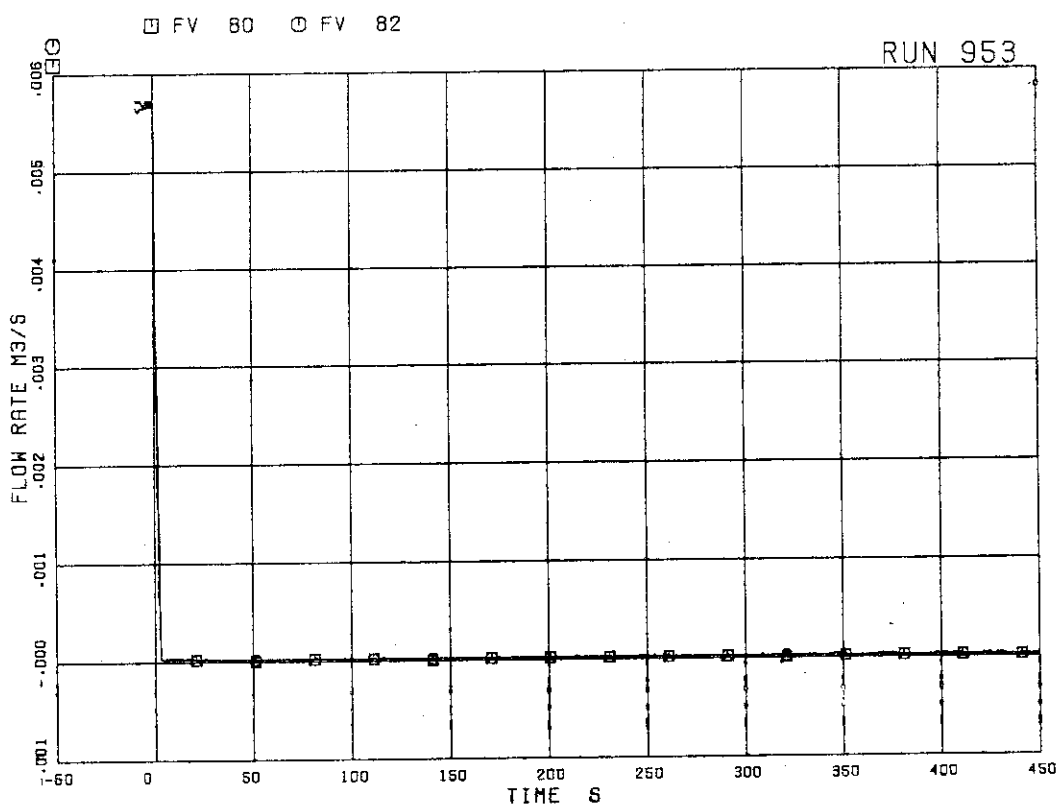


FIG. 5. 40 JP-3,4 DISCHARGE FLOW RATE

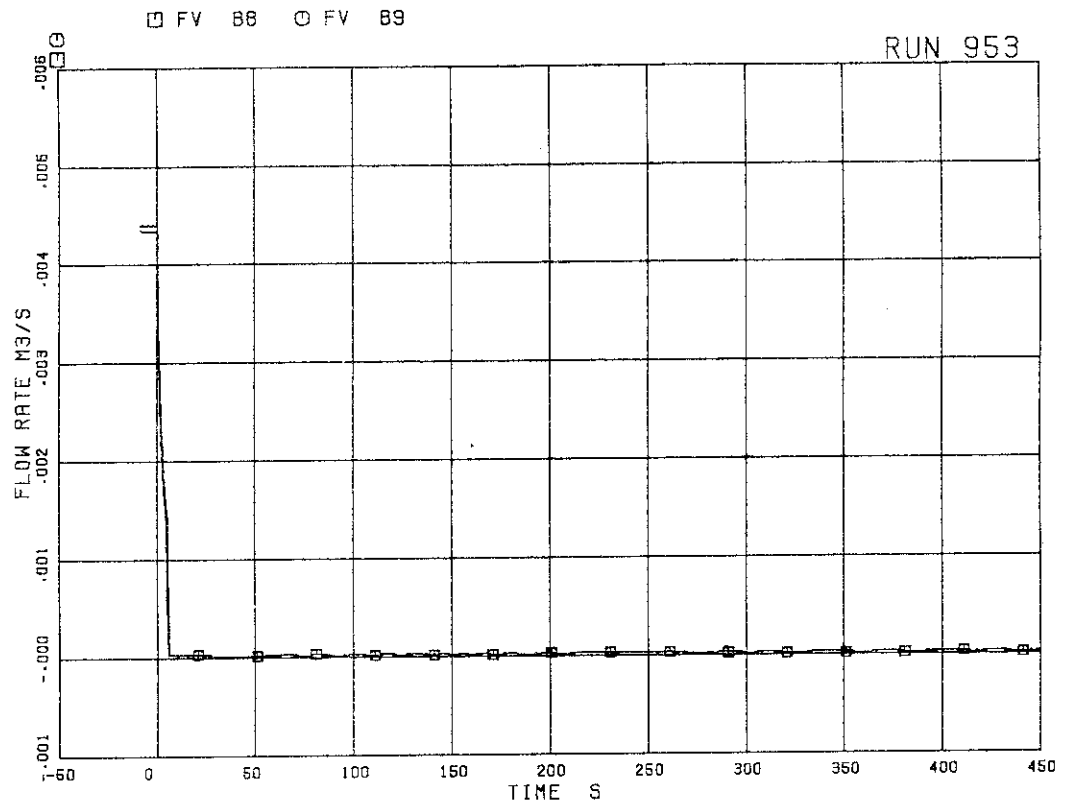
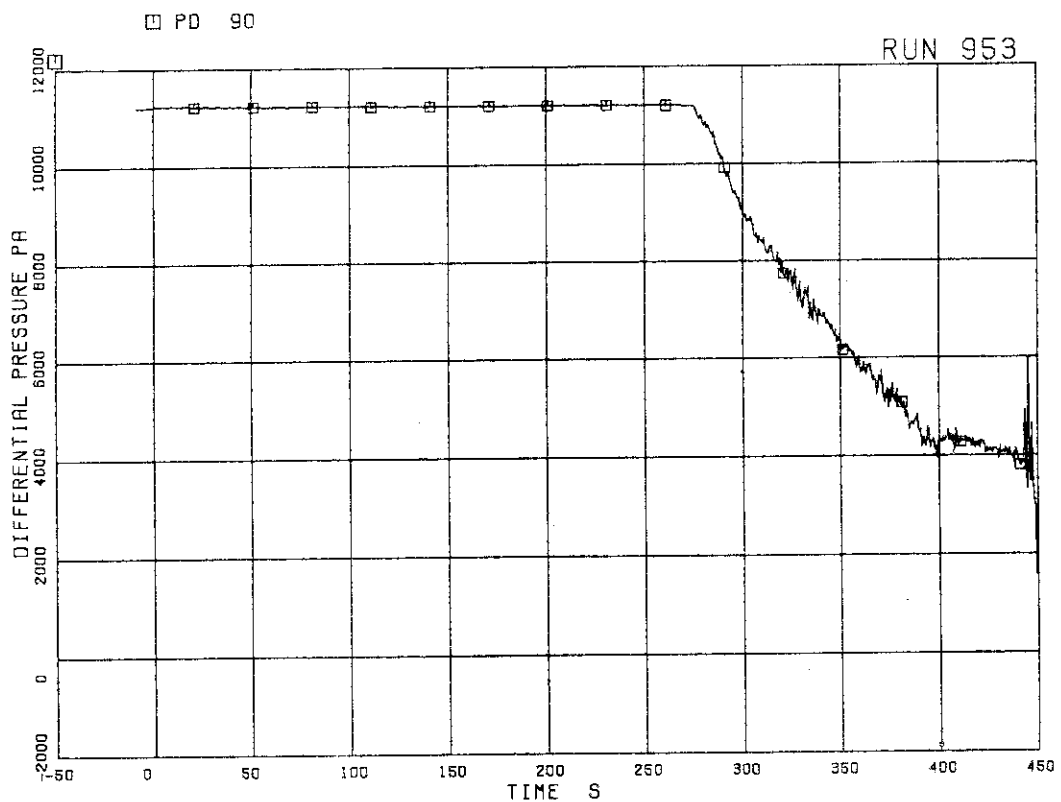


FIG. 5. 41 MRP FLOW RATE

FIG. 5. 42 DIFF. PRESSURE ACROSS ORIFICE  
F-1 IN MSL (LOW)

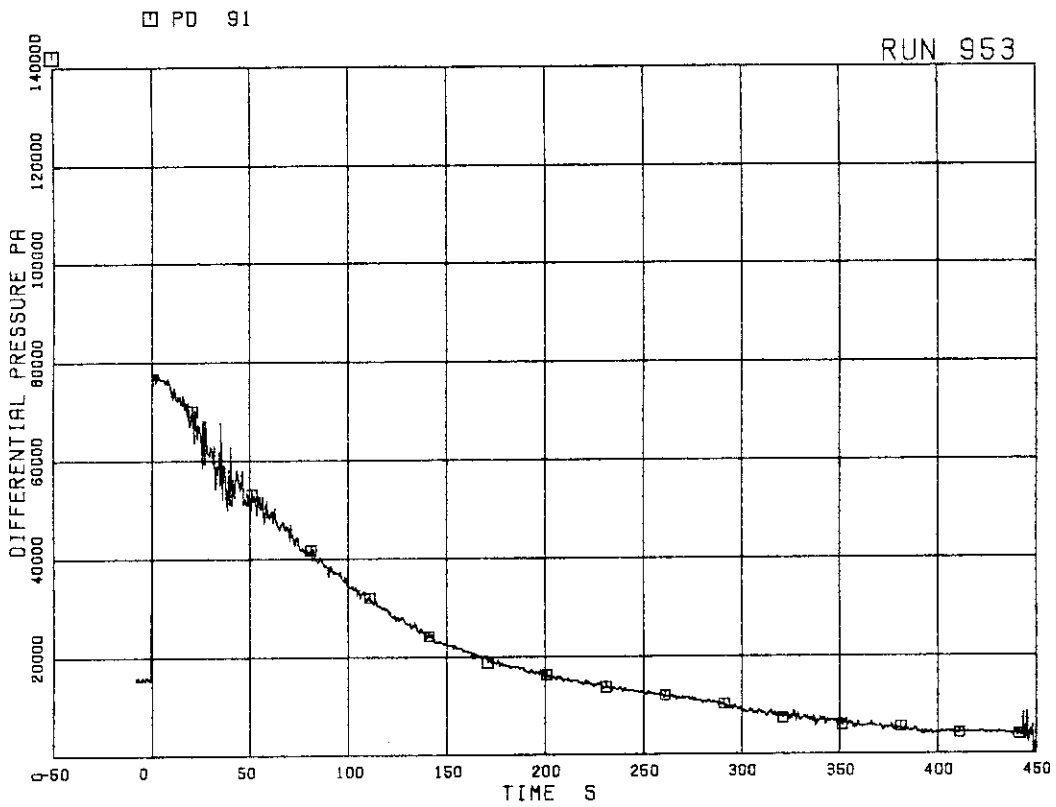


FIG. 5. 43 DIFF. PRESSURE ACROSS ORIFICE  
F-2 IN MSL (MID)

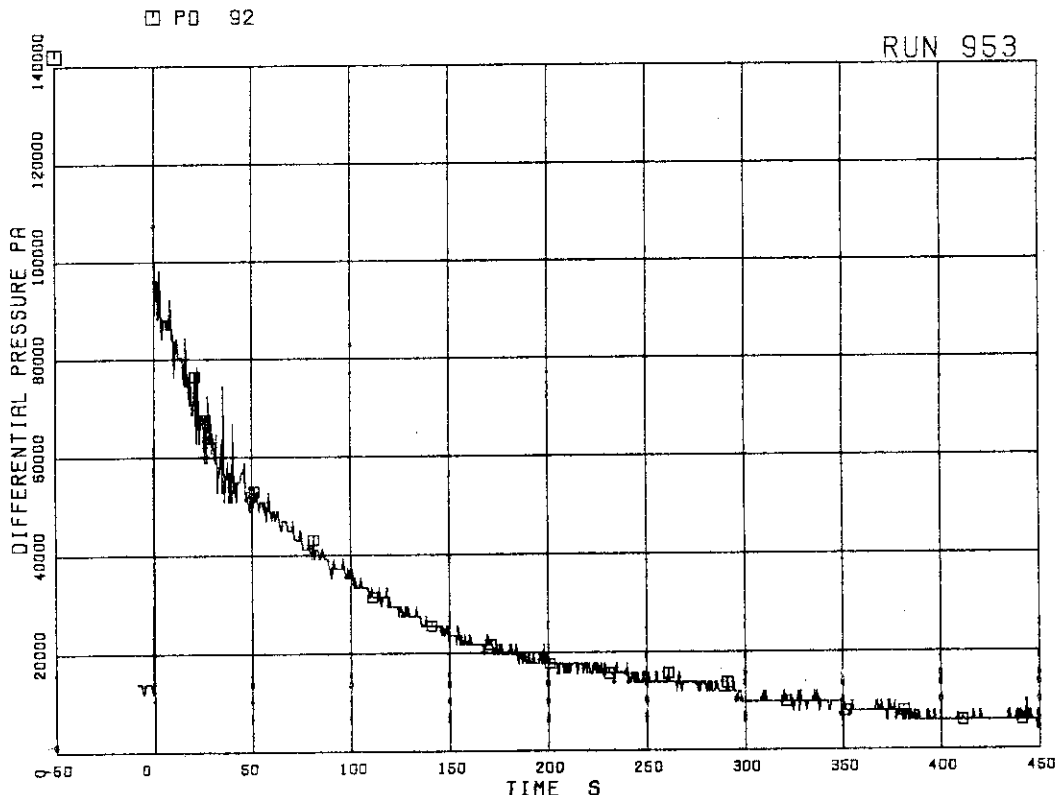


FIG. 5. 44 DIFF. PRESSURE ACROSS ORIFICE  
F-3 IN MSL (HIGH)

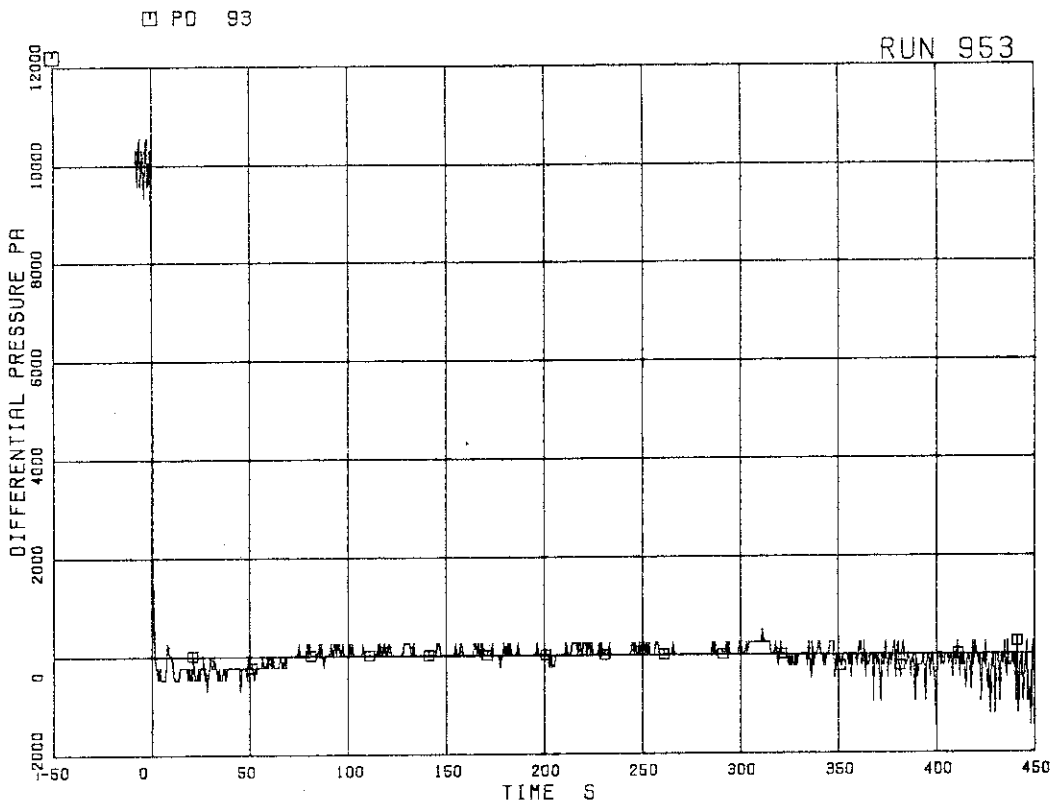


FIG.5. 45 DIFF. PRESSURE ACROSS VENTURI  
F-17 IN JP1

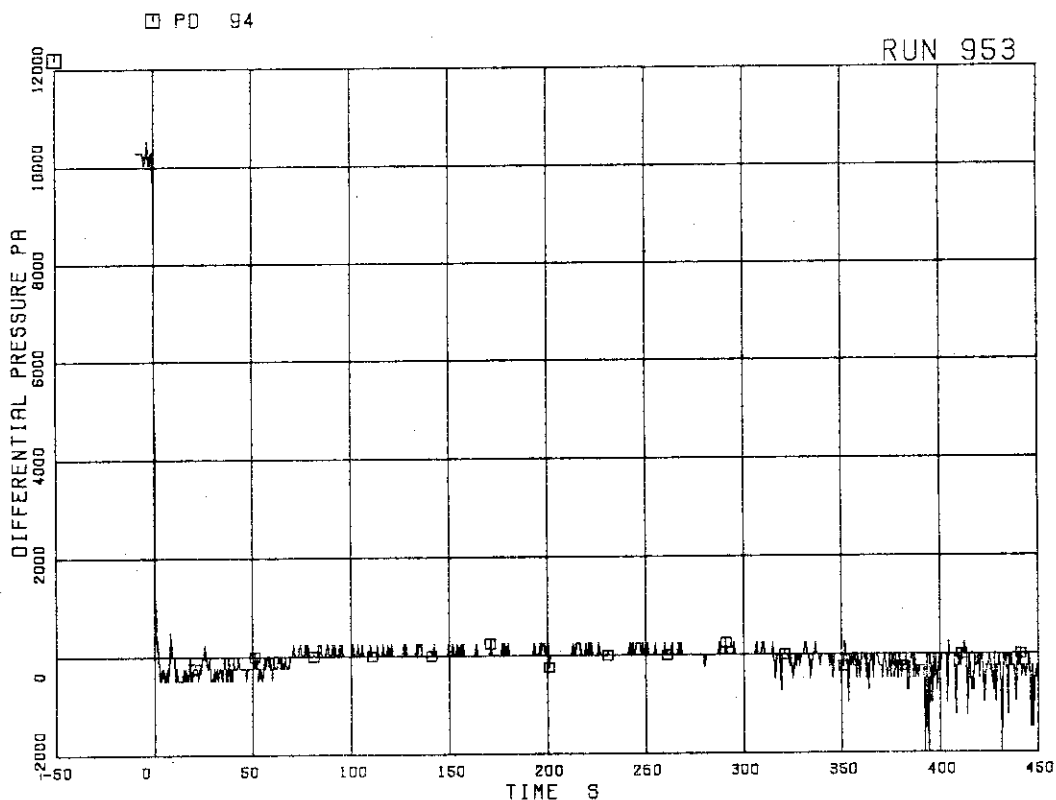


FIG.5. 46 DIFF. PRESSURE ACROSS VENTURI  
F-18 IN JP2

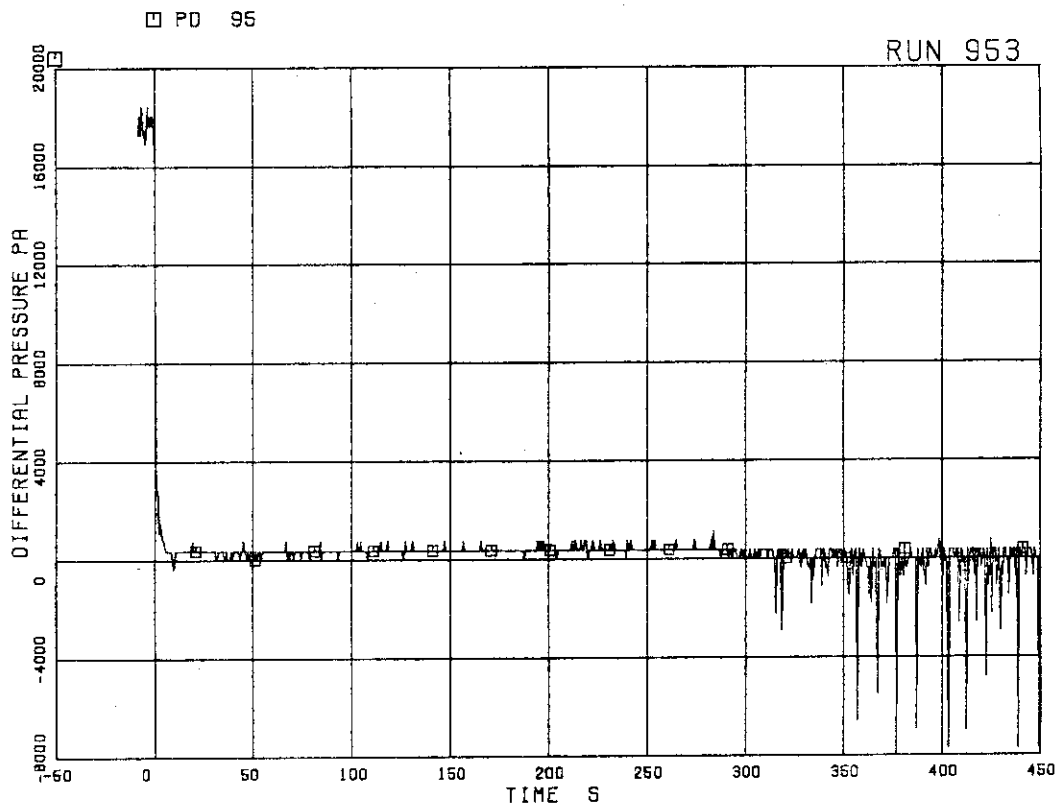


FIG. 5. 47 DIFF. PRESSURE ACROSS ORIFICE  
F-19 IN JP3

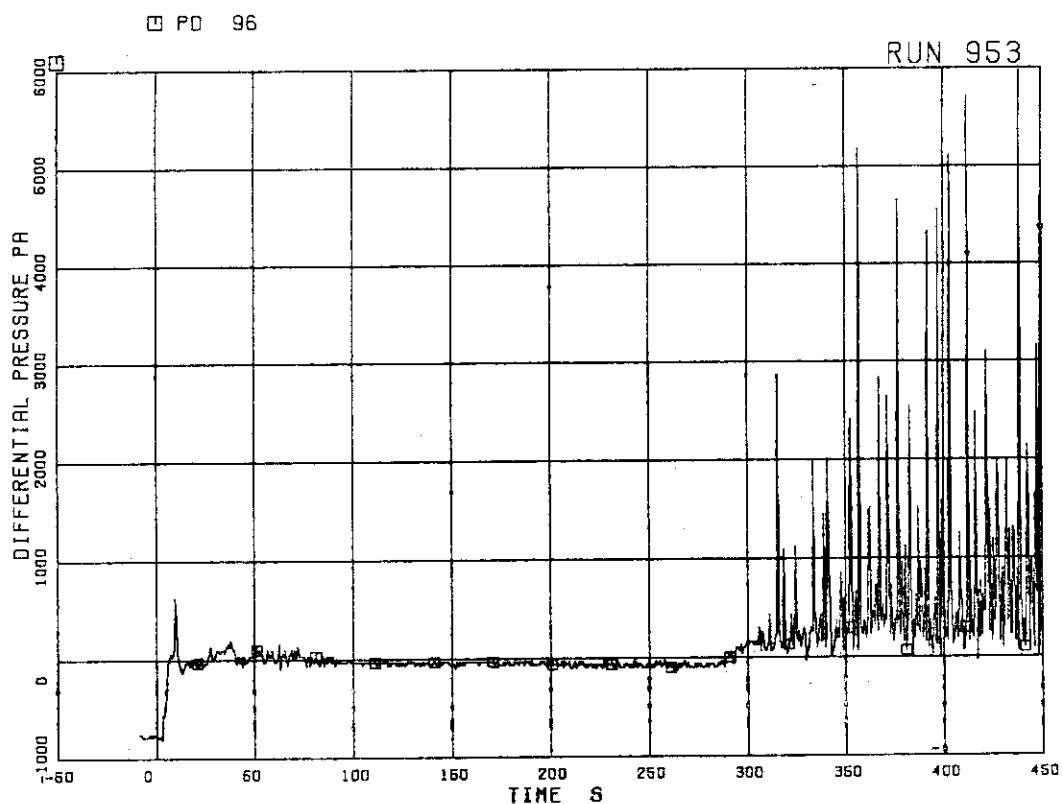


FIG. 5. 48 DIFF. PRESSURE ACROSS ORIFICE  
F-20 IN JP4

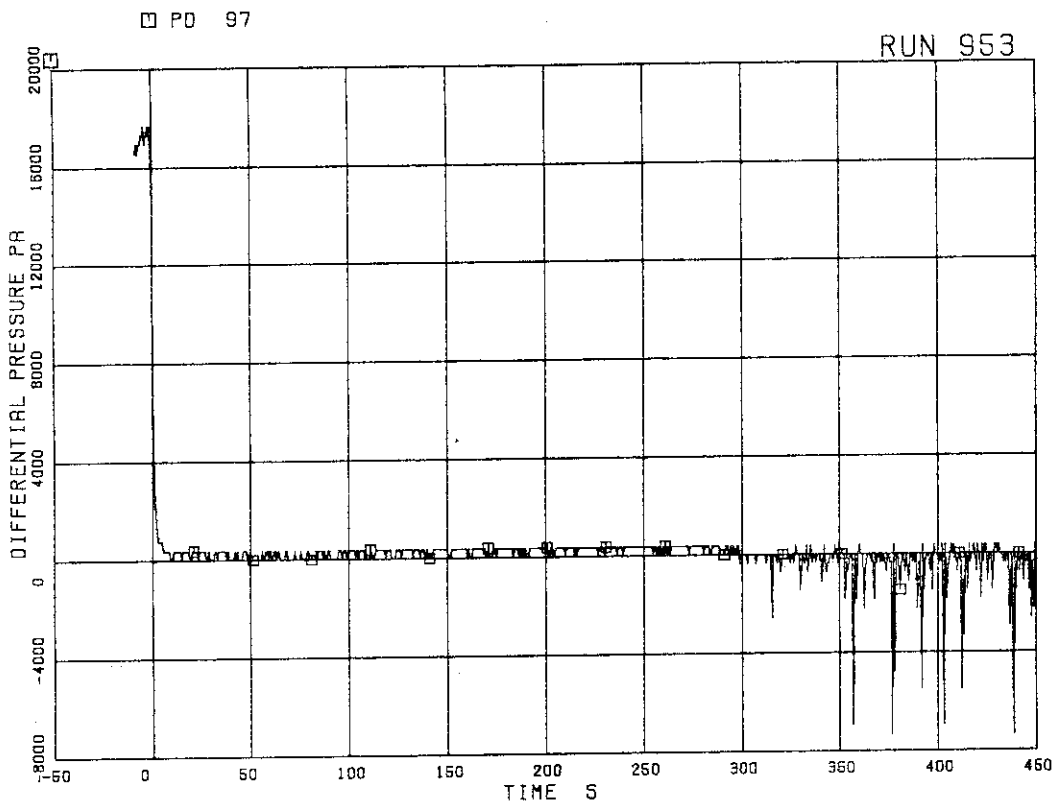


FIG. 5. 49 DIFF. PRESSURE ACROSS ORIFICE  
F-21 IN JP3

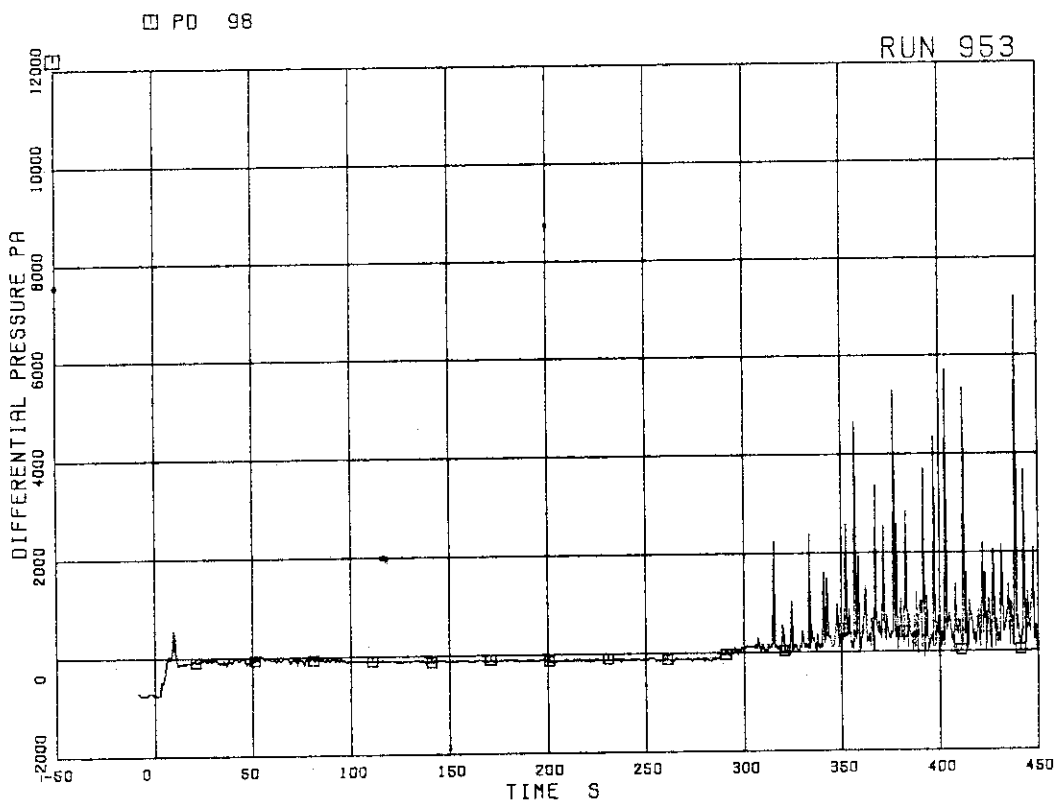


FIG. 5. 50 DIFF. PRESSURE ACROSS ORIFICE  
F-22 IN JP4

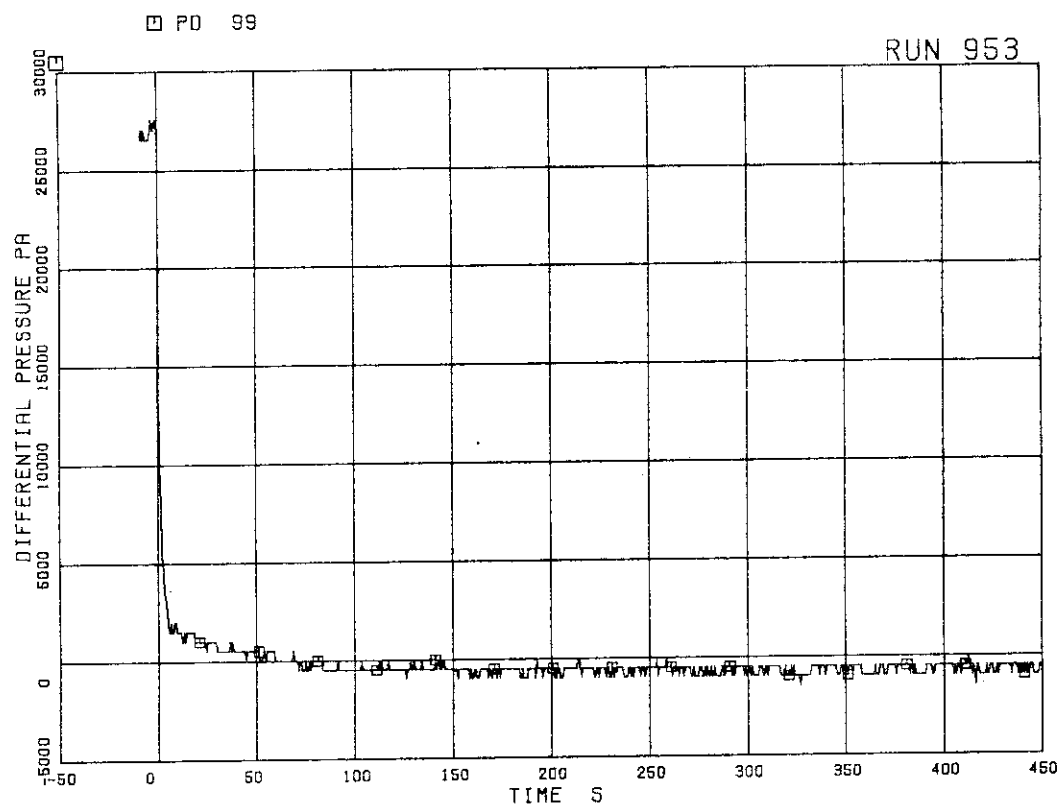


FIG. 5. 51 DIFF. PRESSURE ACROSS VENTURI  
F-27 IN MRP-1

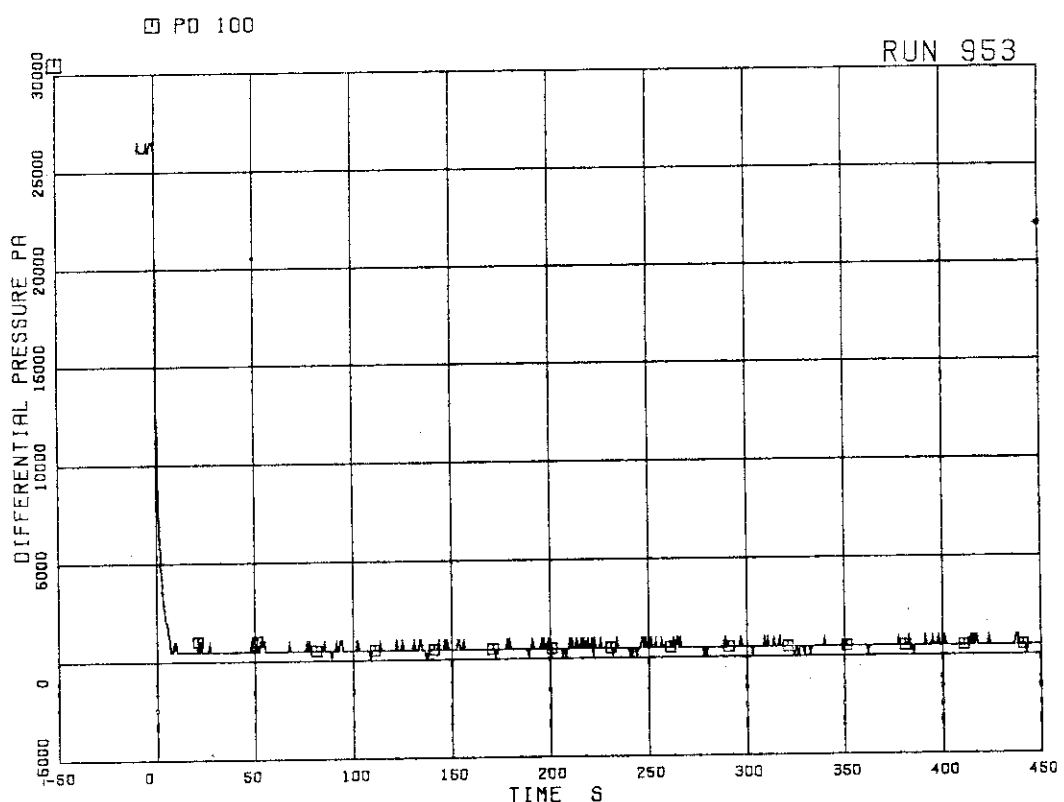


FIG. 5. 52 DIFF. PRESSURE ACROSS VENTURI  
F-28 IN MRP-2

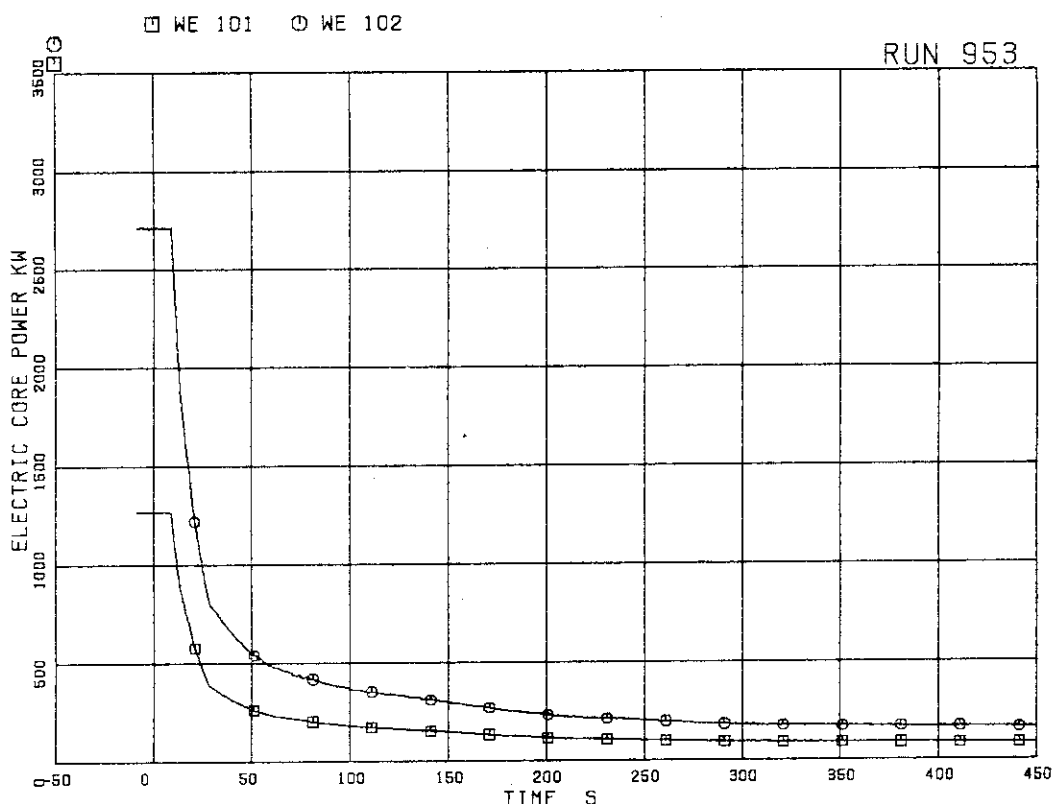


FIG. 53 ELECTRIC CORE POWER

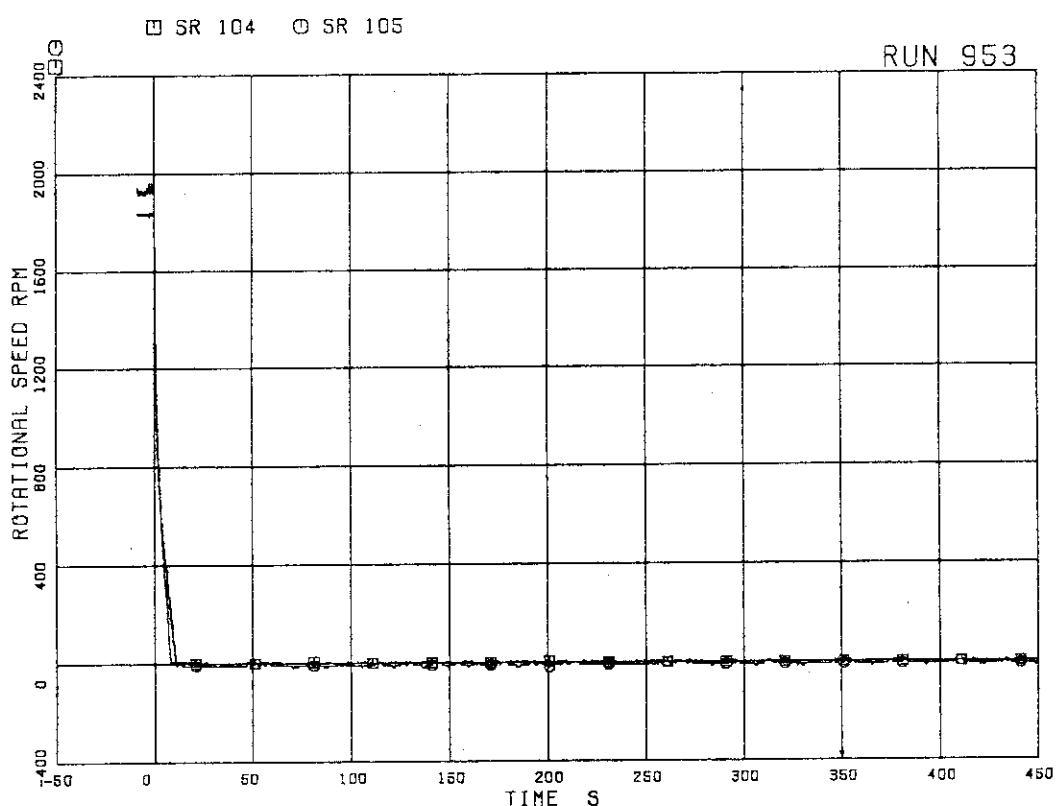


FIG. 54 MRP REVOLUTION

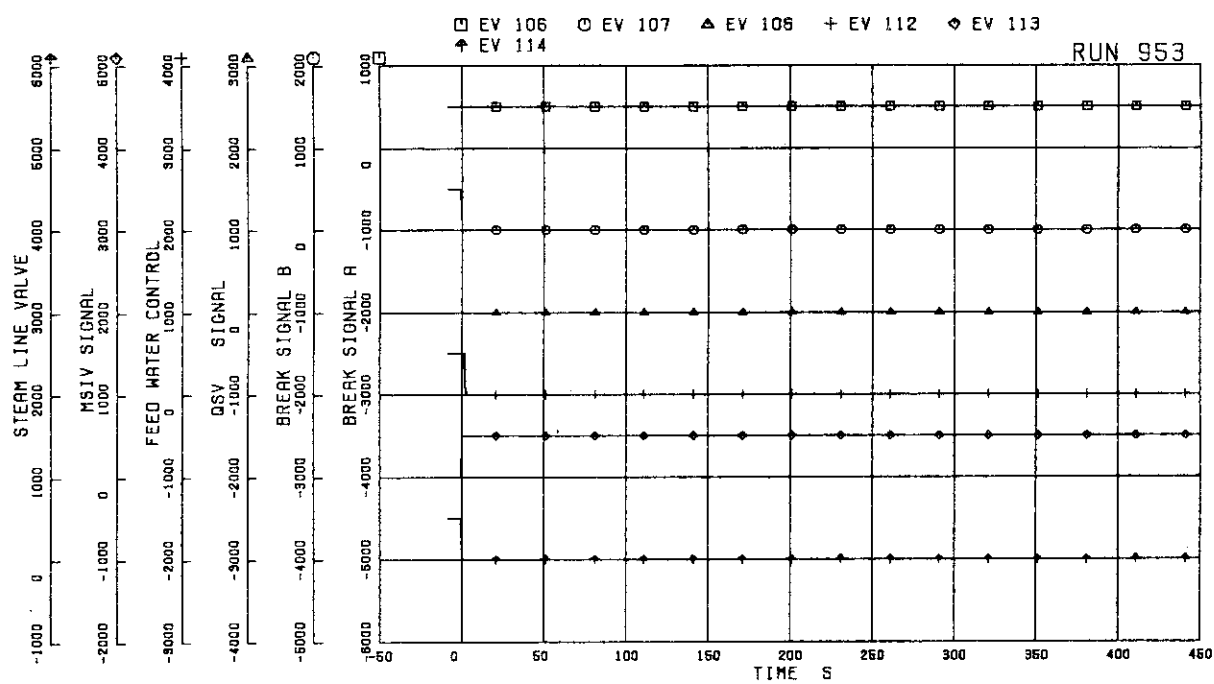


FIG. 5. 55 VALVE OPERATION SIGNALS

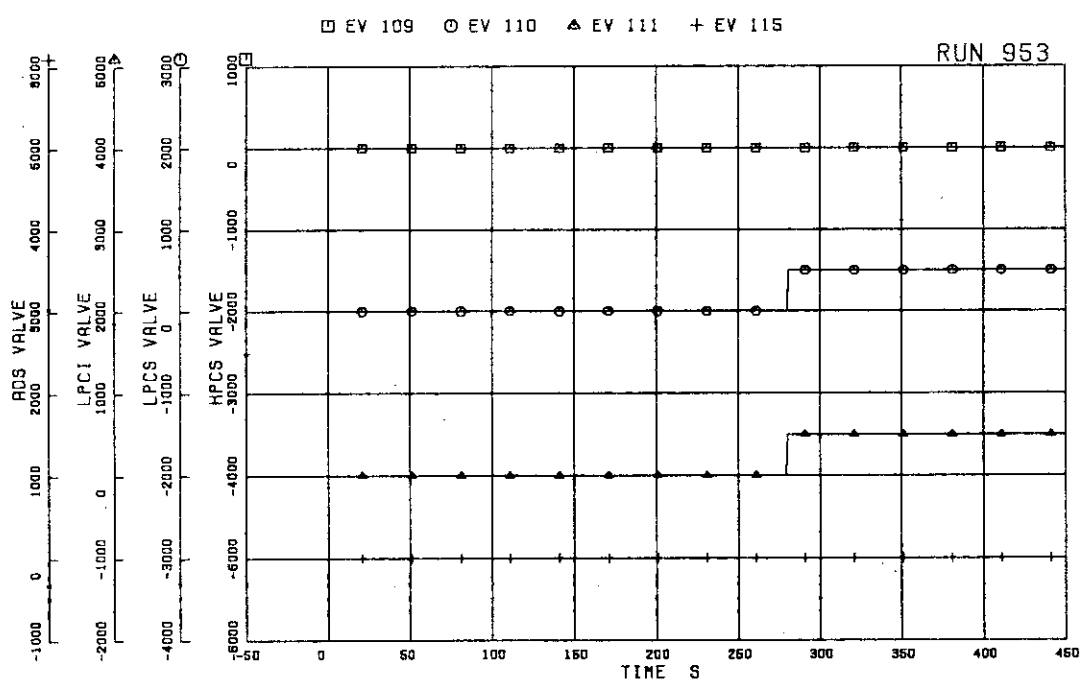


FIG. 5. 56 ECCS OPERATION SIGNALS

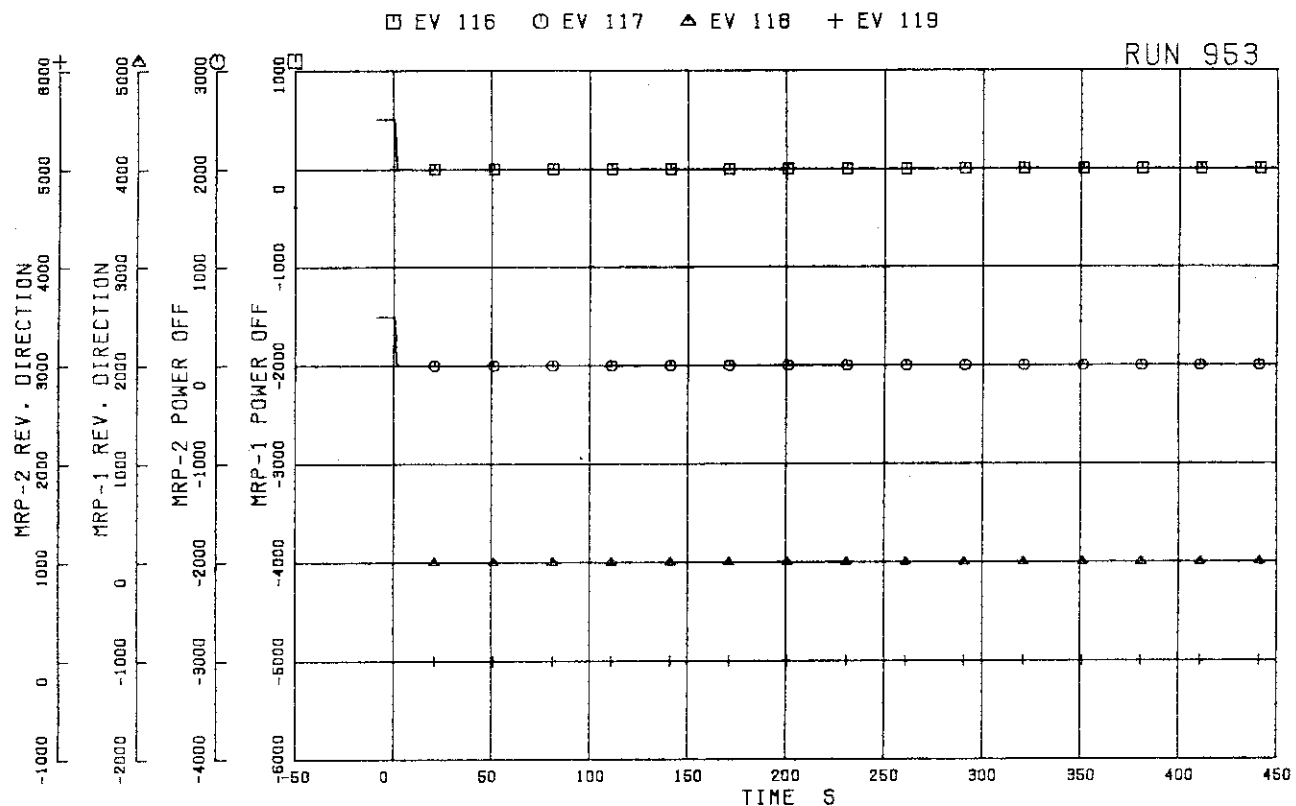


FIG. 5. 57 MRP OPERATION SIGNALS

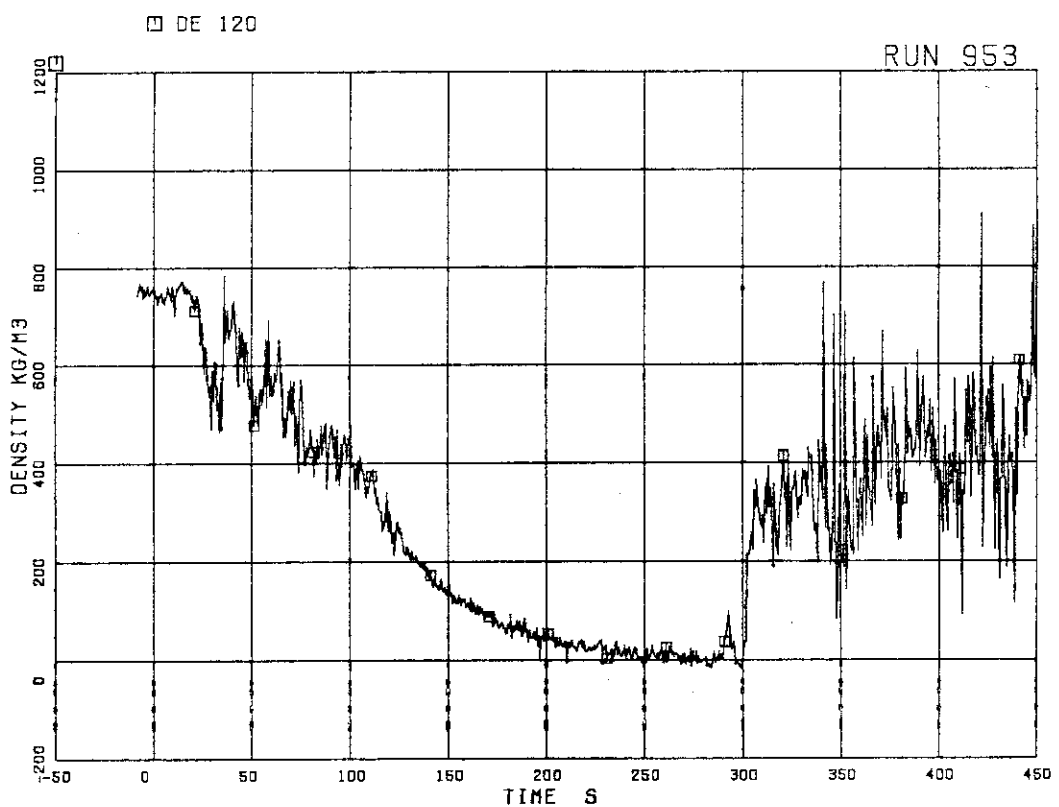


FIG. 5. 58 FLUID DENSITY AT JP-1,2 OUTLET, BEAM A

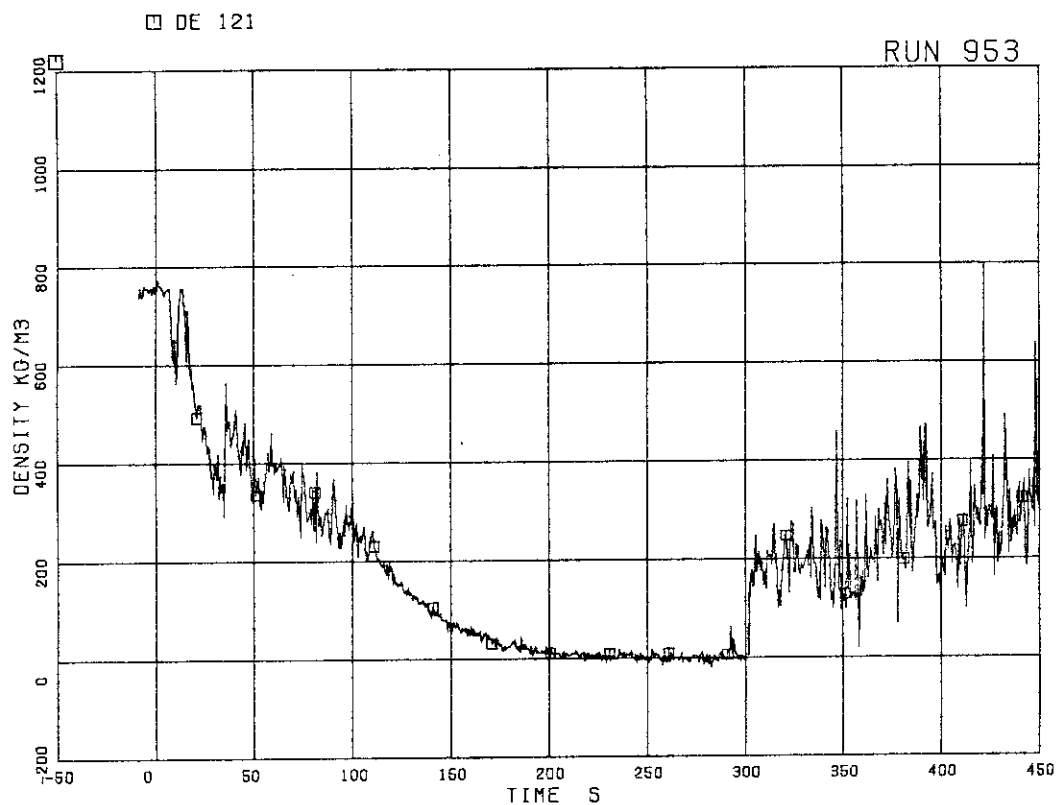


FIG. 5. 59 FLUID DENSITY AT JP-1,2 OUTLET, BEAM B

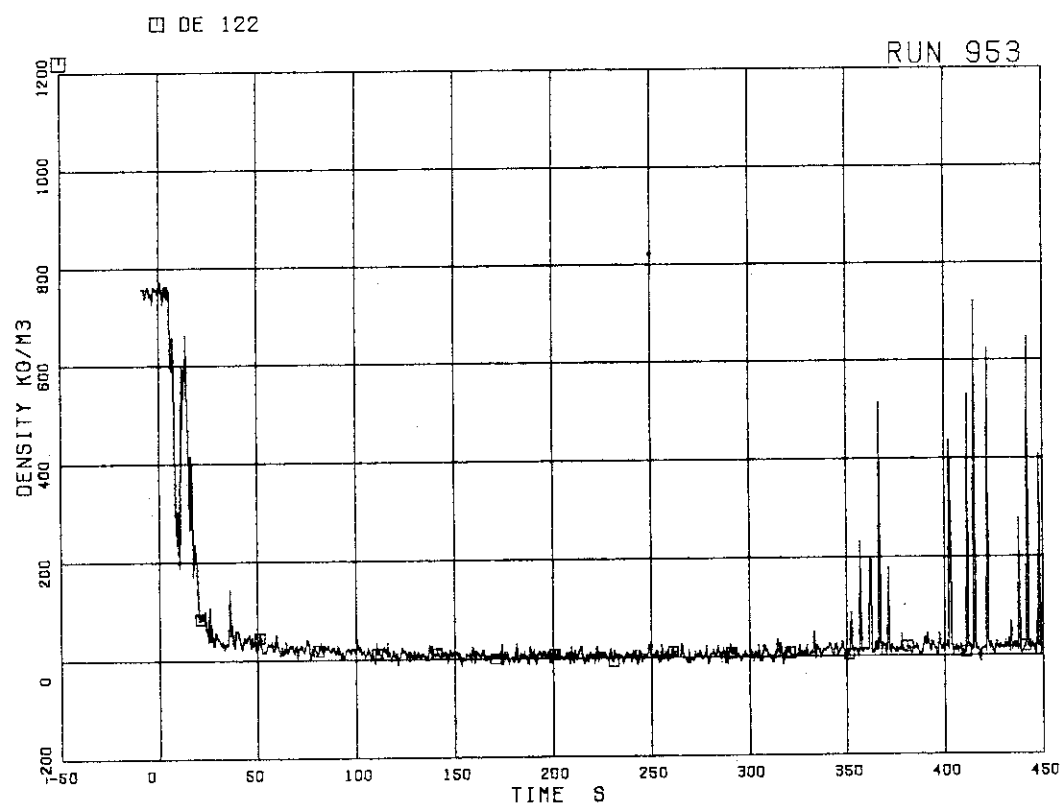


FIG. 5. 60 FLUID DENSITY AT JP-1,2 OUTLET, BEAM C

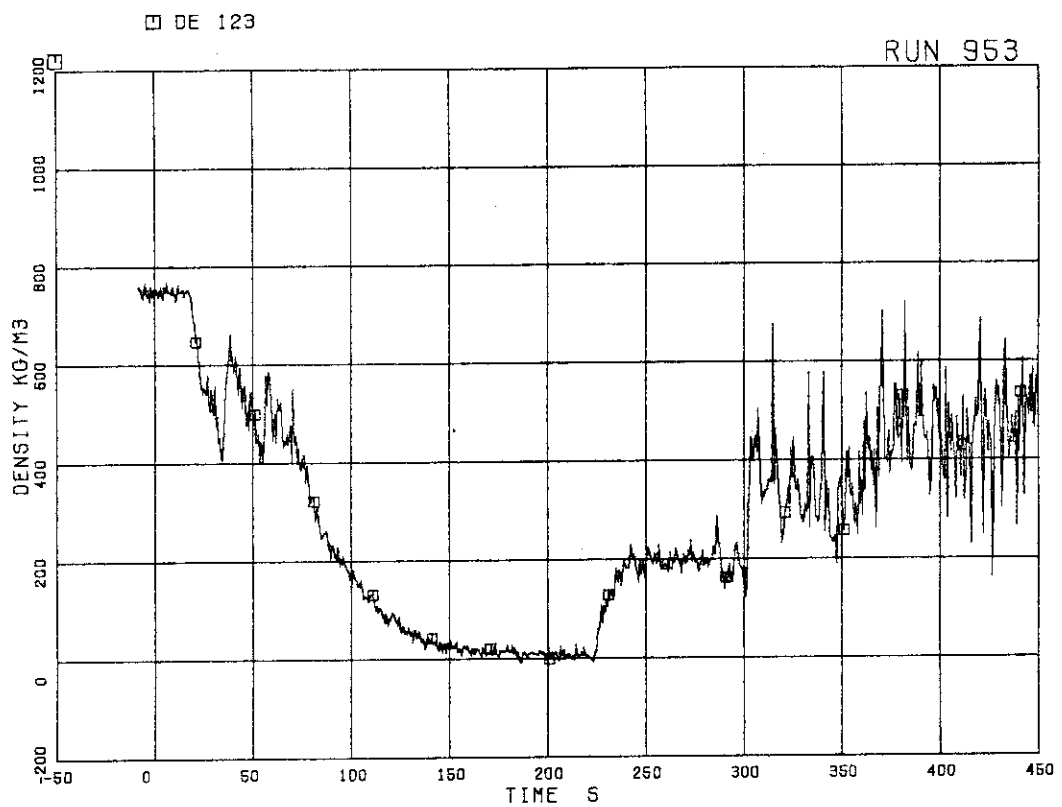


FIG. 5. 61 FLUID DENSITY AT JP-3,4 OUTLET, BEAM A

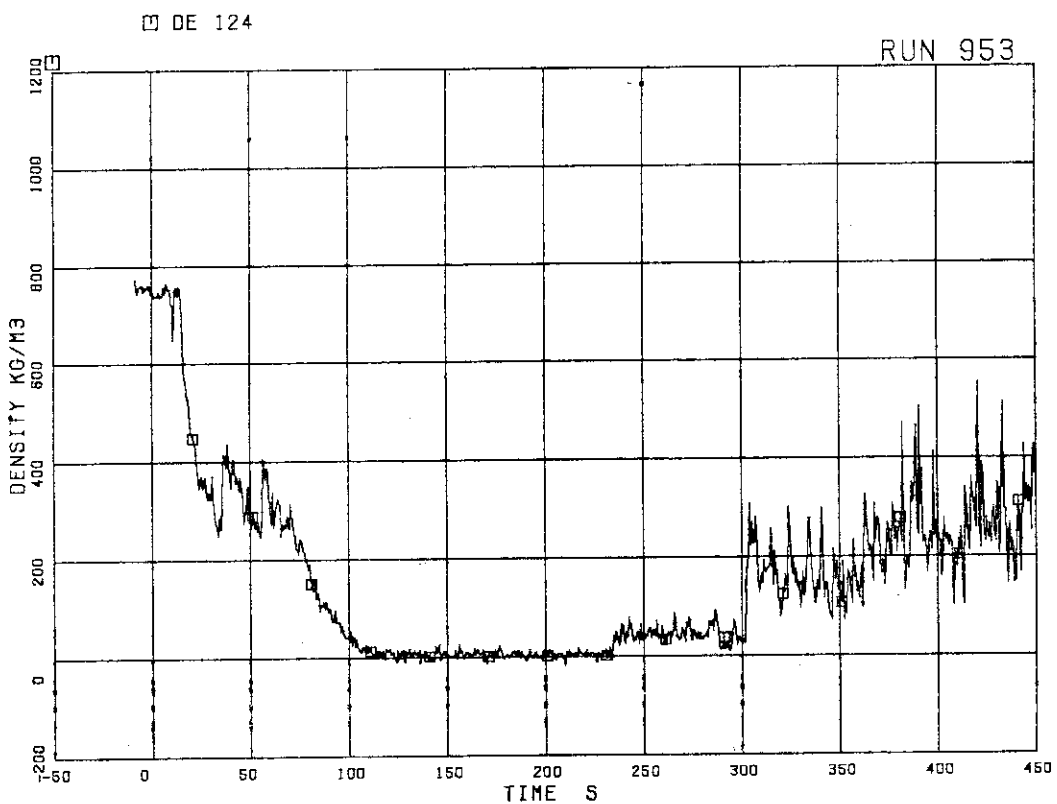


FIG. 5. 62 FLUID DENSITY AT JP-3,4 OUTLET, BEAM B

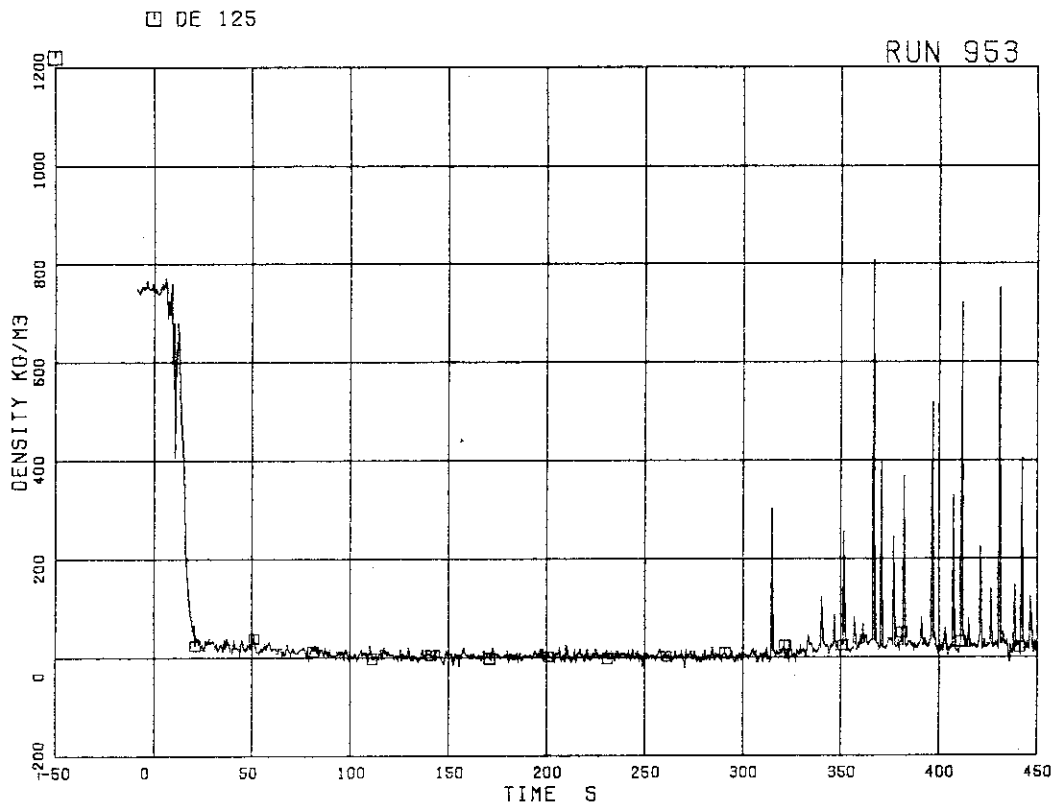


FIG. 5. 63 FLUID DENSITY AT JP-3,4 OUTLET, BEAM C

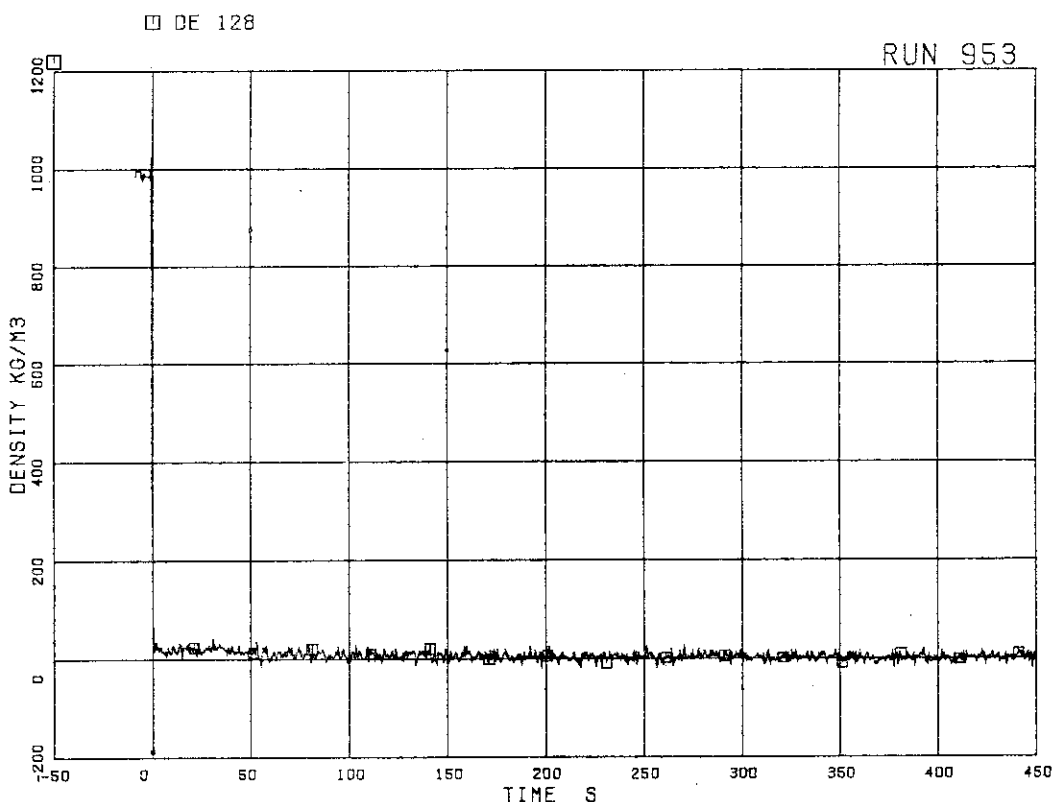


FIG. 5. 64 FLUID DENSITY AT BREAK,(BEAM A)

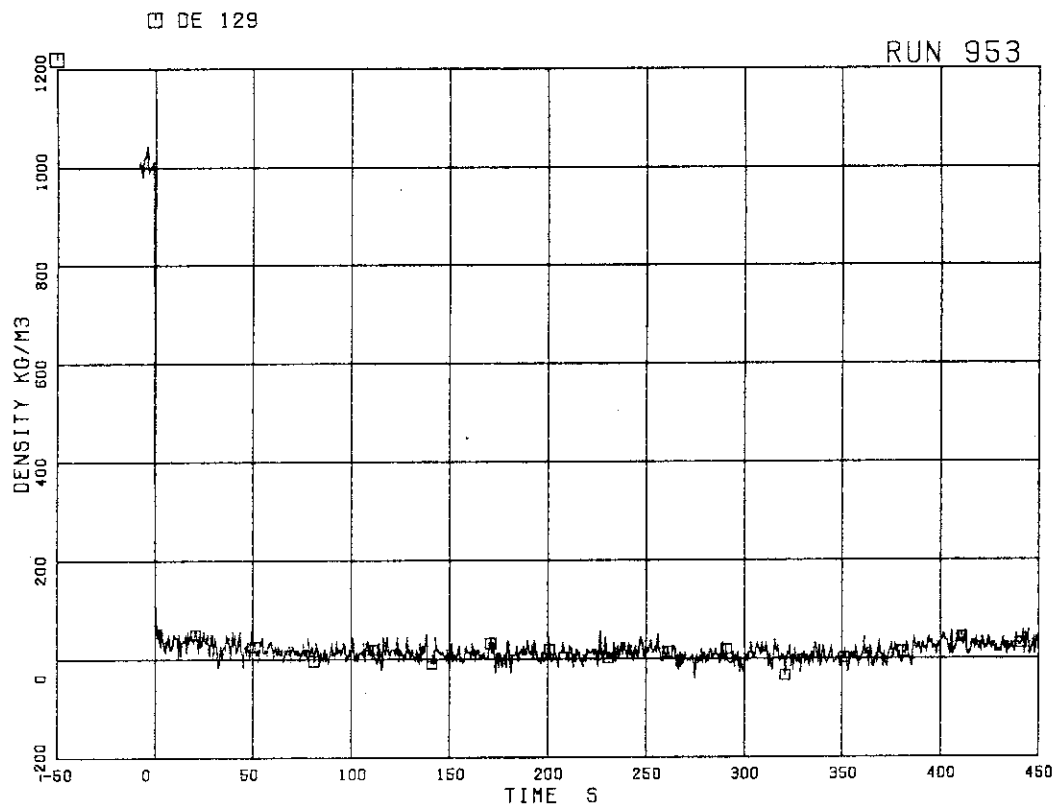


FIG. 5. 65 FLUID DENSITY AT BREAK,(BEAM B)

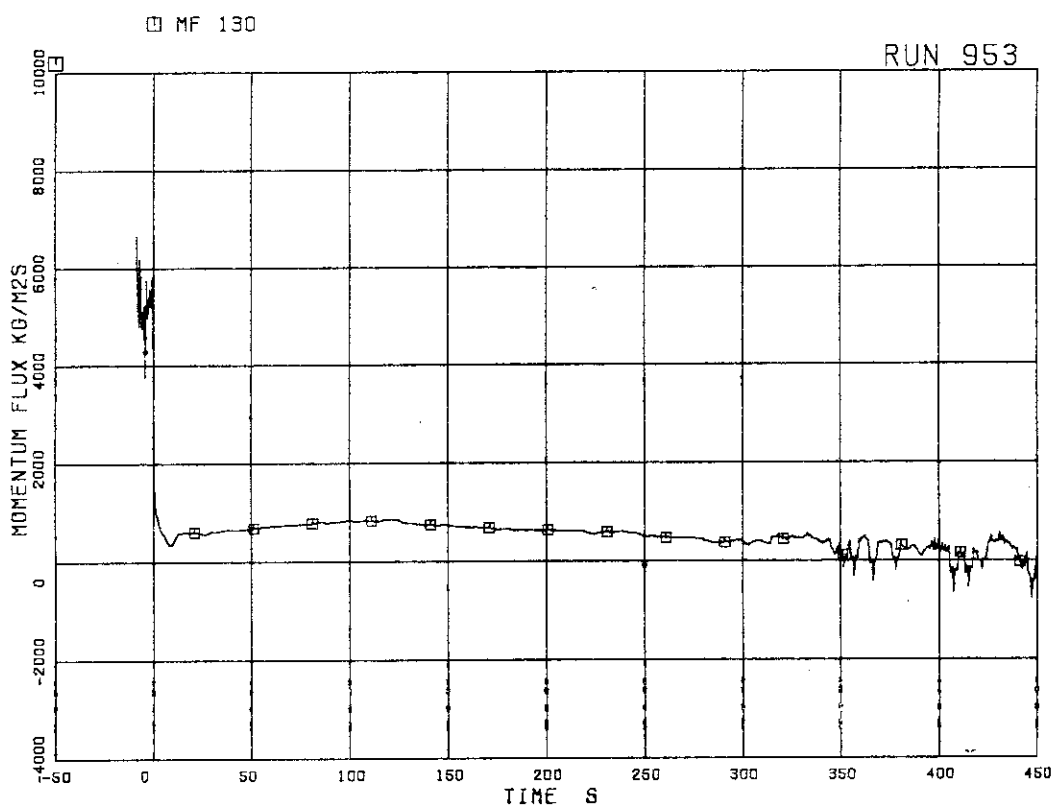


FIG. 5. 66 MOMENTUM FLUX AT JP-1,2 OUTLET

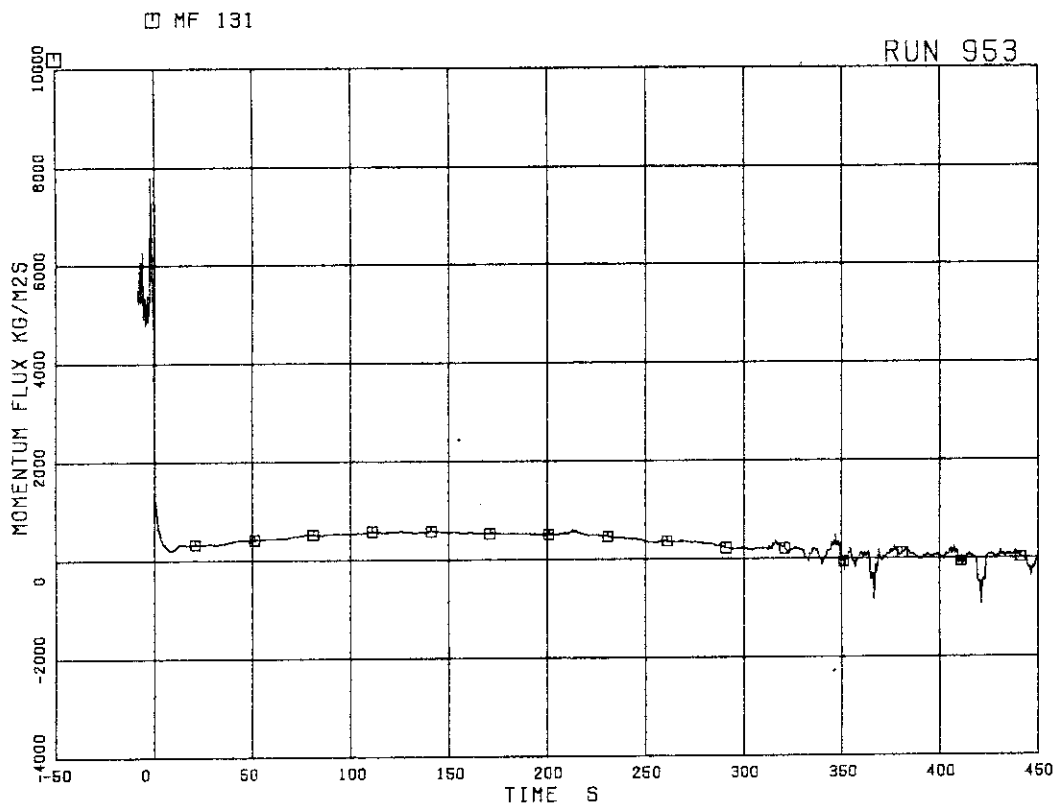
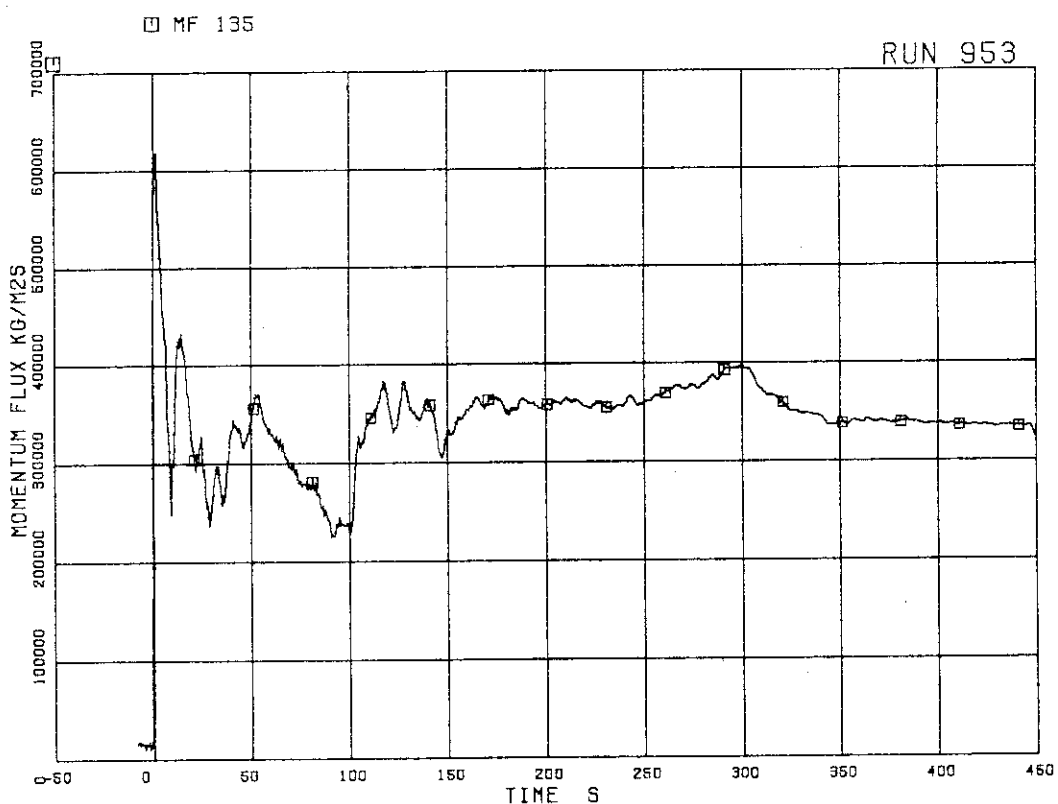


FIG. 5. 67 MOMENTUM FLUX AT JP-3,4 OUTLET

FIG. 5. 68 MOMENTUM FLUX AT BREAK B SPOOL PIECE  
(HIGH RANGE)

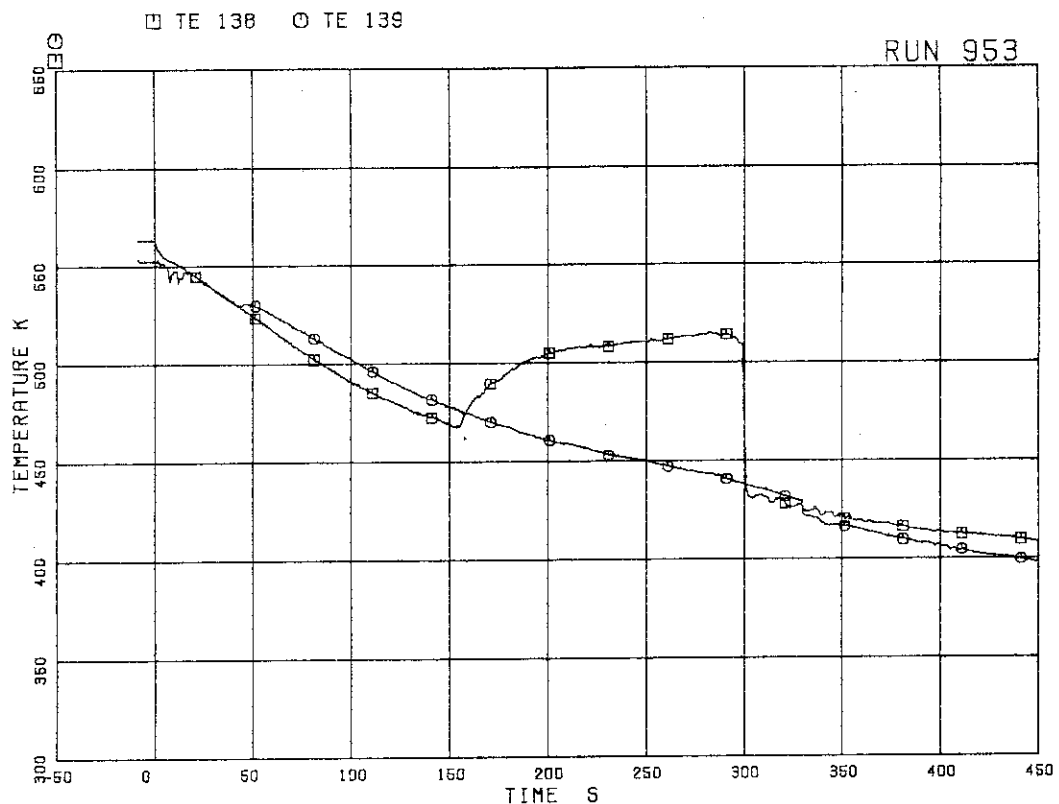


FIG. 5. 69 FLUID TEMPERATURES IN  
LOWER PLENUM AND UPPER PLENUM

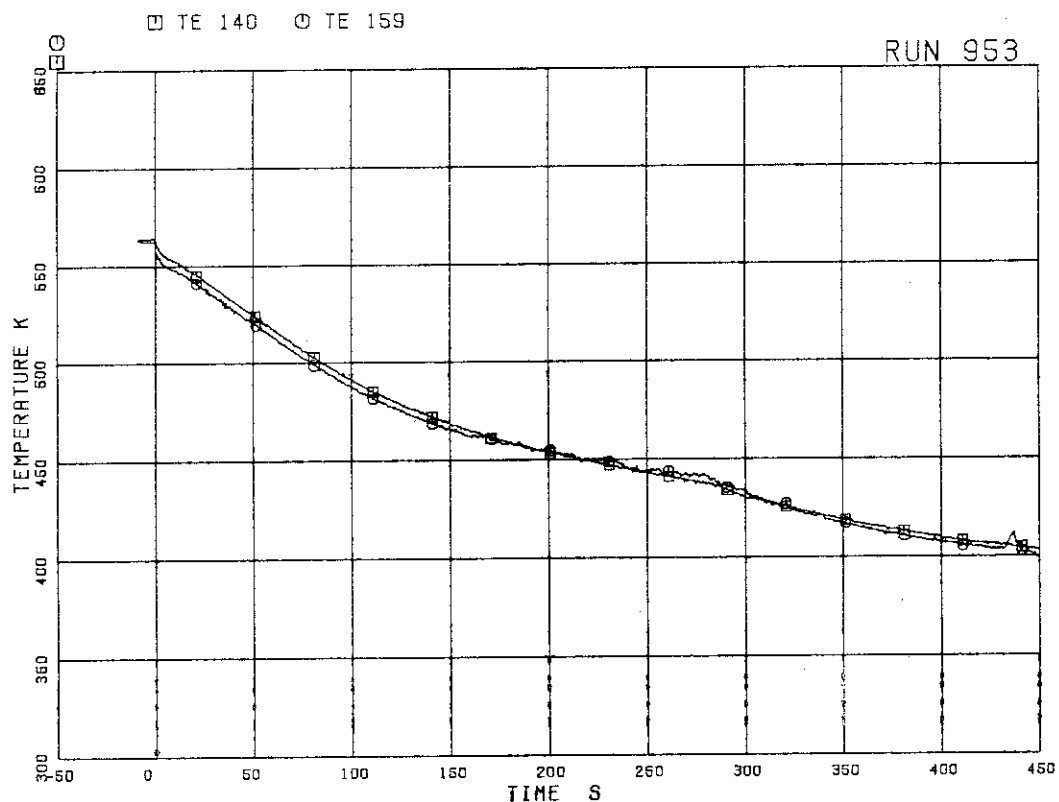


FIG. 5. 70 FLUID TEMPERATURES IN STEAM DOME AND MSL

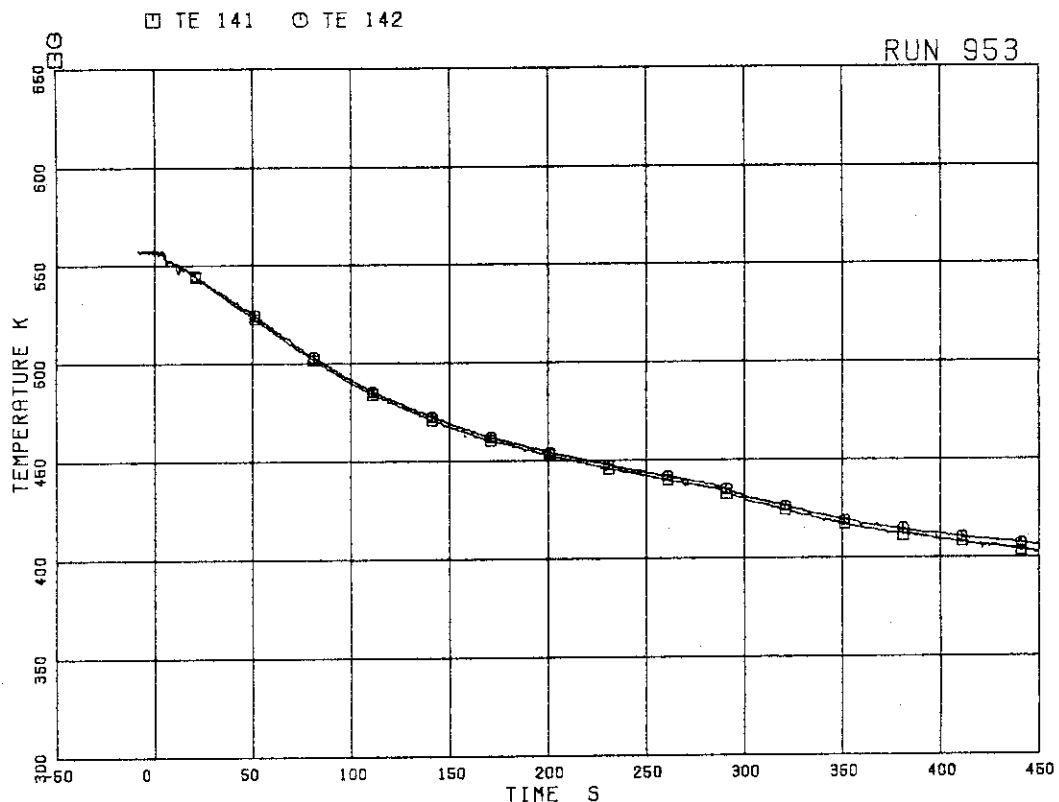


FIG. 5. 71 FLUID TEMPERATURES IN DOWNCOMER

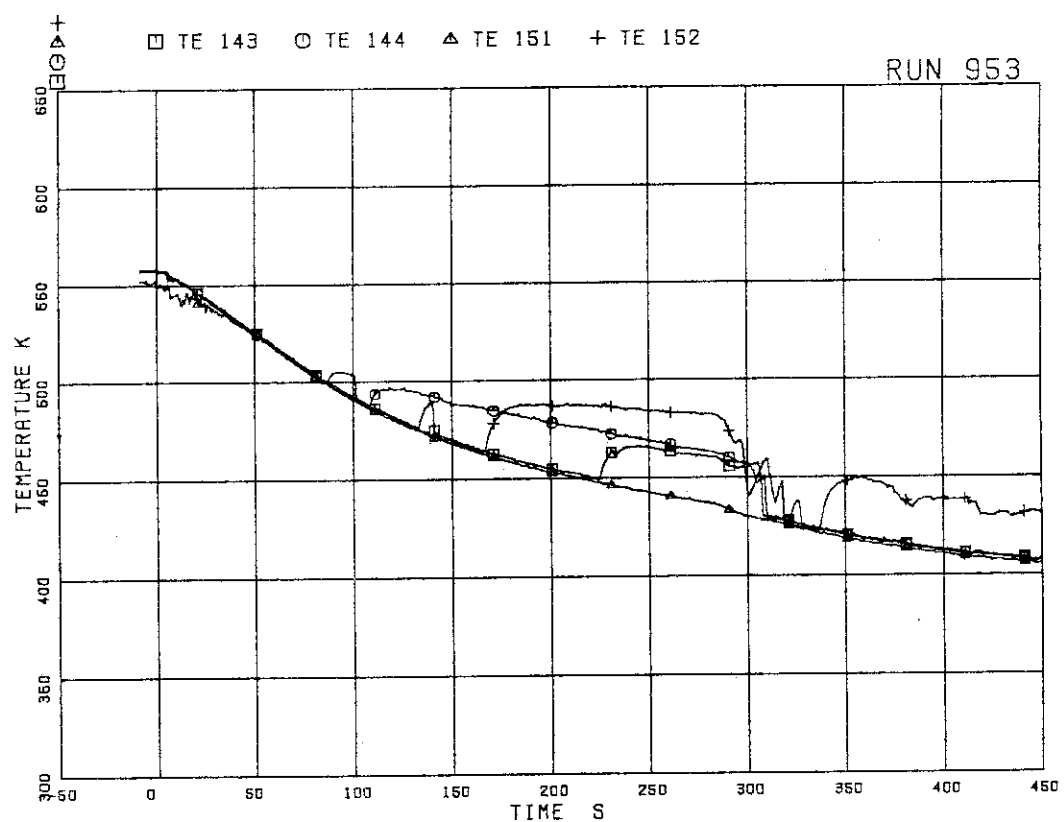


FIG. 5. 72 FLUID TEMPERATURES IN RECIRCULATION LOOP A

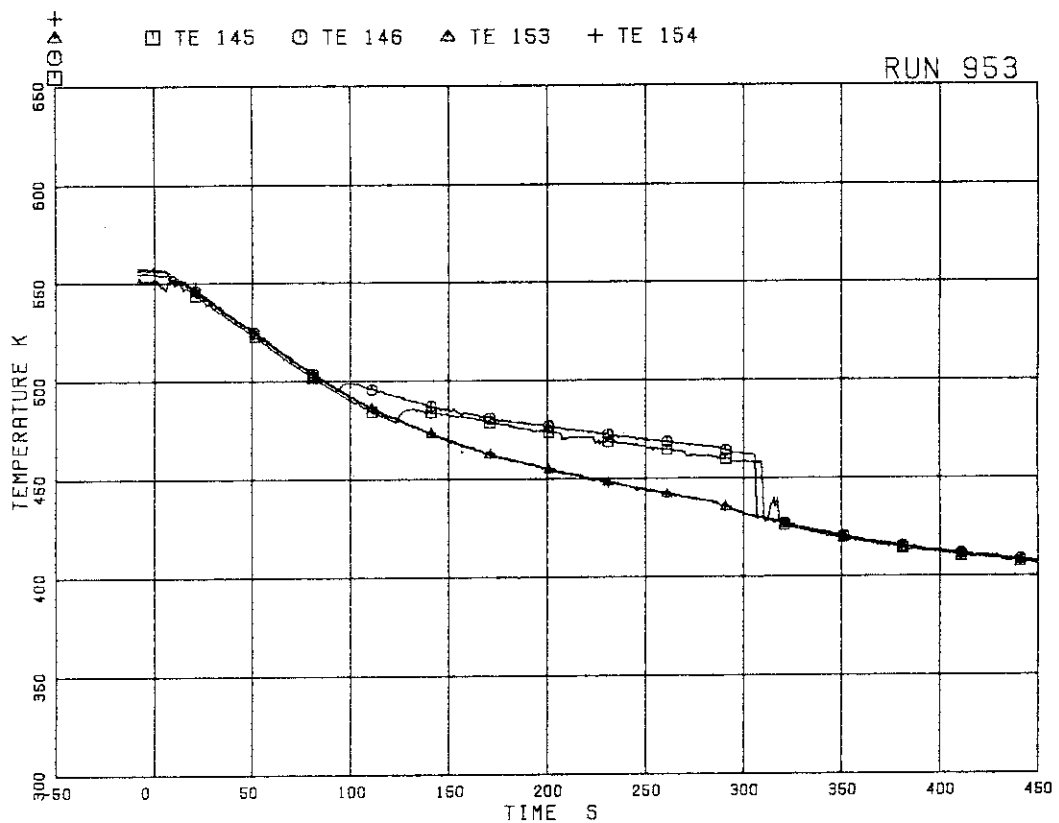


FIG. 5. 73 FLUID TEMPERATURES IN RECIRCULATION LOOP B

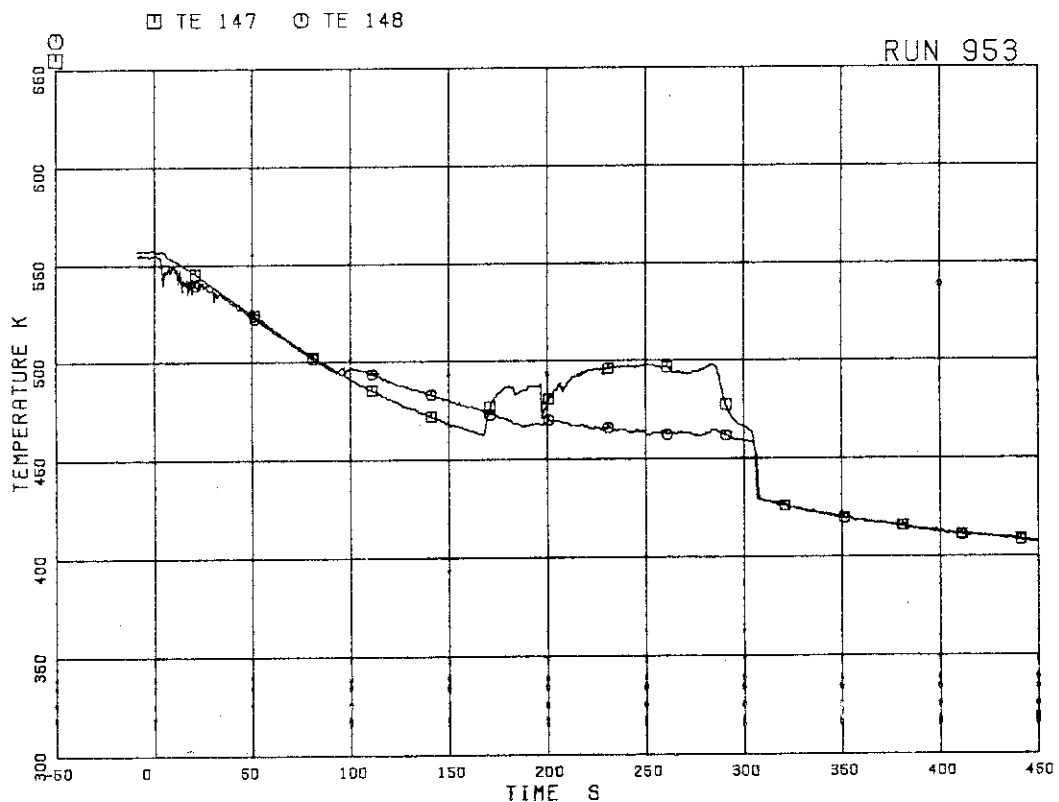


FIG. 5. 74 FLUID TEMPERATURES AT JP-1,2 OUTLET

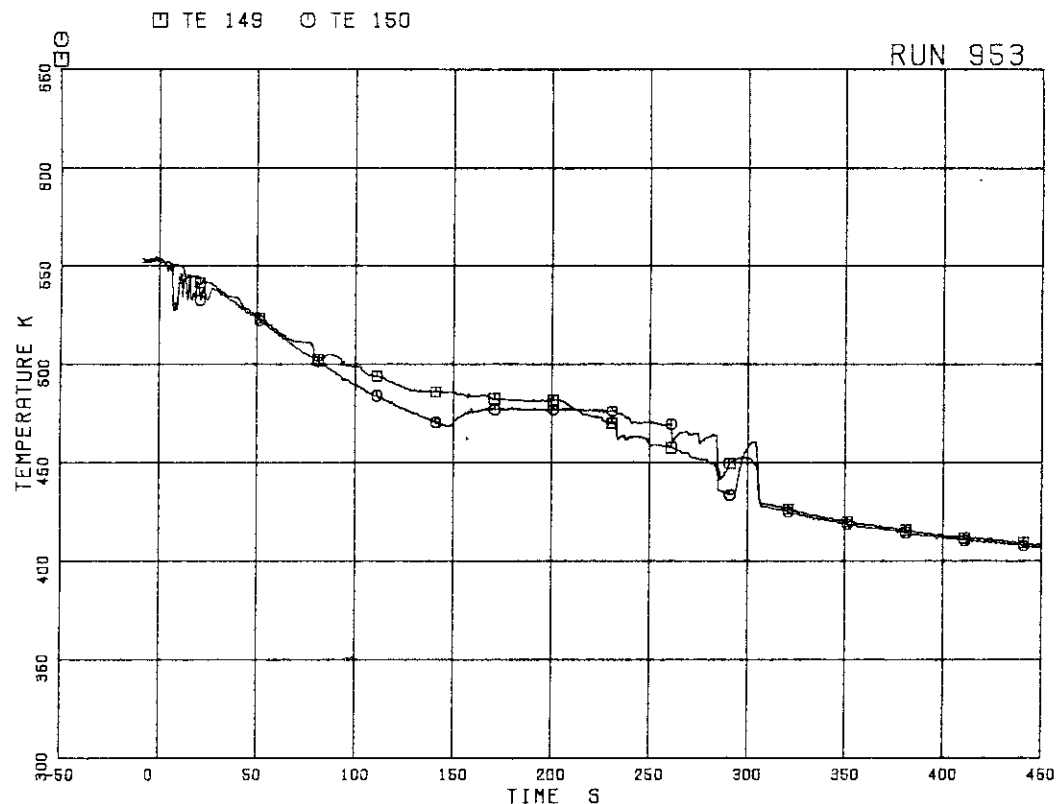


FIG. 5. 75 FLUID TEMPERATURES AT JP-3,4 OUTLET

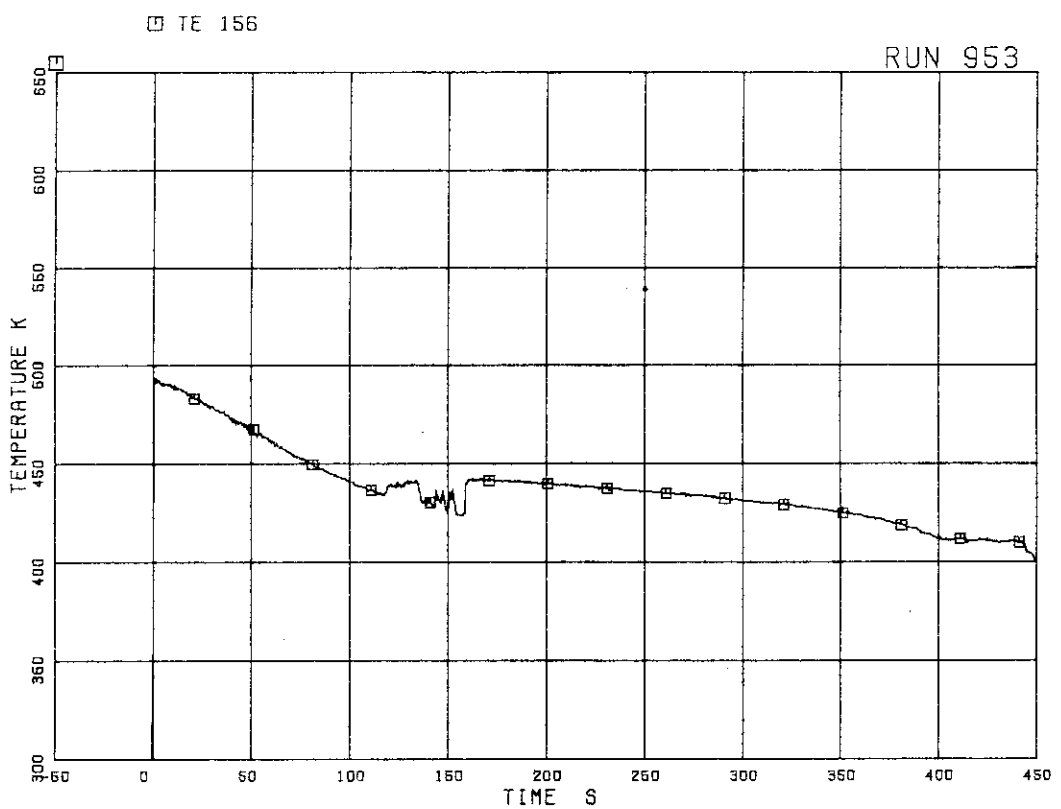


FIG. 5. 76 FLUID TEMPERATURE UPSTREAM OF BREAK

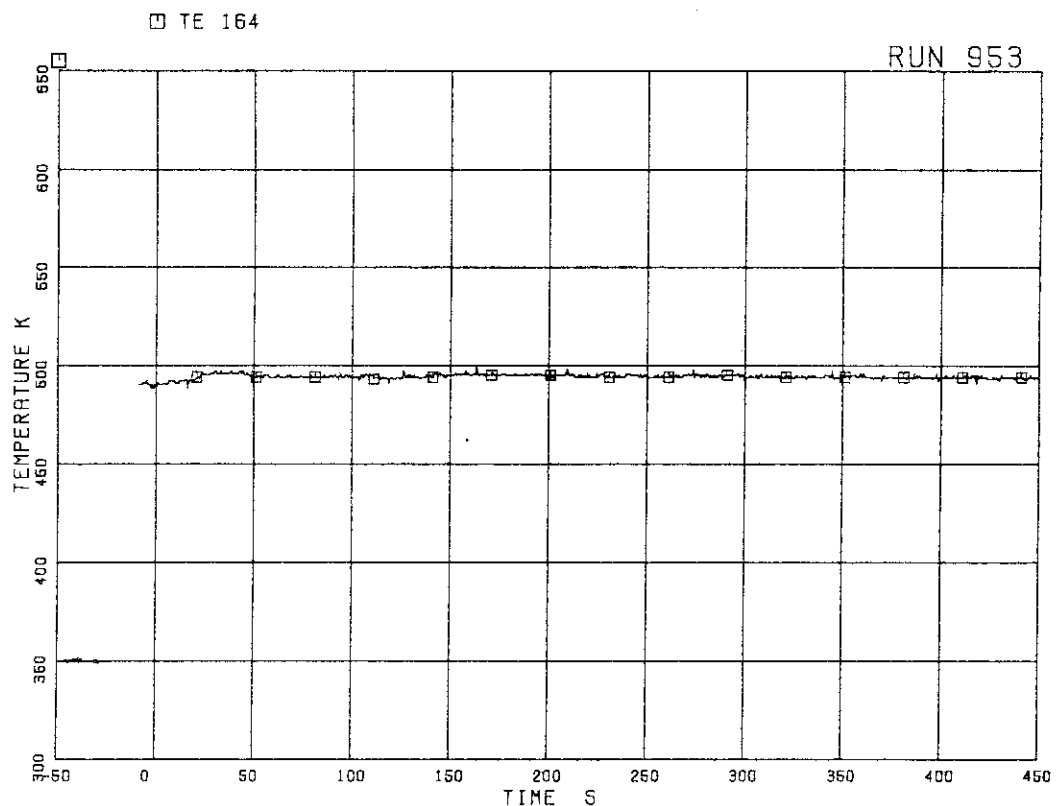


FIG. 5. 77 FEEDWATER TEMPERATURE

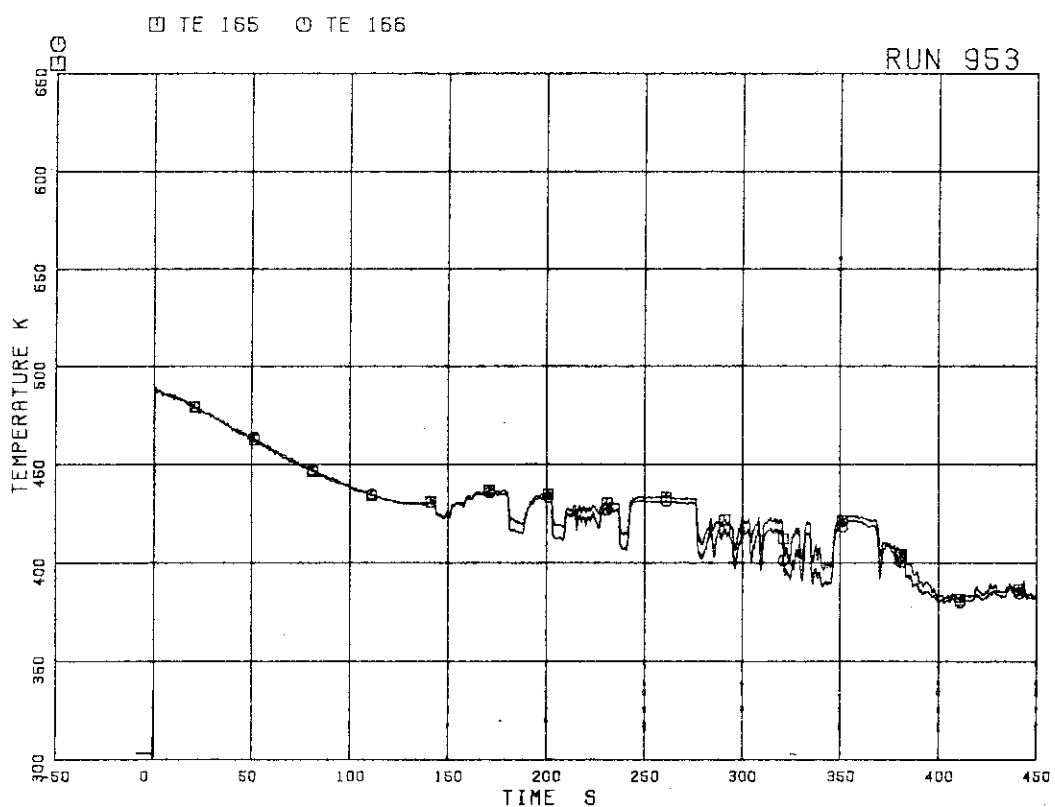


FIG. 5. 78 FLUID TEMPERATURES AT BREAK ORIFICE

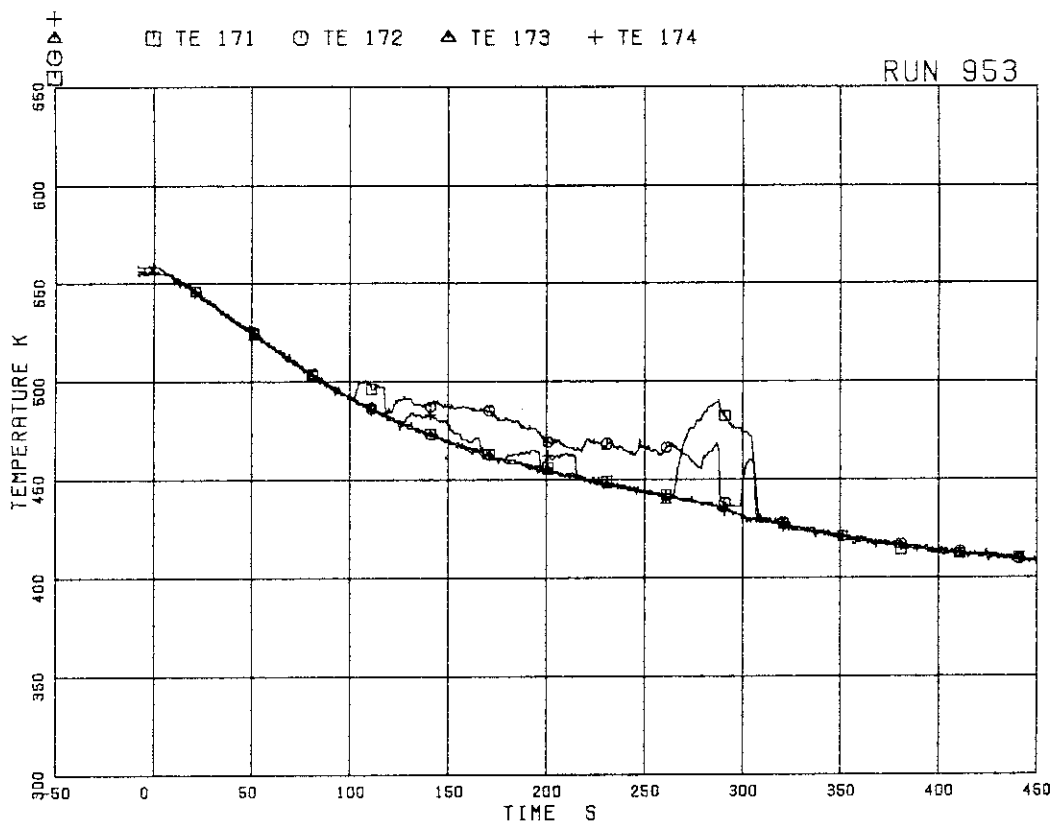


FIG. 5. 79 JP DIFFUSER WALL TEMPERATURES

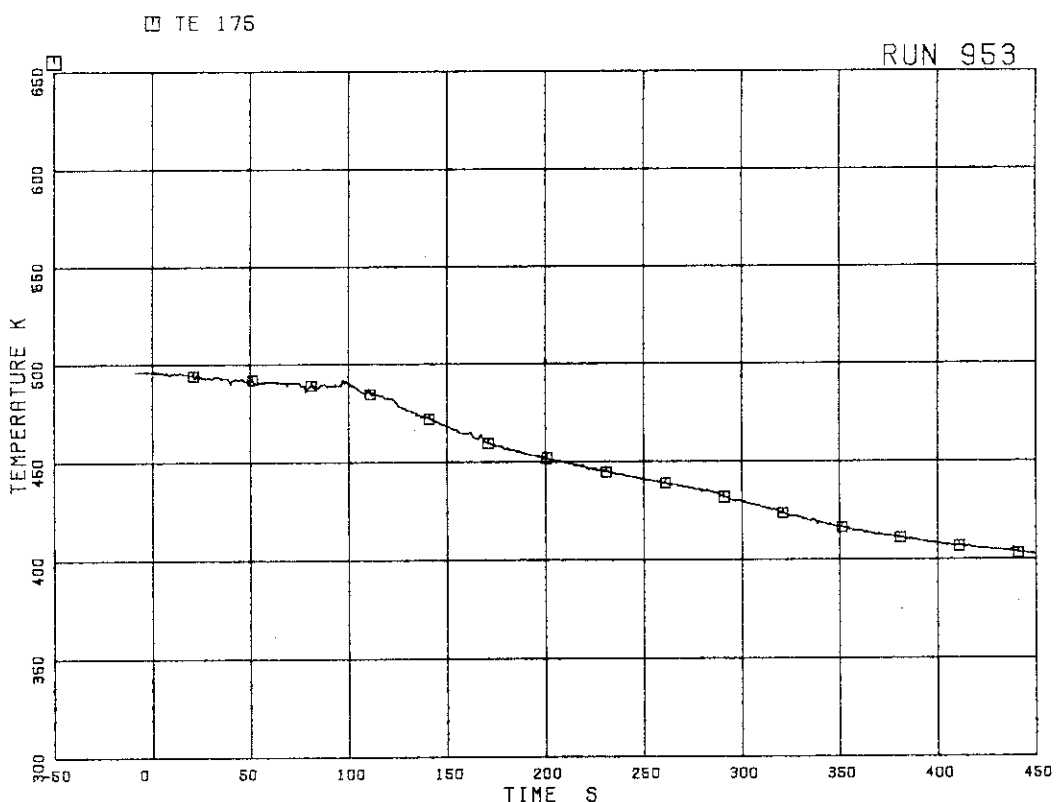


FIG. 5. 80 PV FEEDWATER FLUID TEMPERATURE

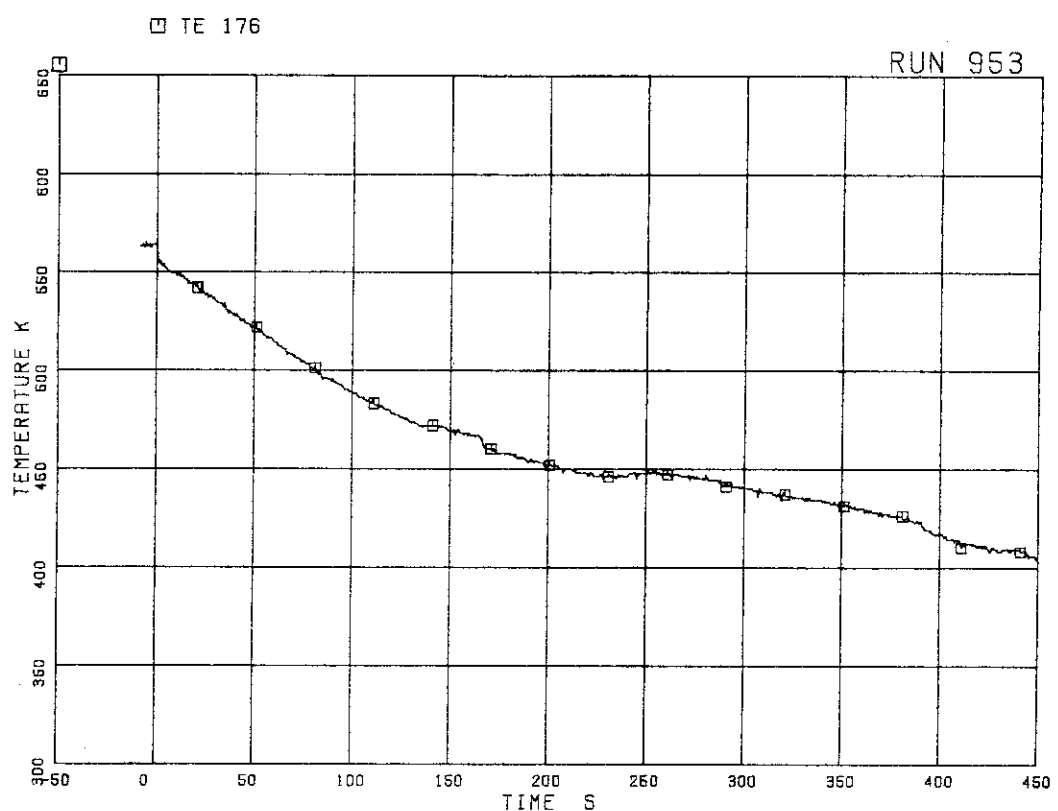


FIG. 5. 81 DISCHARGED STEAM TEMPERATURE

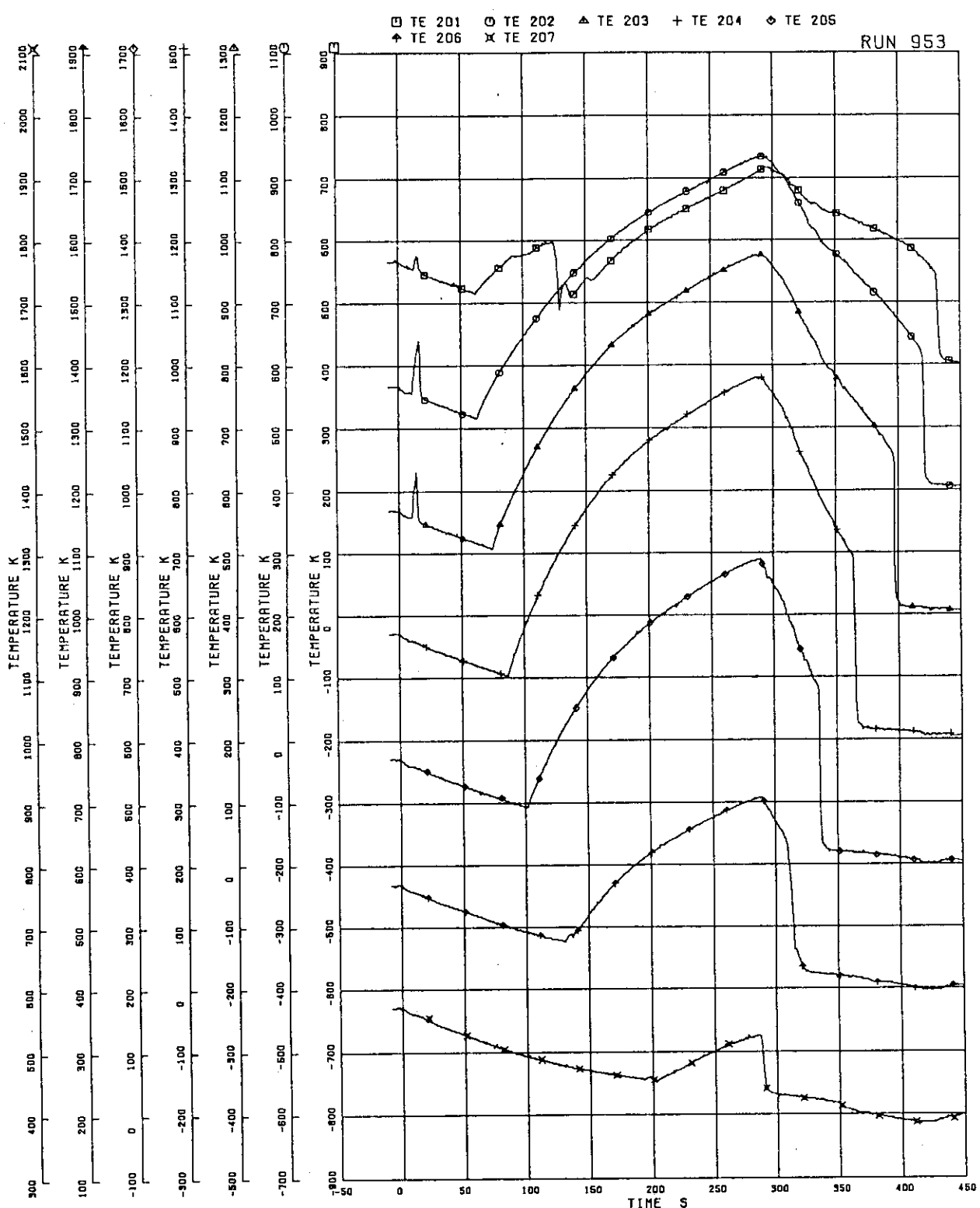


FIG. 5. 82 SURFACE TEMPERATURES OF FUEL ROD A11

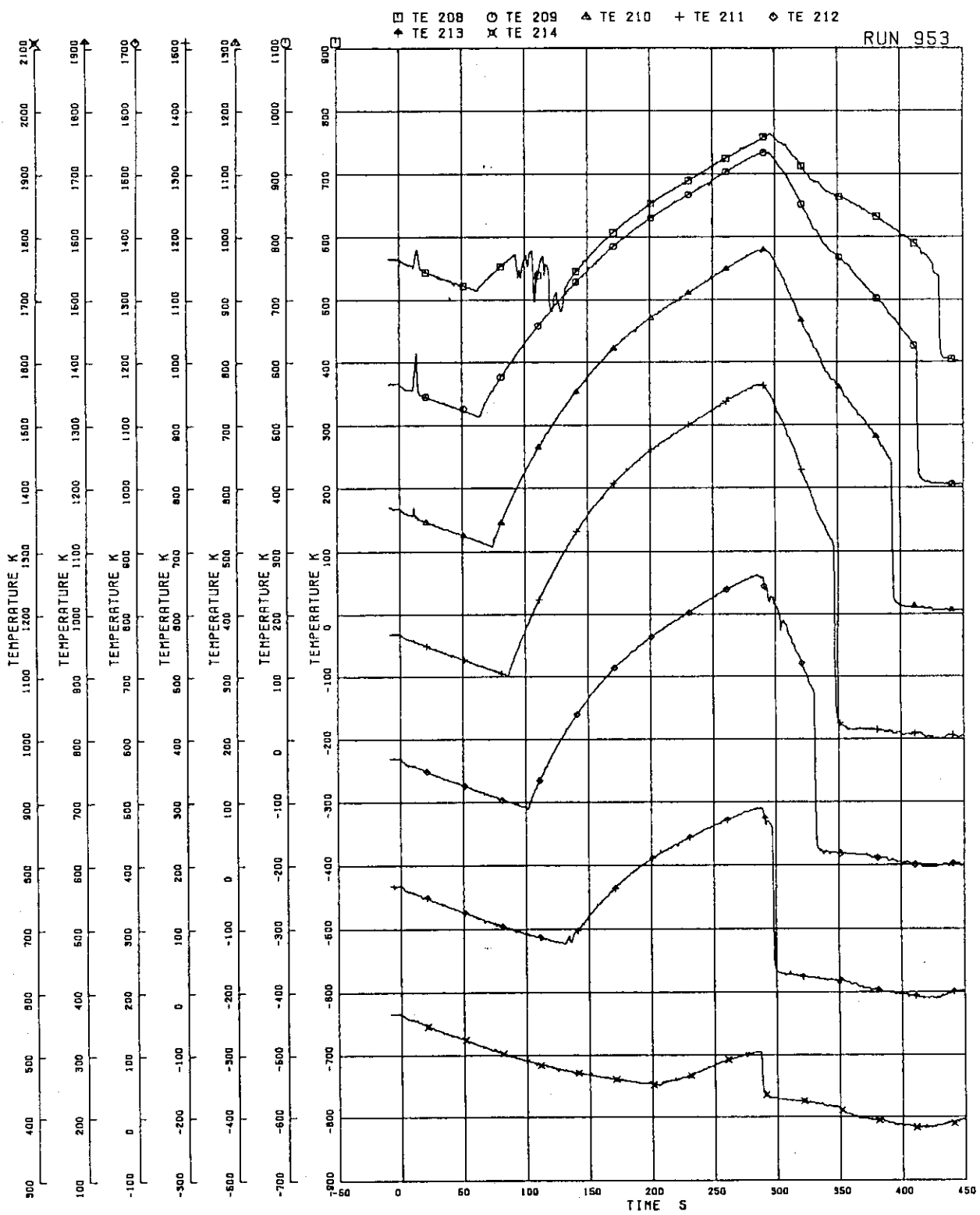


FIG. 5. 83 SURFACE TEMPERATURES OF FUEL ROD A12

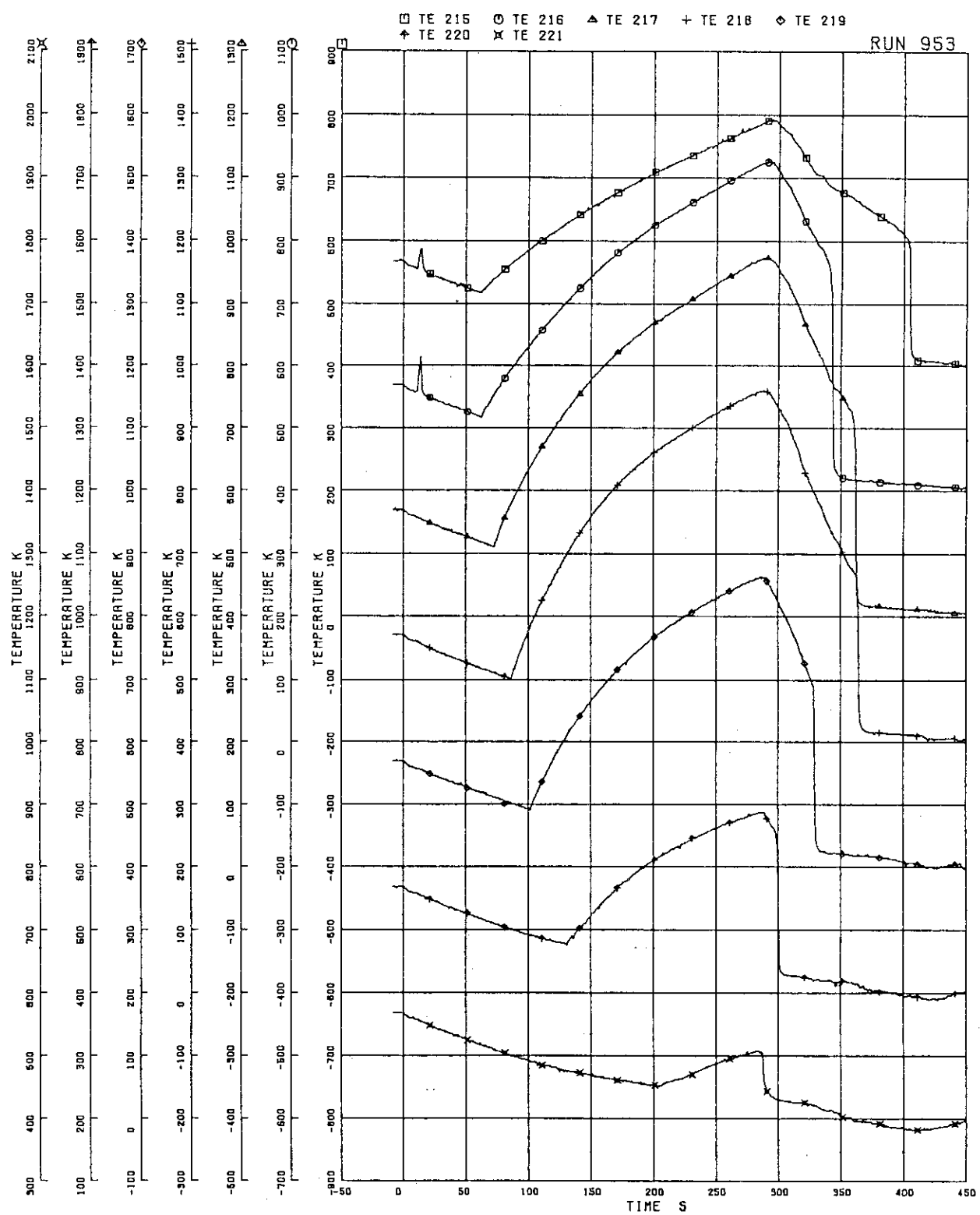


FIG. 5. 84 SURFACE TEMPERATURES OF FUEL ROD A13

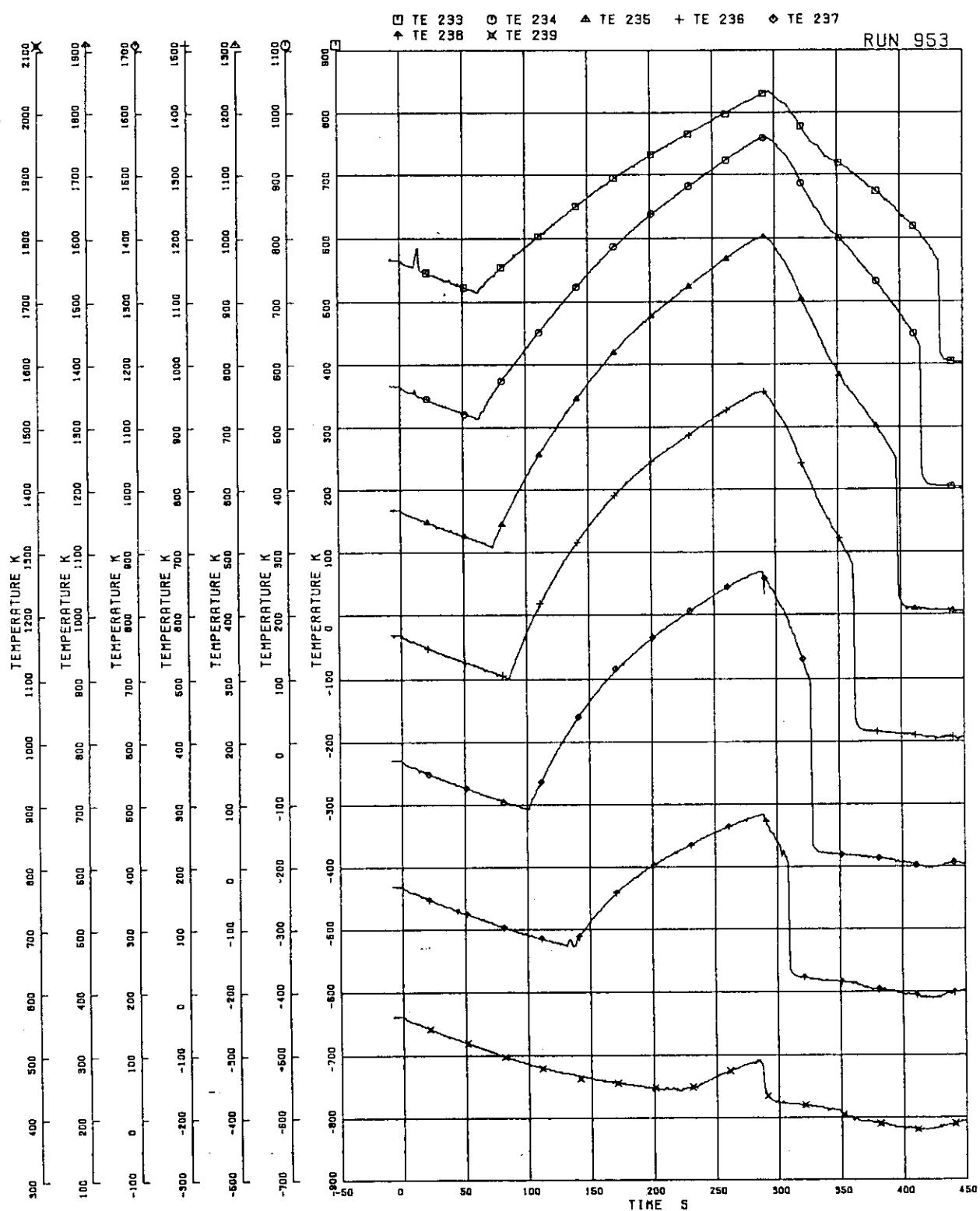


FIG. 5. 85 SURFACE TEMPERATURES OF FUEL ROD A22

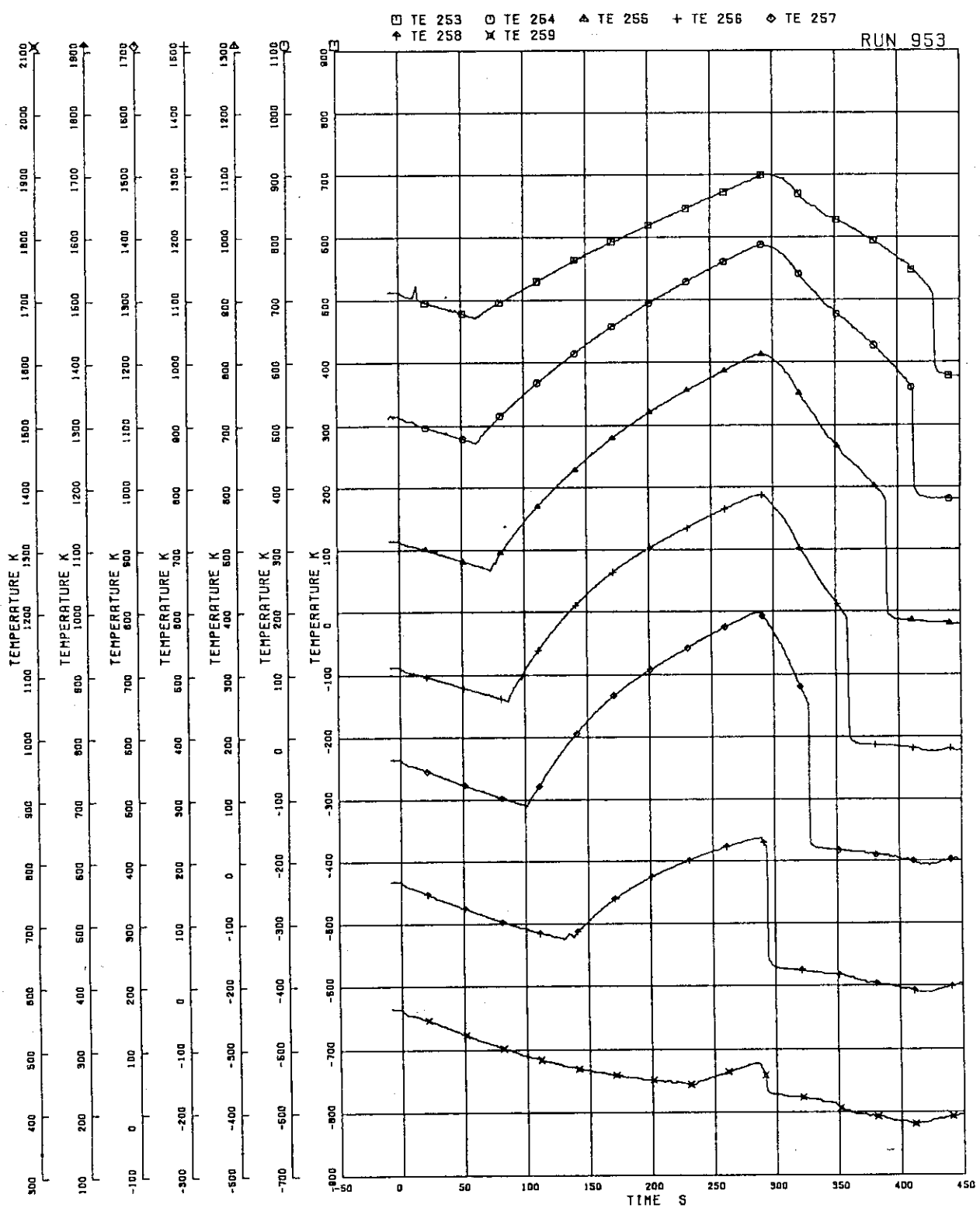


FIG. 5. 86 SURFACE TEMPERATURES OF FUEL ROD A33

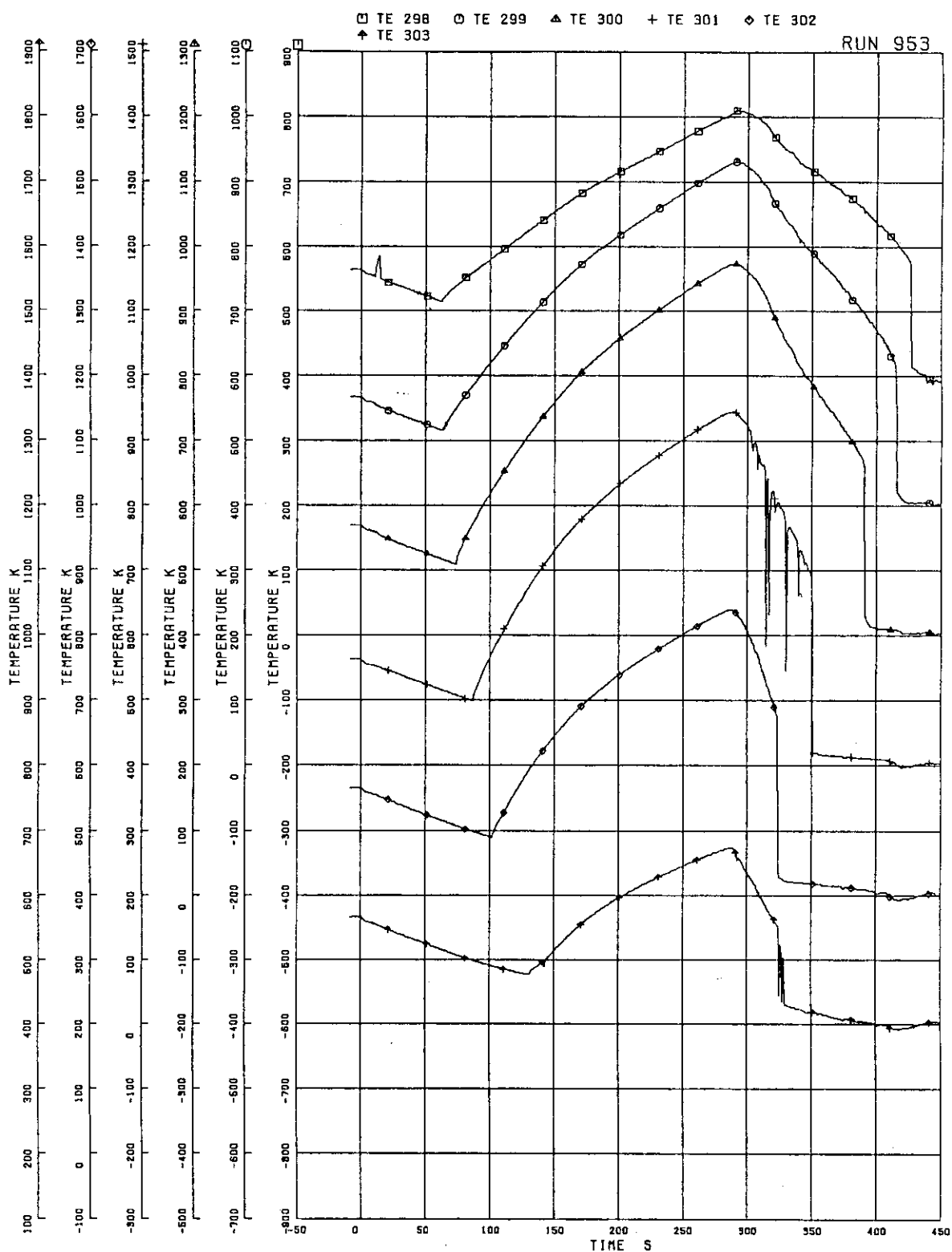


FIG. 5-87 SURFACE TEMPERATURES OF FUEL ROD A77

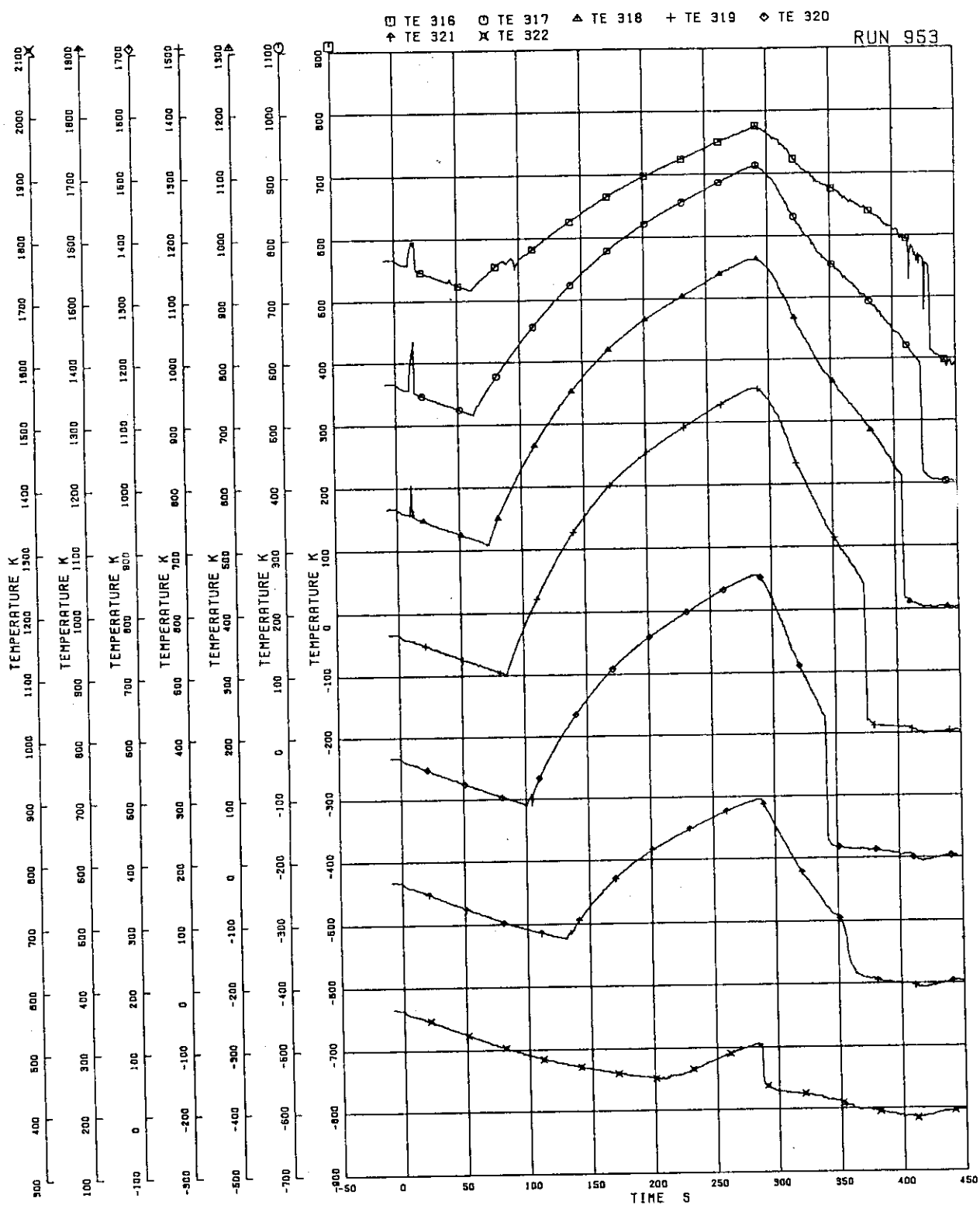


FIG. 5. 88 SURFACE TEMPERATURES OF FUEL ROD A87

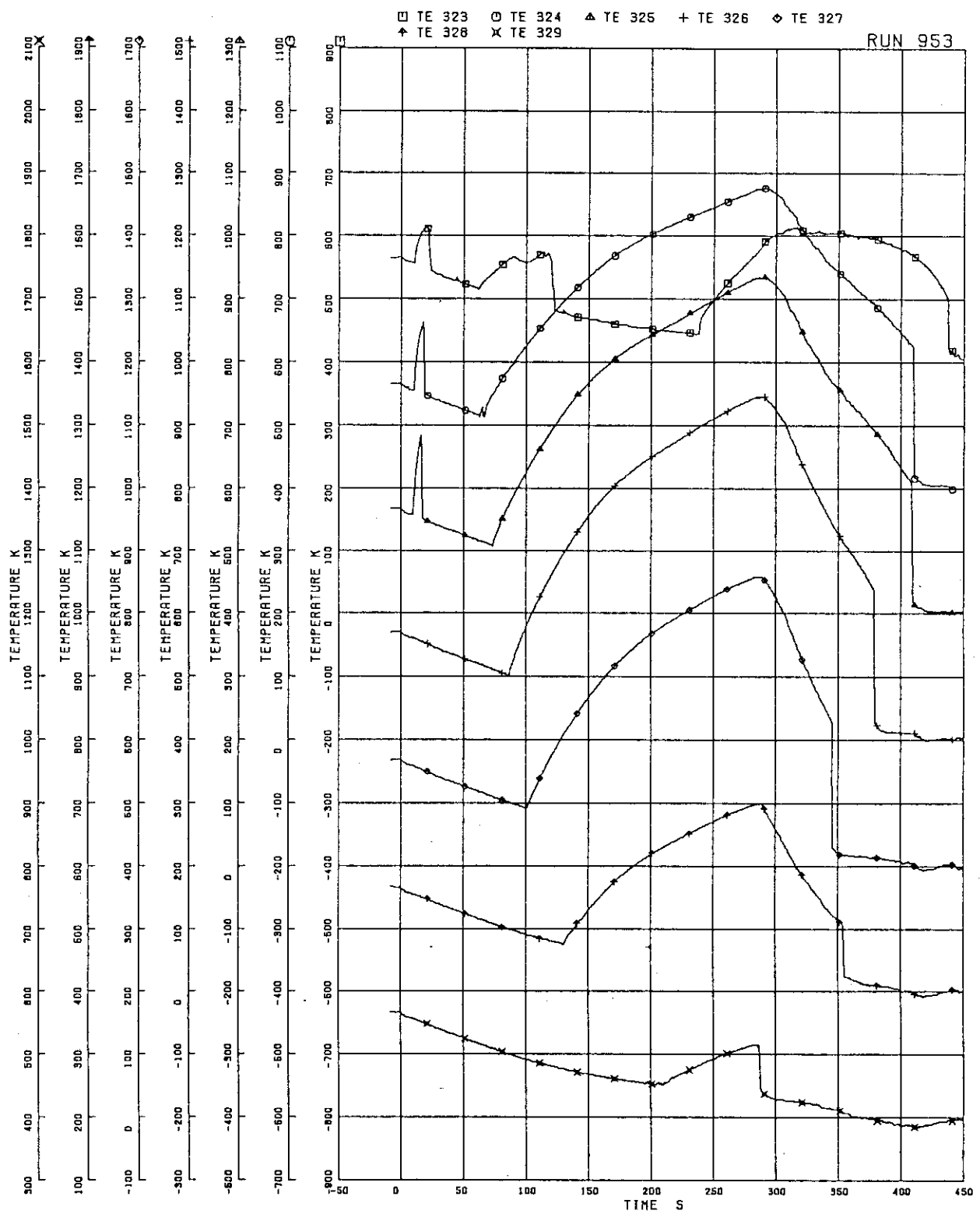


FIG. 5. 89 SURFACE TEMPERATURES OF FUEL ROD A88

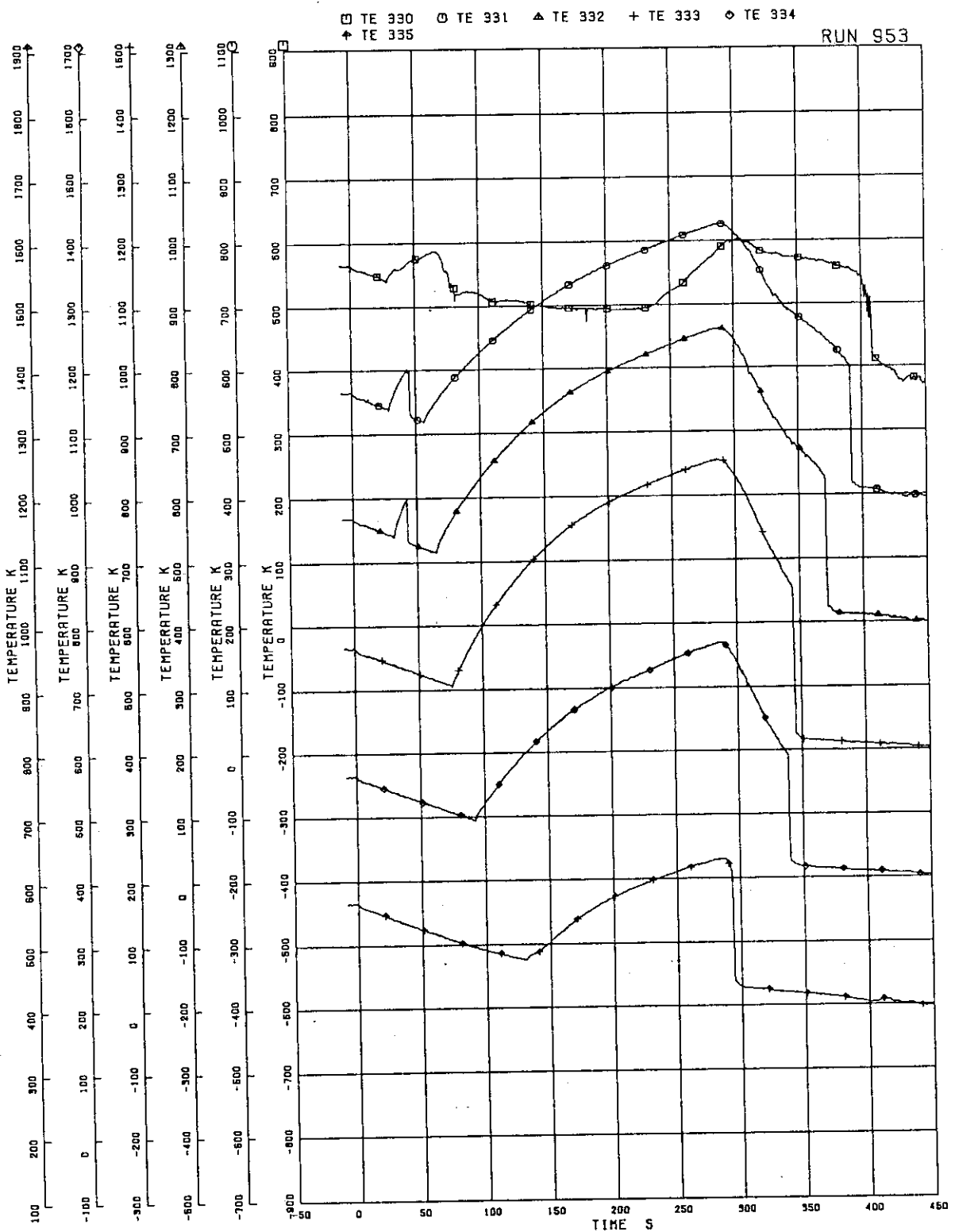


FIG. 5. 90 SURFACE TEMPERATURES OF FUEL ROD B11

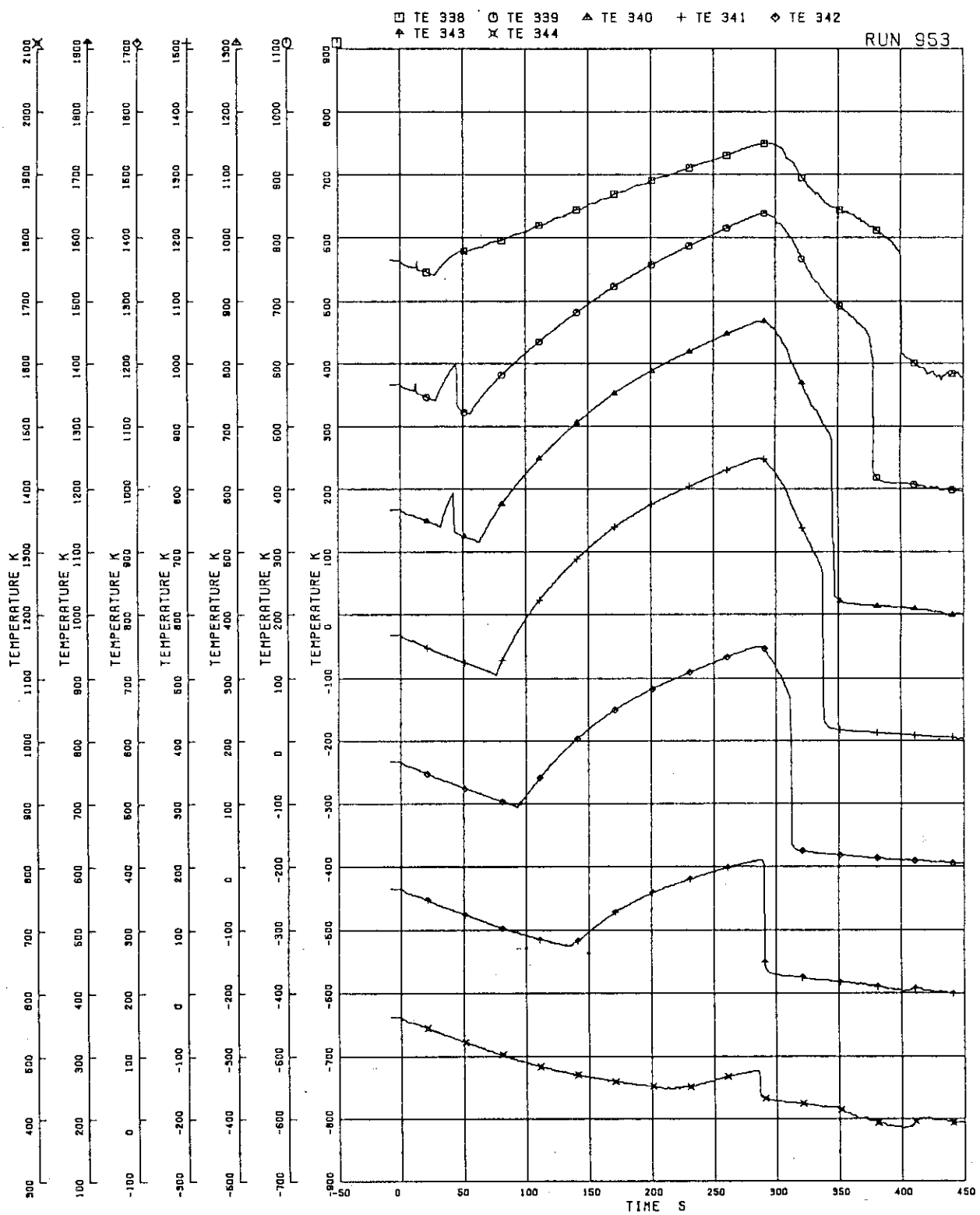


FIG. 5. 91 SURFACE TEMPERATURES OF FUEL ROD 822

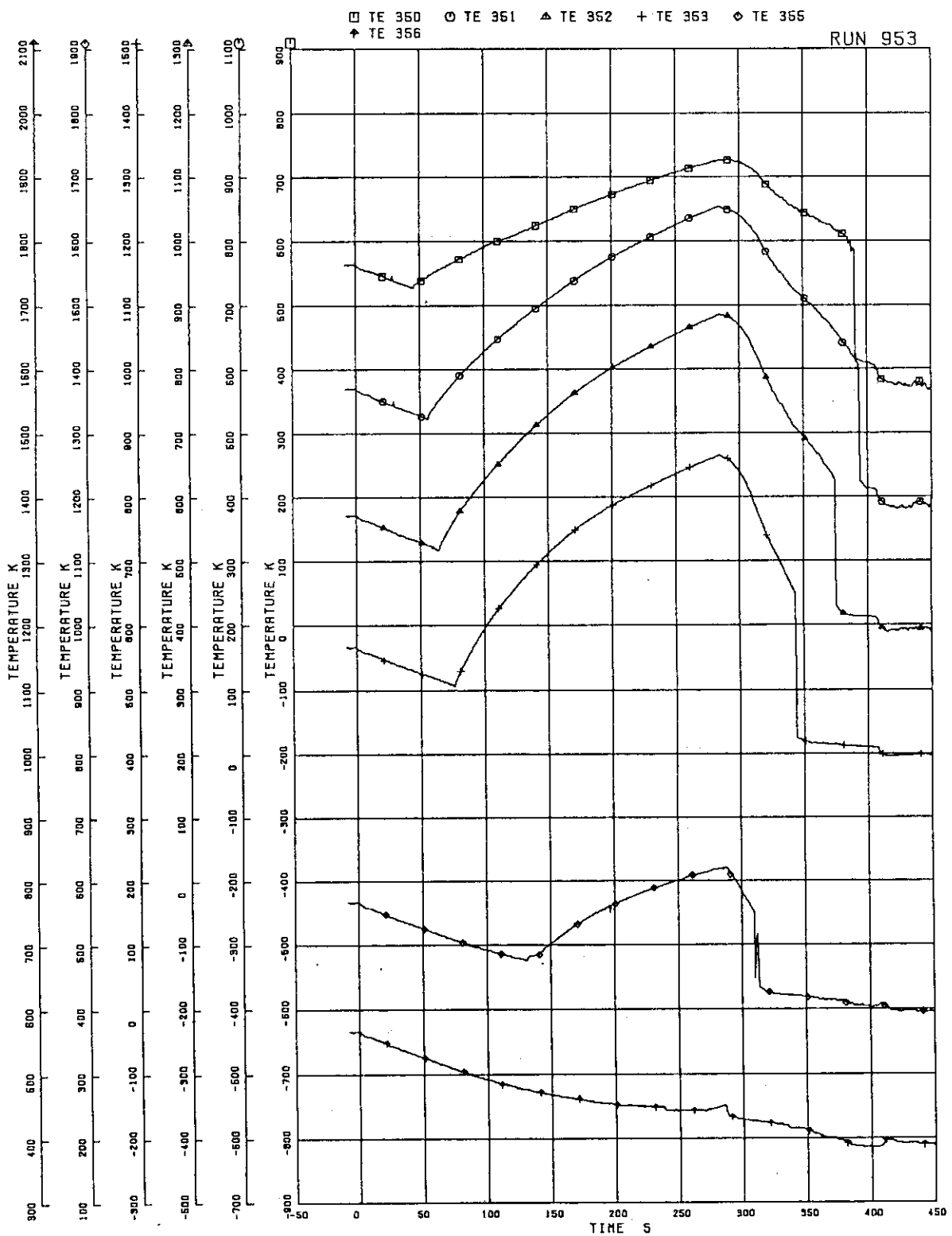


FIG. 5. 92 SURFACE TEMPERATURES OF FUEL ROD B77

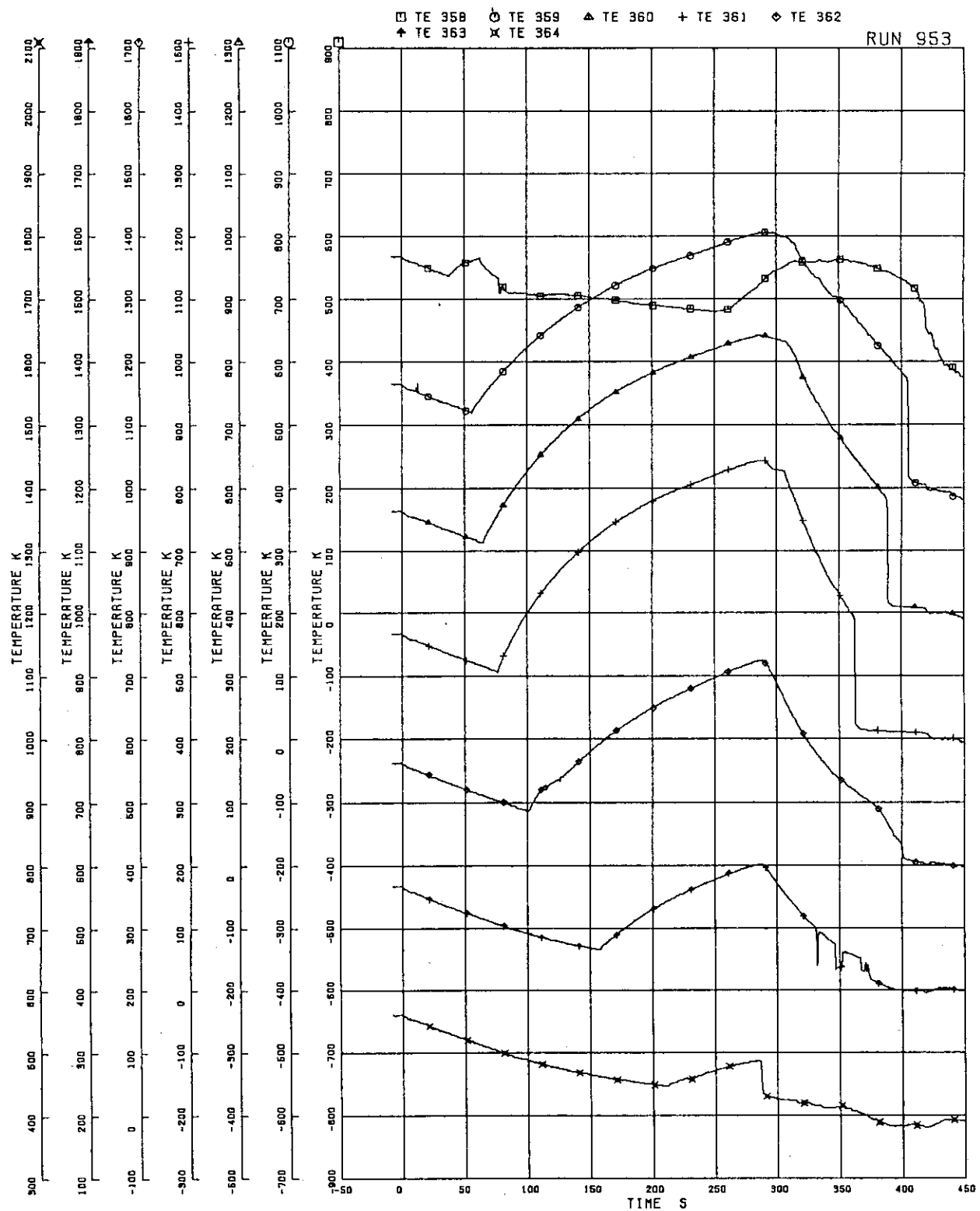


FIG. 5. 93 SURFACE TEMPERATURES OF FUEL ROD C11

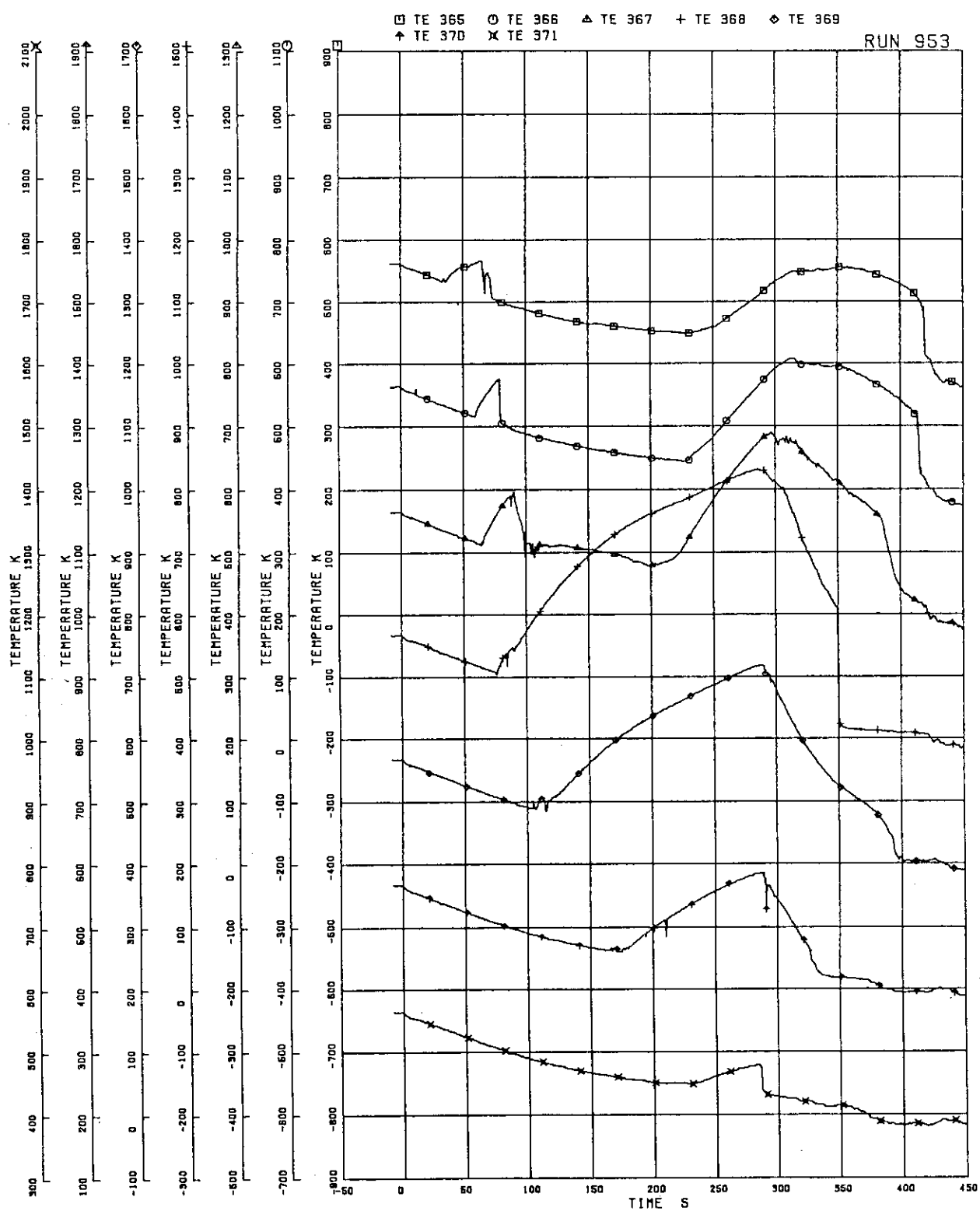


FIG. 5. 94 SURFACE TEMPERATURES OF FUEL ROD C13

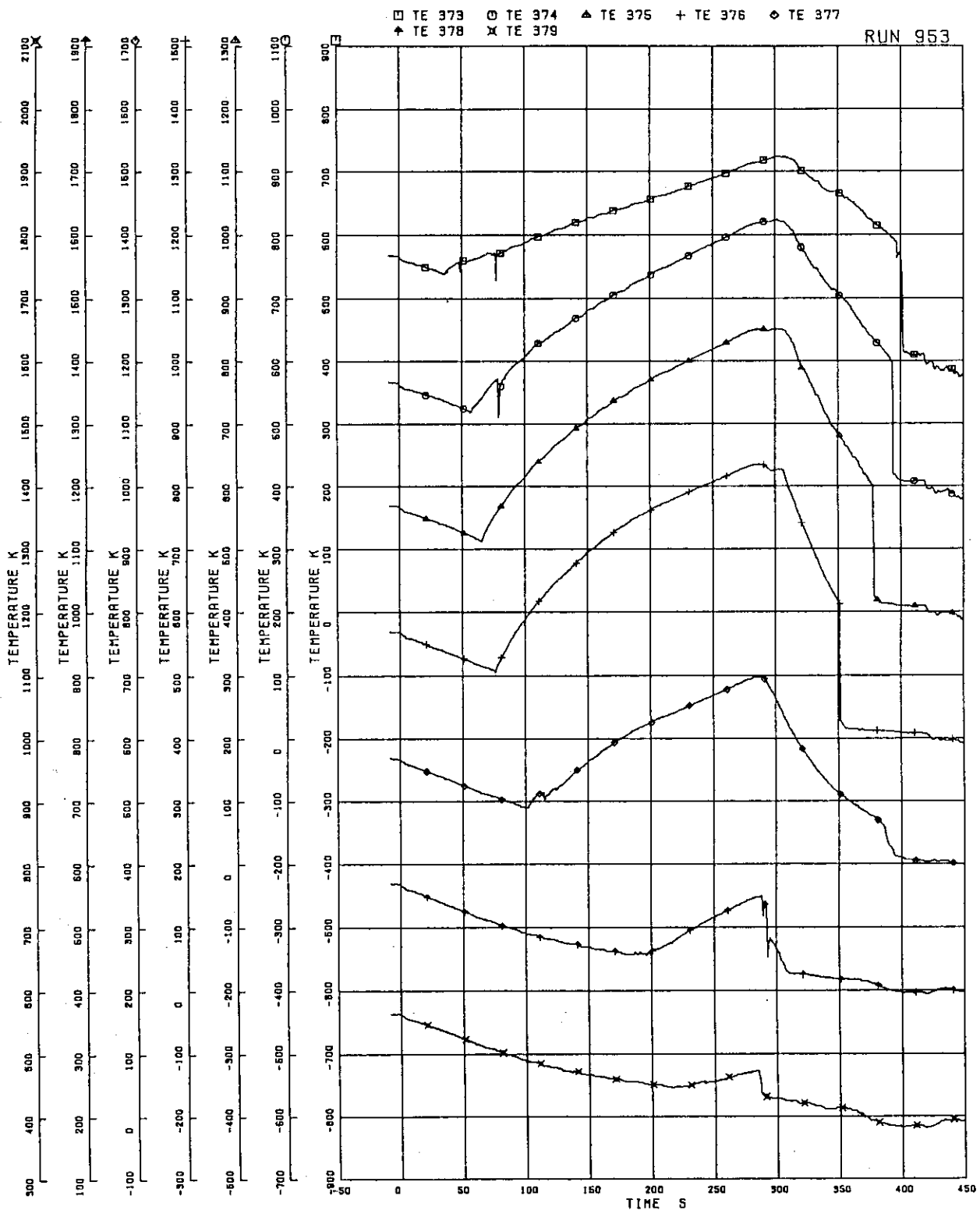


FIG. 5. 95 SURFACE TEMPERATURES OF FUEL ROD C22

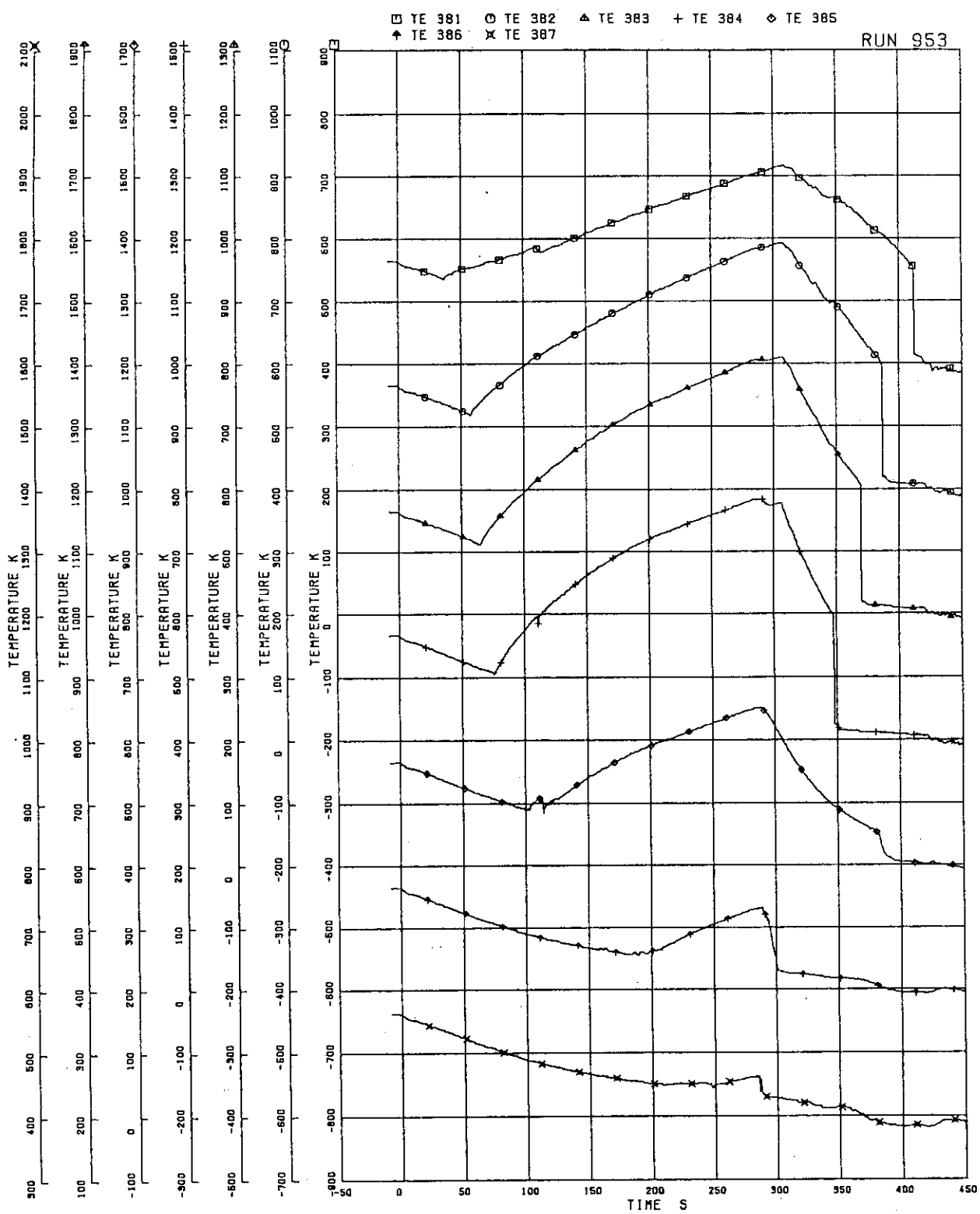


FIG. 5-96 SURFACE TEMPERATURES OF FUEL ROD C33

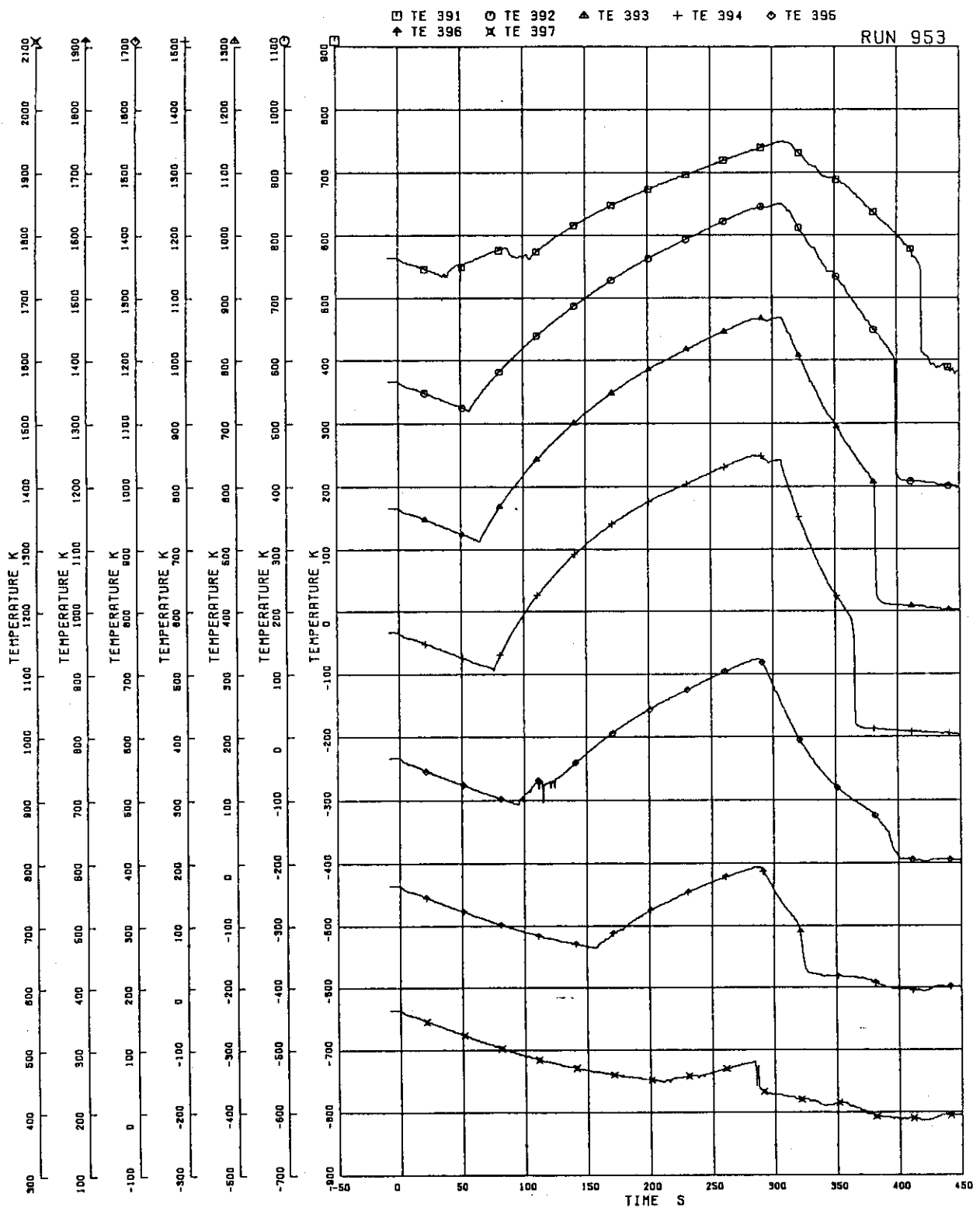


FIG. 5. 97 SURFACE TEMPERATURES OF FUEL ROD C77

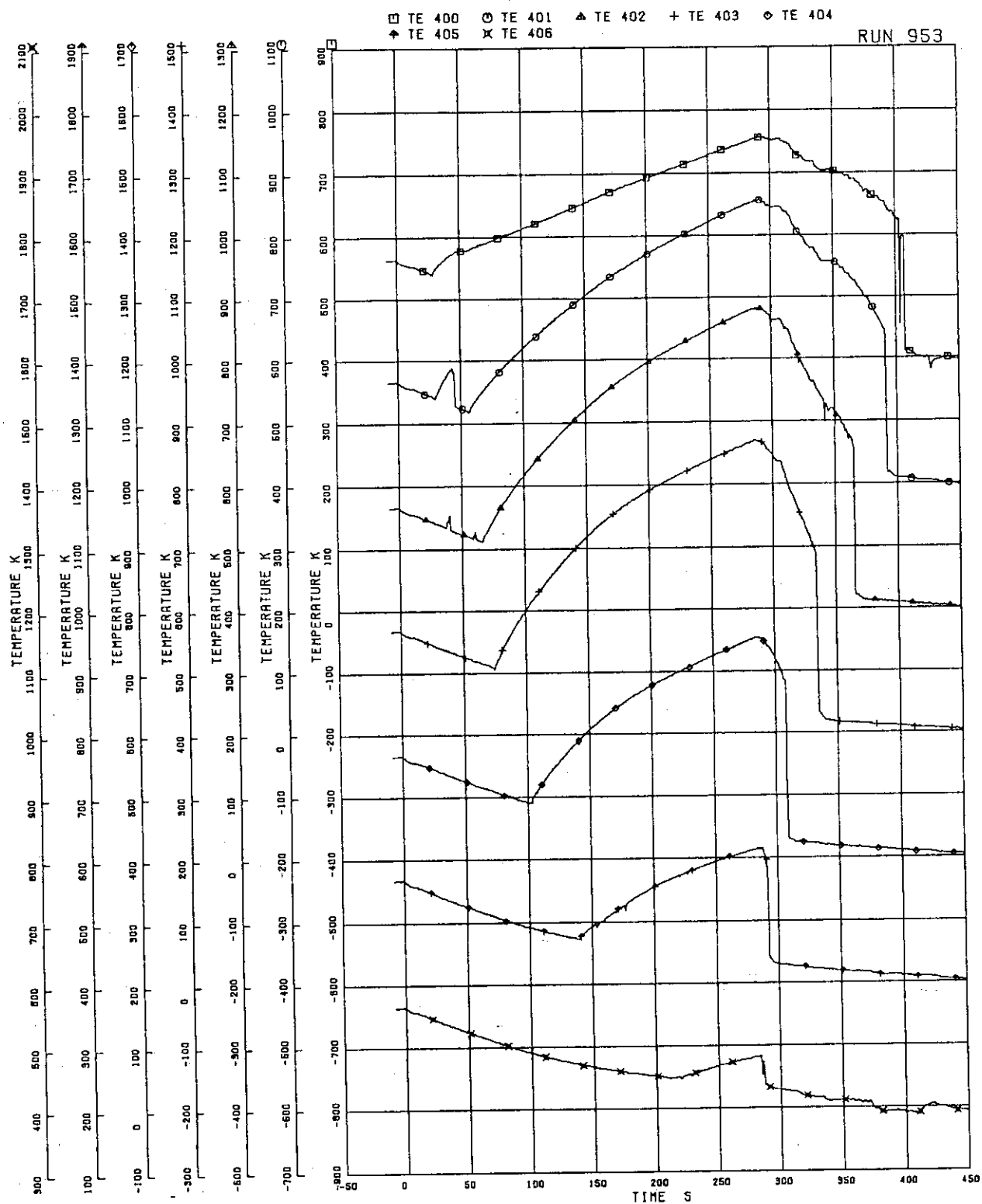


FIG. 5. 98 SURFACE TEMPERATURES OF FUEL ROD D22

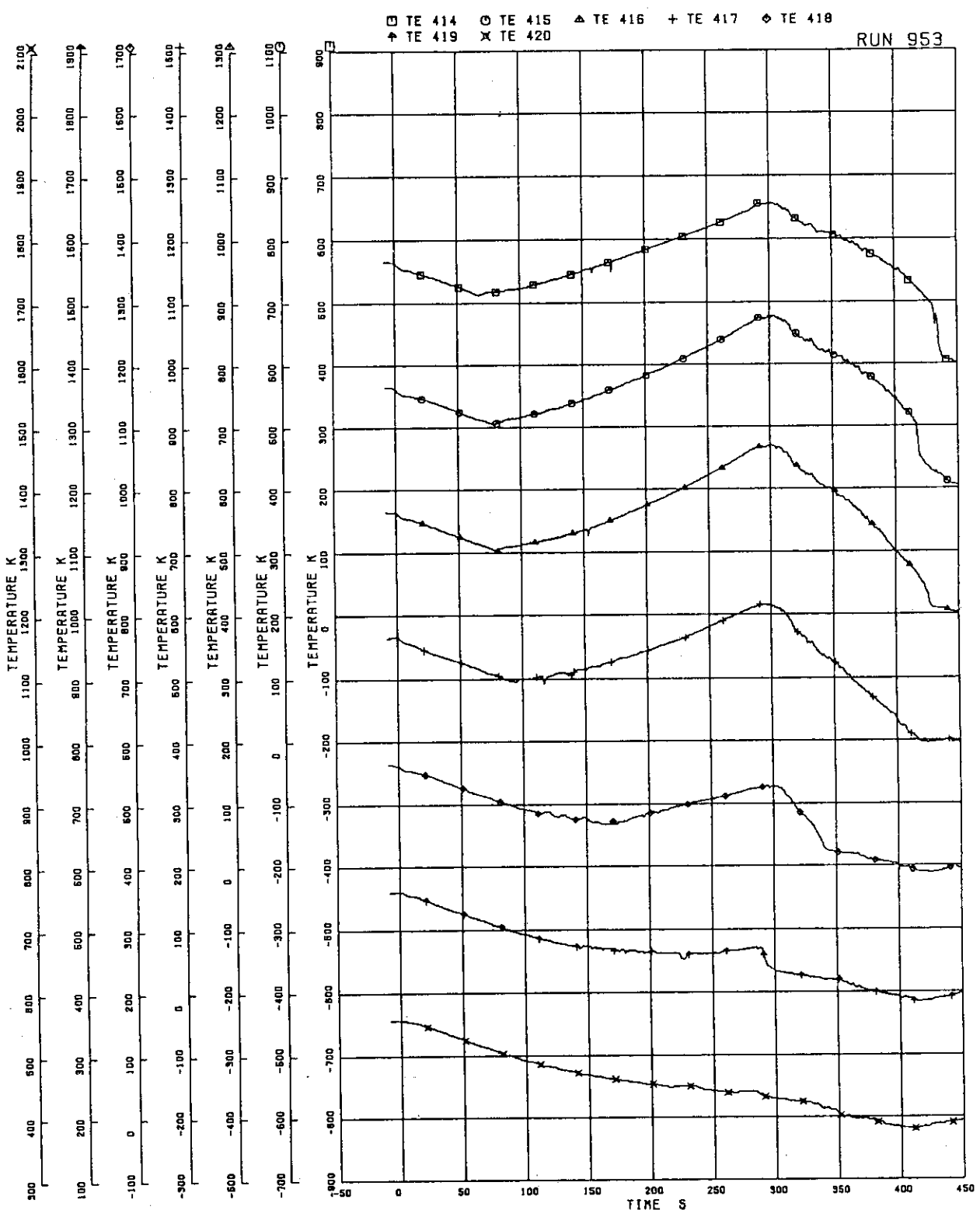
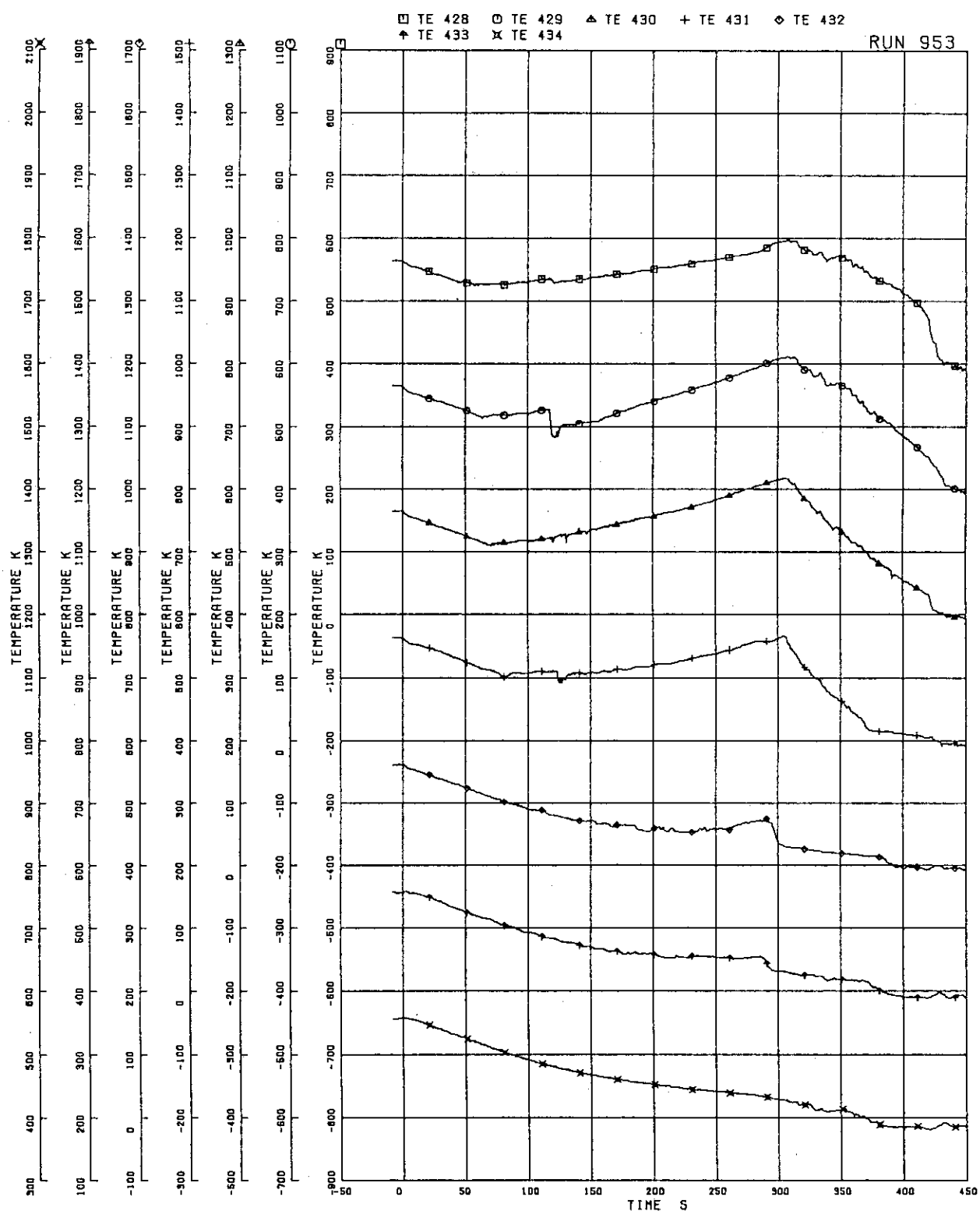


FIG. 5. 99 SURFACE TEMPERATURES OF  
WATER ROD SIMULATOR R45

FIG.5.100 SURFACE TEMPERATURES OF  
WATER ROD SIMULATOR C45

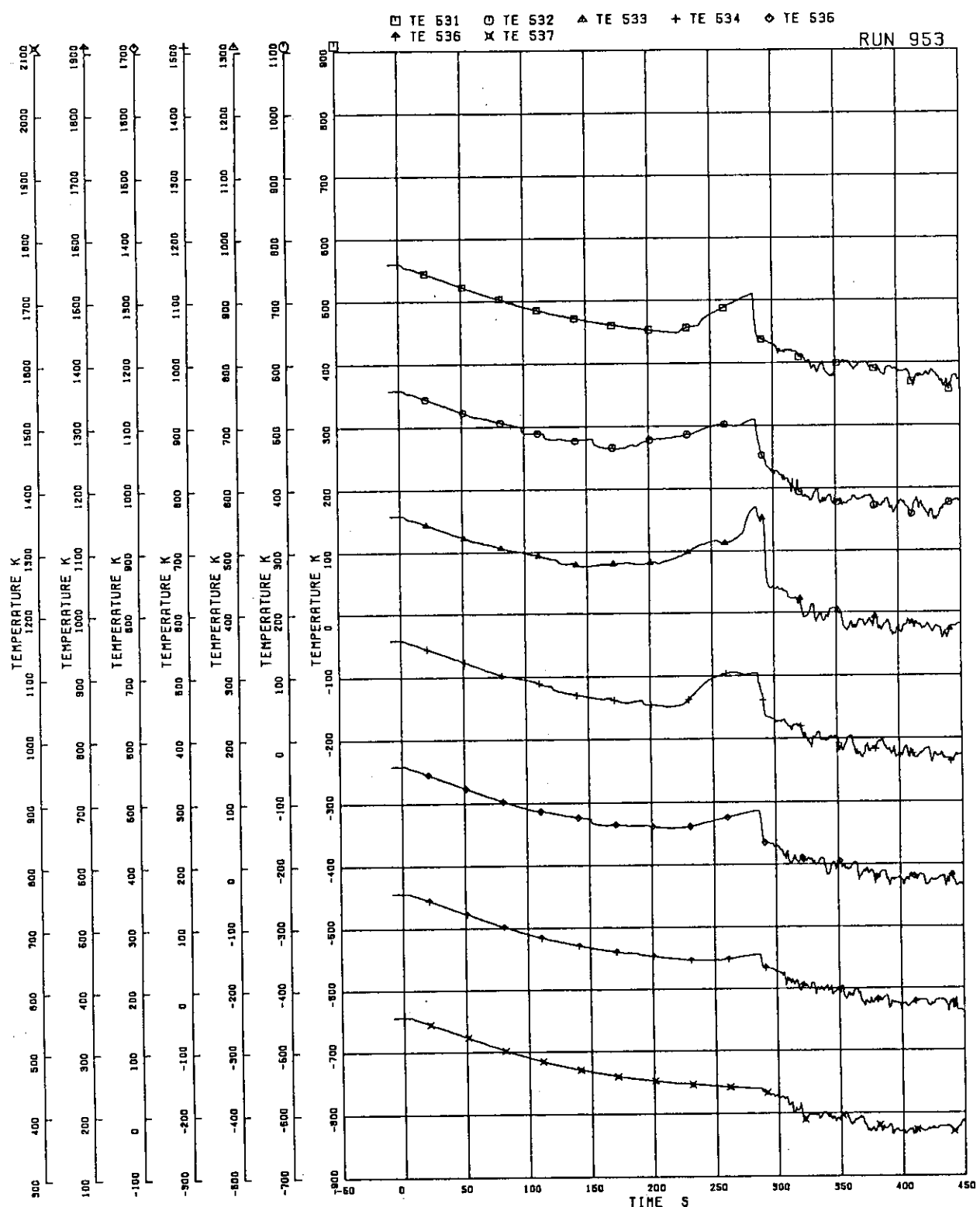


FIG.5.101 OUTER SURFACE TEMPERATURES OF CHANNEL BOX A

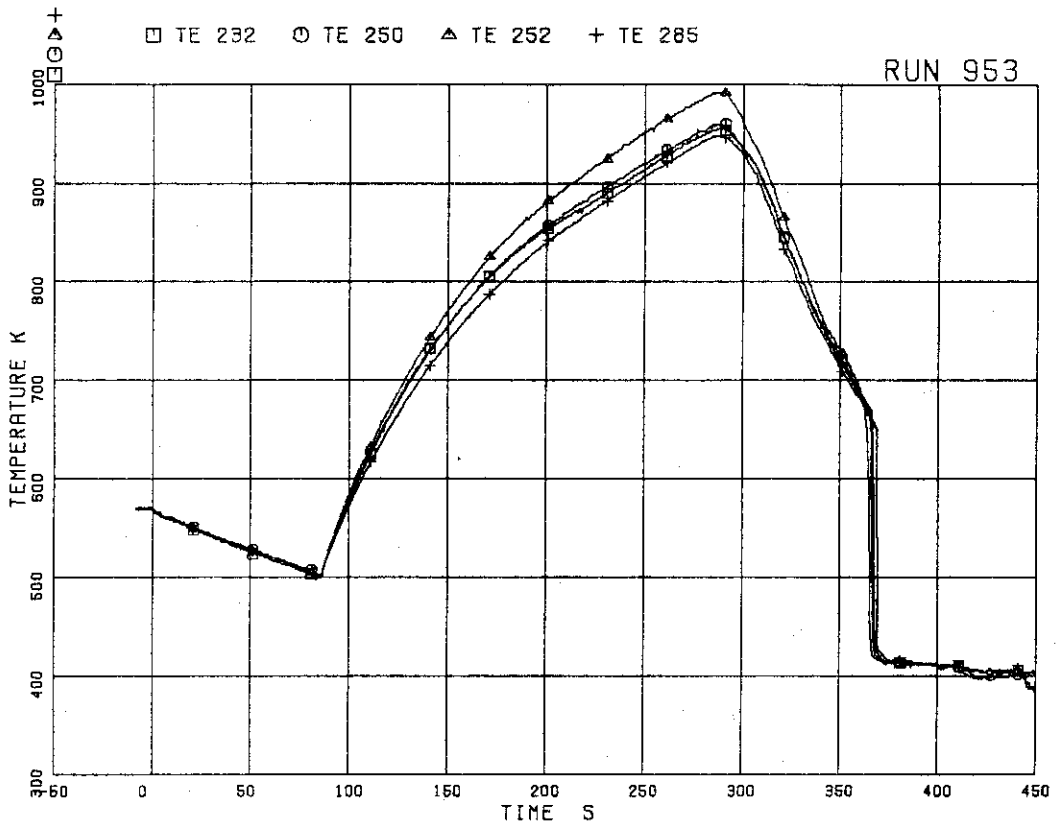


FIG.5.102 SURFACE TEMPERATURE OF FUEL RODS  
A17,A28,A31,A57 AT POSITION 4

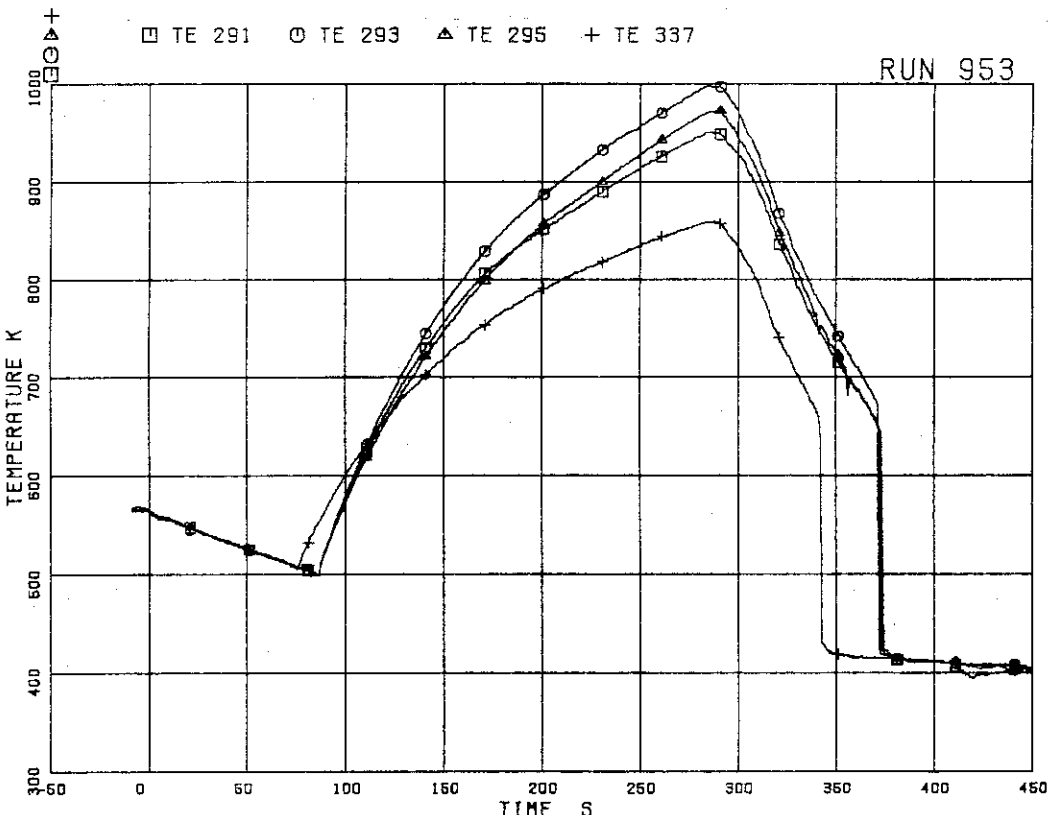


FIG.5.103 SURFACE TEMPERATURE OF FUEL RODS  
A68,A71,A73,B13 AT POSITION 4

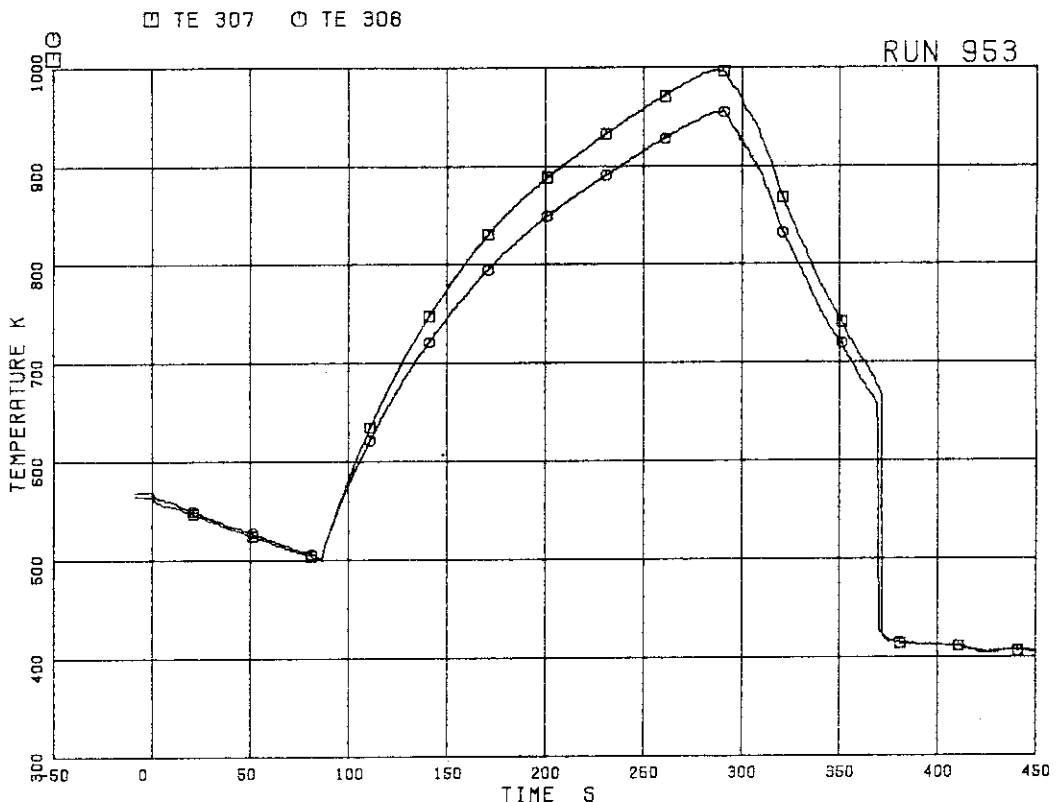


FIG.5.104 SURFACE TEMPERATURES OF FUEL ROD A84  
AT POSITIONS 1 AND 4

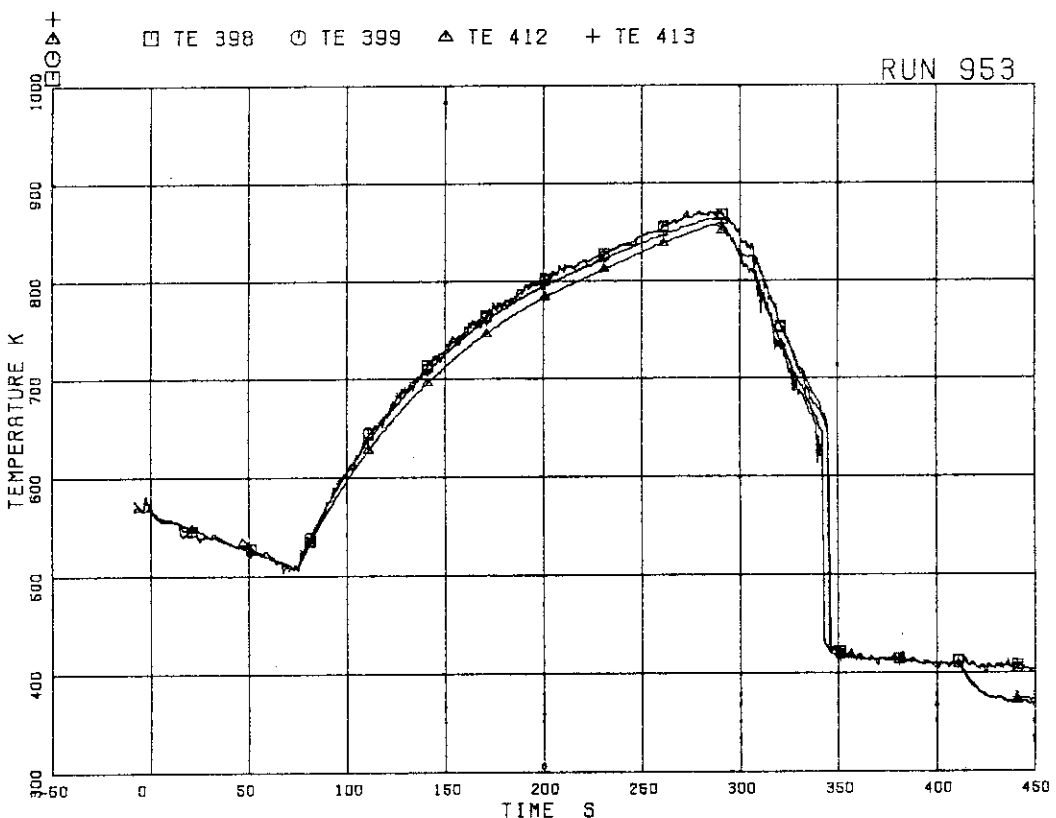


FIG.5.105 SURFACE TEMPERATURES OF FUEL RODS  
D11,D13,D77,D86 AT POSITION 4

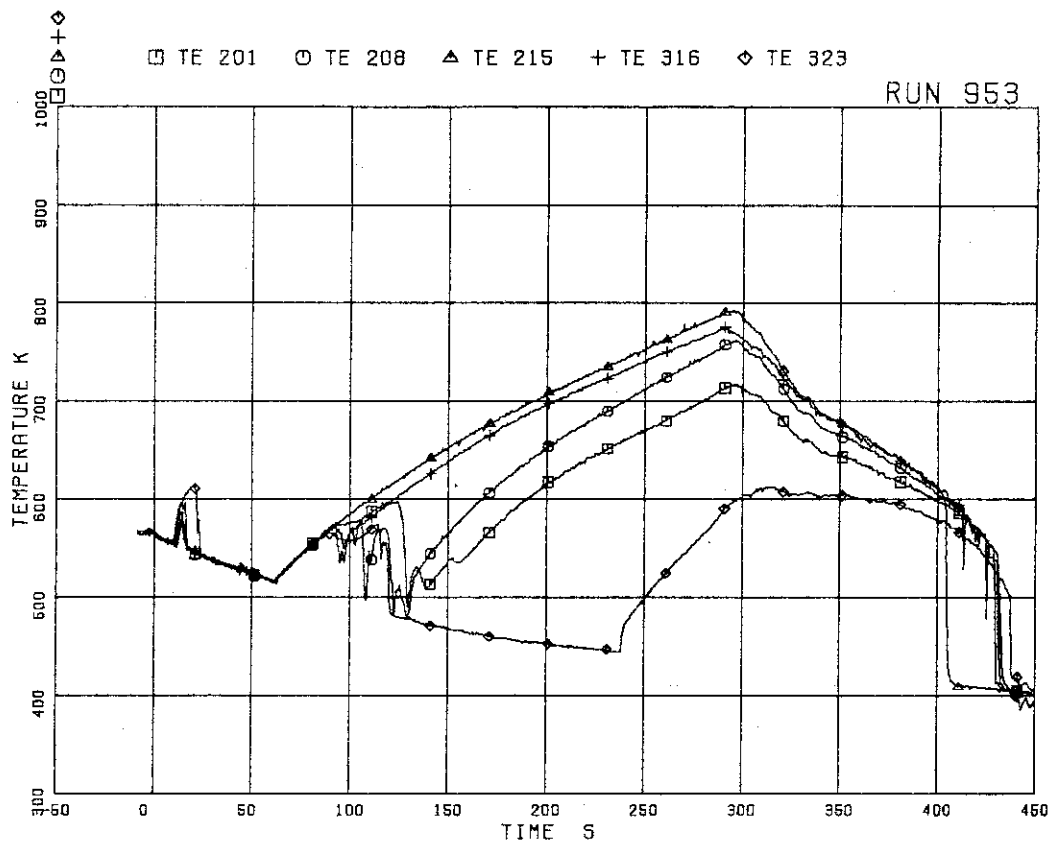


FIG.5.106 SURFACE TEMPERATURES OF FUEL RODS  
A11,A12,A13,A87,A88 AT POSITION 1

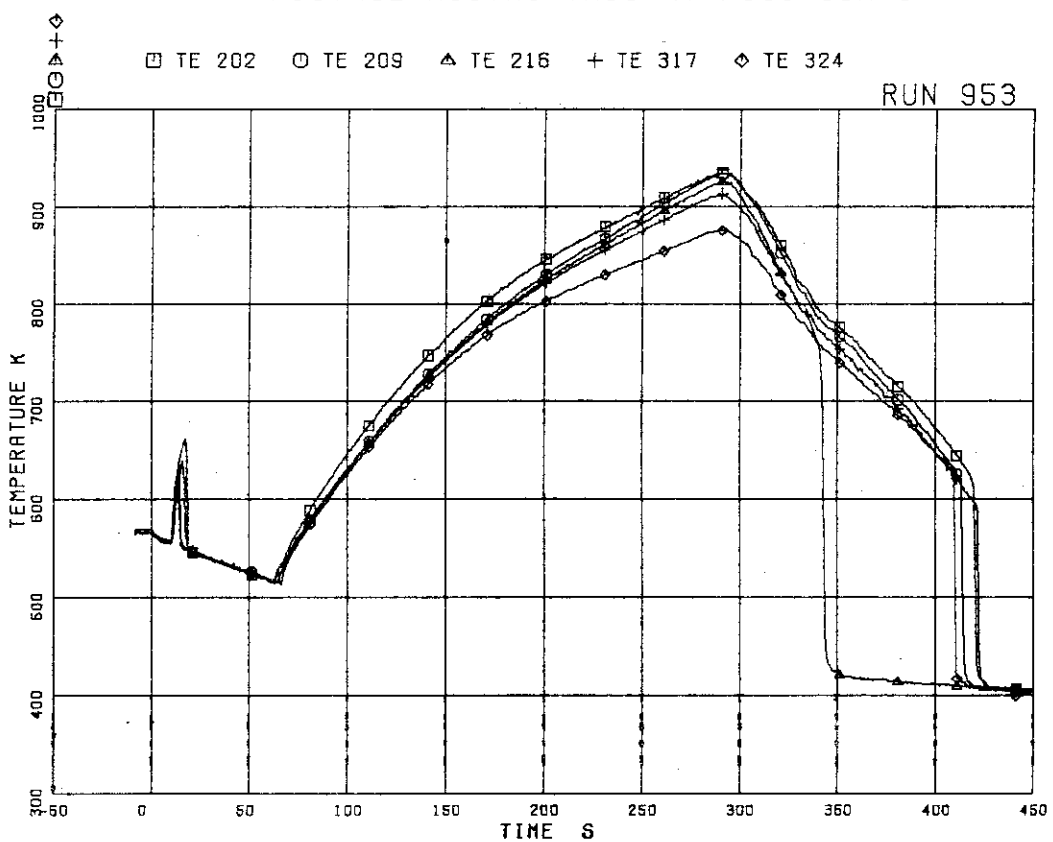


FIG.5.107 SURFACE TEMPERATURES OF FUEL RODS  
A11,A12,A13,A87,A88 AT POSITION 2

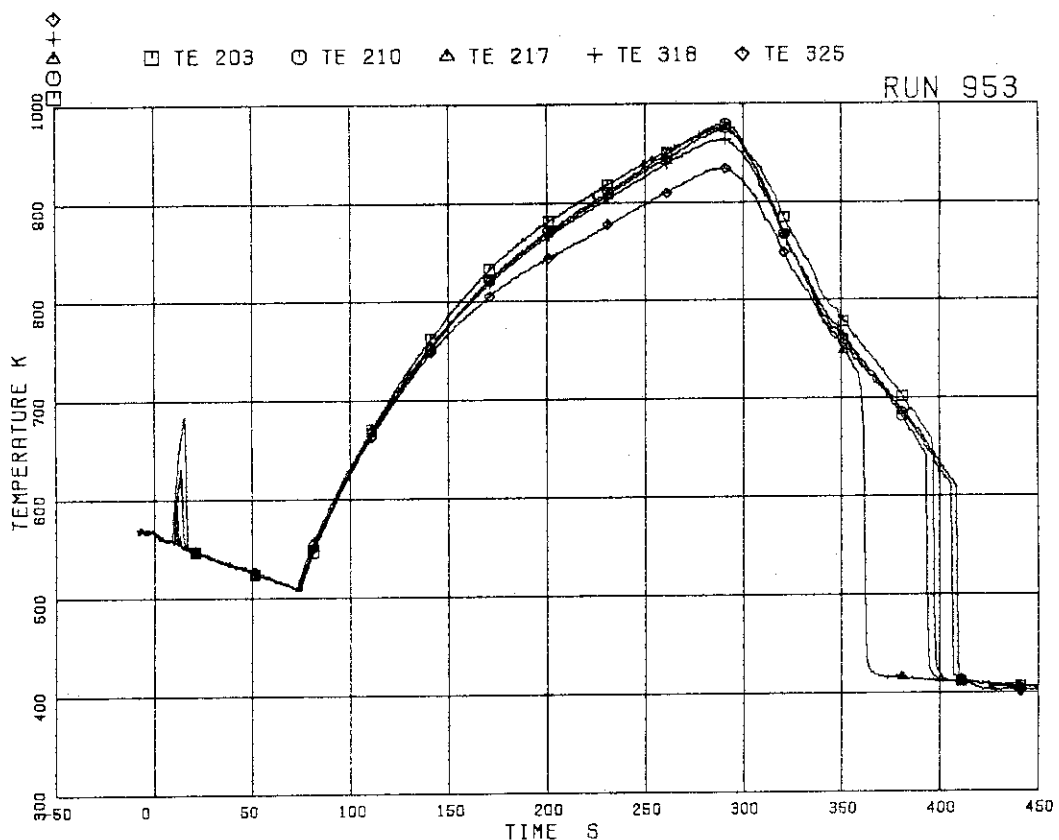


FIG.5.108 SURFACE TEMPERATURES OF FUEL RODS  
A11,A12,A13,A87,A88 AT POSITION 3

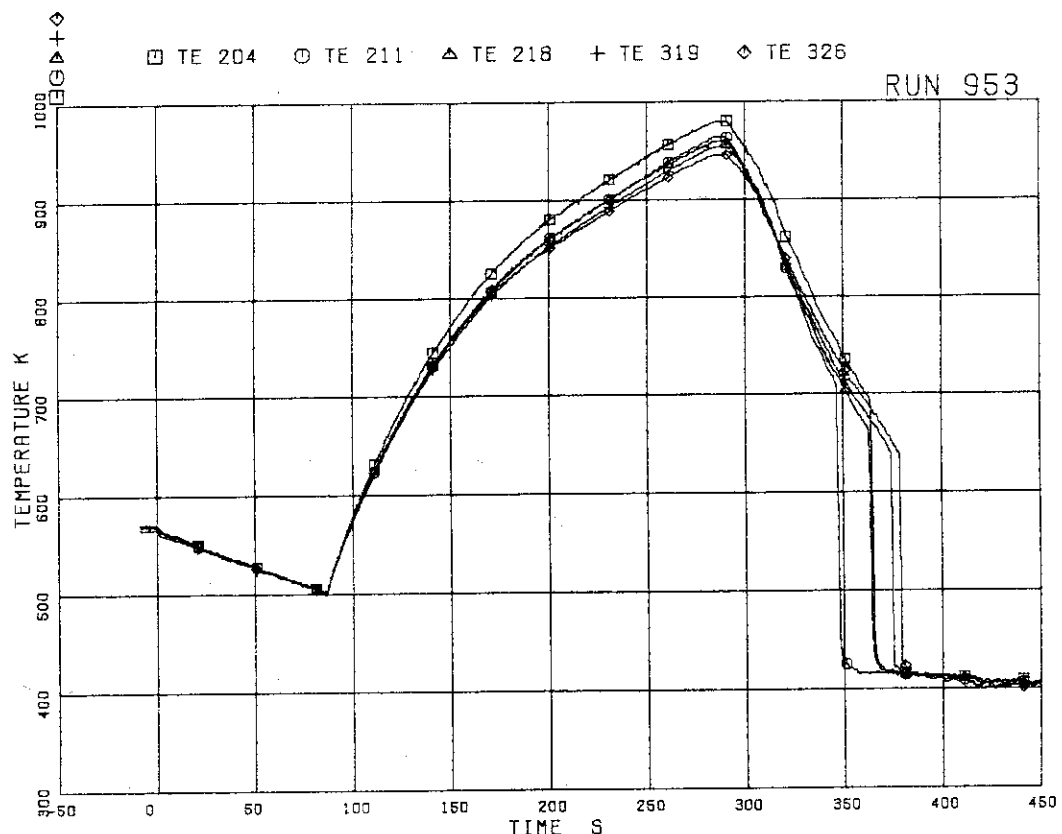


FIG.5.109 SURFACE TEMPERATURES OF FUEL RODS  
A11,A12,A13,A87,A88 AT POSITION 4

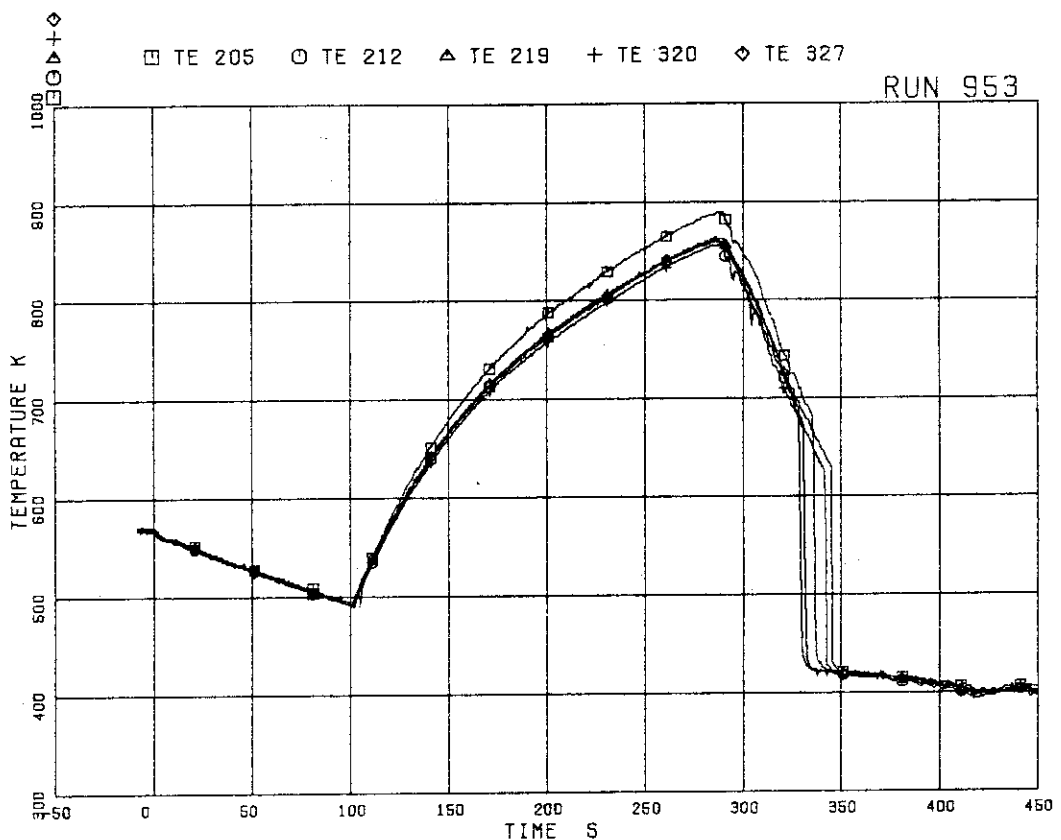


FIG. 5.110 SURFACE TEMPERATURES OF FUEL RODS  
A11, A12, A13, A87, A88 AT POSITION 5

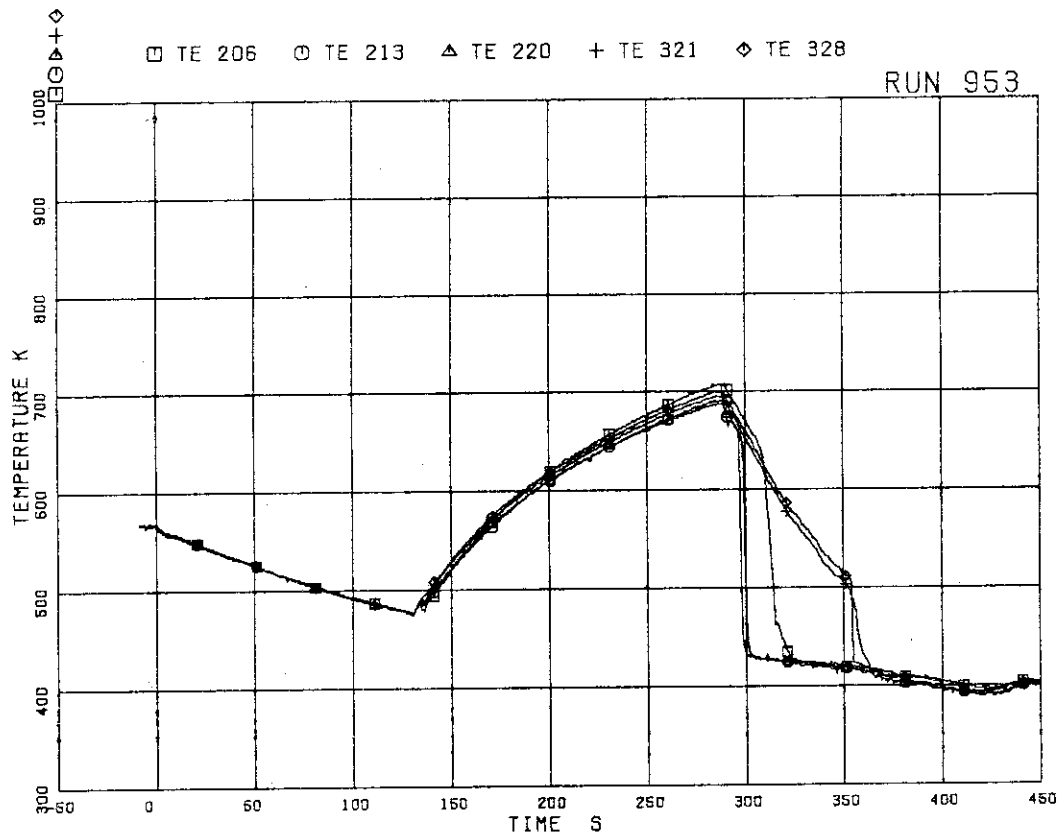


FIG. 5.111 SURFACE TEMPERATURES OF FUEL RODS  
A11, A12, A13, A87, A88 AT POSITION 6

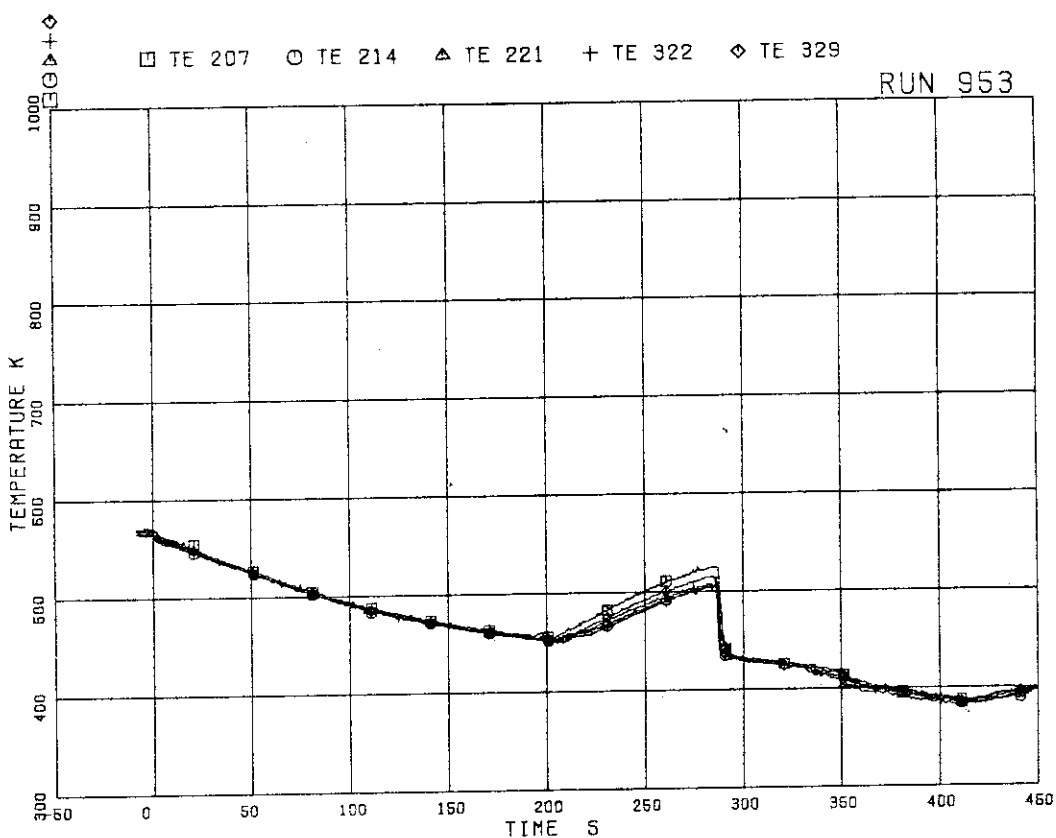


FIG.5.112 SURFACE TEMPERATURES OF FUEL RODS  
A11,A12,A13,A87,A88 AT POSITION 7

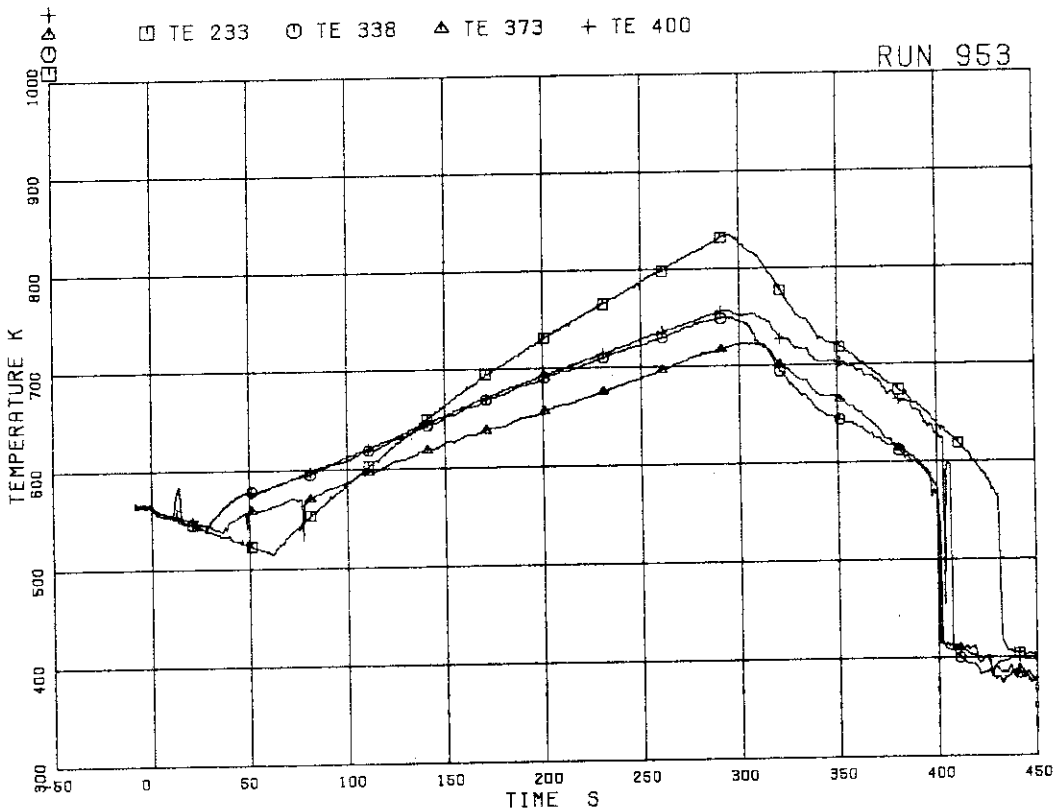


FIG.5.113 SURFACE TEMPERATURES OF FUEL RODS  
A22,B22,C22,D22 AT POSITION 1

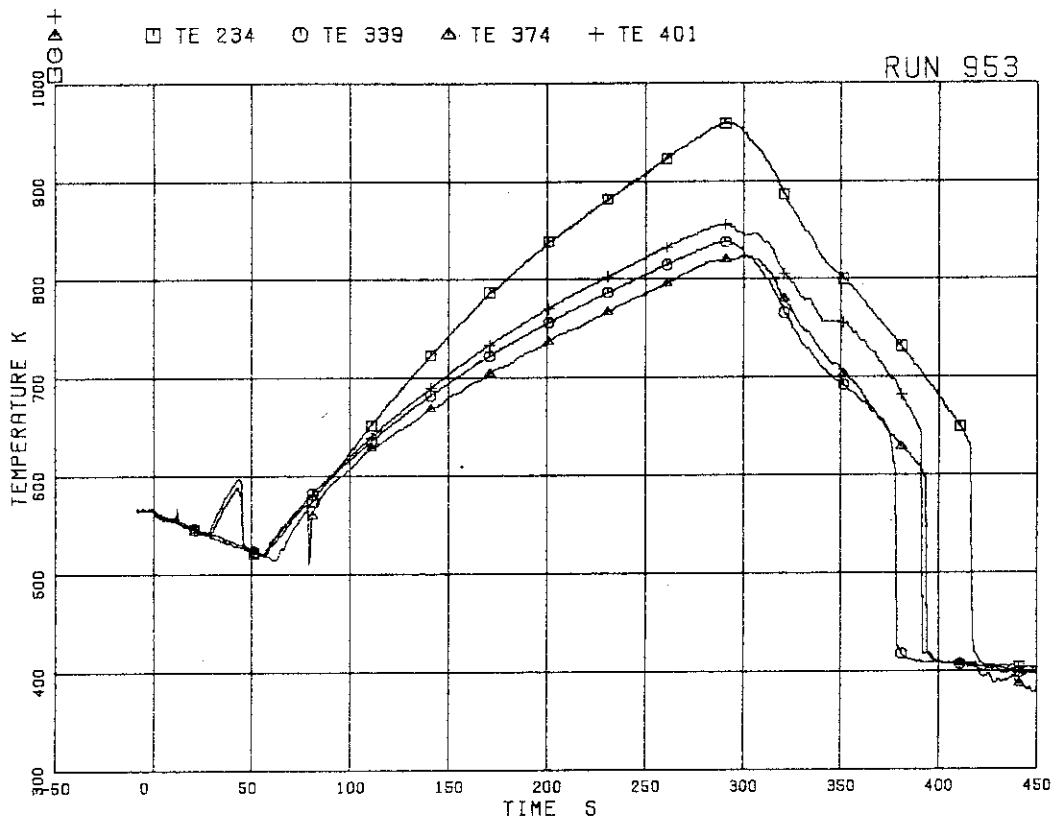


FIG. 5.114 SURFACE TEMPERATURES OF FUEL RODS  
A22,B22,C22,D22 AT POSITION 2

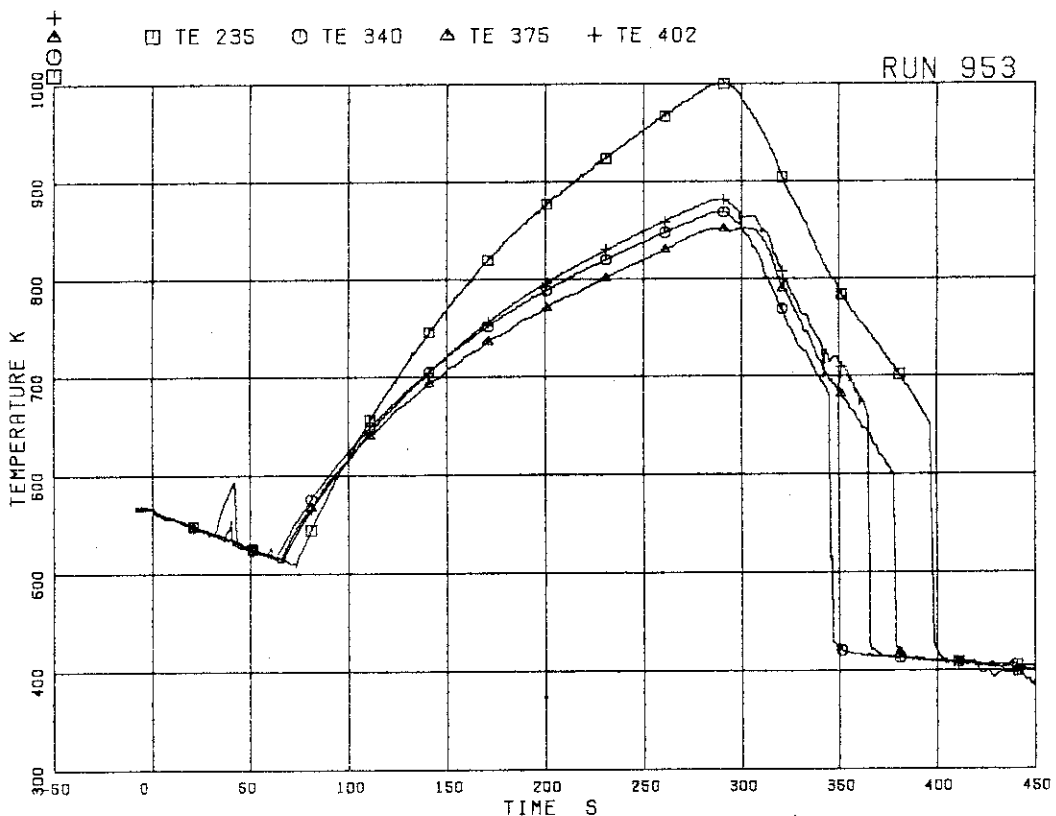


FIG. 5.115 SURFACE TEMPERATURES OF FUEL RODS  
A22,B22,C22,D22 AT POSITION 3

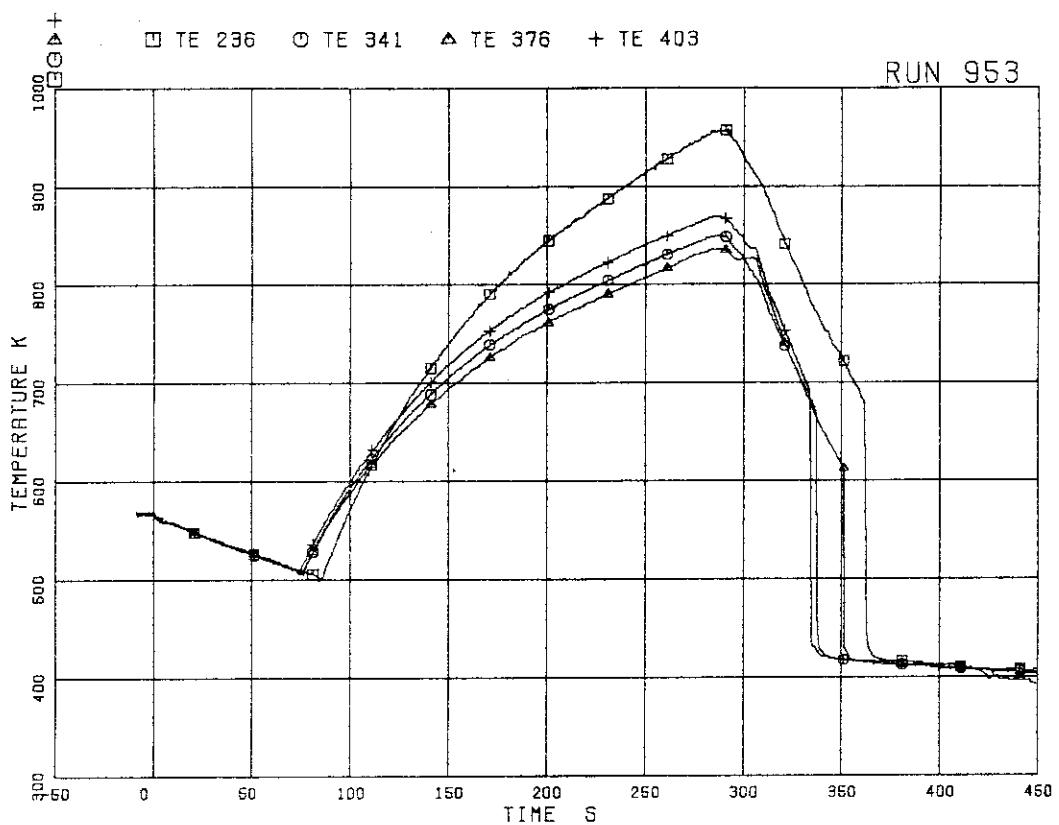


FIG.5.116 SURFACE TEMPERATURES OF FUEL RODS  
A22,B22,C22,D22 AT POSITION 4

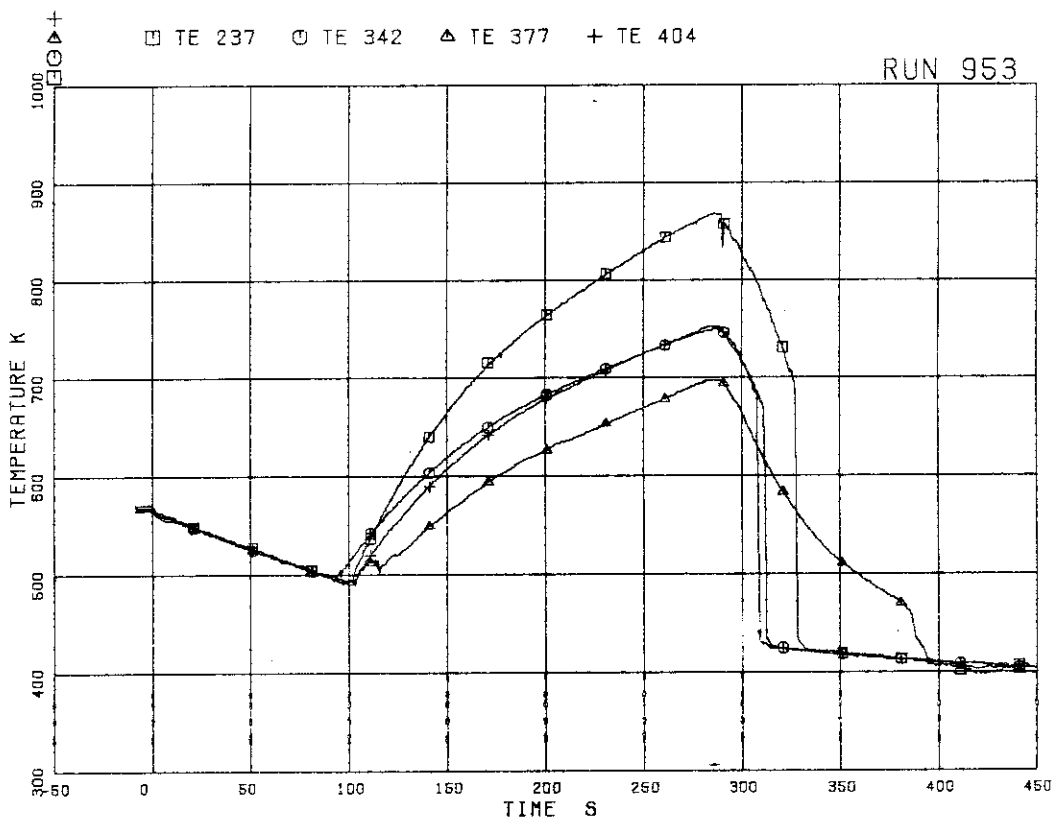


FIG.5.117 SURFACE TEMPERATURES OF FUEL RODS  
A22,B22,C22,D22 AT POSITION 5

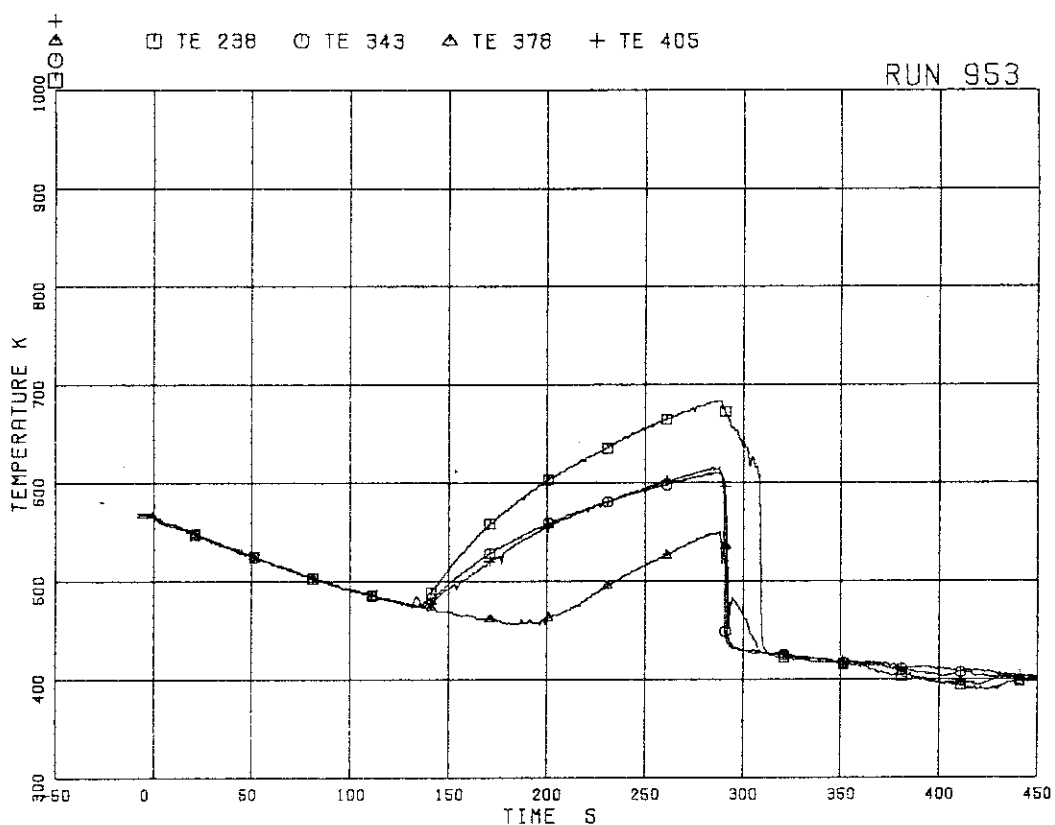


FIG.5.118 SURFACE TEMPERATURES OF FUEL RODS  
A22,B22,C22,D22 AT POSITION 6

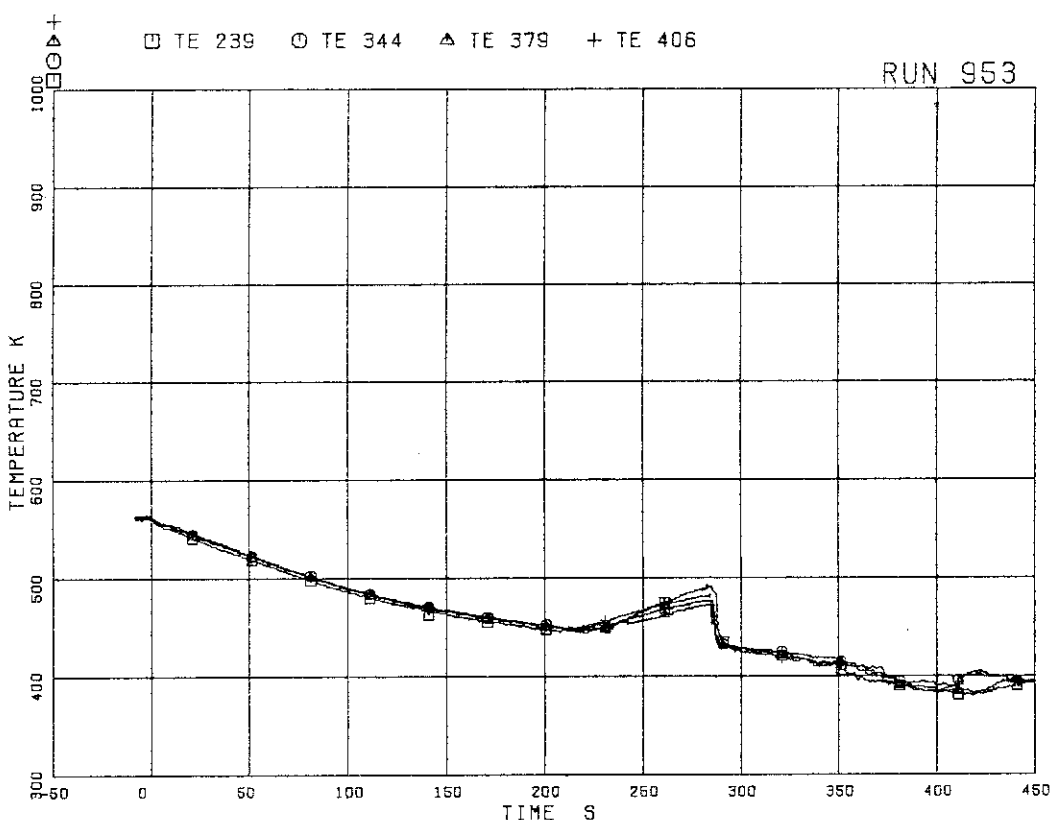


FIG.5.119 SURFACE TEMPERATURES OF FUEL RODS  
A22,B22,C22,D22 AT POSITION 7

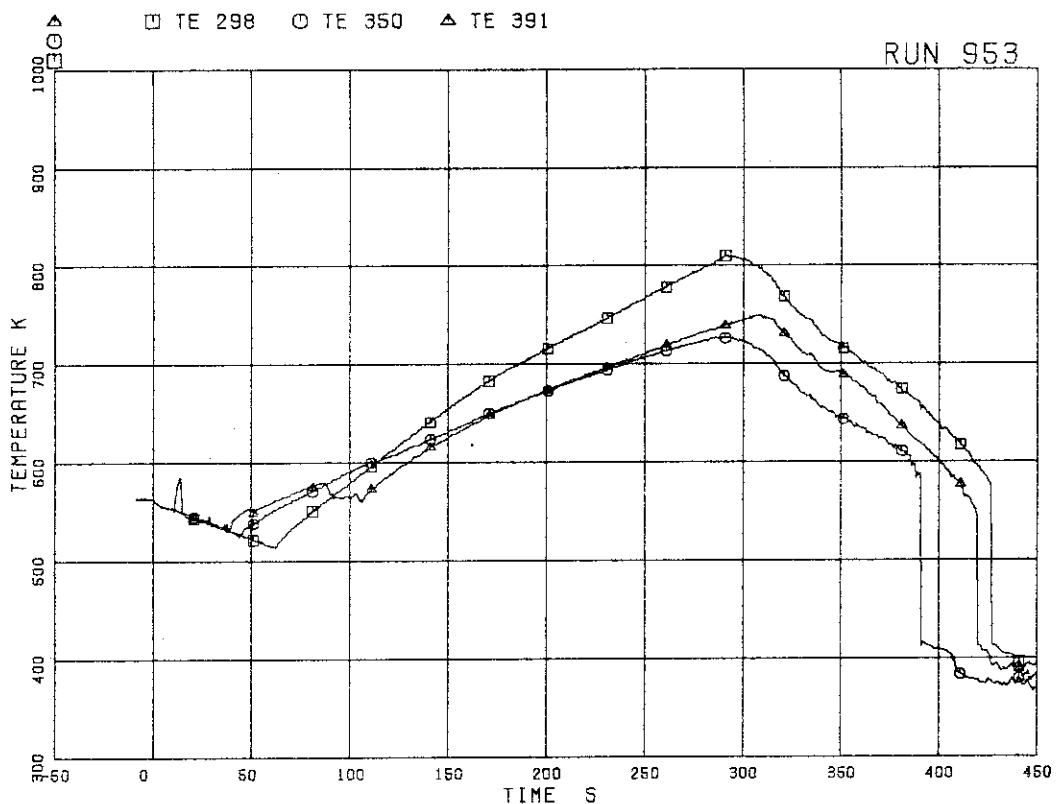


FIG. 5.120 SURFACE TEMPERATURES OF FUEL RODS  
A77,B77,C77 AT POSITION 1

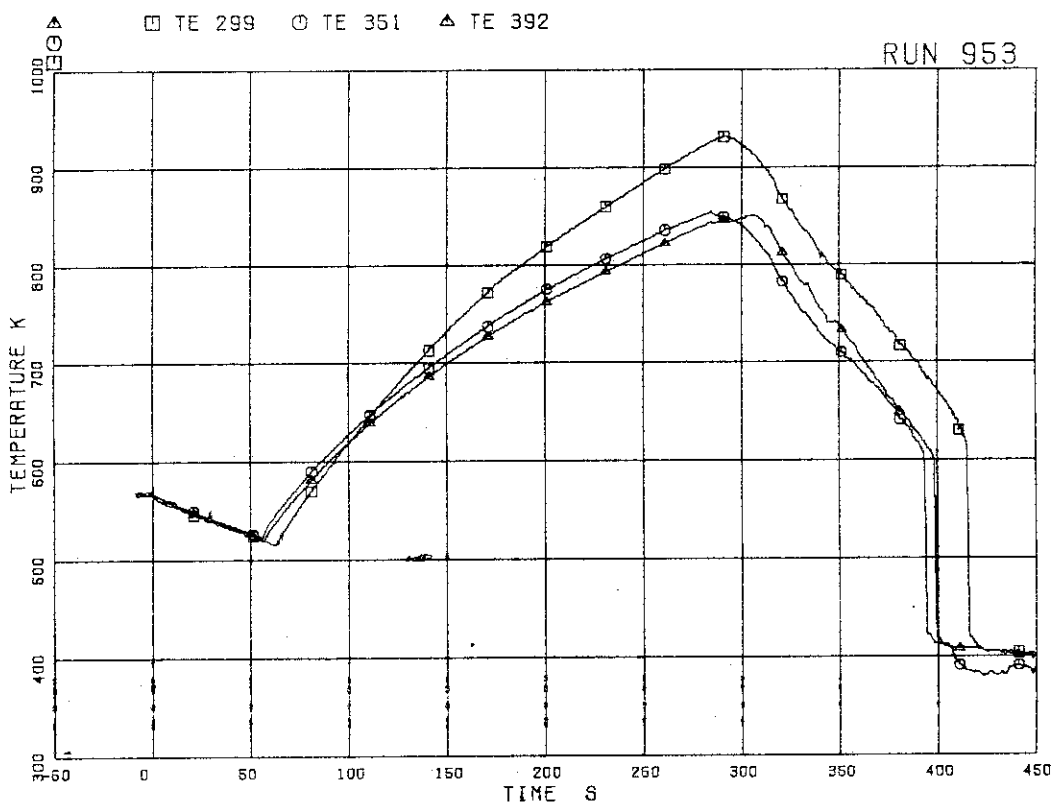


FIG. 5.121 SURFACE TEMPERATURES OF FUEL RODS  
A77,B77,C77 AT POSITION 2

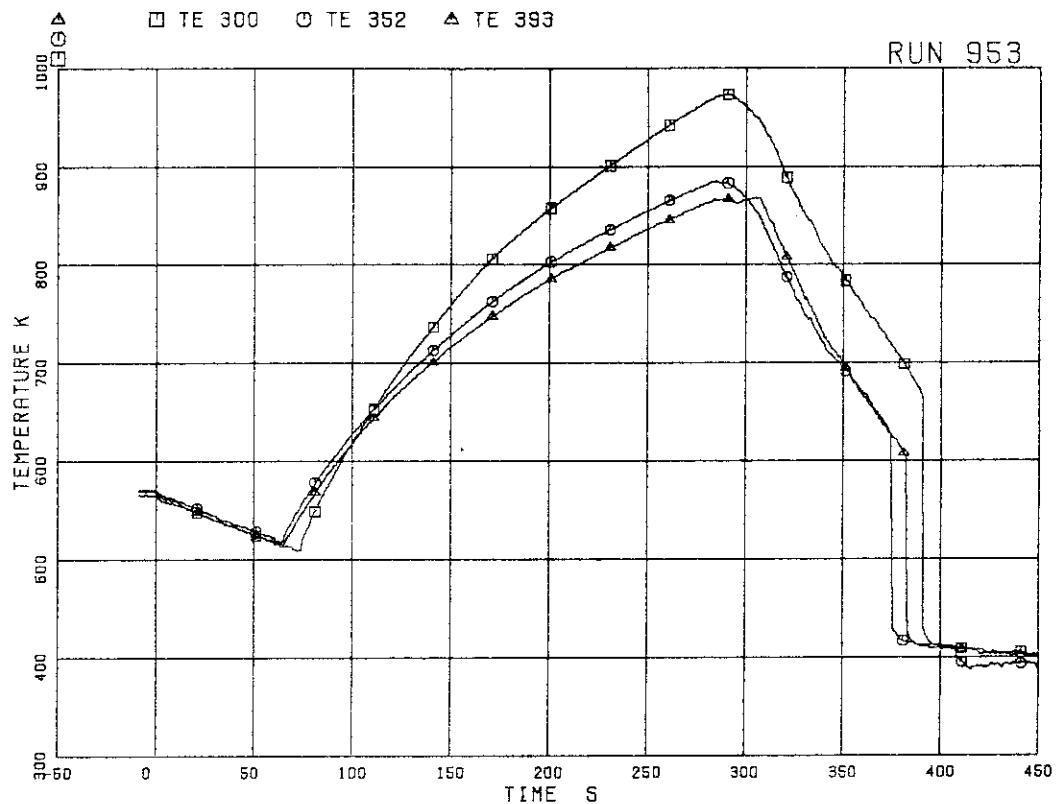


FIG.5.122 SURFACE TEMPERATURES OF FUEL RODS  
A77,B77,C77 AT POSITION 3

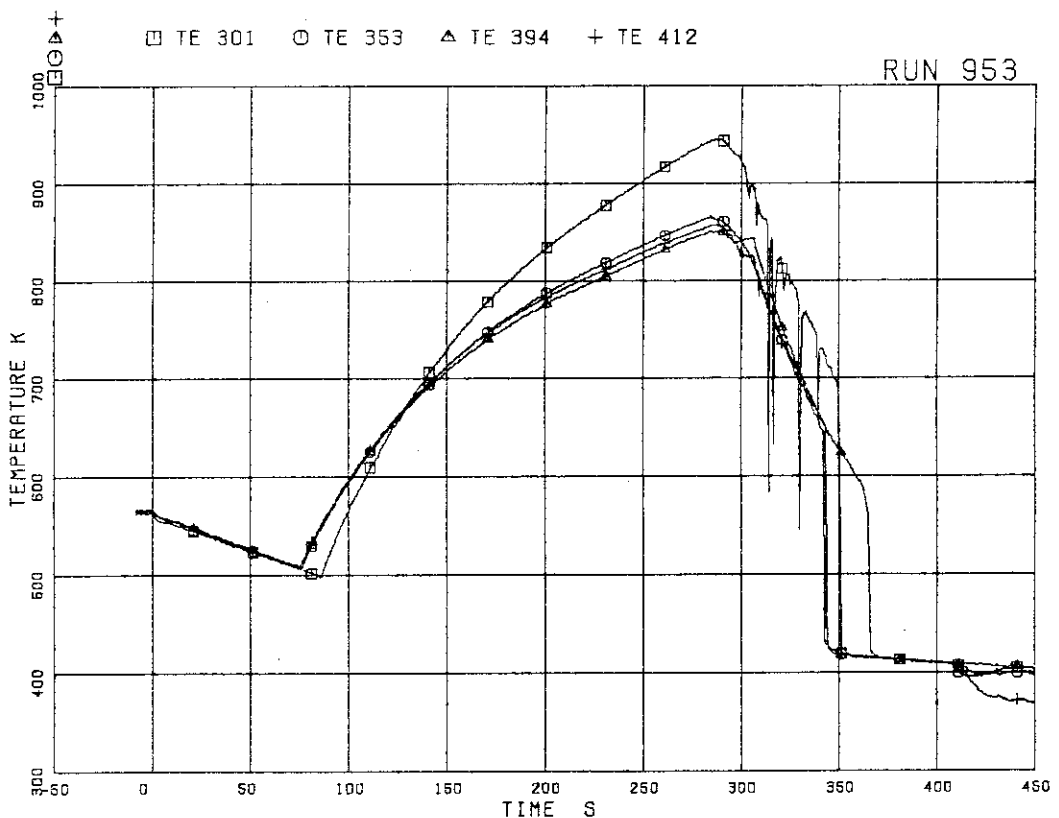


FIG.5.123 SURFACE TEMPERATURES OF FUEL RODS  
A77,B77,C77 AT POSITION 4

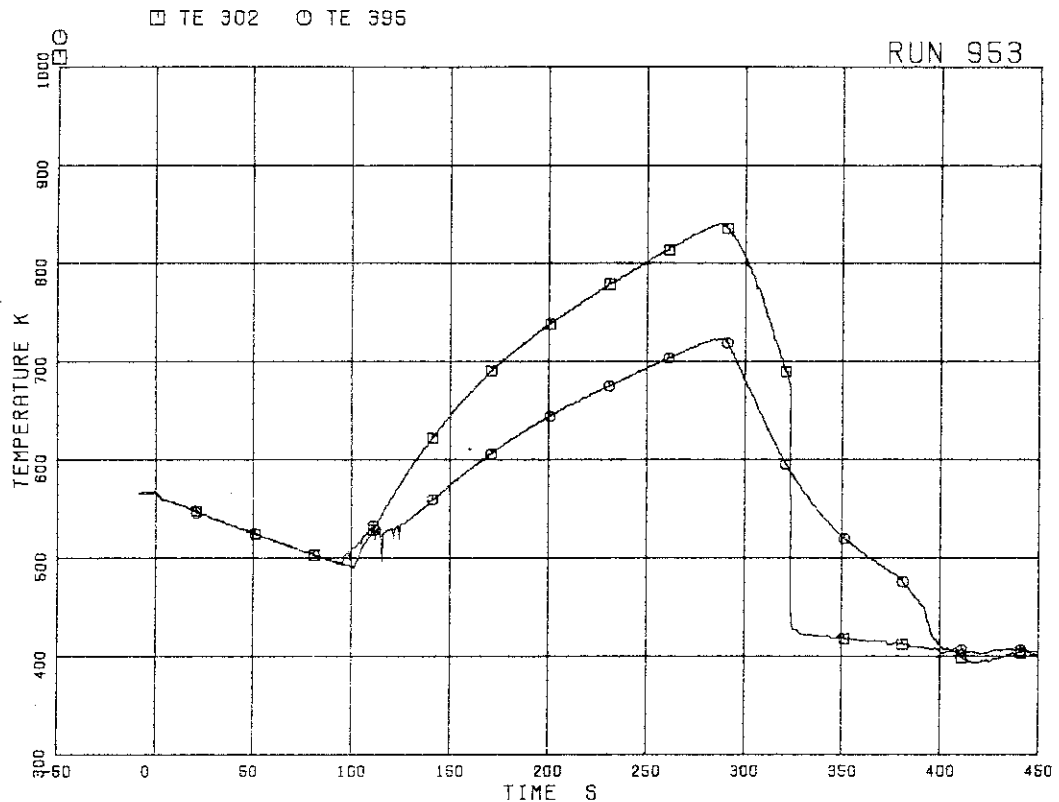


FIG. 5.124 SURFACE TEMPERATURES OF FUEL RODS  
A77, C77 AT POSITION 5

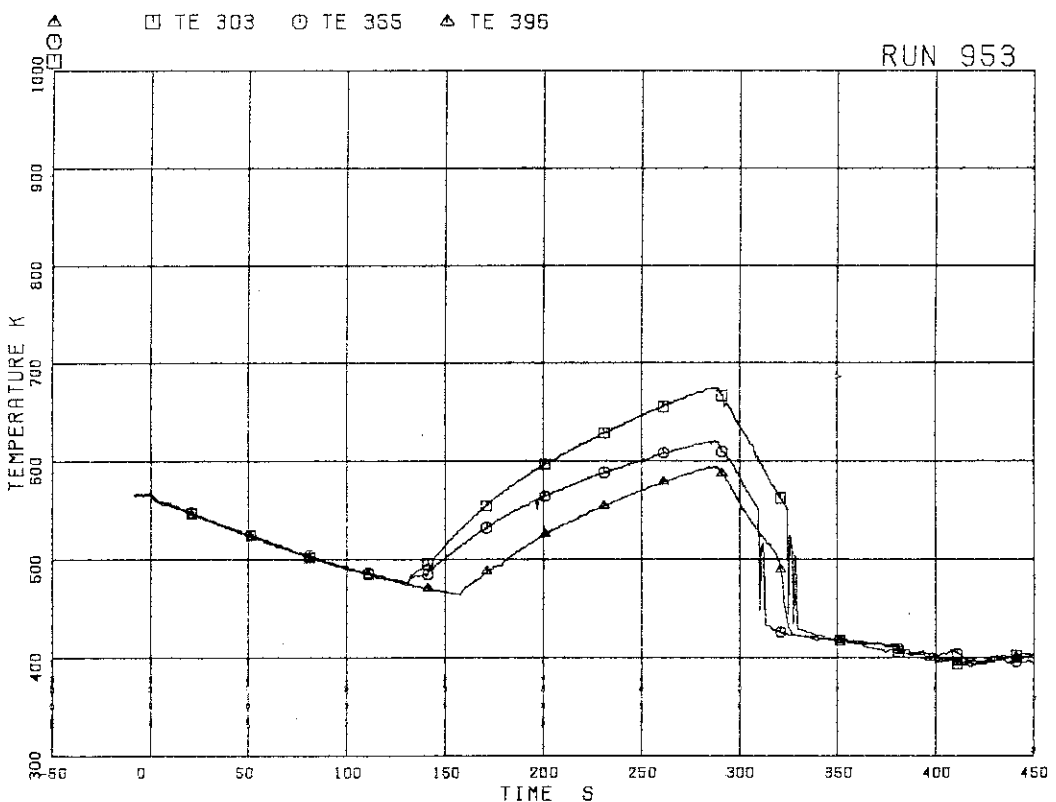


FIG. 5.125 SURFACE TEMPERATURES OF FUEL RODS  
A77, B77, C77 AT POSITION 6

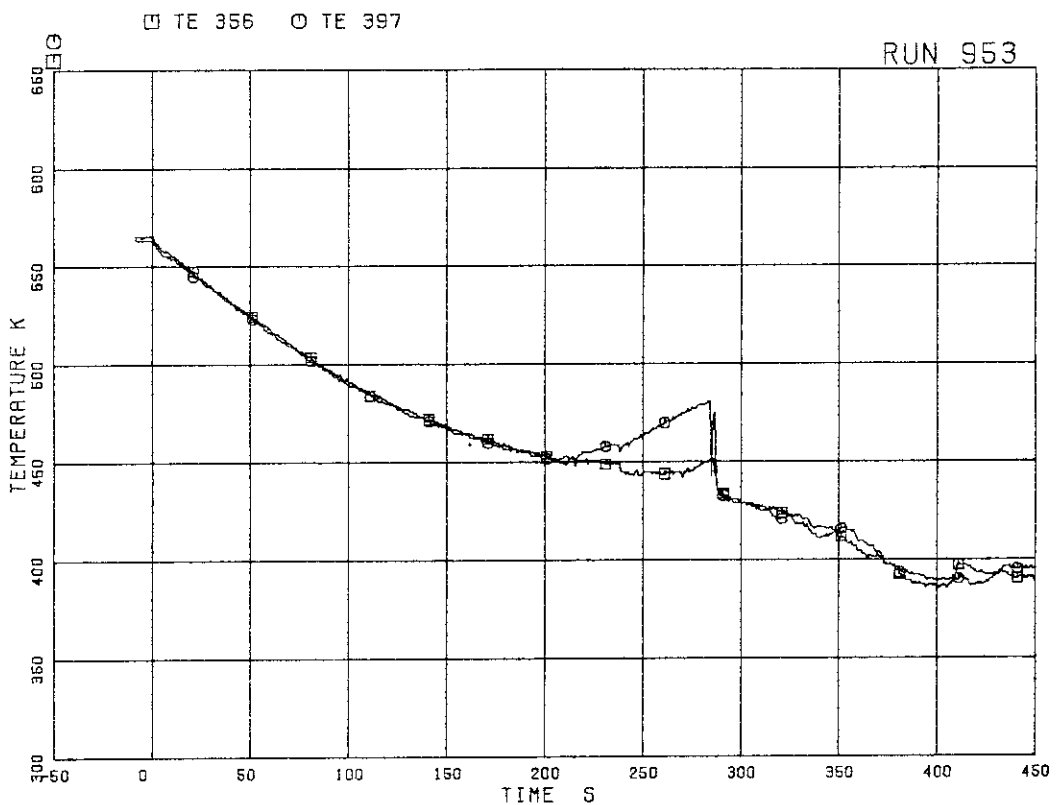


FIG.5.126 SURFACE TEMPERATURES OF FUEL RODS  
B77,C77 AT POSITION 7

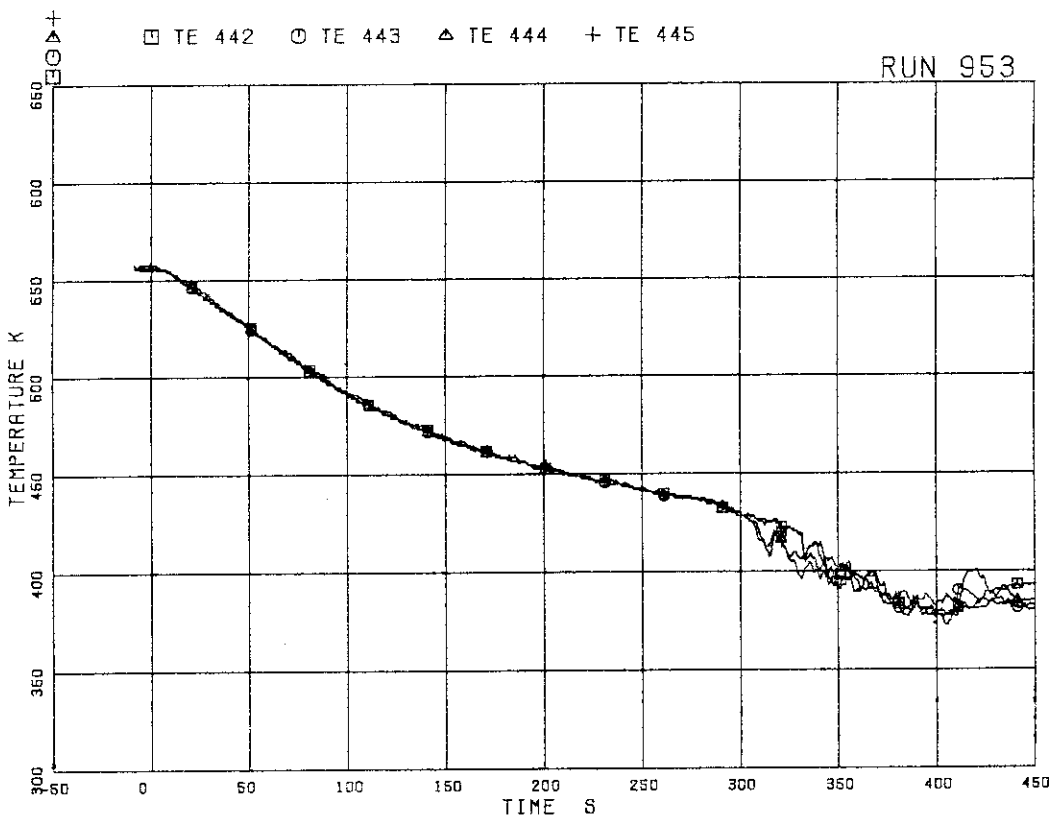


FIG.5.127 FLUID TEMPERATURES AT CHANNEL INLET

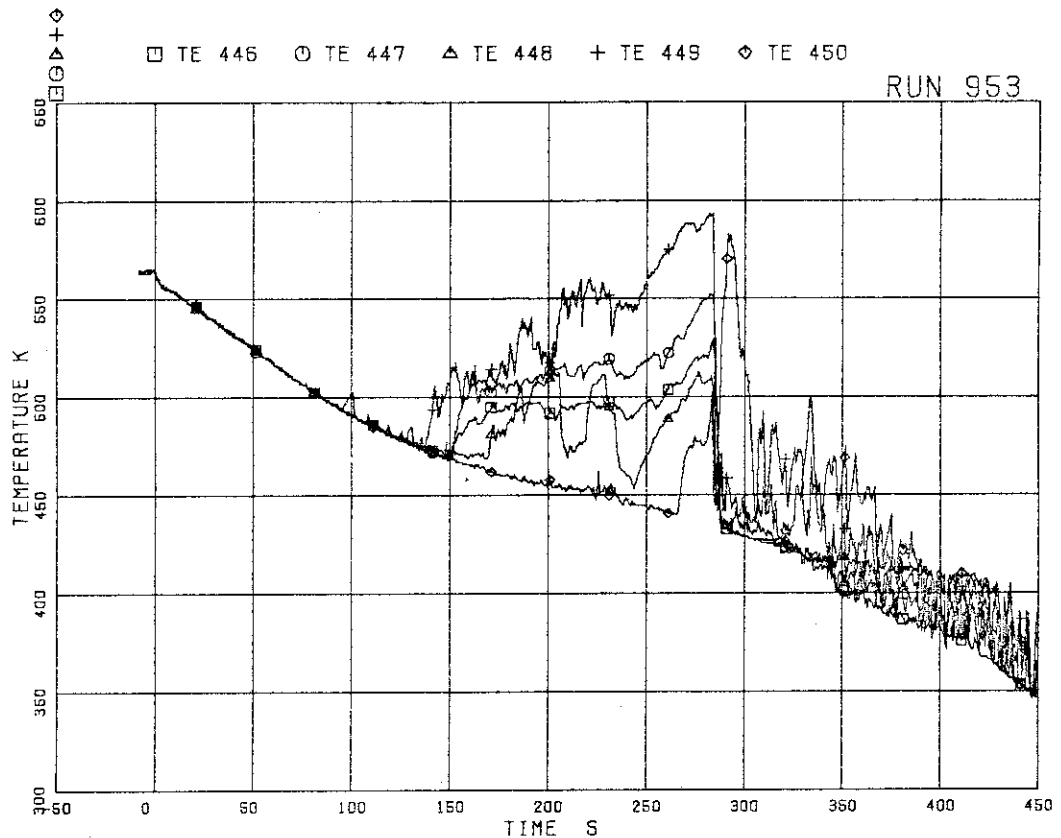


FIG.5.128 FLUID TEMPERATURES AT CHANNEL A OUTLET

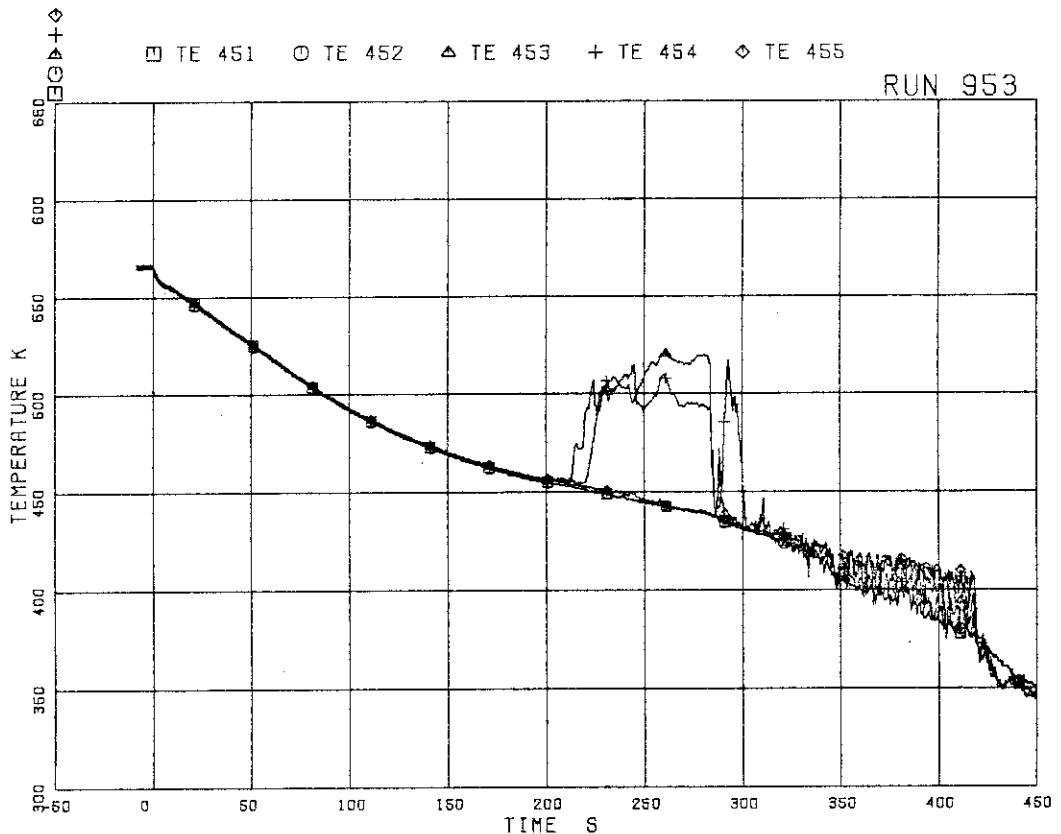


FIG.5.129 FLUID TEMPERATURES AT CHANNEL C OUTLET

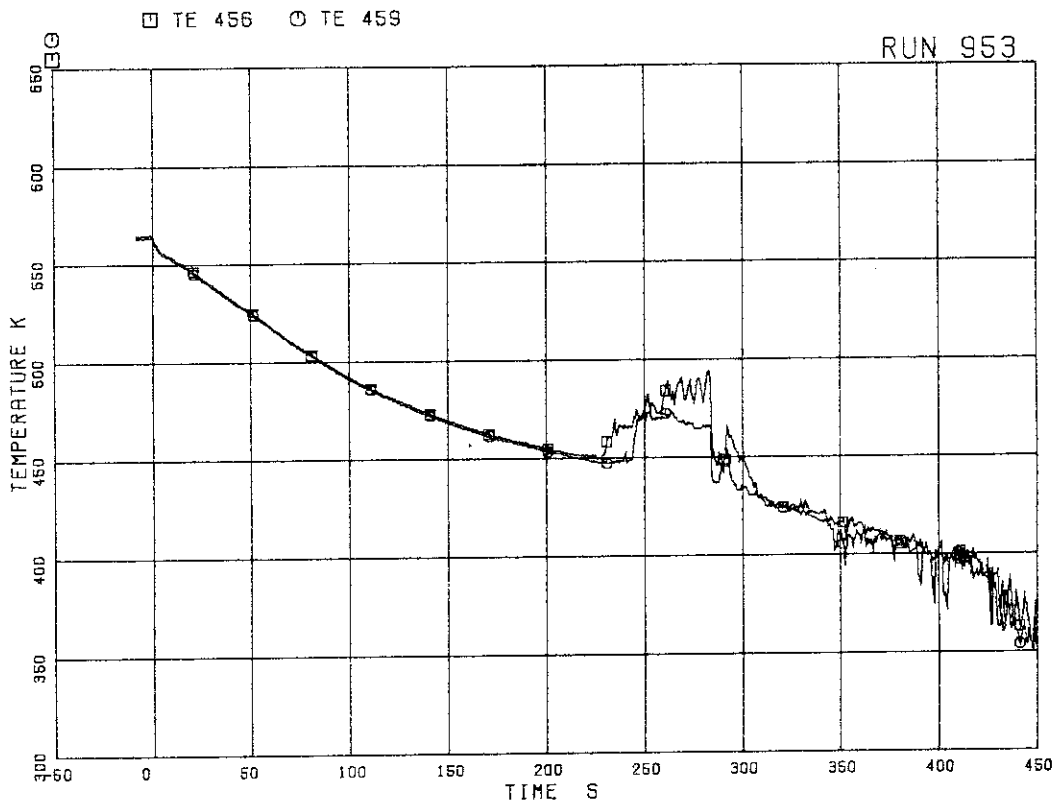


FIG.5.130 FLUID TEMPERATURES ABOVE UTP OF CHANNEL A, OPENINGS 1 AND 4

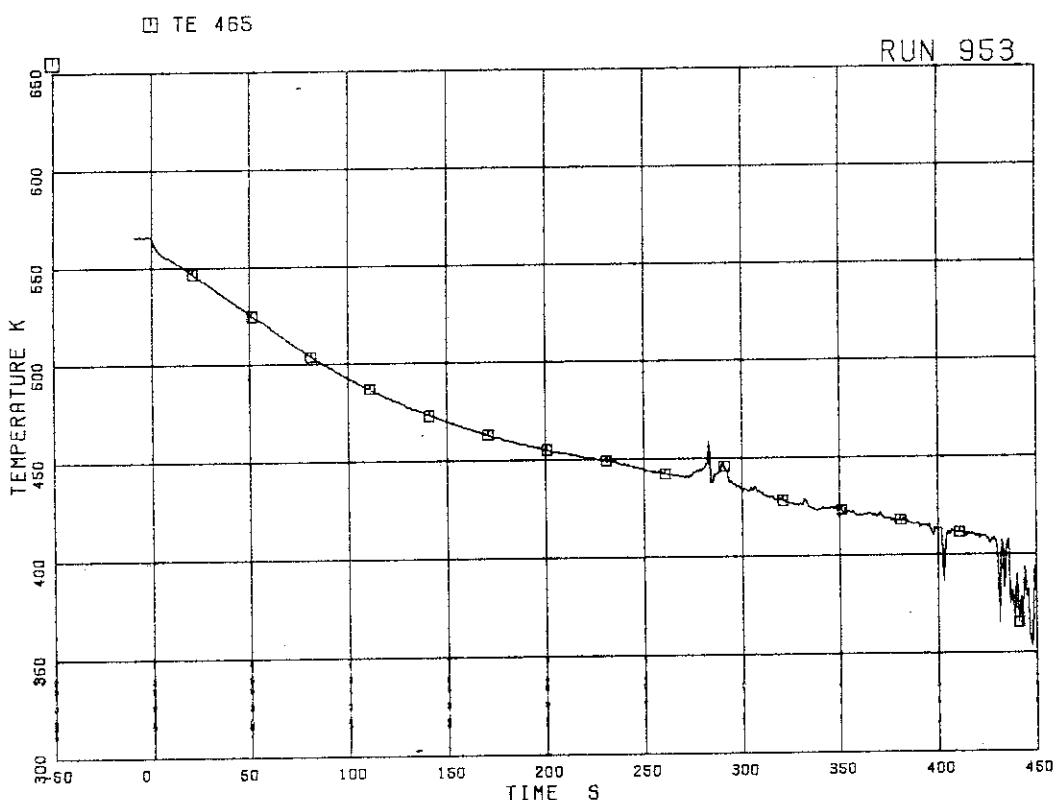


FIG.5.131 FLUID TEMPERATURE ABOVE UTP OF CHANNEL A, OPENING 10

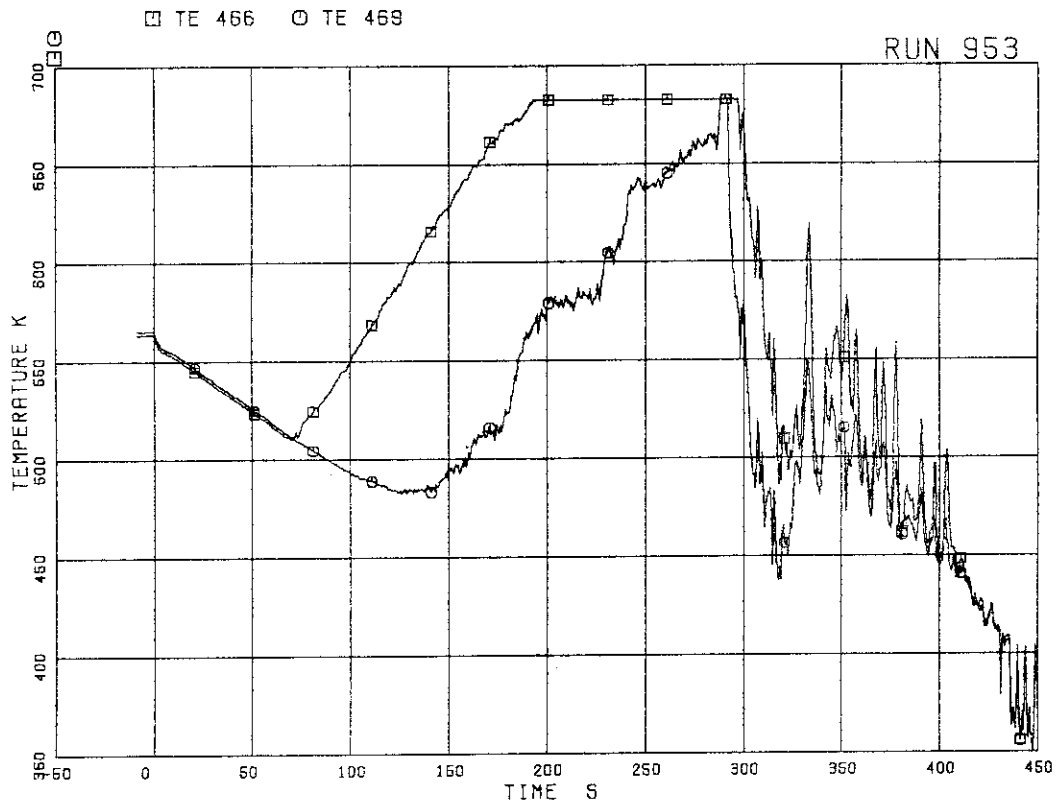


FIG.5.132 FLUID TEMPERATURES BELOW UTP OF CHANNEL A, OPENING 1 AND 4

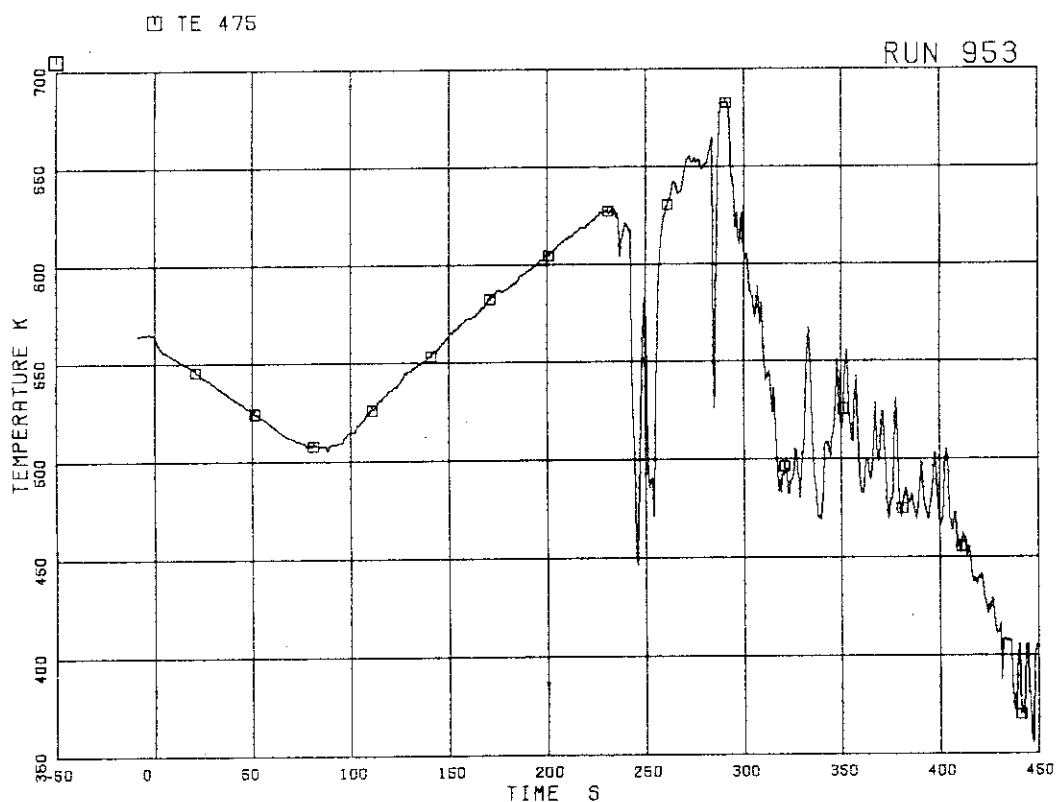


FIG.5.133 FLUID TEMPERATURES BELOW UTP OF CHANNEL A, OPENING 10

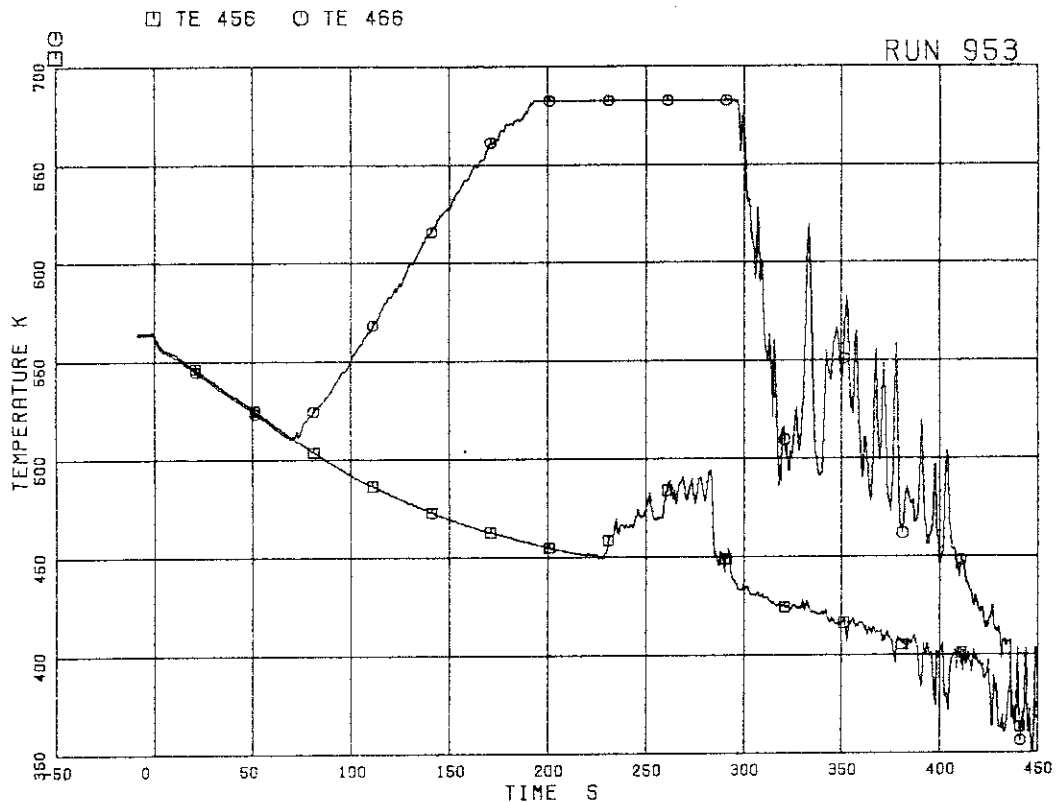


FIG.5.134 FLUID TEMPERATURES ACROSS UTP IN CHANNEL A, OPENING 1

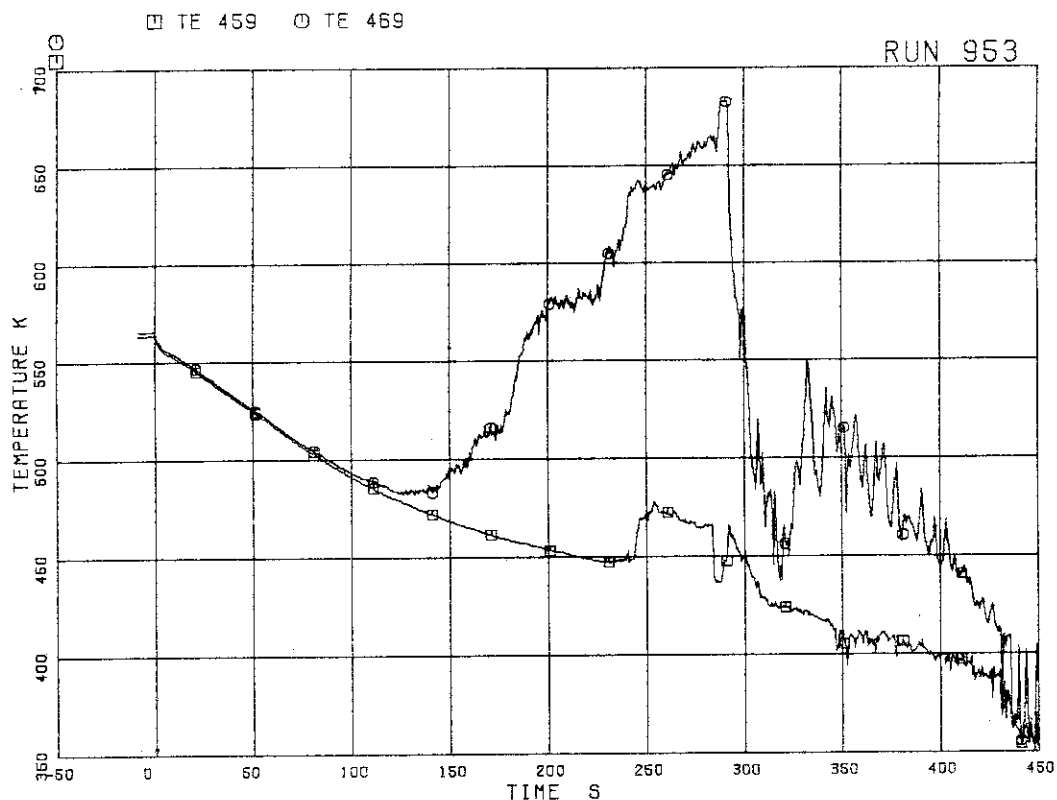


FIG.5.135 FLUID TEMPERATURES ACROSS UTP IN CHANNEL A, OPENING 4

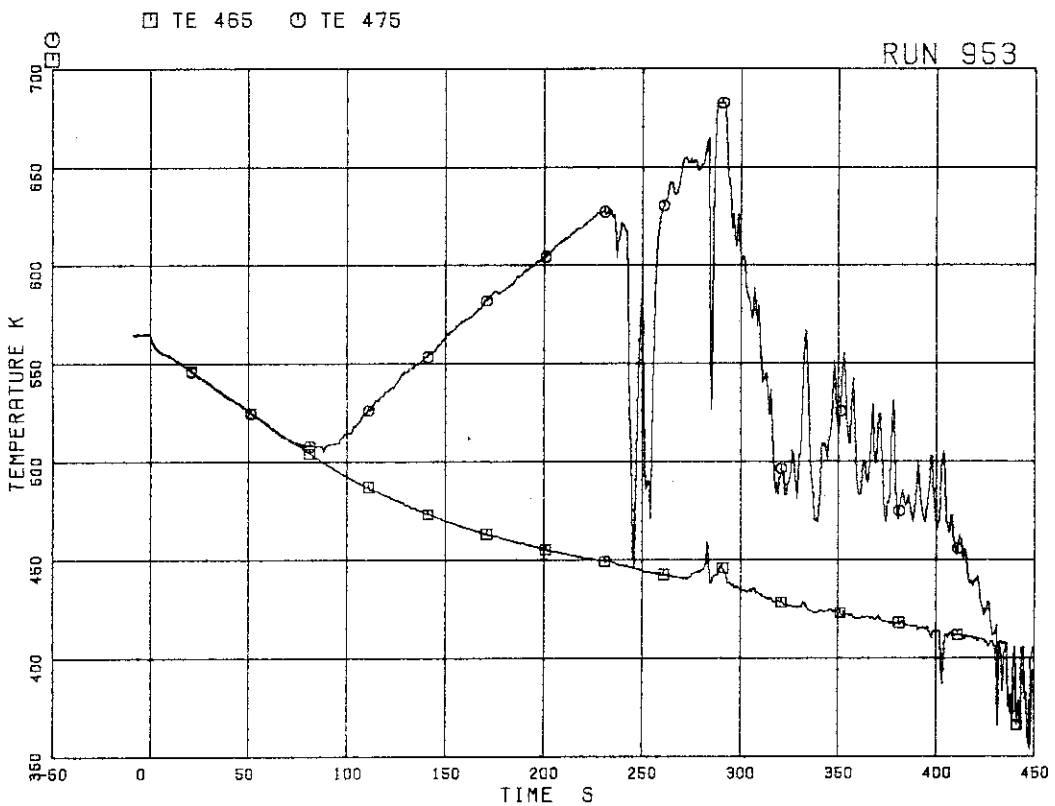


FIG.5.136 FLUID TEMPERATURES ACROSS UTP IN CHANNEL A, OPENING 10

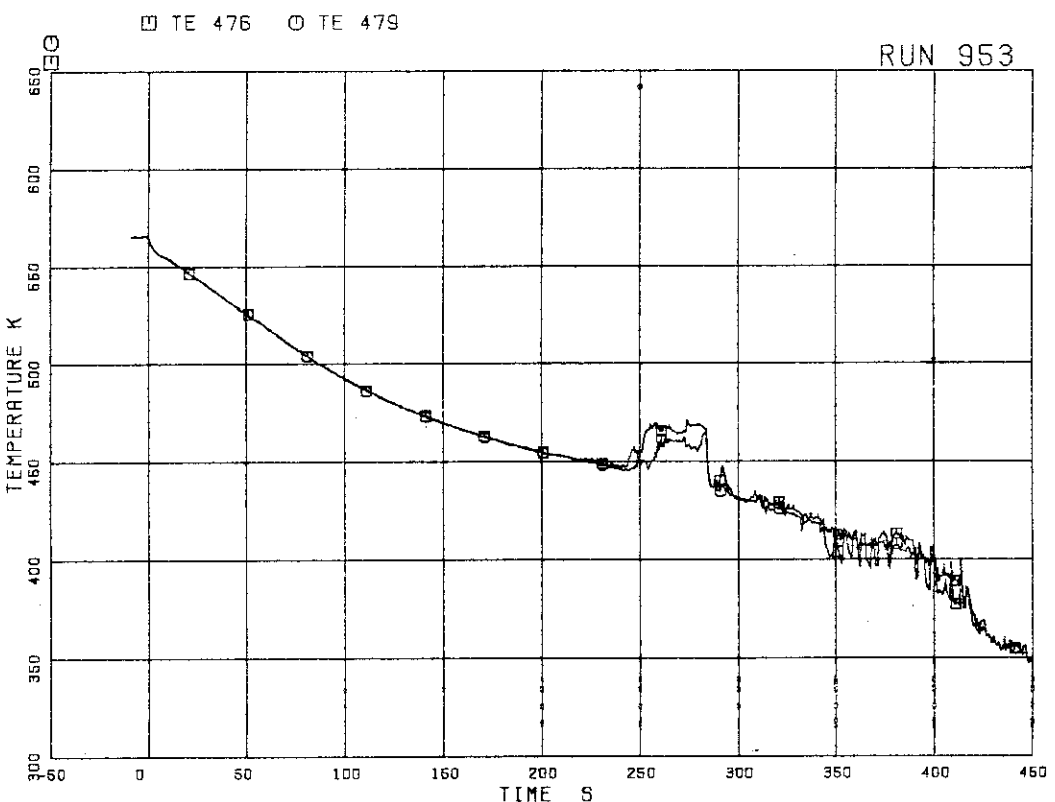


FIG.5.137 FLUID TEMPERATURES ABOVE UTP OF CHANNEL C, OPENINGS 1 AND 4

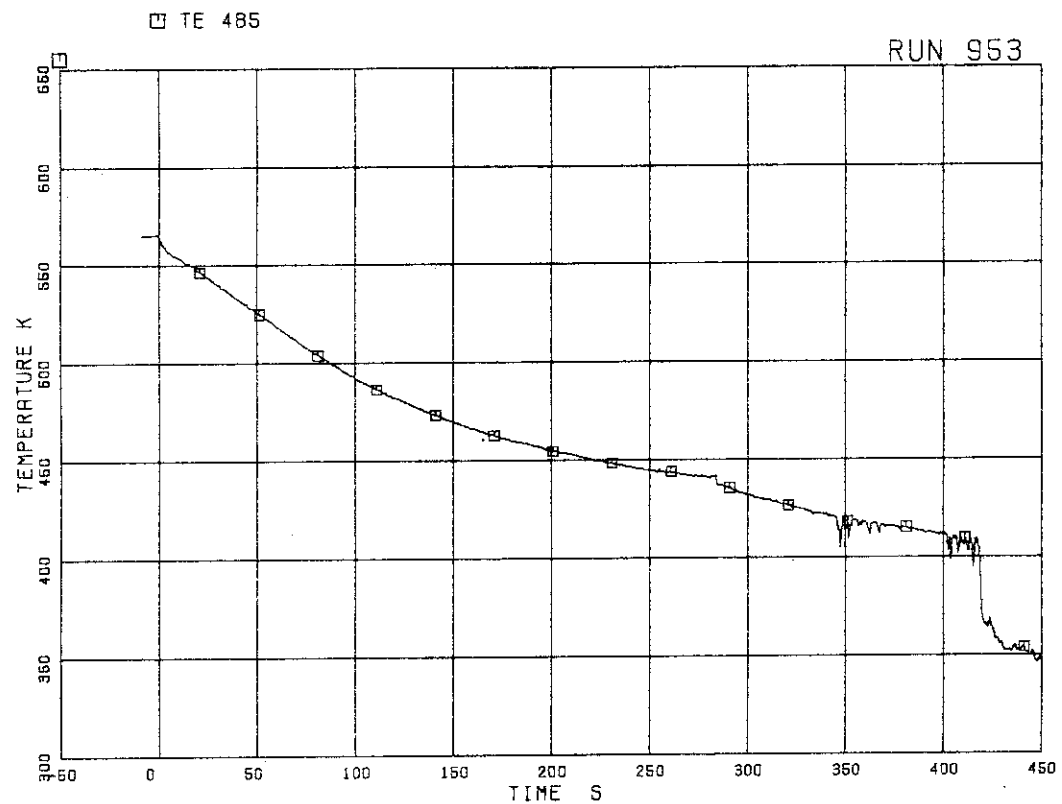


FIG. 5.138 FLUID TEMPERATURES ABOVE UTP OF CHANNEL C, OPENING 10

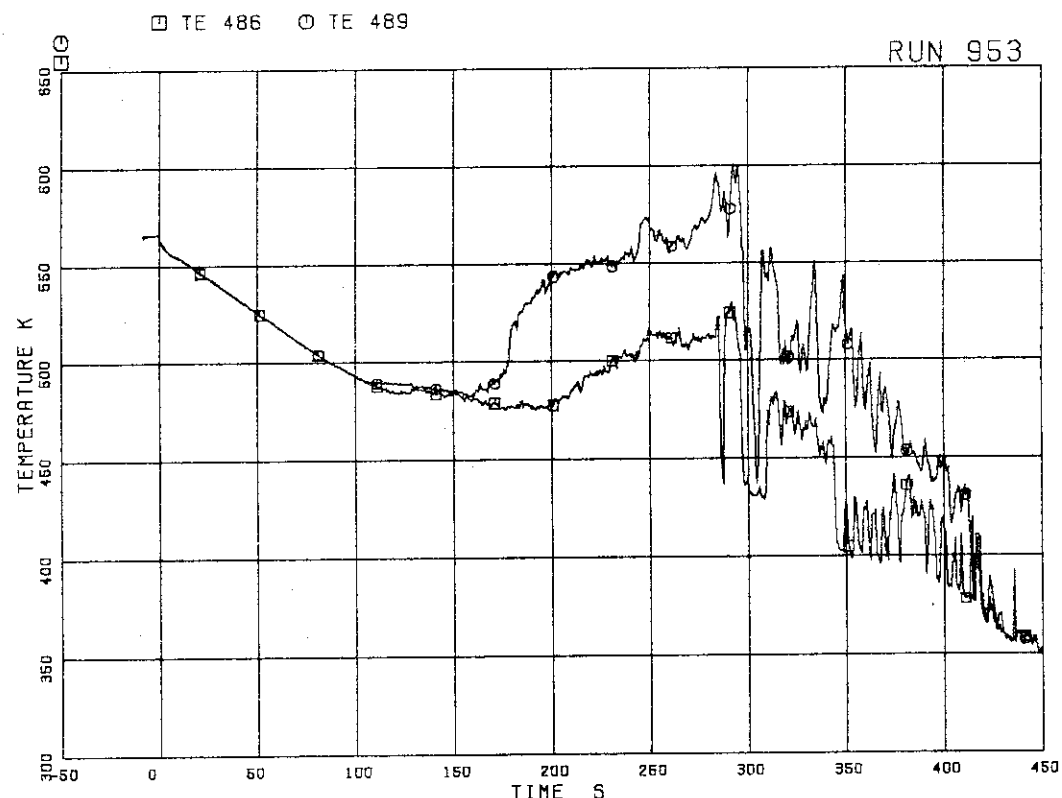


FIG. 5.139 FLUID TEMPERATURES BELOW UTP OF CHANNEL C, OPENINGS 1 AND 4

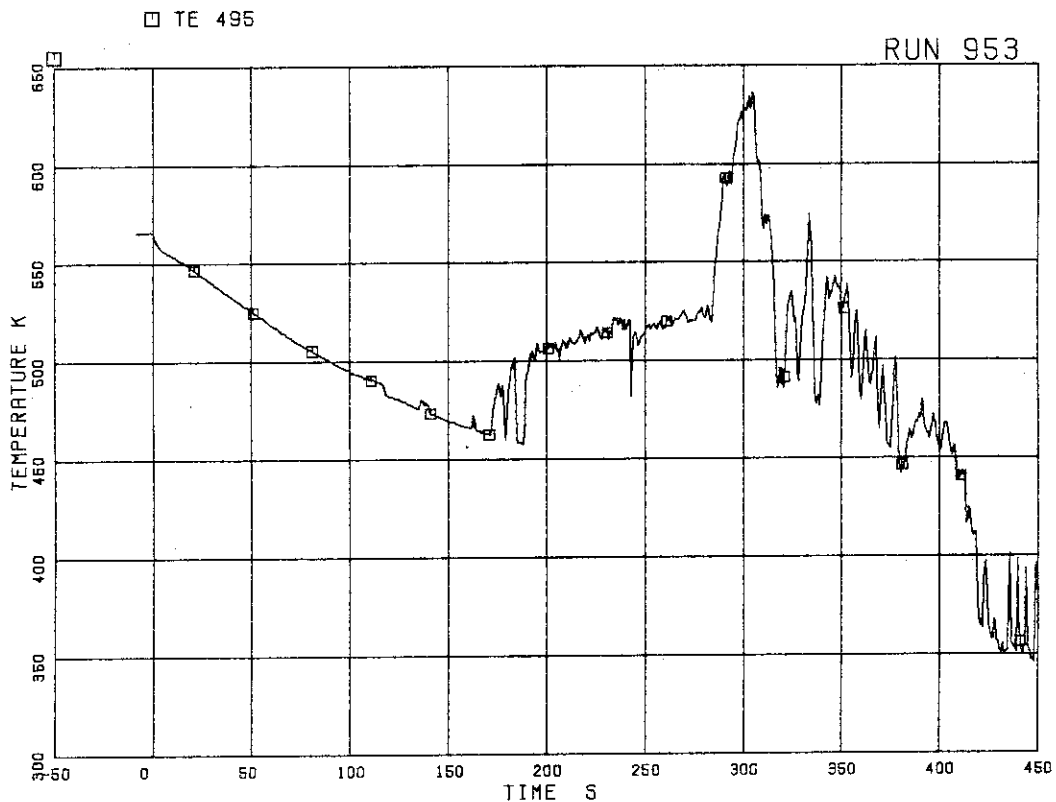


FIG.5.140 FLUID TEMPERATURES BELOW UTP OF CHANNEL C, OPENING 10

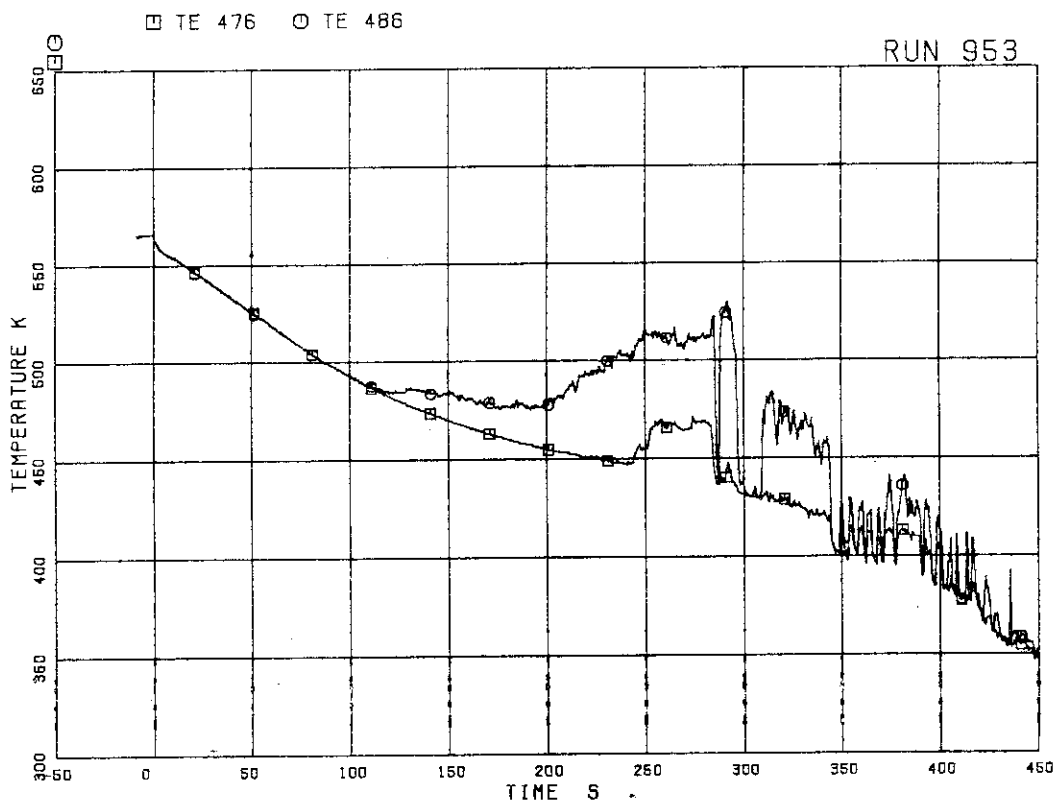


FIG.5.141 FLUID TEMPERATURES ACROSS UTP IN CHANNEL C, OPENING 1

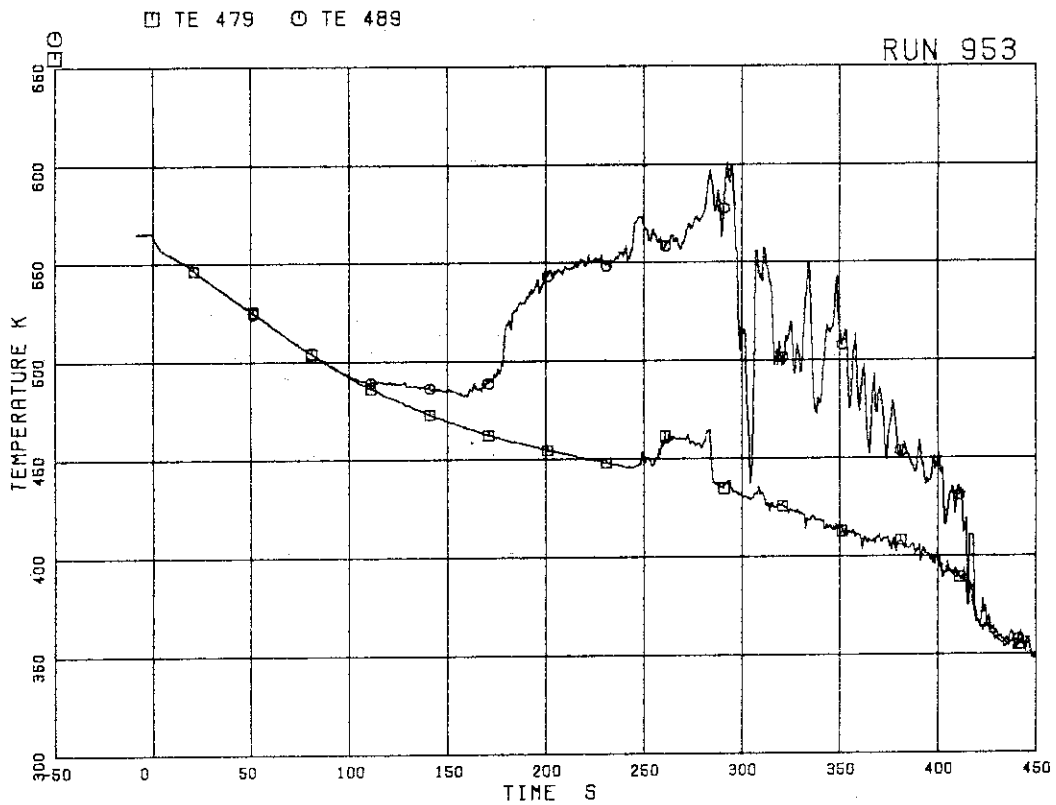


FIG.5.142 FLUID TEMPERATURES ACROSS UTP IN CHANNEL C, OPENING 4

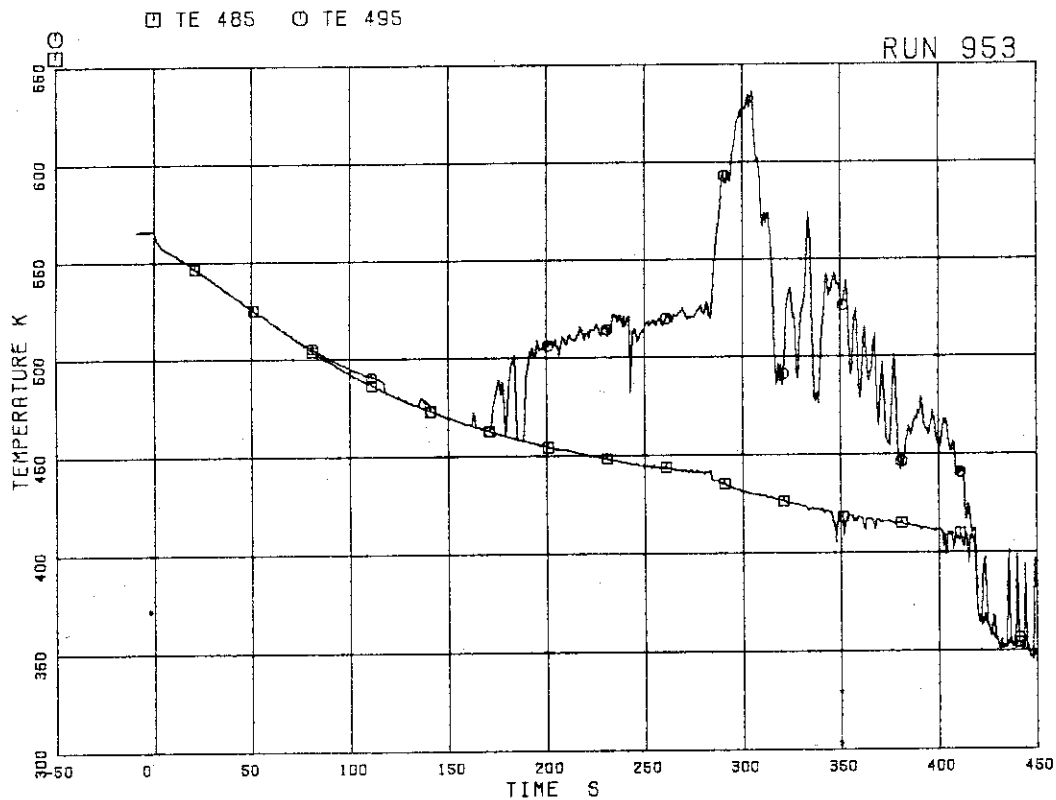


FIG.5.143 FLUID TEMPERATURES ACROSS UTP IN CHANNEL C, OPENING 10

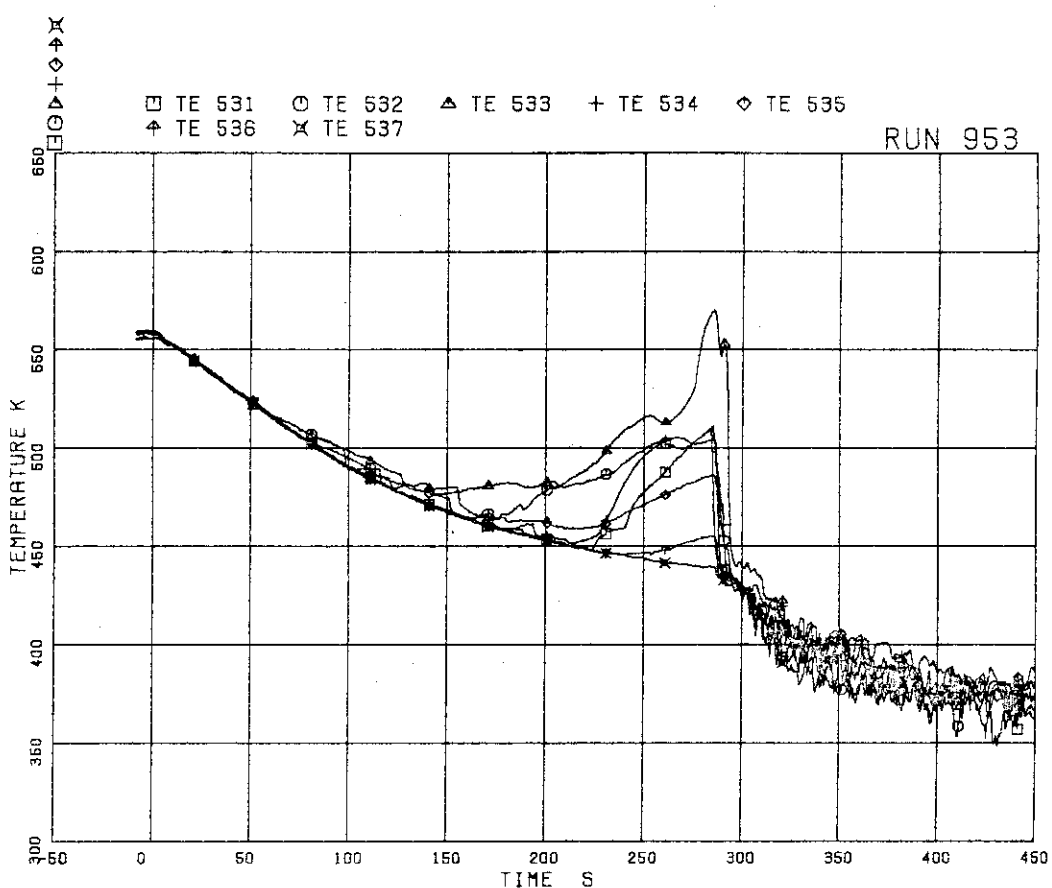


FIG.5.144 OUTER SURFACE TEMPERATURES OF CHANNEL BOX A

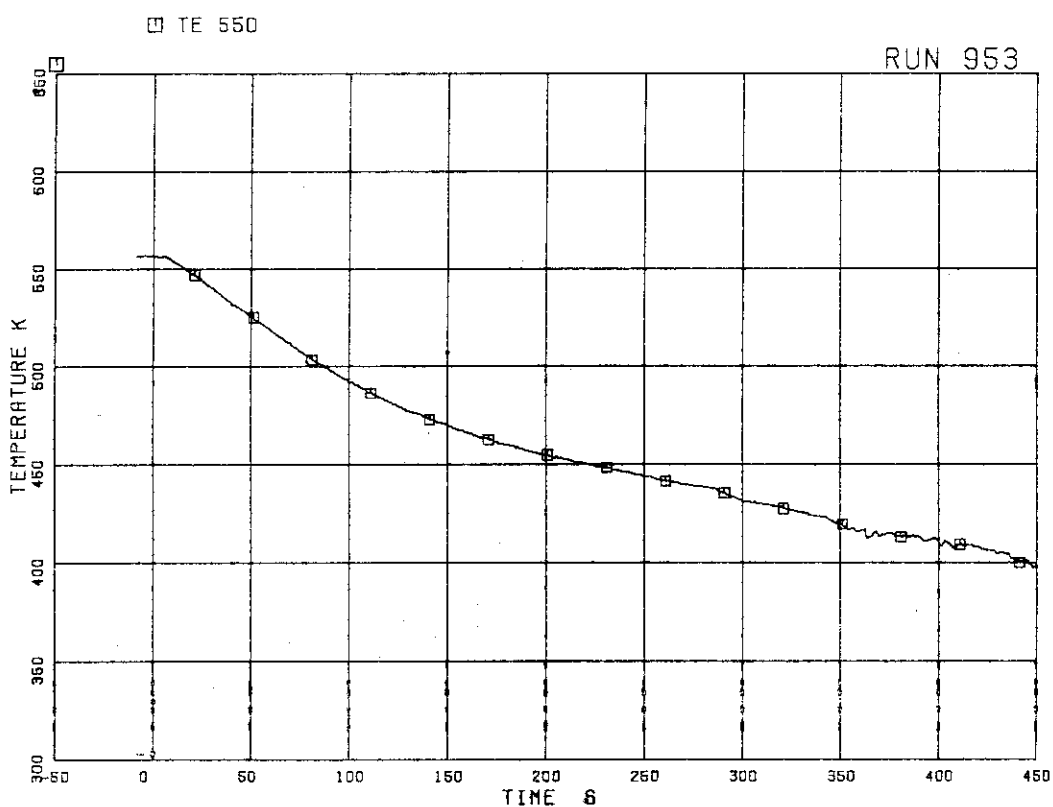


FIG.5.145 FLUID TEMPERATURE IN LOWER PLENUM, CENTER

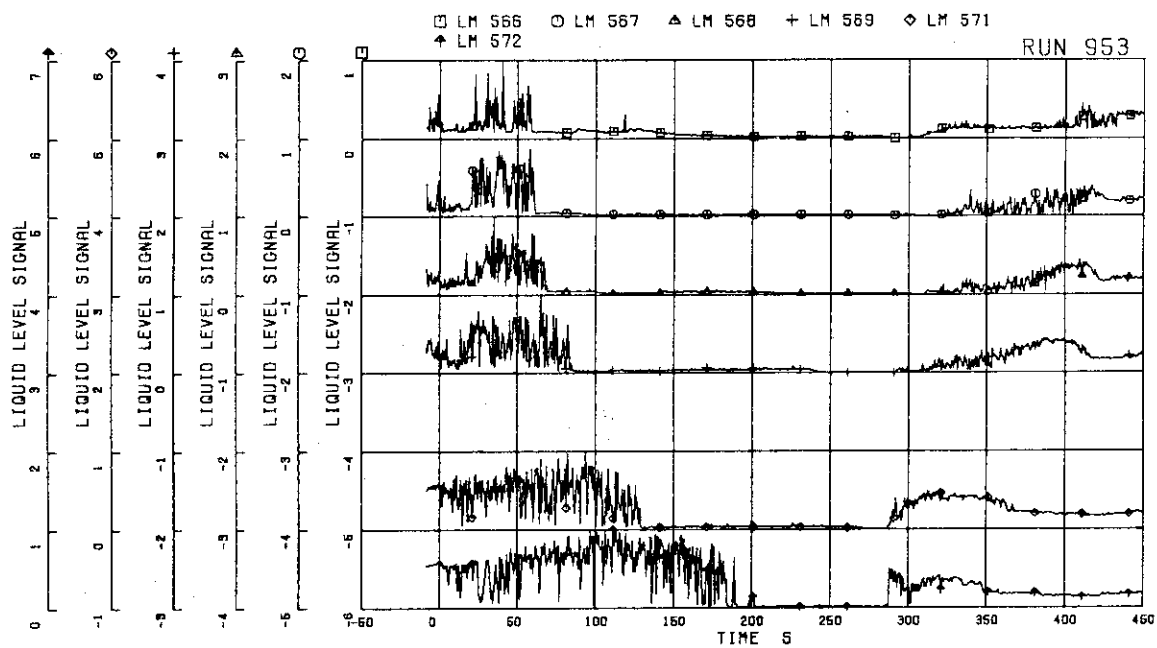
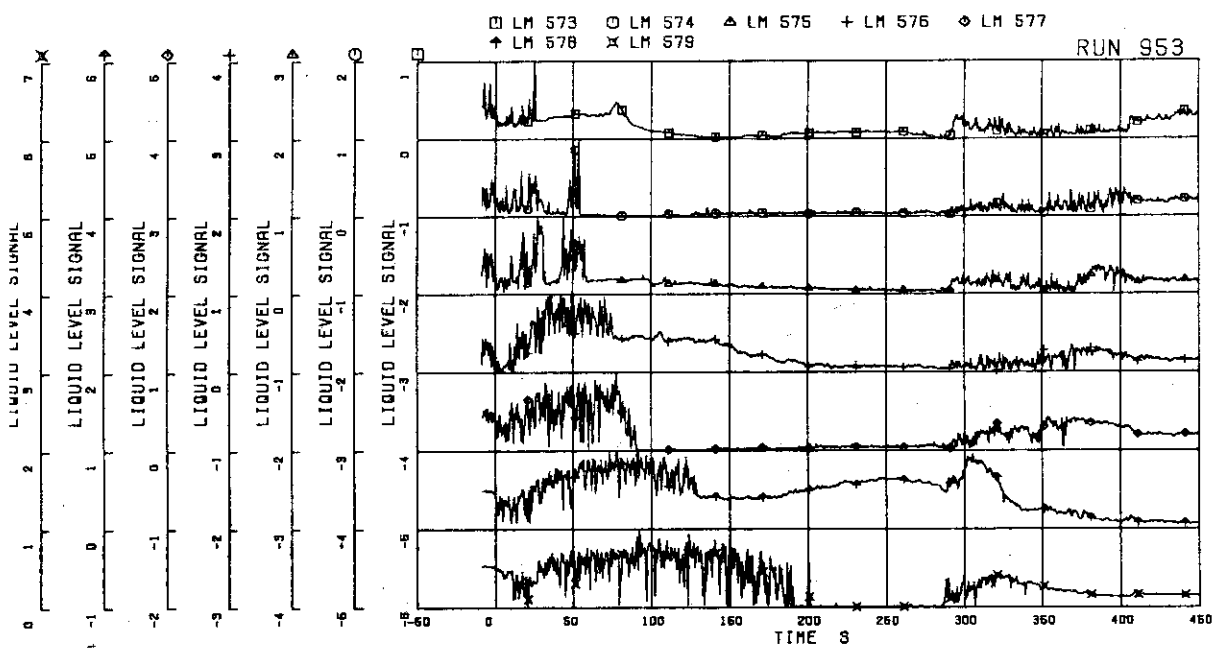
FIG.5.146 LIQUID LEVEL SIGNALS IN CHANNEL BOX A  
LOCATION A2

FIG.5.147 LIQUID LEVEL SIGNALS IN CHANNEL BOX B

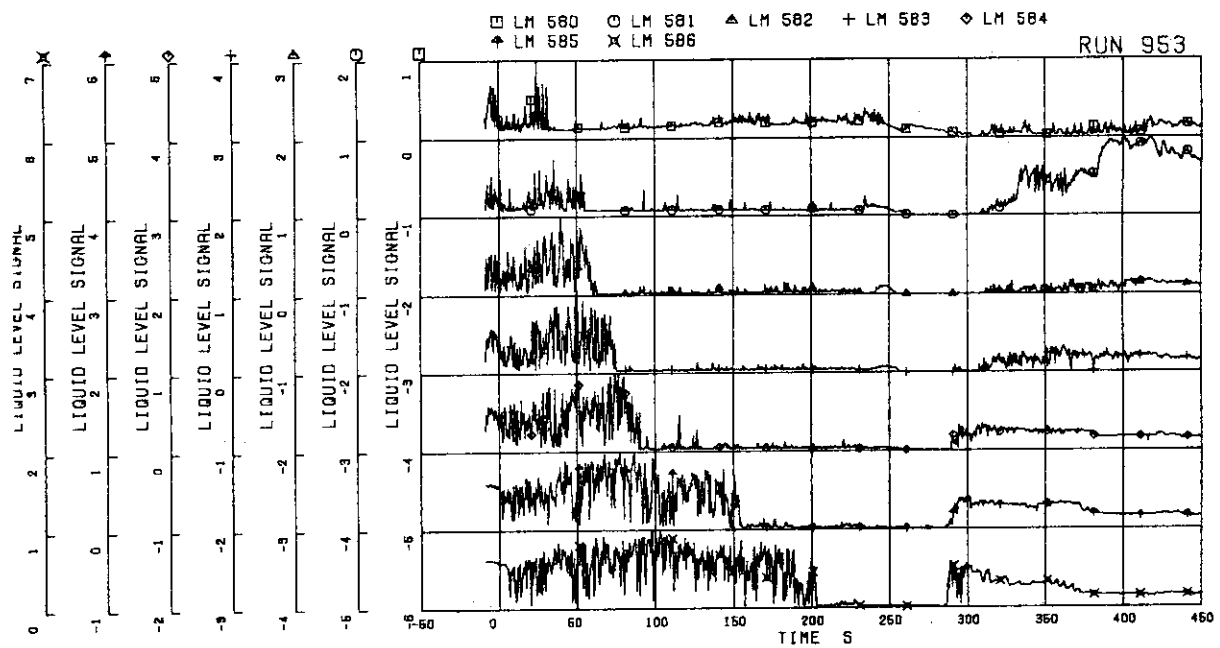


FIG.5.148 LIQUID LEVEL SIGNALS IN CHANNEL BOX C

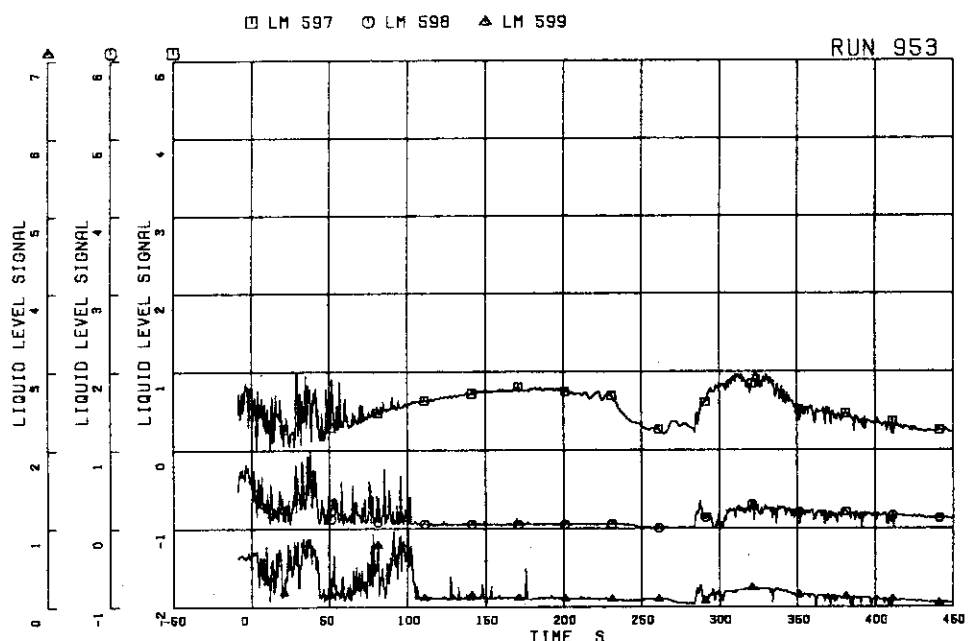


FIG.5.149 LIQUID LEVEL SIGNALS IN CHANNEL A OUTLET LOCATION A2

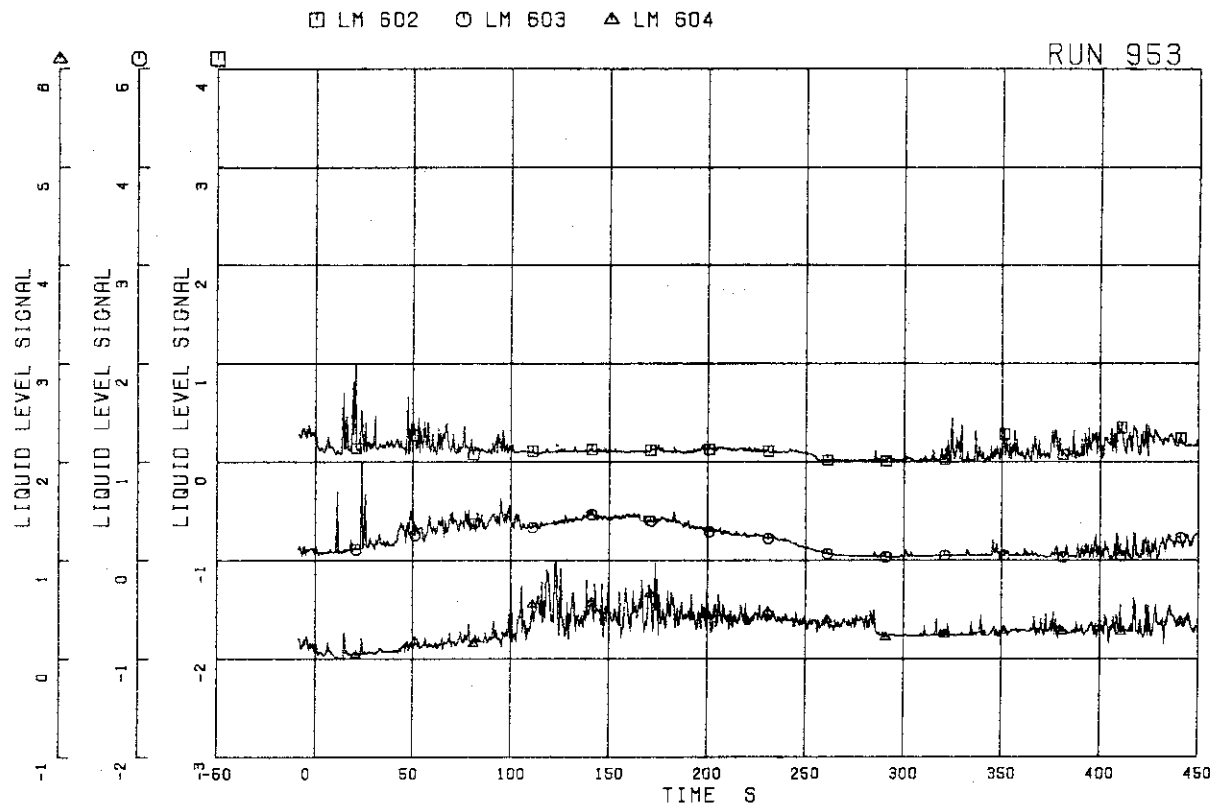


FIG.5.150 LIQUID LEVEL SIGNALS IN CHANNEL A OUTLET CENTER

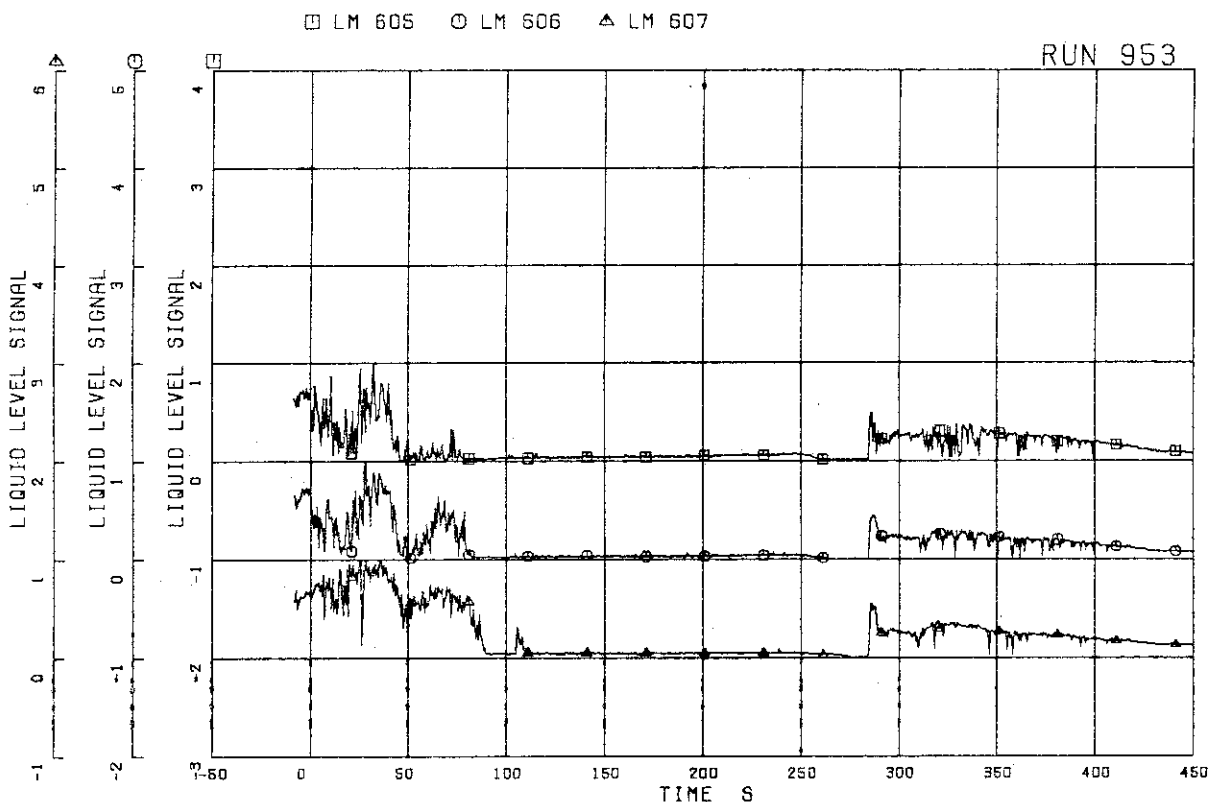


FIG.5.151 LIQUID LEVEL SIGNALS IN CHANNEL C OUTLET LOCATION C1

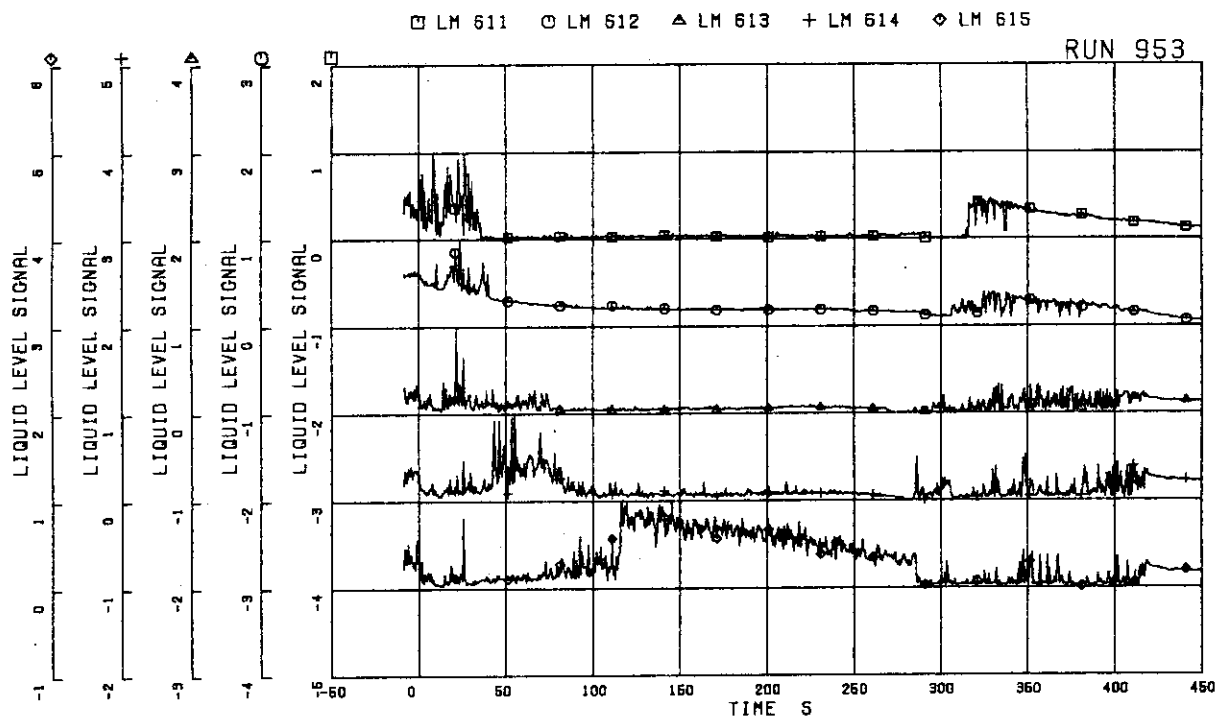


FIG.5.152 LIQUID LEVEL SIGNALS IN CHANNEL C OUTLET CENTER

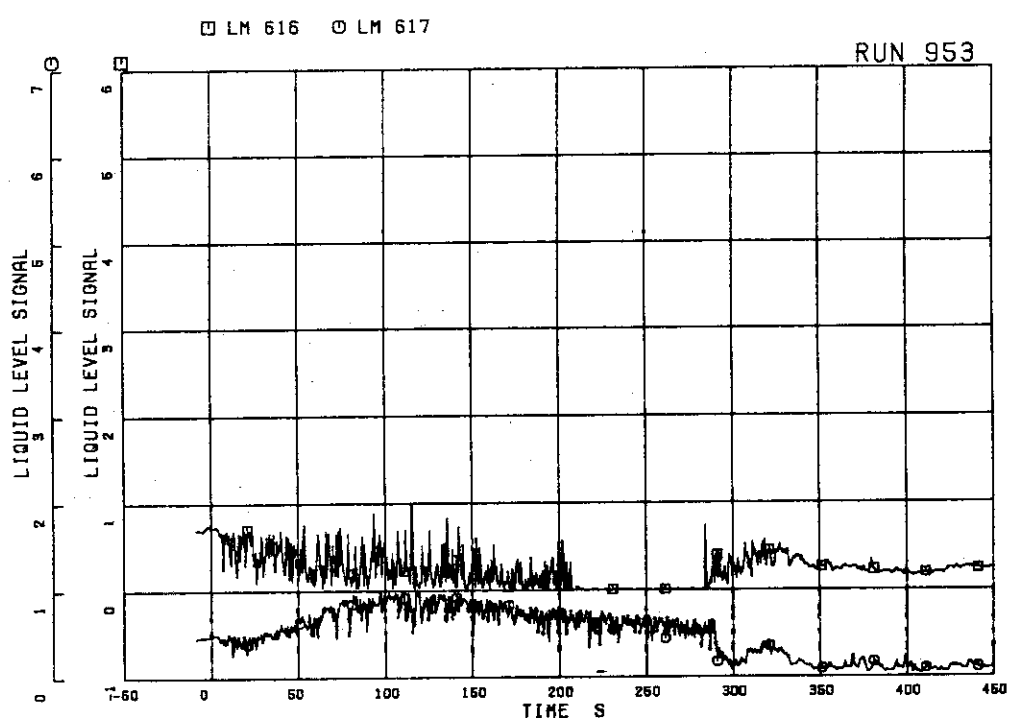


FIG.5.153 LIQUID LEVEL SIGNALS IN CHANNEL A INLET

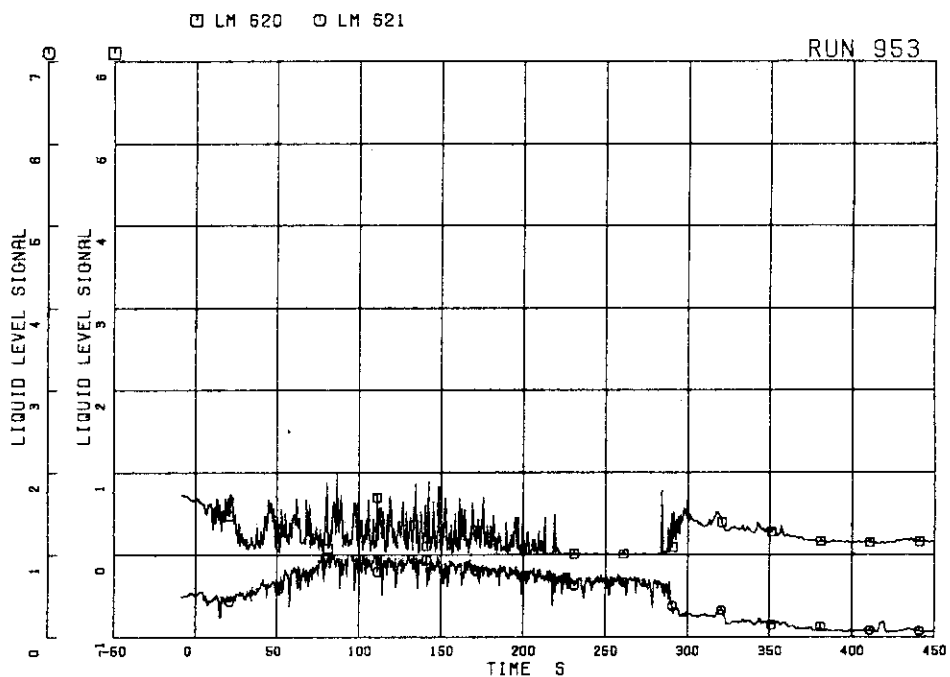
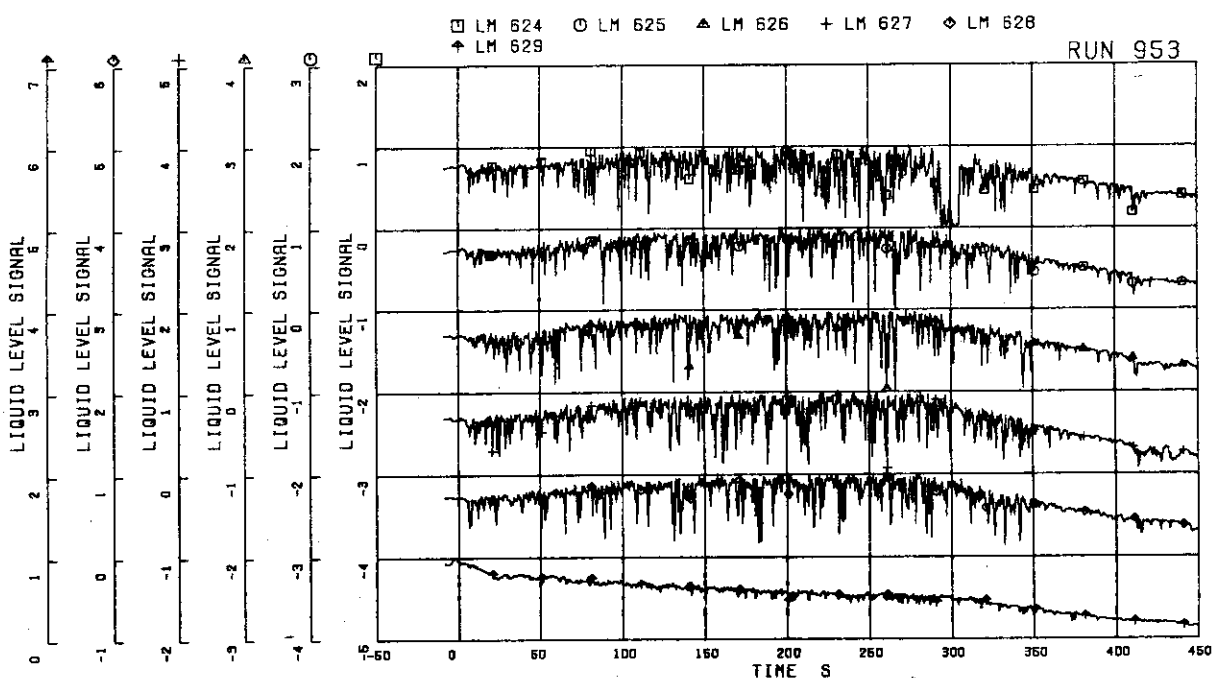


FIG.5.154 LIQUID LEVEL SIGNALS IN CHANNEL C INLET

FIG.5.155 LIQUID LEVEL SIGNALS IN LOWER PLENUM  
NORTH

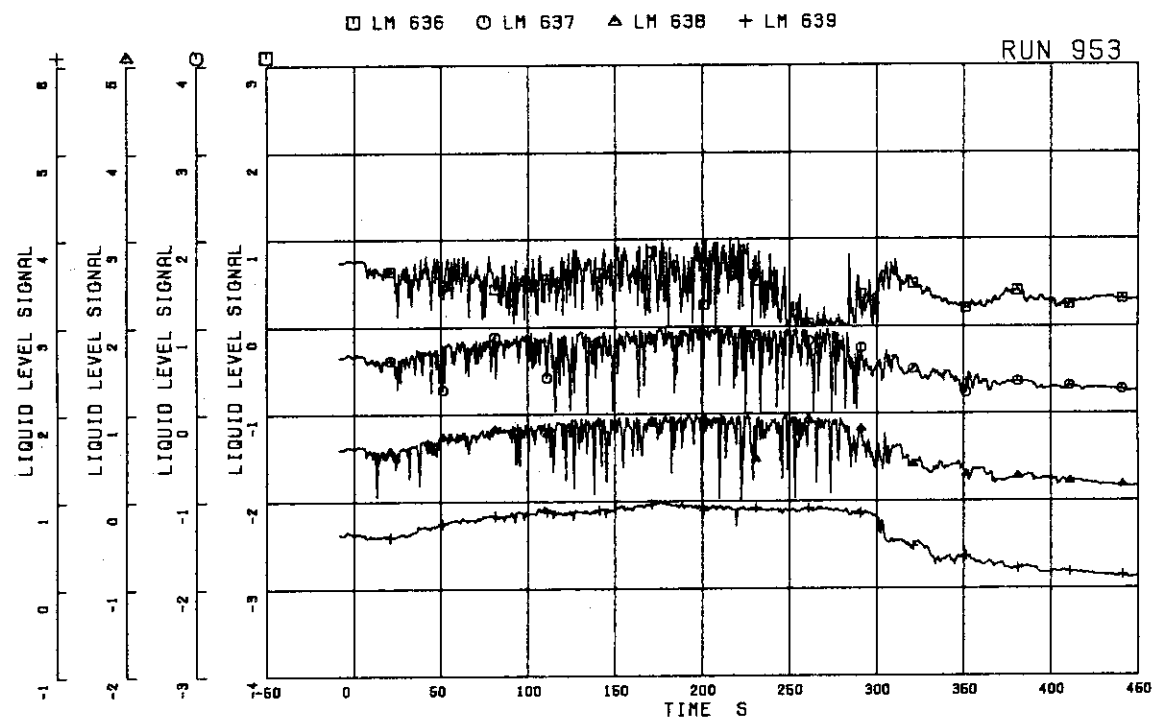


FIG.5.156 LIQUID LEVEL SIGNALS IN GUIDE TUBE  
NORTH

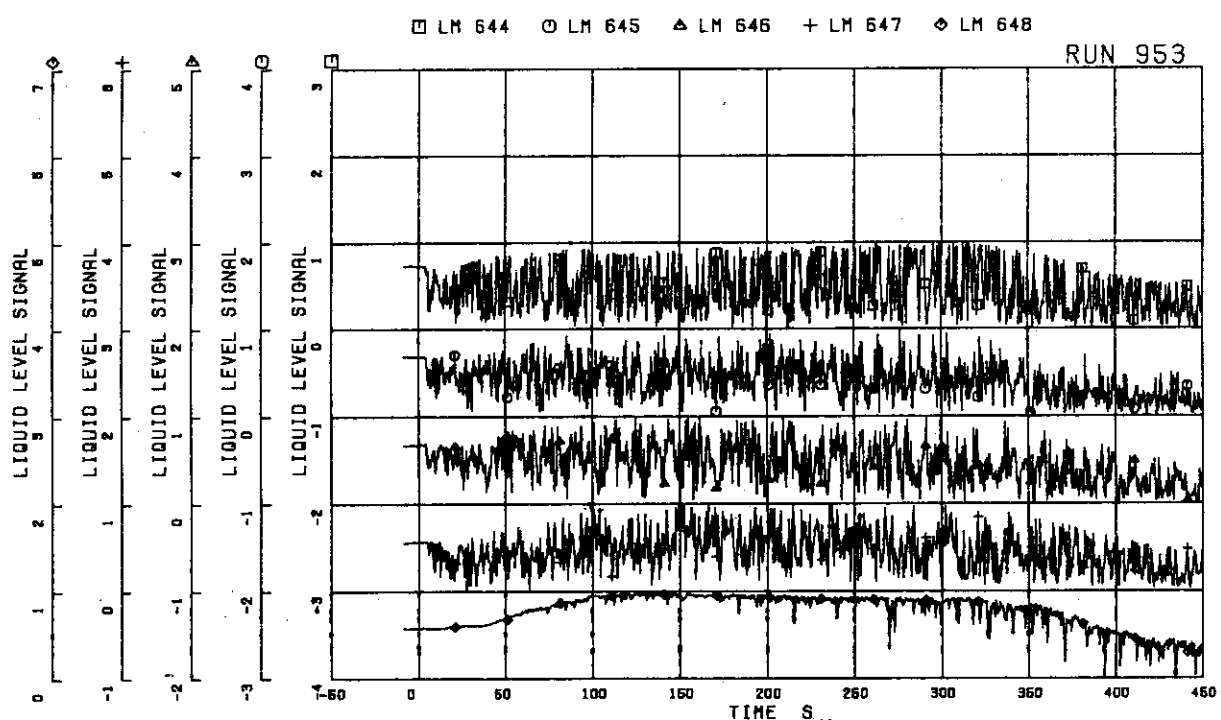


FIG.5.157 LIQUID LEVEL SIGNALS IN DOWNCOMER  
D SIDE

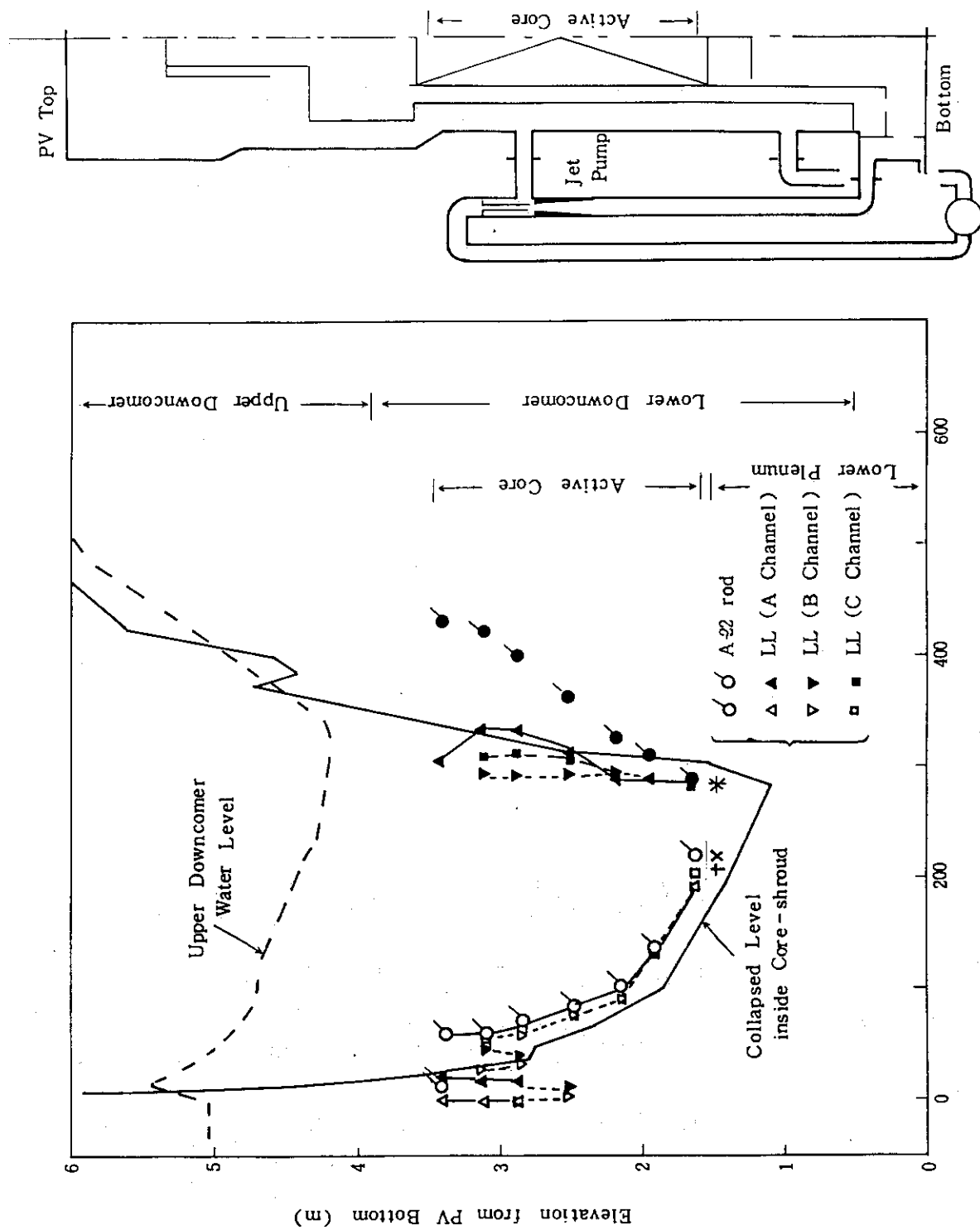


Fig. 5.158 Liquid level in core and downcomer

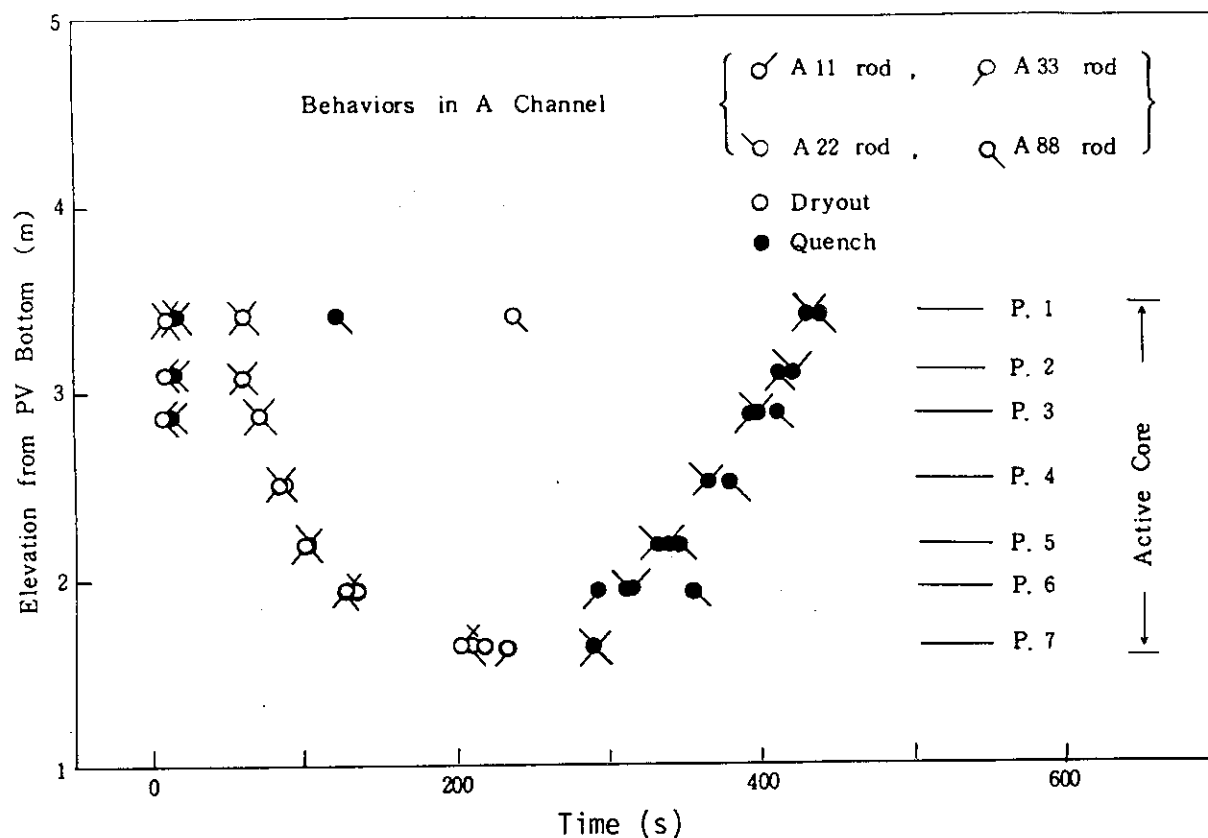


Fig. 5.159 Dryout and quench front transients in channel A

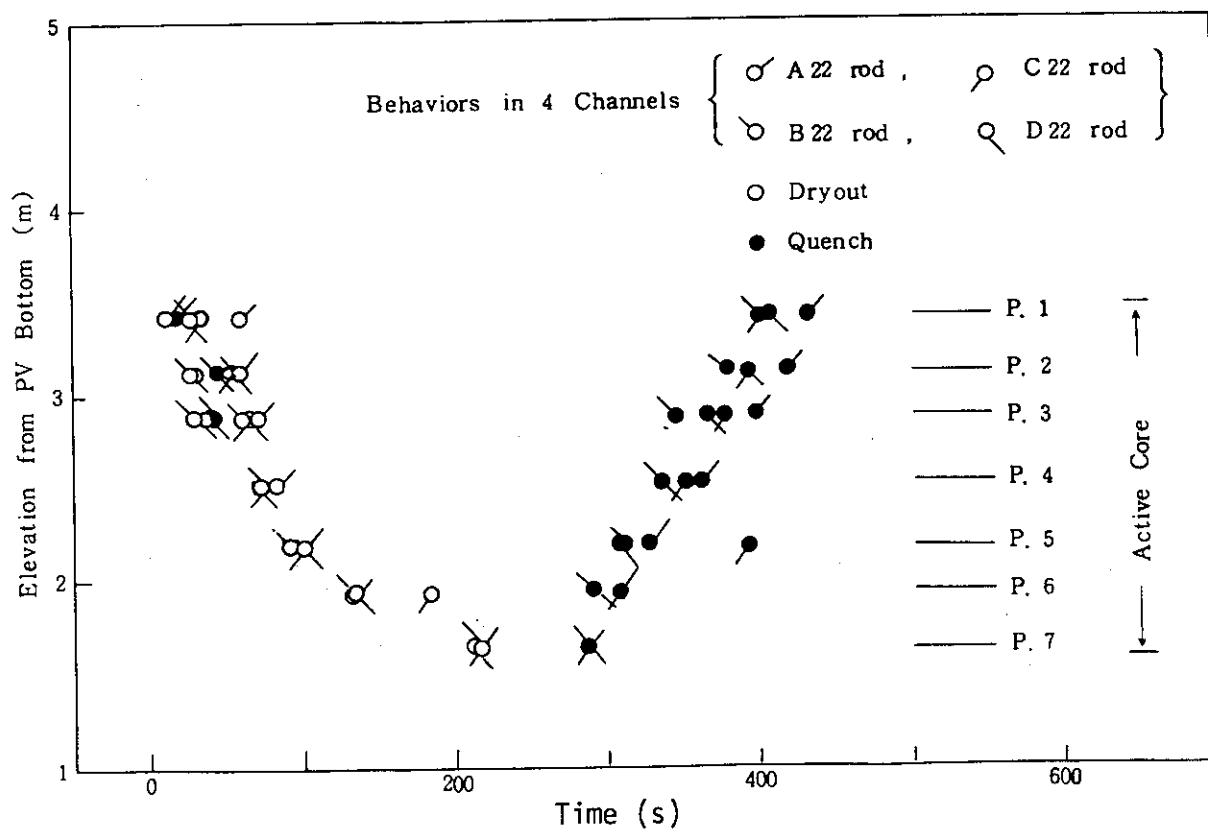


Fig. 5.160 Dryout and quench front transients in channels A,B,C and D

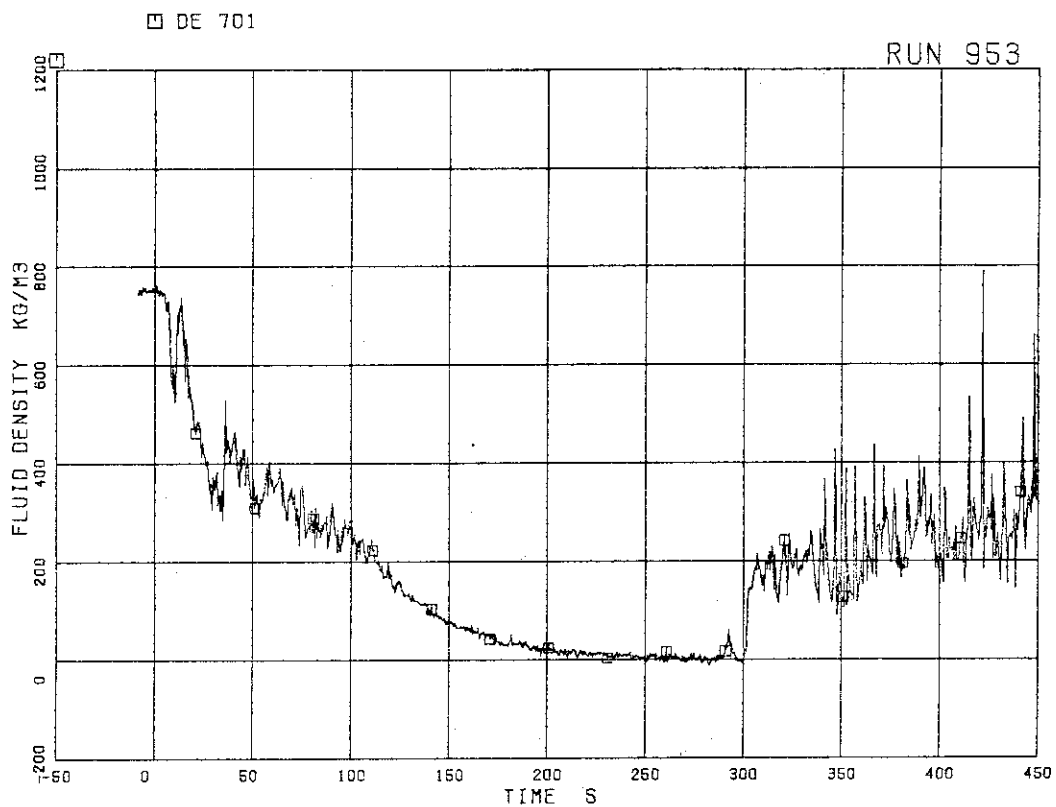


FIG.5.161 AVERAGE DENSITY AT JP-1,2 OUTLET

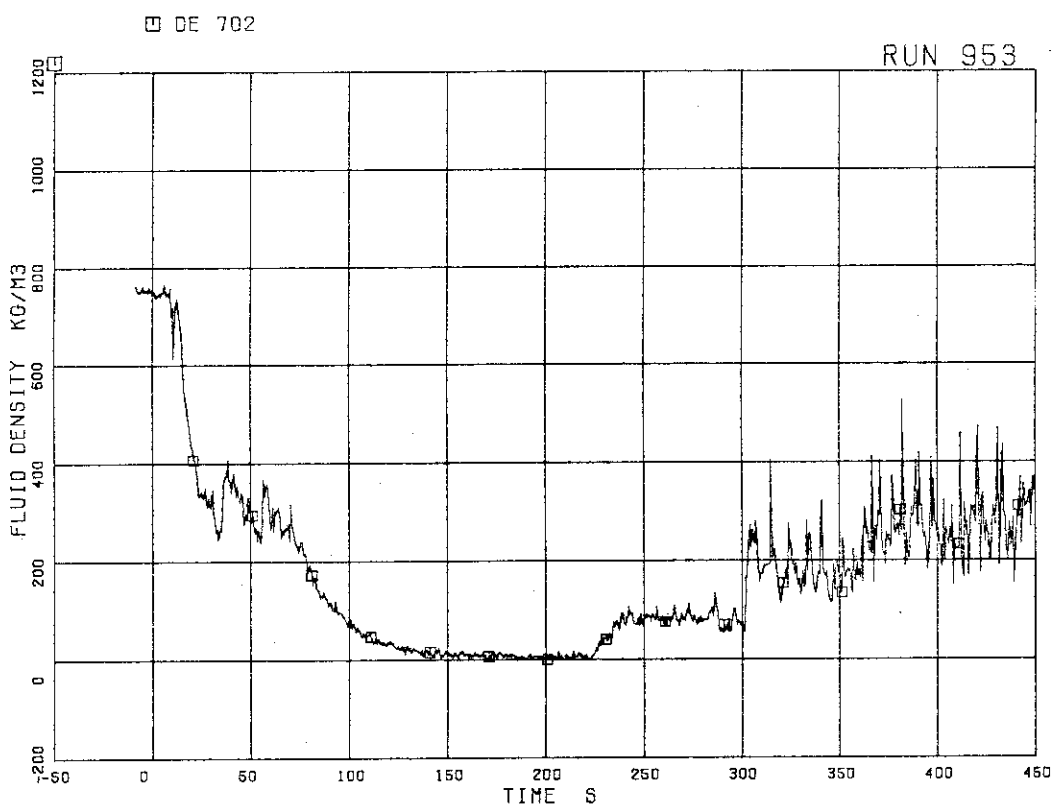


FIG.5.162 AVERAGE DENSITY AT JP-3,4 OUTLET

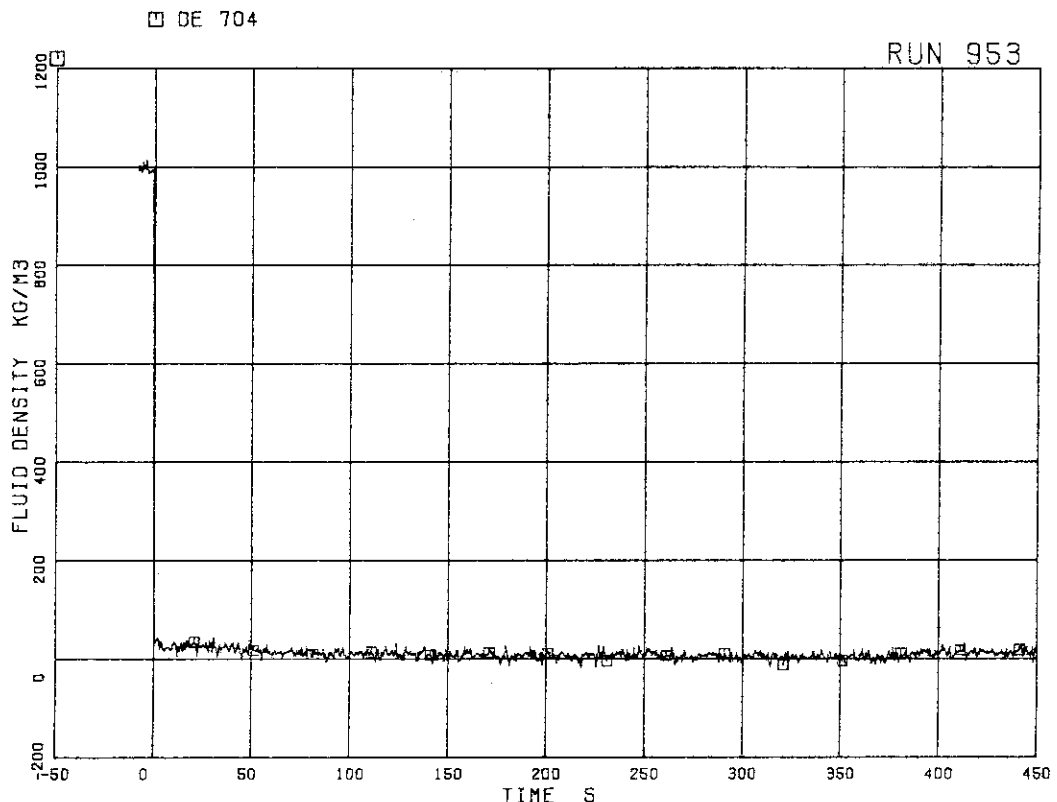
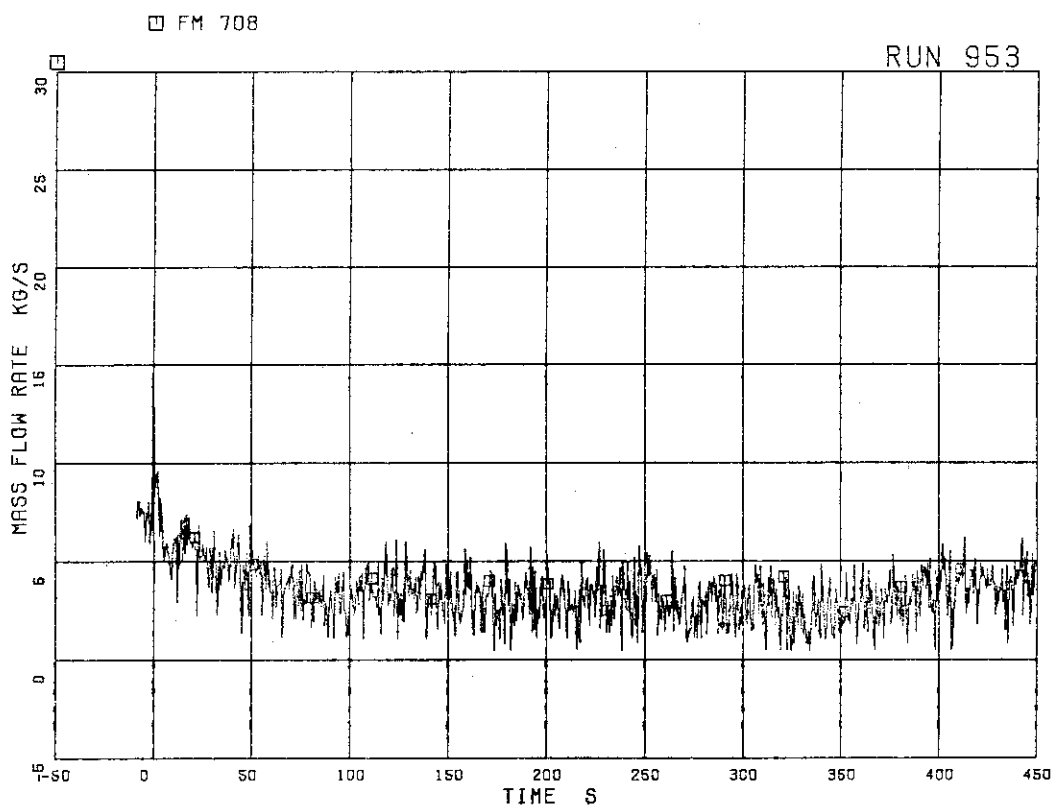


FIG.5.163 AVERAGE DENSITY AT BREAK

FIG.5.164 FLOW RATE AT BREAK  
(BASED ON HIGH RANGE DRAG DISK DATA)

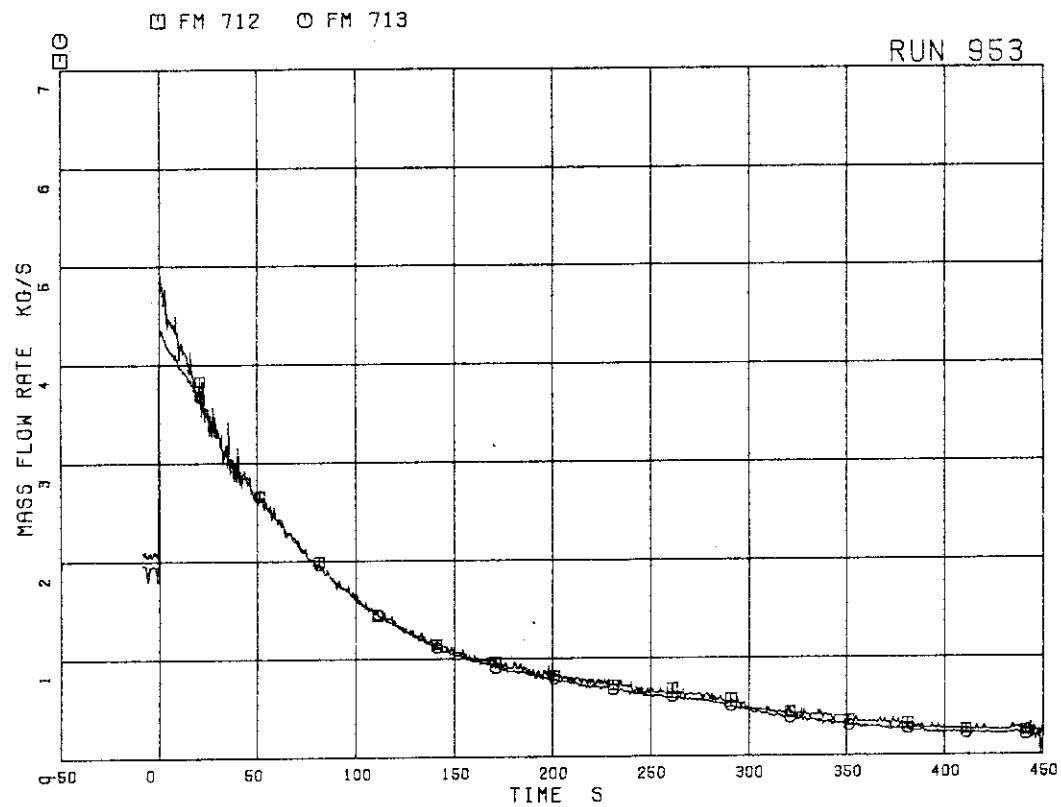


FIG.5.165 STEAM DISCHARGE FLOW RATE THROUGH MSL

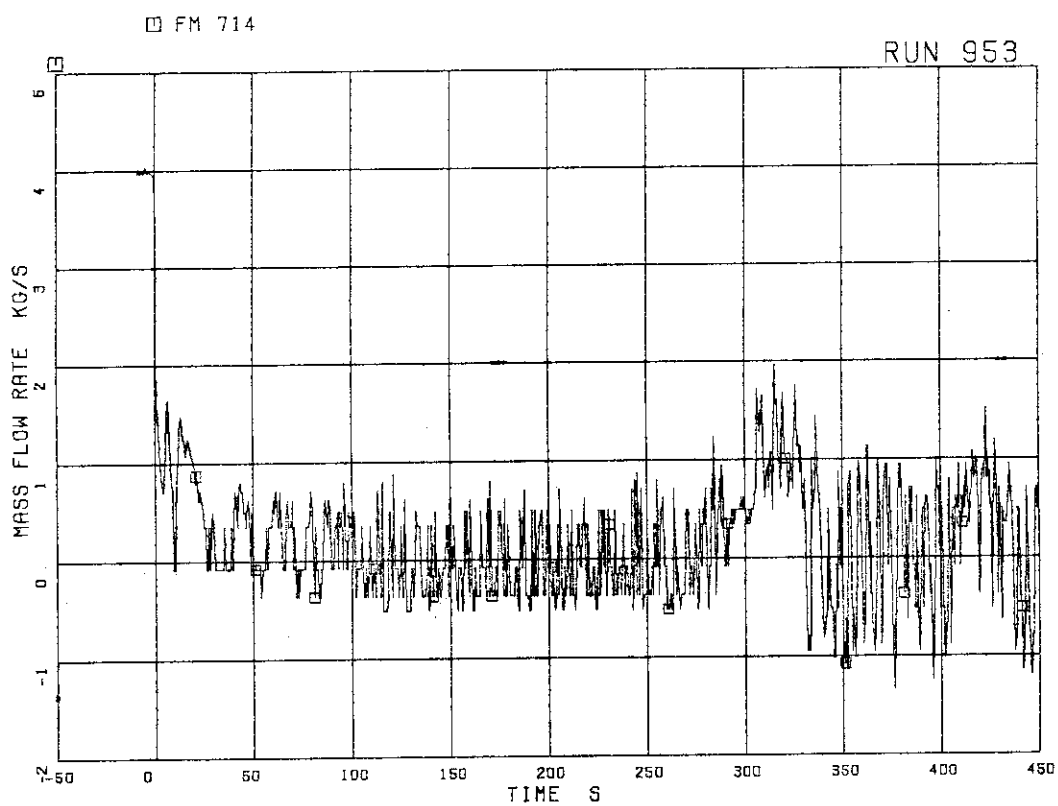


FIG.5.166 FLOW RATE AT CHANNEL A INLET

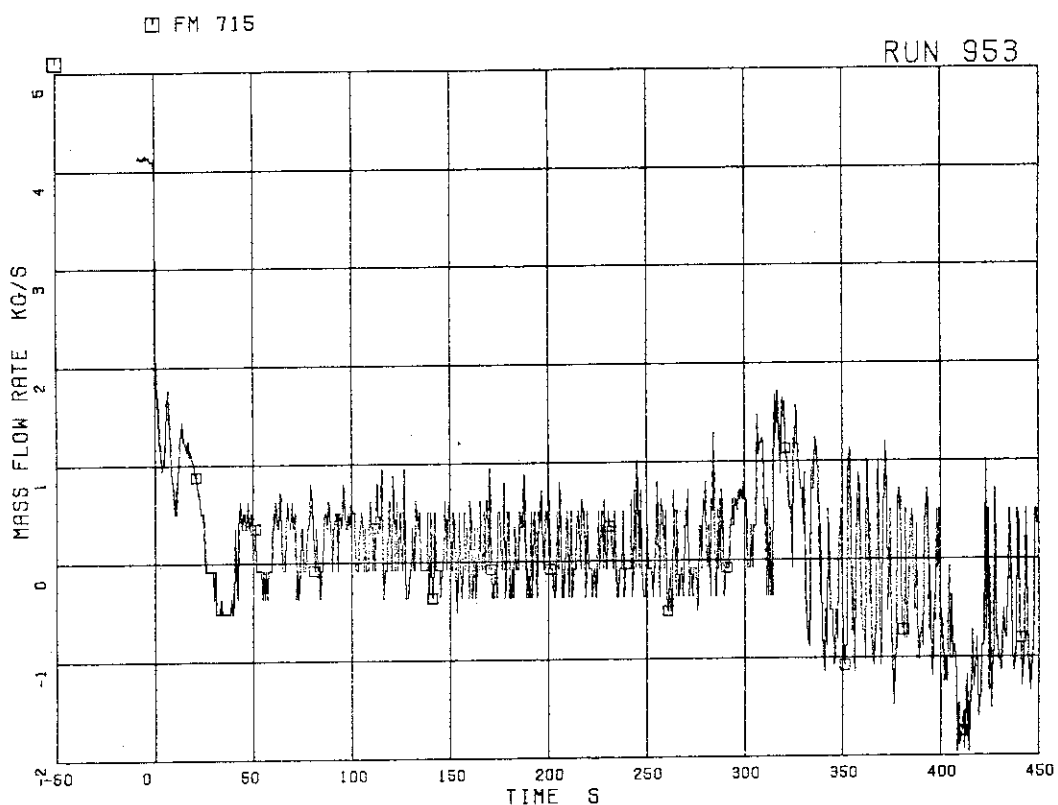


FIG.5.167 FLOW RATE AT CHANNEL B INLET

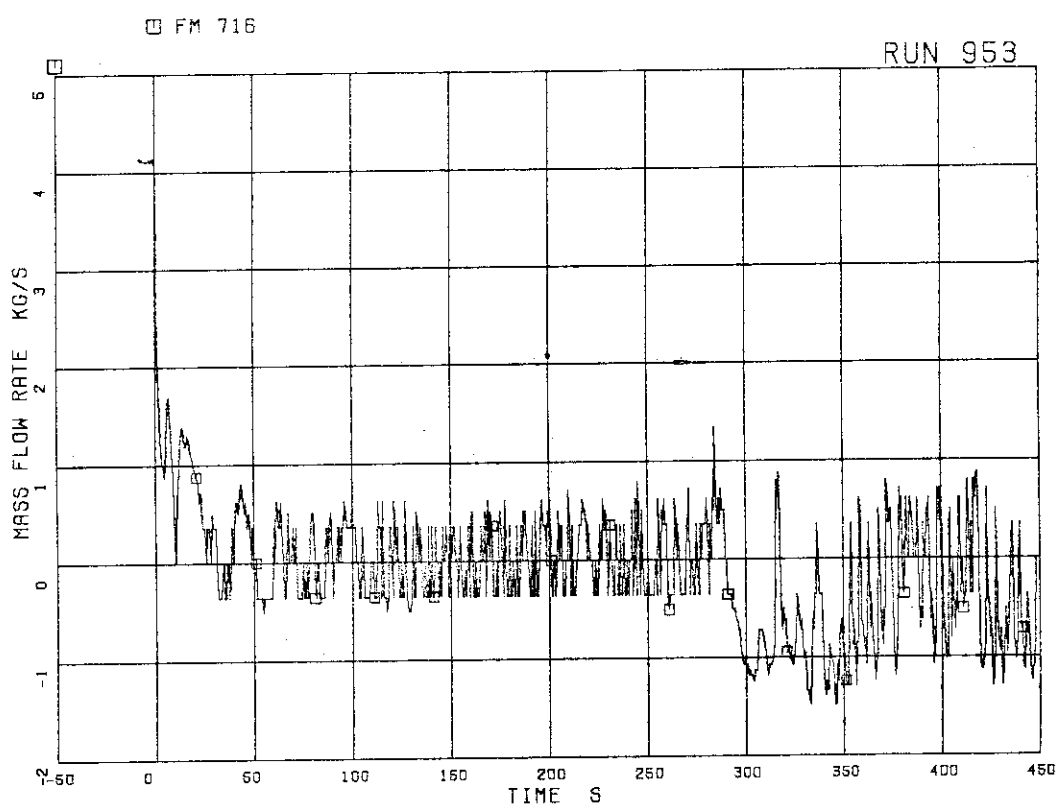


FIG.5.168 FLOW RATE AT CHANNEL C INLET

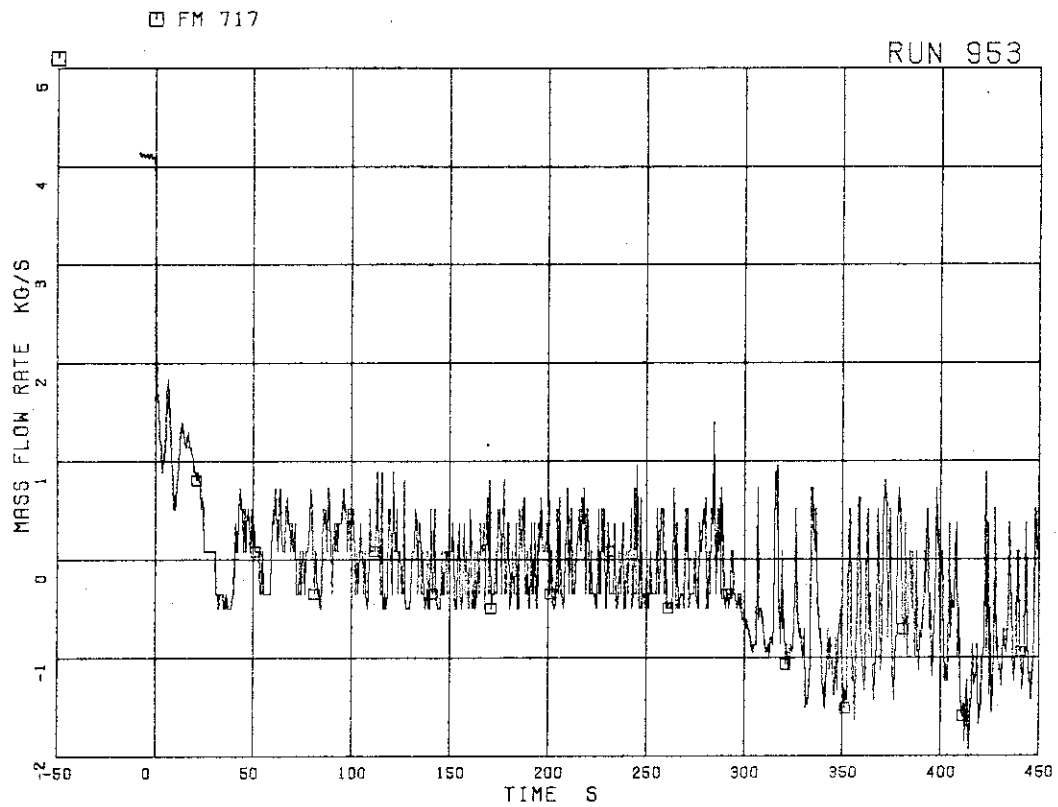


FIG.5.169 FLOW RATE AT CHANNEL D INLET

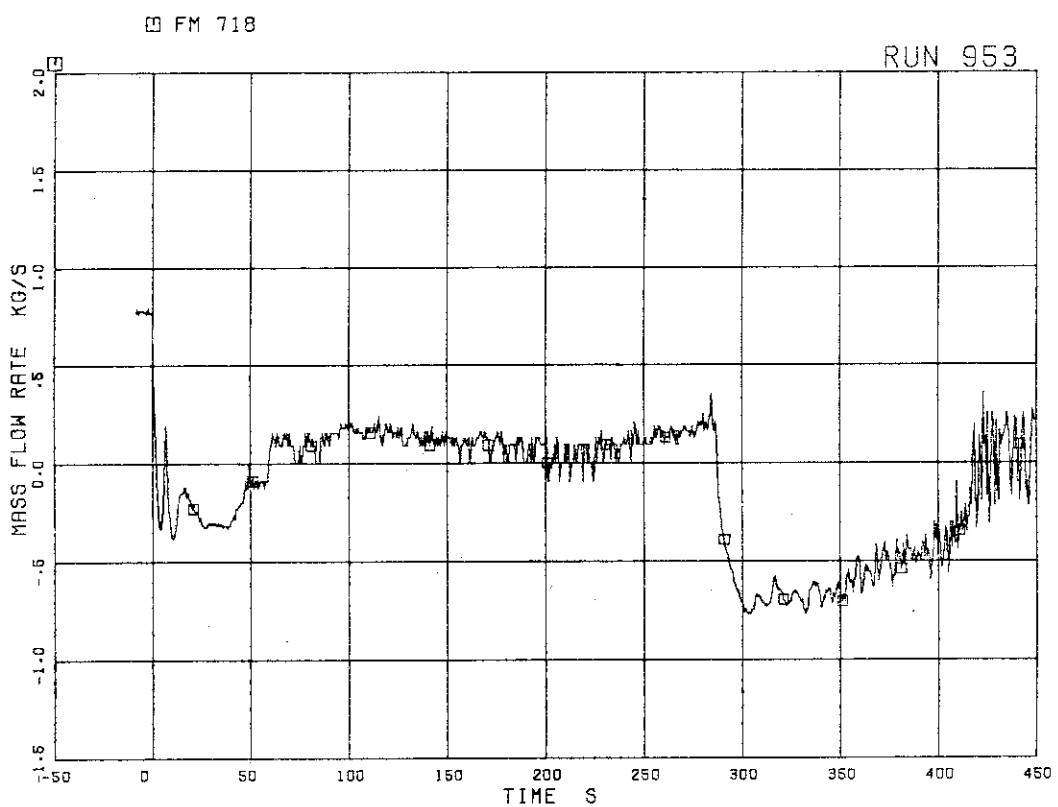


FIG.5.170 FLOW RATE AT BYPASS HOLE

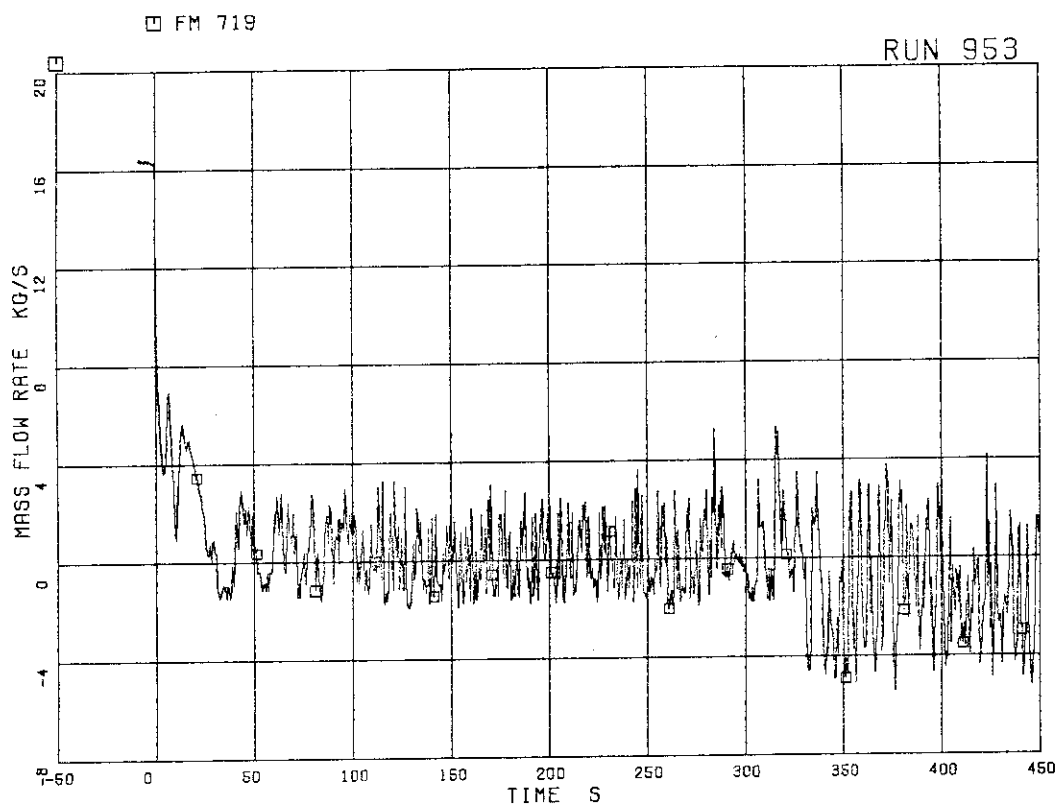


FIG.5.171 TOTAL CHANNEL INLET FLOW RATE

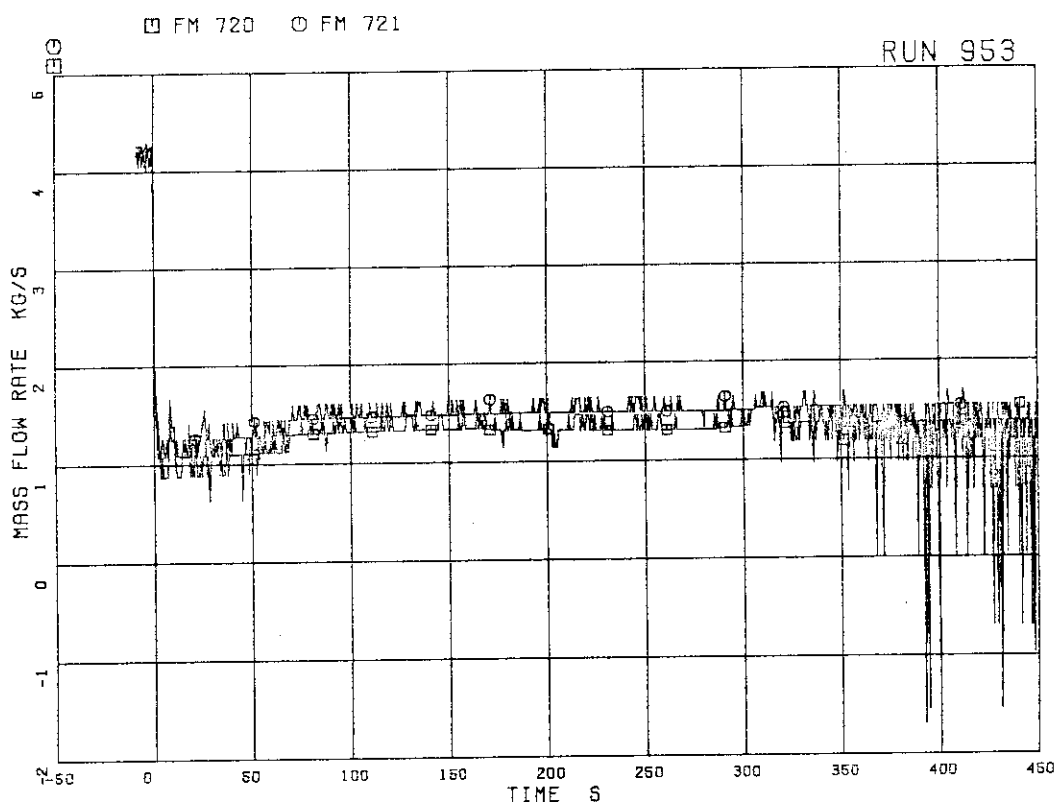


FIG.5.172 FLOW RATE AT JP-1,2 OUTLET (POS.FLOW)

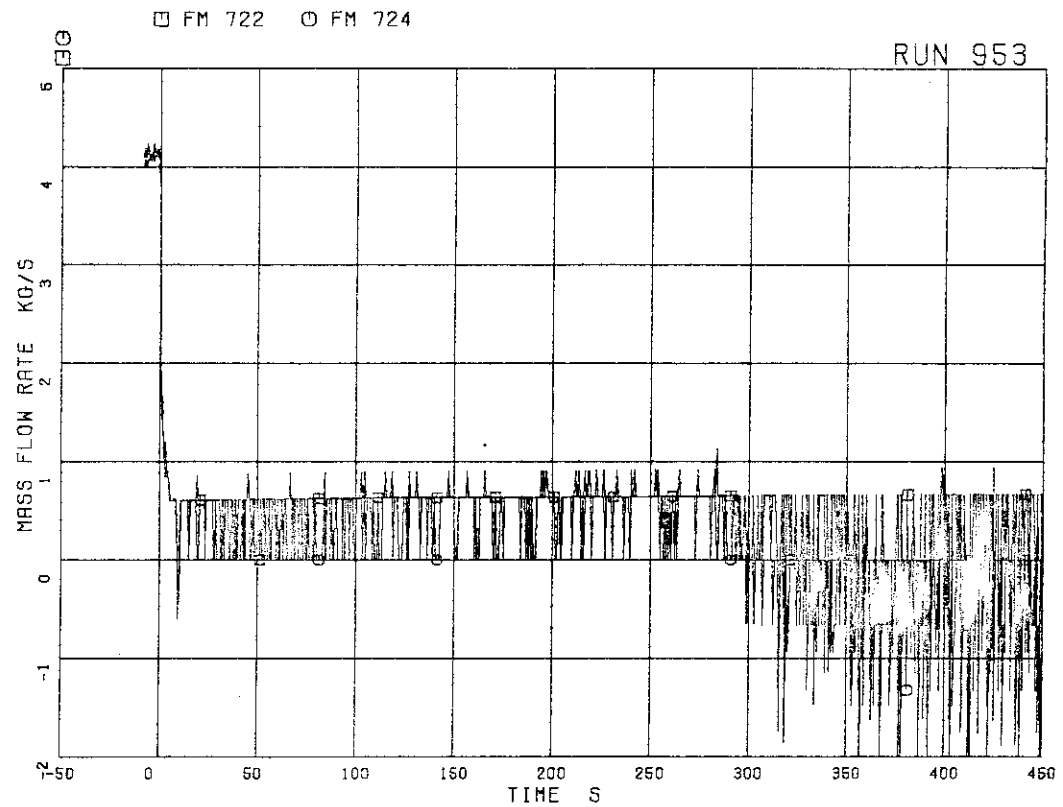


FIG.5.173 FLOW RATE AT JP-3,4 OUTLET (POS.FLOW)

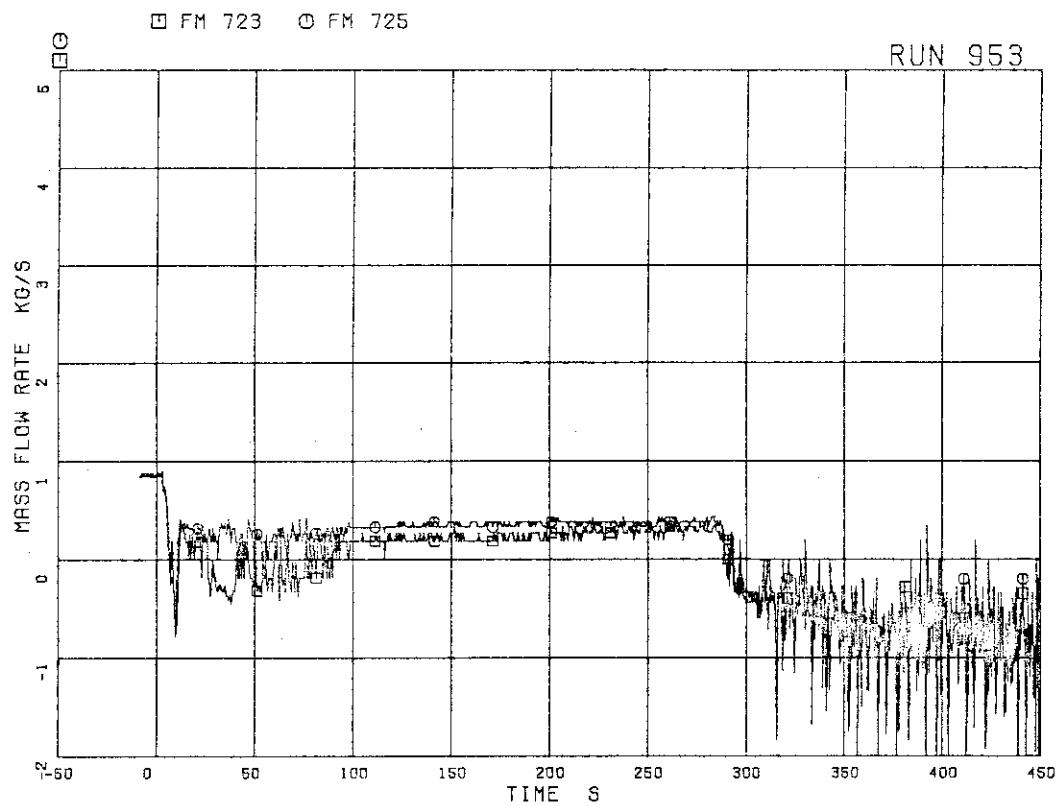


FIG.5.174 FLOW RATE AT JP-3,4 OUTLET (NEG.FLOW)

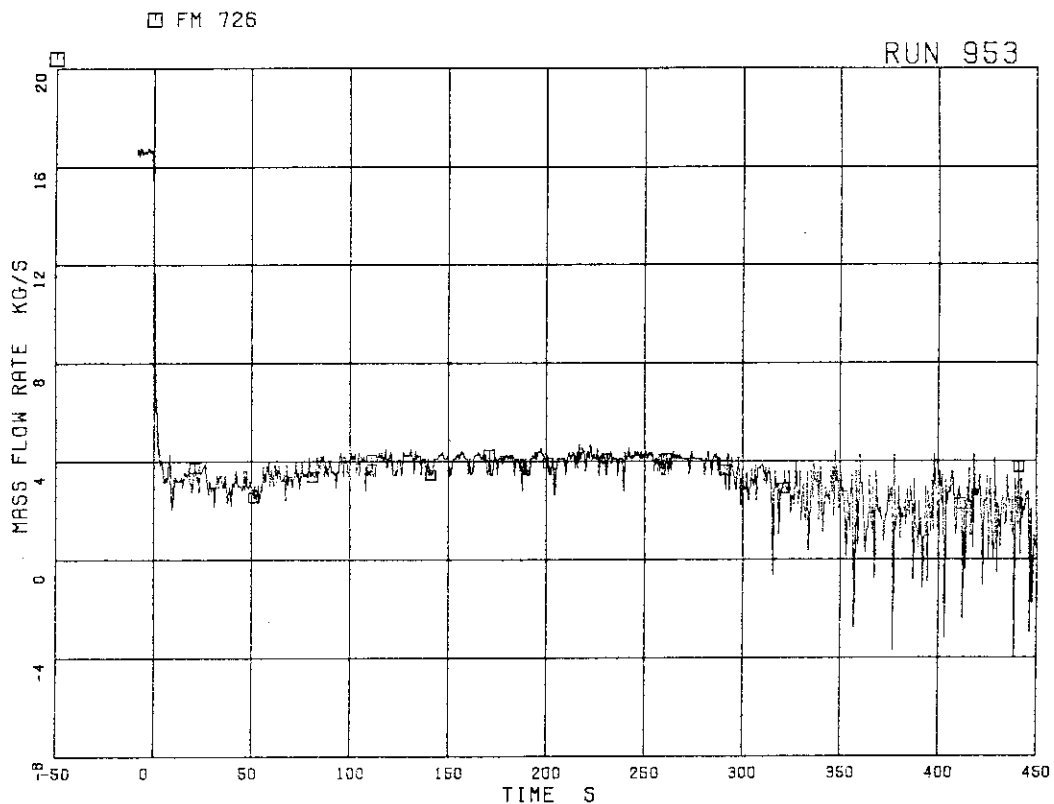


FIG.5.175 TOTAL JP OUTLET FLOW RATE (POS.FLOW)

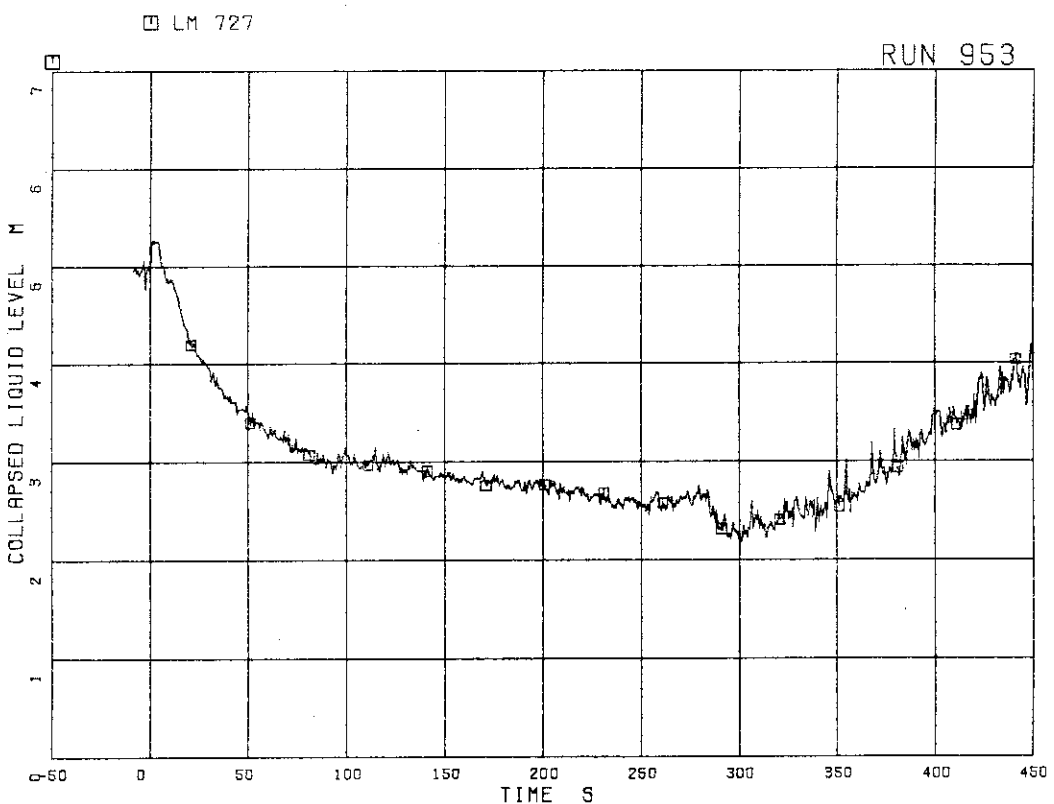


FIG.5.176 COLLAPSED LIQUID LEVEL IN DOWNCOMER

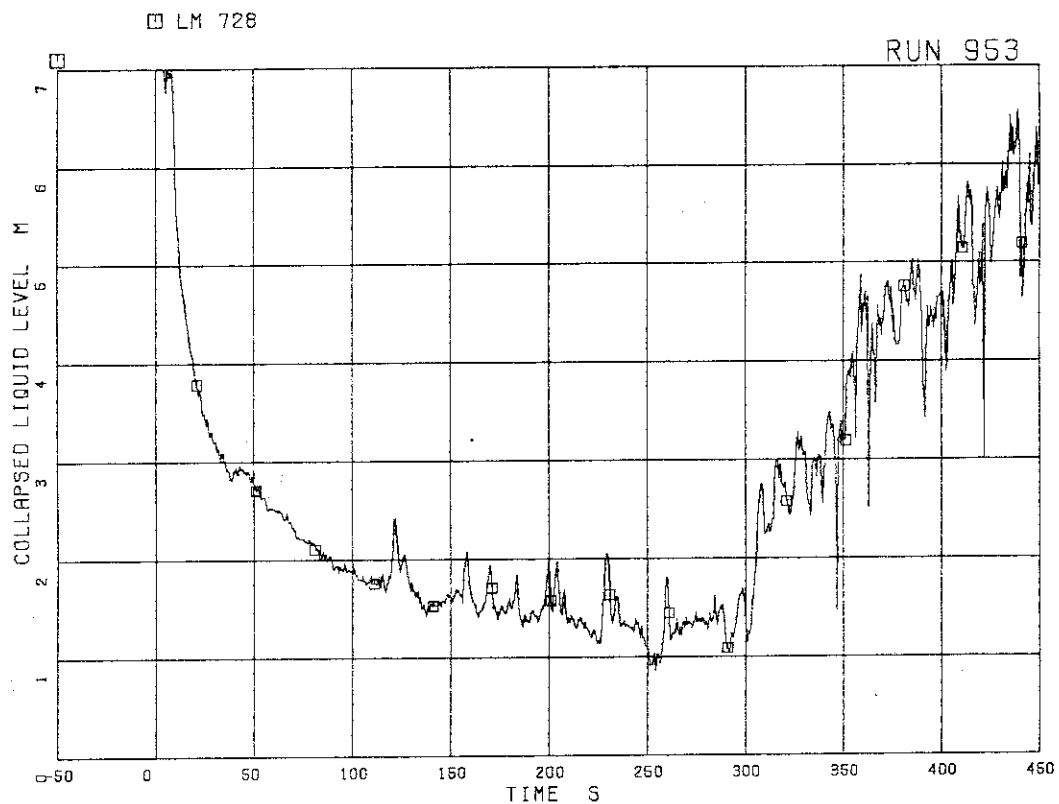


FIG.5.177 COLLAPSED LIQUID LEVEL INSIDE CORE SHROUD

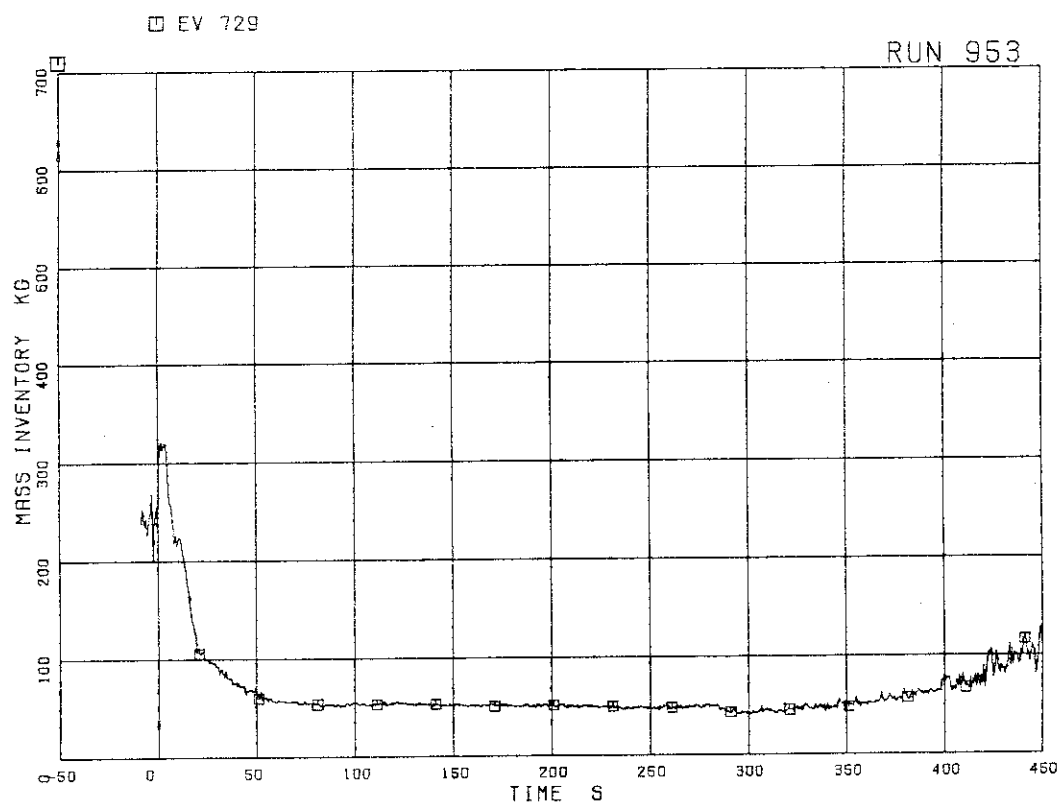


FIG.5.178 FLUID INVENTORY IN DOWNCOMER

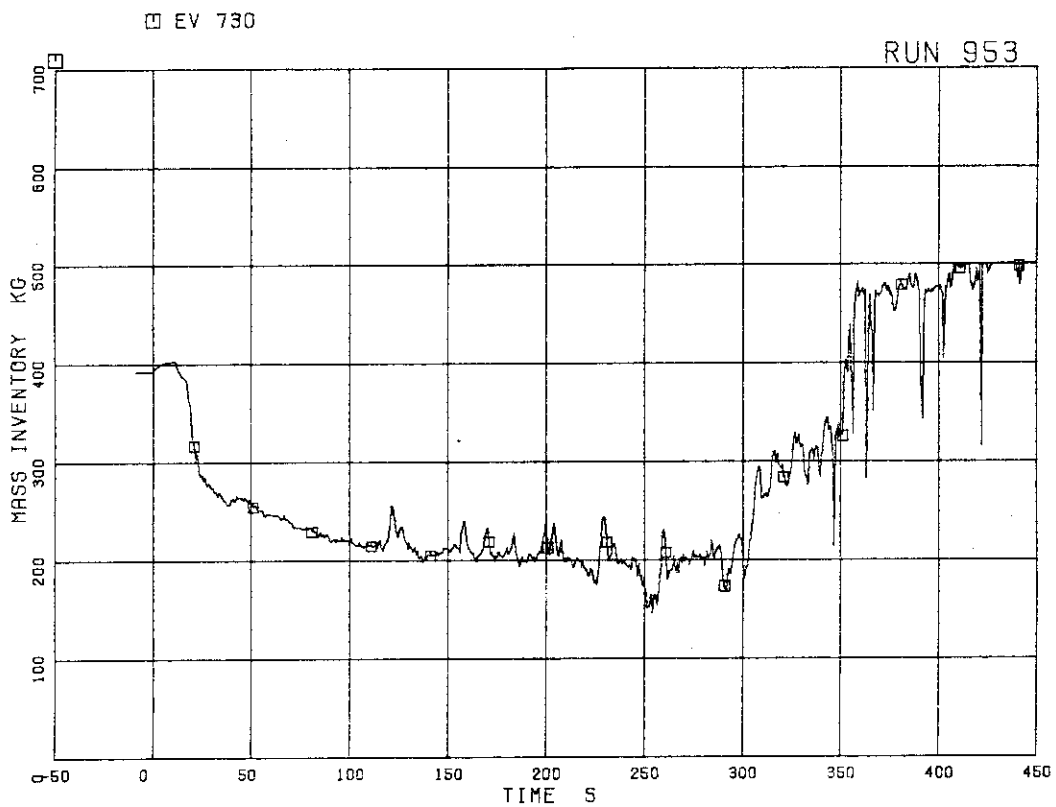


FIG.5.179 FLUID INVENTORY INSIDE CORE SHROUD

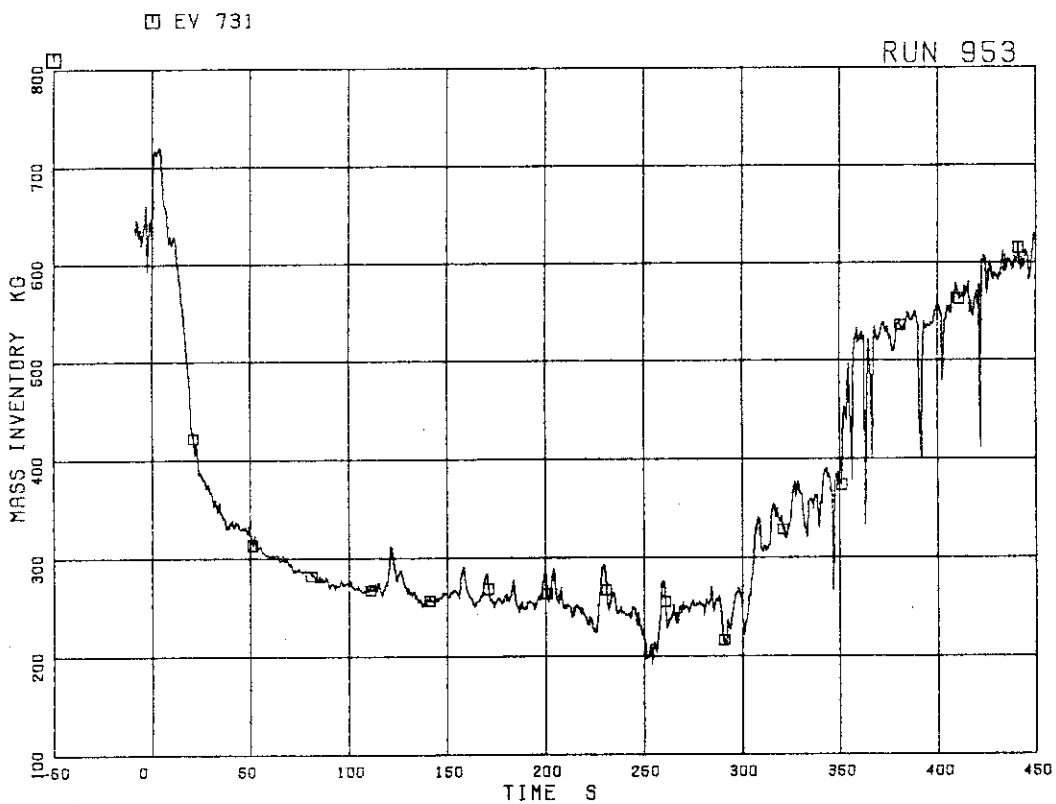


FIG.5.180 TOTAL FLUID INVENTORY IN PRESSURE VESSEL

## 6. Discussion of Test Results

Experimental data for RUN 953 are discussed in this section.

### 6.1 Pressure Response and Sequence of Events

The pressure response in various parts of the pressure vessel, recirculation line and break unit are shown in Figs. 5.1 through 5.5. The pressure response shows monotonous depressurization throughout the test, which is reasonable in a steam line break or a continuous steam discharge transient with a large amount of vapor generation in the whole system.

Initiation of vapor generation or flashing at each location of the ROSA-III system can be determined from the liquid level, differential pressure and fluid temperature data. The liquid in the middle downcomer began to evaporate at 4.6 s after break as shown in the differential pressure data (see Fig. 5.8). The fluid in the top part of jet pumps began to evaporate also at 4.6 s (see Fig. 5.16). At 5.4 s, flashing started to occur in the lower plenum, resulting in a decrease in the depressurization rate. The fluid in the feedwater line with an initial temperature of 489 K began to flash at a pressure of 2.2 MPa at 95 s after break (see Fig. 5.38).

The LPCS and LPCI were simultaneously actuated by the L1 trip signal with a time delay of 40 s at a system pressure of 0.65 MPa at 281 s after break. The actuation pressure was lower than the designed pressure set point due to a delay in tripping the signal for ECCS, i.e., L1 water level signal in the upper downcomer. The high water level in the upper downcomer (see Fig. 5.35) was caused by the vapor generation in the lower downcomer, lower plenum and recirculation line. Core uncovering started to occur from

the top of the core at 29 s after break. The bottom part of the core was uncovered and exposed to the steam environment at about 200 s after break. The reflooding of the core followed the LPCS and LPCI actuation and the entire core was quenched at 438 s after break (157 s after LPCS actuation).

## 6.2 Differential Pressure

Differential pressure and collapsed water level in the pressure vessel are discussed in this section. The collapsed water level is estimated from the corresponding differential pressure data neglecting the effects of friction and acceleration terms.

Figures 5.6 through 5.9 show differential pressure data between the lower and upper plena (D1), between the upper plenum and steam dome (D2), between the bottom and middle regions of the downcomer (D4), and between the lower plenum and steam dome (D5) respectively. (For differential pressure designation, refer to Table 3.2) Flow stagnation due to coasting down of the recirculation pumps occurred shortly after the break, resulting in a rapid decrease in the differential pressure (D1).

The differential pressure, D1, shows large fluctuations after LPCS and LPCI actuation at 281 s after break. D1 increased rapidly after LPCS and LPCI actuation indicating an increase in mass inventory.

The differential pressure, D2, between the upper plenum and steam dome shows a rapid increase due to the fluid acceleration in the steam line immediately after the break. The effect of lower plenum flashing is observed after 5.4 s. D2 remained unaffected for a while even after LPCS and LPCI actuation.

The differential pressure, D4, in the lower downcomer shows a rapid decrease after 4.6 s indicating coolant flashing in the downcomer. Following LPCS and LPCI actuation, the differential pressure in the lower down-

comer shows a sudden decrease prior to a start of mass recovery at about 300 s after break. The void fraction in the downcomer was estimated from the data to be approximately 56% between 100 s and 250 s. The maximum void fraction was estimated to be 67% occurring at about 300 s. It is noted from the D4 data that steam generation occurred in the downcomer for a long time even after LPCS and LPCI actuation until the lower downcomer was entirely refilled with subcooled water. The differential pressure, D5, between the top and bottom of the pressure vessel is the same as the sum of D1 and D2. A sudden increase and a rapid drop in D5 just after break reflects a similar behavior observed in the D2 data. After about 30 s, D5 decreased less rapidly but nevertheless indicated a decrease in the pressure vessel mass inventory. D5 began to increase gradually after 281 s due to LPCS and LPCI actuation. The collapsed water levels inside and outside the core shroud estimated from the differential pressure data are shown in Figs. 5.176 and 5.177 and will be discussed shortly.

Figures 5.10 through 5.52 show differential pressure data in the pressure vessel and recirculation line, which represent primarily the changes in the flow rate and mass inventory. Rapid decreases in differential pressure shown in these figures immediately after break indicate flow stagnation caused by the recirculation pump coast down. The coolant in the recirculation lines began to flash at 5.4 s after break and the transient differential pressure data, D16 (Fig. 5.15), D17 (Fig. 5.16), and D21 (Fig. 5.18) show decreases in the mass inventory. After LPCS and LPCI actuation at 281 s, D21 began to decrease indicating gradual accumulation of coolant at the jet pump discharge piping. On the other hand, D16 and D17 decreased to very small values indicating that a small quantity of coolant remained in the recirculation line.

Figures 5.29 through 5.33 show the differential pressures measured across the core inlet orifices of the four channel boxes and the bypass

hole simulating a leakage path from the lower plenum to the guide tube in BWR/6. At steady state before the break, the differential pressure across the core inlet orifice of the peak power channel A is slightly lower than those of the average power channels due to larger vapor generation rate in channel A. The differential pressures dropped to small values immediately after break due to flow stagnation. At the time of lower plenum flashing (5.4 s), the differential pressure increased temporarily. The differential pressure across the bypass hole shows negative values for a while following the break, indicating a downward flow through the bypass hole. The negative values after 281 s indicate a downward flow caused by the LPCS and LPCI water accumulating in the core bypass.

The collapsed water levels in the upper and the lower regions of the downcomer are estimated from the corresponding differential pressure data and shown in Figure 5.35. The collapsed water level in the upper downcomer (between 3.90m EL and 6.04m EL) dropped to the L2 level (4.75 m EL) at 74 s and to the L1 level (4.25m EL) at 245 s, while the water level in the downcomer (between 0.938m EL and 3.90m EL) decreased after 4.2 s indicating generation of a large amount of steam due to flashing. The steam generated due to flashing of the coolant in the lower downcomer contributed to the water hold up in the upper downcomer. Continuous flashing and high water level in the downcomer are uniquely observed in the MSL break test.

Figures 5.176 and 5.177 show the collapsed water level in the pressure vessel. The collapsed water level inside the core shroud was estimated from the differential pressure data shown in Fig. 5.9 assuming no friction and acceleration terms. The total water head in the downcomer was obtained by adding the collapsed water levels in the upper and lower regions of the downcomer. It is evident from these figures, that the collapsed water level in the upper downcomer was always higher than the water level inside the core shroud until LPCS and LPCI injection increased the mass inventory

inside the core shroud.

### 6.3 Coolant Flow Rate

The steam flow rate in the MSL, as well as HPCS and feedwater flow rates were measured in RUN 953. Figure 5.36 shows the steam mass flow rates measured by the high range and high-high range orifice flow meters. The steam flow rate was initially at 2.08 kg/s, but increased instantaneously to above 5.0 kg/s at the initiation of break and subsequently decreased following the system pressure transient shown in Fig. 5.1. The steam flow rate is slightly lower than the break flow rate measured with the drag disk and gamma densitometer in the break unit (see Fig. 5.164). Figure 5.37 shows the ECCS flow rates. HPCS was not actuated in the present test. LPCS and LPCI were triggered by the L1 level signal in the upper downcomer with a time delay of 40 s. The LPCS and LPCI flow rates were steady at 0.00115 m<sup>3</sup>/s (0.00115 kg/s) and 0.00415 m<sup>3</sup>/s (0.00415 kg/s) respectively.

Figure 5.38 shows the feedwater flow rate. The average steady flow rate was equal to  $2.4 \times 10^{-3}$  m<sup>3</sup>/s (2.04kg/s). The feedwater flow started to decrease at 1.5 s after break and was terminated completely at 3.8 s. A large spike appeared in the flow rate at about 95 s indicating the flashing of the feedwater remaining in the feedwater line at a system pressure of 2.22 MPa. Spikes repeatedly occurred at 288 s and 568 s indicating similar inflow of feedwater into the pressure vessel.

The volumetric flow rates through the jet pumps and the main recirculation pumps are shown in Figures 5.39 through 5.41. The flow rates dropped to near zero immediately after break following the pump coast down and remained near zero thereafter.

Figures 5.42 through 5.52 show the differential pressures measured across the orifice or venturi flow meters in the MSL, jet pumps and recirc-

culation pumps. These pressure drop data were used to calculate the flow rates in the respective locations shown previously.

#### 6.4 Process Control

There are two electric power supply systems used to heat up the core, namely A system (2.1 MW max.) for the peak power channel A, and the B system (3.15MW max.) for the other three average power channels, B, C, and D. The power transients of A and B systems are shown in Fig. 5.53. Initial power was 1.265 MW for the system A and 2.712 MW for system B. The corresponding maximum linear heat rates of heater rods are shown in Table 4.1. The radial and axial power distributions in the core are shown in Figs. 2.6 and 2.7. The steady state power was maintained for the first 9.0 s after break and then reduced along the decay curve shown in Fig. 4.2.

The coast down characteristics of the main recirculation pumps are shown in Fig. 5.54. The coast down was initiated at the time of break and completed in about 10 s for both pumps.

The on-off signals indicating the operation of valves, ECCS and the main recirculation pumps are shown in Fig. 5.55 through 5.57. The LPCS and LPCI are seen to be actuated at 281 s.

#### 6.5 Density and Momentum Flux

Fluid density was measured by using two-beam and three-beam gamma densitometers.

Figures 5.58 through 5.63 show the fluid density data of beams A, B, and C at a location downstream of jet pumps 1,2 and jet pumps 3,4, respectively. These data indicate that the fluid density decreased due to steam generation after the initiation of flashing at 4.6 s until 300 s and

increased thereafter due to the arrival of LPCS and LPCI water. Flow separation is also indicated in these figures.

Figures 5.64 and 5.65 show the fluid density data of beams A and B at the break. The density before break was nearly  $1000 \text{ kg/m}^3$ , because the steam that leaked out through AV165 was condensed and accumulated at the cooler measurement location far downstream of the MSL. Immediately after break, steam began to pass through the measurement location. Pressure and fluid temperature at the break unit were 7.15 MPa and 300 K prior to the break initiation, and 0.91 MPa and 455 K at 200 s after break.

Figures 5.66 through 5.68 show the momentum fluxes measured at the jet pump outlet and the break. The break flow is seen to gradually decrease with time initially, but remain constant after about 100 s.

## 6.6 Coolant Temperature

The coolant temperatures measured at various parts of the pressure vessel and recirculation loops except at the core inlet and outlet are shown in Figs. 5.69 through 5.81. The data show a gradual decrease that corresponds to the rate of system depressurization, and in some cases superheated conditions due to core dryout.

The fluid temperatures at the core inlet and outlet, and at lower plenum are shown in Figs. 5.127 through 5.145. The temperature of the fluid entering the core decreases gradually following the saturation temperature corresponding to the system pressure. The fluid exiting the core, however, shows superheating during the period of core dryout.

## 6.7 Fuel Rod Surface Temperature

Fuel rod surface temperatures were measured by CA thermocouples of 0.5

mm O.D. imbedded in the fuel rod sheath made of Inconel 600. Figures 5.82 through 5.89 show the fuel rod surface temperatures of the rods A11, A12, A13, A22, A33, A77, A87 and A88 in the peak power channel A. Each fuel rod has seven thermocouples along the axial direction.

Figures 5.90 through 5.98 show the surface temperatures of the fuel rods B11, B22, B77, C11, C13, C22, C33, C77 and D22 in the average power channels. The surface temperatures of water rod simulators, A45 and C45, and the outer surface temperatures of the channel box A are shown in Figs. 5.99 through 5.101. The upper part of the water rod simulators experienced a temperature increase due to heat transfer by thermal radiation during the fuel rod dryout. On the other hand, the channel box temperature was not affected significantly by the dryout of fuel rods. The temperatures of different fuel rods at the same elevation are compared in Figs. 5.102 through 5.126.

Following observations have been obtained from the fuel rod surface temperature data. (1) The peak cladding temperature (PCT) of 1004 K was obtained at position 3 of A22 rod at 292 s after break. This PCT value is the highest attained in all the previous ROSA-III tests with a single failure assumption in ECCS except for RUNs 805 and 8051 in which the ADS actuation was delayed. (2) Temporary dryout occurred at the upper part (pos. 1-3) of channel A between 10 and 20 s after break prior to the major core uncovering. Similar dryout was observed between 30 s and 50 s in the top part of average power channels B, C and D. This difference in time of occurrence of temporary dryout is due to the higher power in channel A than the other channels. Local core cooling was observed shortly after the major core uncovering started at the top of the core due to the coolant falling from the upper plenum. (3) Turn-around of the fuel surface temperatures occurred soon after LPCS and LPCI actuation. (4) Quenching proceeded primarily from bottom of the core upward and was completed at 438 s after

break (157 s after LPSC and LPCI actuation). The dryout and quench front propagation will be discussed in detail in the next section.

### 6.8 Liquid Level

Liquid levels in the pressure vessel were detected by the conduction probes (CP). Figures 5.146 through 5.148 show conduction probe signals obtained at the inner surfaces of channel boxes A, B, and C. Seven conduction probes are attached axially on the channel box wall. Liquid level fall and its recovery in each channel are clearly shown in these figures.

Figures 5.149 through 5.152 show the conduction probe signals near the outlet of channels A and C. Figures 5.153 and 5.154 show the signals obtained at the inlet of the same channels. It is shown in these figures that a clear liquid level was not formed in the lower plenum except near the core inlet. Figure 5.155 shows the CP signals at the north side of the lower plenum. Figures 5.156 and 5.157 show the signals in the guide tube and the downcomer, respectively. These data indicate that the lower plenum, guide tube and the lower part of the downcomer (0.525m - 3.325 m EL) were not exposed to the steam environment throughout the whole test.

The liquid level transients estimated from the liquid level signals shown in Figs. 5.146 through 5.157 are presented in Fig. 5.158 for the upper plenum and core. Following can be observed from this figure. (1) The core uncovering started at 29 s in the average channel C and at 62 s in the peak power channel A. The core is completely voided at about 200 s in all channels. (2) Following the LPSC and LPCI actuation, the two-phase mixture appears immediately in all channels.

Figure 5.159 shows the dryout and quench front movements in channel A, which are estimated from the heater rod surface temperature transients shown earlier. Figure 5.160 compares the dryout and quench front movements

in channels A,B,C and D. The liquid level data shown in Fig. 5.158 are also duplicated for comparison. The propagation of the dryout front coincides with the fall in the core liquid level, however, the rise in the core liquid level significantly precedes the upward movement of the quench front.

### 6.9 Density, Momentum Flux and Mass Flow Rates

Figures 5.161 through 5.163 show the average fluid densities downstream of the jet pumps and at the break. The average densities were obtained by weighted averaging of the chordal density data shown in Figs. 5.58 through 5.65. The flow rate at the break, namely the discharge flow through the MSL, is calculated from the average density and the momentum flux measured with the high range drag disk as shown in Fig. 5.164.

The steam discharge flow through the MSL was also measured at a location upstream of the orifice, OR-5, by orifice flow meters as shown in Fig. 5.165. The flow rates measured by the orifice and drag disk show similar trends through the transient, however, the orifice flow meter data are not reliable, because a single-phase vapor flow was assumed throughout the test during conversion to the mass flow rate.

Mass flow rates in the core and recirculation loops are calculated from the orifice flow meter data and are shown in Figs. 5.166 through 5.175. The coolant flow through the core inlet decreased rapidly after break and stagnated throughout the test, however, large oscillations are observed after about 300 s as shown in Fig. 5.171. The flow through the recirculation loops also dropped rapidly after break due to the pump coast down. The values shown are, however, not quantitatively accurate during the two-phase flow conditions which prevailed following the initiation of lower plenum flashing.

The collapsed liquid levels in the downcomer and the core shroud are shown in Figs. 5.176 and 5.177. From these figures, the coolant inventory in the downcomer and inside the core shroud as well as the total coolant inventory are calculated and shown in Figs. 5.178 through 5.180. The coolant inventory in the pressure vessel decreased steadily after break until the liquid level in the downcomer dropped to the L1 level and the LPCS and LPCI were actuated at 281 s. Thereafter, the coolant inventory started to increase inside the core shroud leading to quenching of the whole core at 438 s after break.

## 7. Effect of HPCS failure on MSL break LOCA

The system behavior for an MSL break test with an HPCS failure, RUN 953, has been described in the previous section through examination of the experimental data. Gradual system depressurization, continuous flashing in the pressure vessel, and high water level in the downcomer have been observed to characterize this MSL break LOCA.

In this section, the present results are compared with those of a 100% MSL break test with full ECCS actuation logic, RUN 952, to determine the effect of an HPCS failure on the system response for the MSL break LOCA.<sup>(6)</sup>

The initial conditions and sequence of major events from these two tests are compared in Table 7.1. In both tests, the break location and area are the same.

The lower plenum pressure histories are compared in Fig. 7.1. A gradual decay in pressure is observed in both tests, and, the rate of decrease is nearly equal.

The differential pressure between the top and bottom of the core is shown in Fig. 7.2. This comparison shows a similar decrease in the pressure vessel mass inventory in the early period, but after the HPCS is actuated in RUN 952, the mass inventory increases gradually in comparison with RUN 953. However, the mass inventory in the core recovers rapidly in RUN 953 as LPCS and LPCI are activated at 281 s after break. Because of the large injection rate for LPCI (Fig. 7.3), the core mass inventory in RUN 953 quickly exceeds that in RUN 952 as shown in Fig. 7.4. The collapsed liquid level transients in the upper and lower downcomer (Fig. 7.5) show closely matched behavior until LPCS and LPCI are activated in RUN 953. The effect of HPCS activation in RUN 952 on downcomer mass inventory is observed to be negligibly small (Fig. 7.6). The steam flow rate in the main steam line is

nearly equal between the two tests as shown in Fig. 7.7.

The surface temperatures of the fuel rod, A22, at positions 1, 4 and 6 are compared in Figs. 7.8 through 7.10 respectively. The temperature excursion occurs at nearly the same time in both tests, however, the duration of core heat-up is substantially longer and both the turnaround and quench are delayed. As a consequence, the peak temperatures reached is, in every case, higher in RUN 953 than in RUN 952. Finally, the surface temperatures of the fuel rod, A71 in RUN 953 and A31 in RUN 952, that recorded the PCT respectively are compared in Fig. 7.11. In RUN 952, the PCT of 752 K was reached soon after the HPCS injection and its magnitude was much less than the PCT of 1004 K recorded in RUN 953.

A rather large difference in the PCTs obtained in these tests is attributed to the effectiveness of HPCS in preventing the dryout of the entire core and in arresting the temperature excursion of the fuel rods during an MSL break LOCA. Actuation of HPCS is, however, not totally satisfactory in view of long term cooling of the core during an MSL break LOCA as shown in reference (6). In RUN 952, HPCS water prevented the fall in the downcomer water level to L1, so that LPCS and LPCI were not actuated. Although the core was completely quenched with only HPCS, local dryout of the core occurred in the high heat flux channel. Excursion in fuel rod temperatures of about 100 K above saturation was observed for a long time until LPCS and LPCI were manually activated to bring the core to a stable cooling condition. Though the fuel rod temperature rise was small in magnitude during the local dryout, a remedial procedure to prevent local dryout, such as manual activation of LPCS and LPCI following the HPCS actuation is recommended to secure stable long term cooling of the core during an MSL break LOCA. If the ECCS actuation by the containment pressure signal fails in an actual BWR, as assumed in the present test, an increase in the set point, L1, for LPCS and LPCI actuation is also recommended.

Table 7.1 Test Conditions and Major Events in RUN 953 and RUN 952

## (a) Test Conditions

Items	RUN 953	RUN 952
Break Location	Main Steam Line	Main Steam Line
Break Diameter (mm)	31.0 (orifice)	31.0 (orifice)
Total Break Area (mm <sup>2</sup> )	754.8	754.8
Initial Pressure (MPa)	7.35	7.35
Core Inlet Subcooling (K)	10.7	10.7
HPCS	Actuation	No-Actuation
LPCS	No-Actuation	Actuation
LPCI	No-Actuation	Actuation
ADS	Failure	Failure

## (b) Time of Events (s)

Items	RUN 953	RUN 952
Break Initiation	0.0	0.0
Power-Decay start	9.0	9.0
Lower Plenum Flashing	5.4	4.2
L2 Level Signal	74.0	71.0
HPCS Actuation	-	95.0
L1 Level Signal	245.0	-
LPCS Actuation	281.0	-
LPCI Actuation	281.0	-
Final Core Quench	438.0	230.0

## RUN 953 AND RUN 952

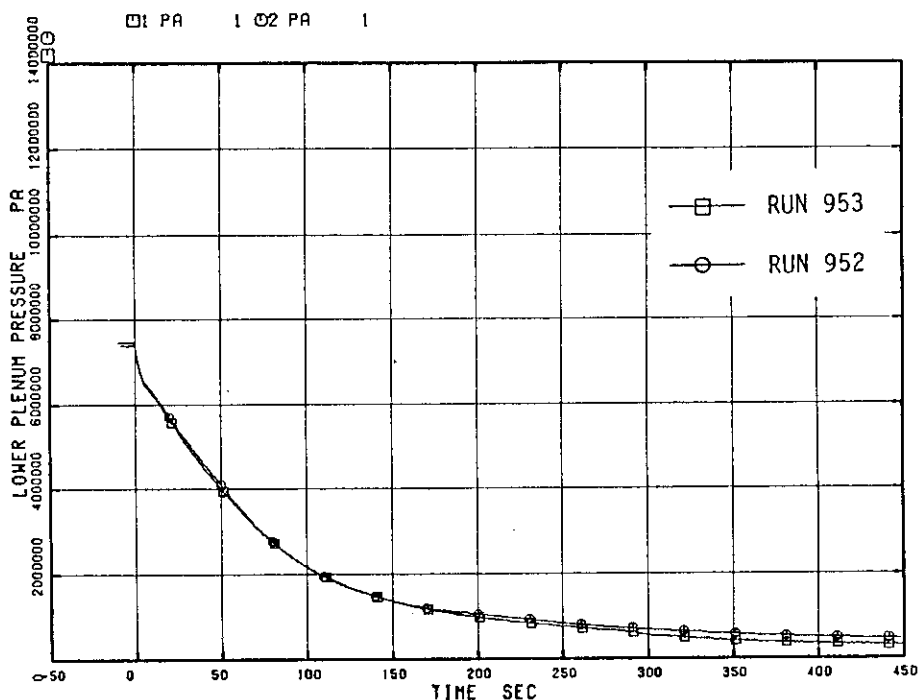


Fig. 7.1 Lower Plenum pressure transients in RUN 953 and RUN 952

## RUN 953 AND RUN 952

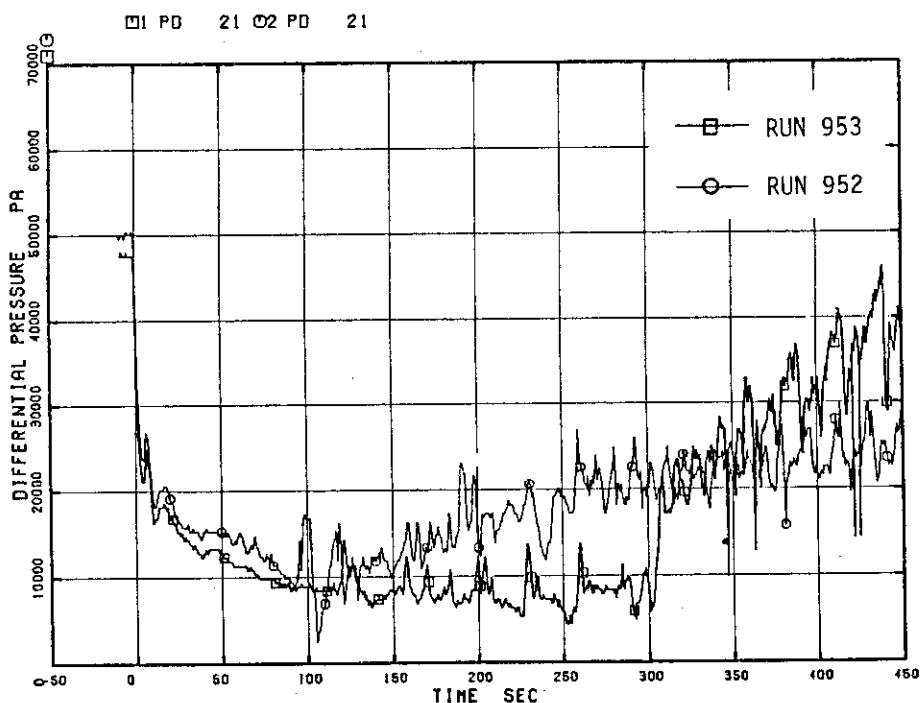


Fig. 7.2 Differential pressure across core

## RUN 953 AND RUN 952

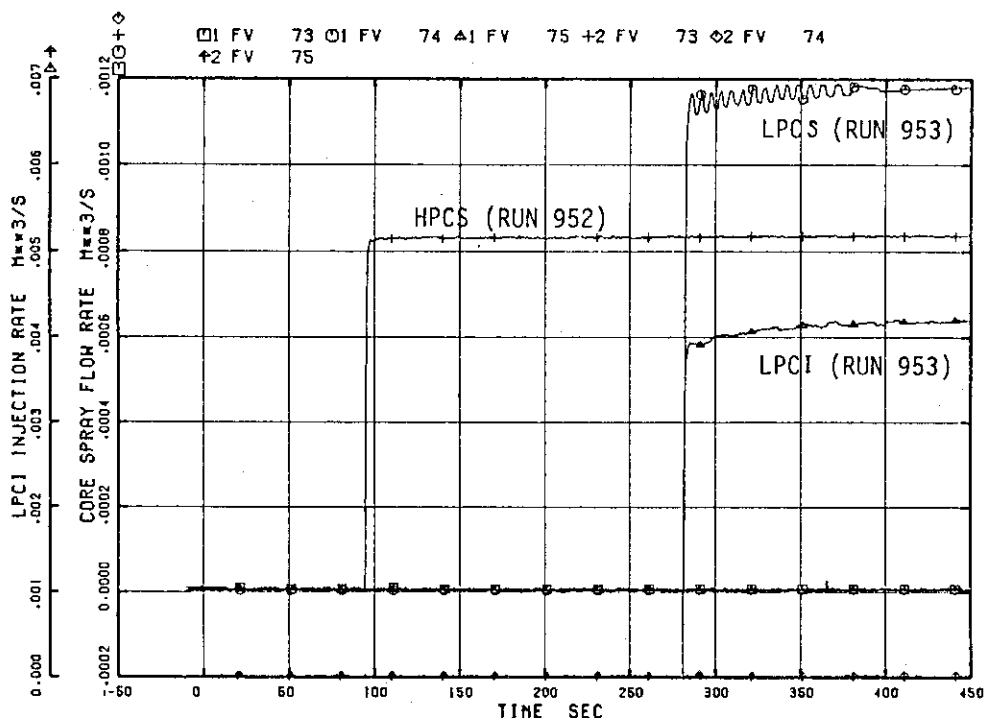


Fig. 7.3 ECCS flow rates

## RUN 953 AND RUN 952

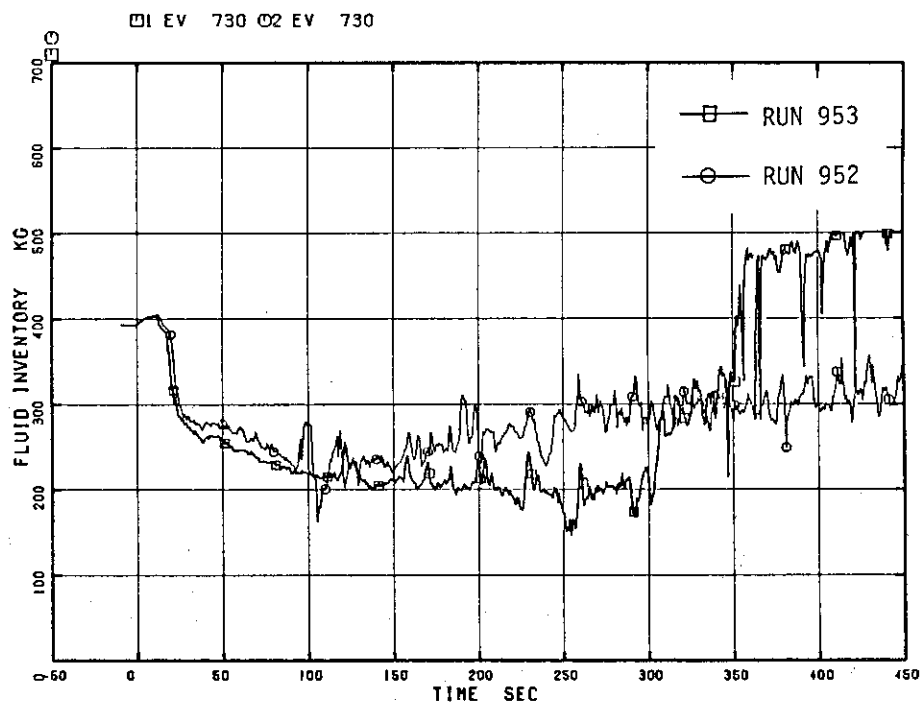


Fig. 7.4 Core mass inventory

## RUN 953 AND RUN 952

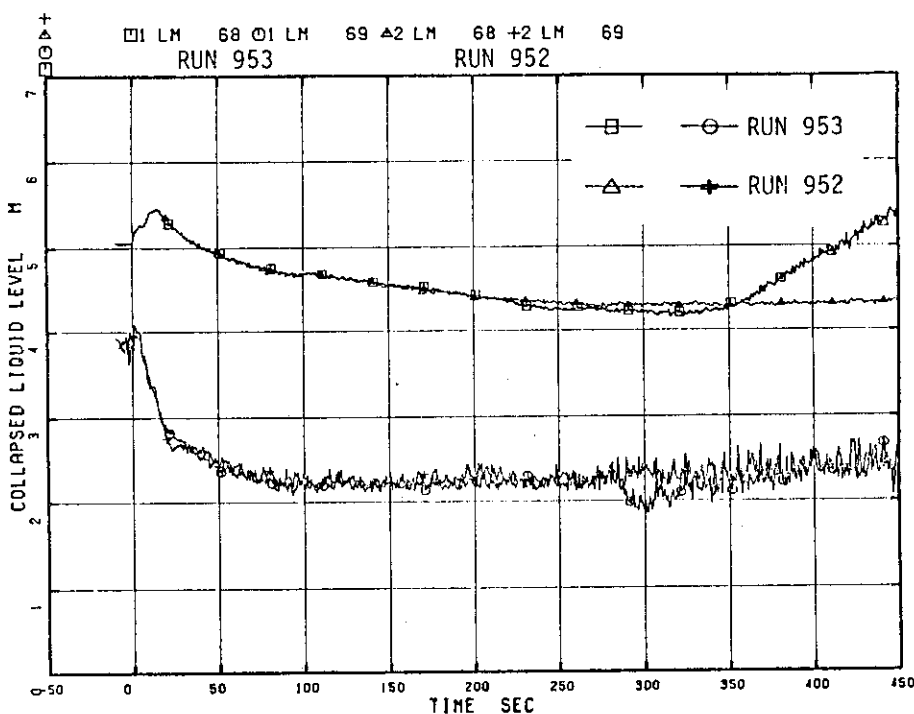


Fig. 7.5 Collapsed liquid level in upper and lower downcomer

## RUN 953 AND RUN 952

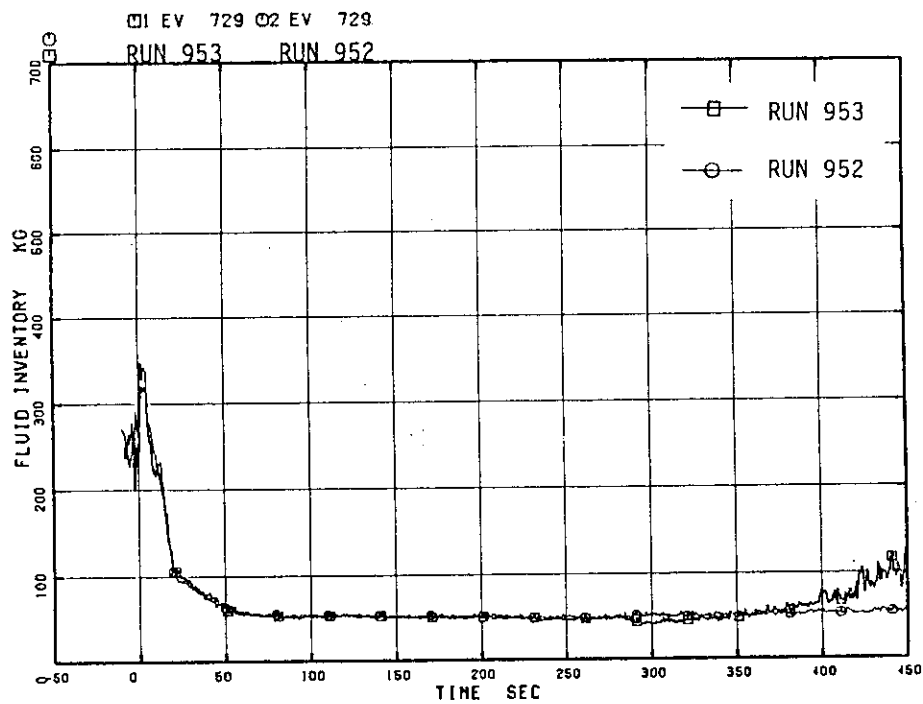


Fig. 7.6 Mass inventory in downcomer

## RUN 953 AND RUN 952

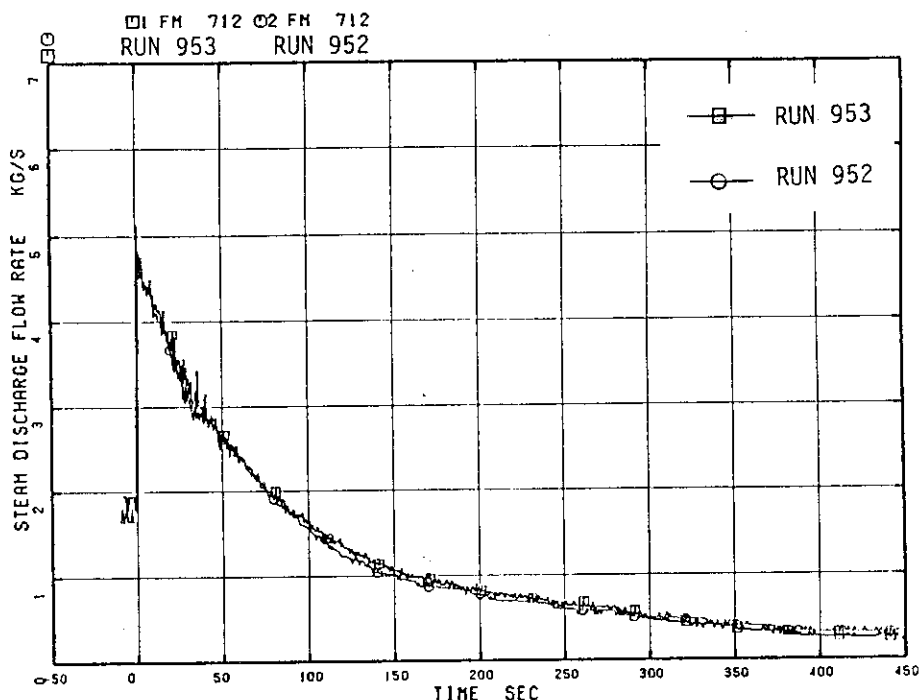


Fig. 7.7 Steam flow rate in the Main Steam line

## RUN 953 AND RUN 952

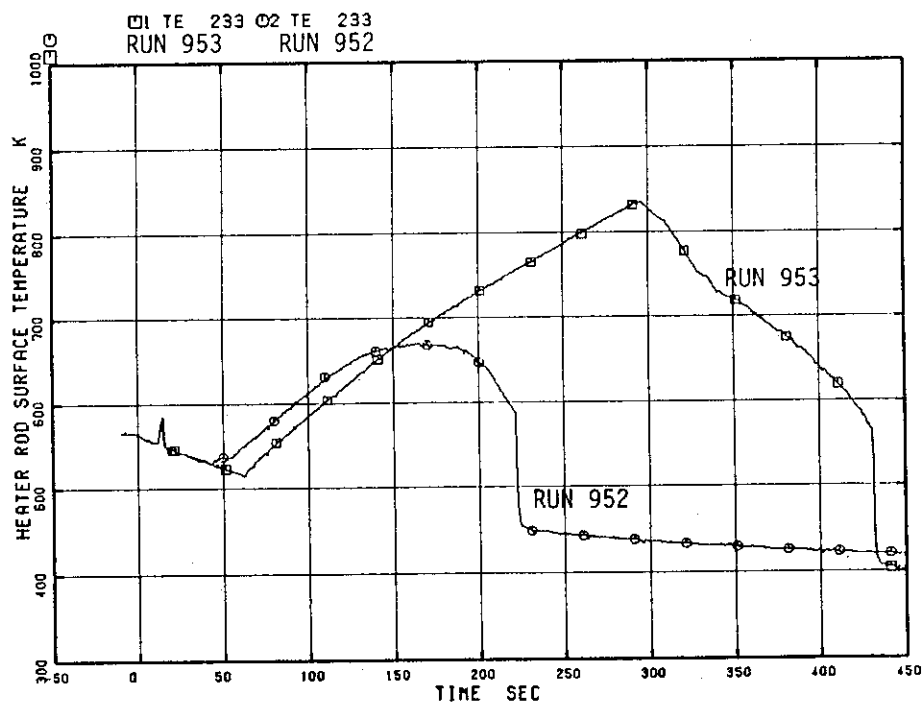


Fig. 7.8 Comparison of surface temperatures at position 1 of fuel rod A22

## RUN 953 AND RUN 952

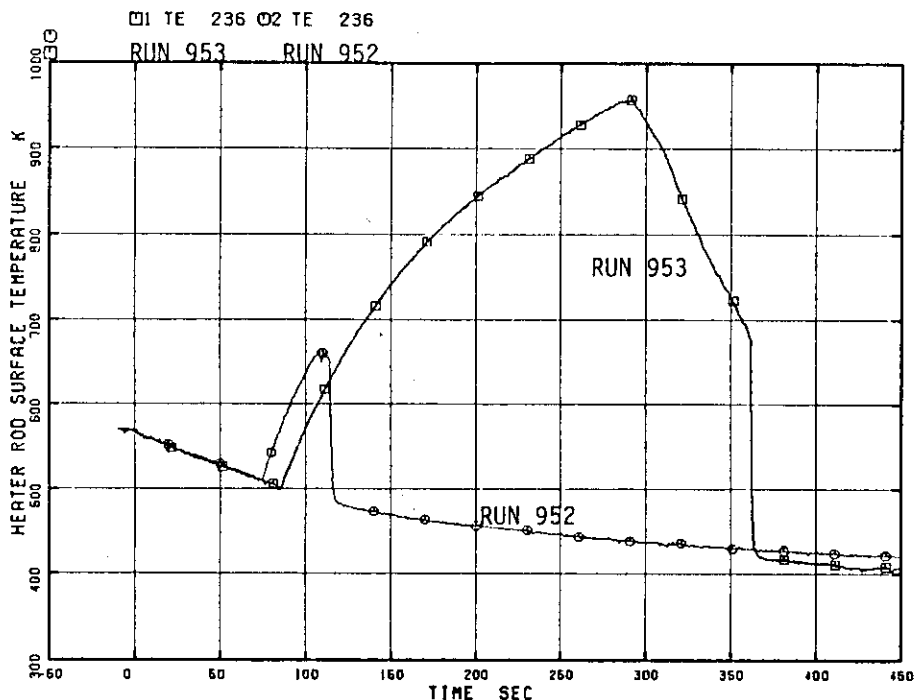


Fig. 7.9 Comparison of surface temperatures at position 4 of fuel rod A22

## RUN 953 AND RUN 952

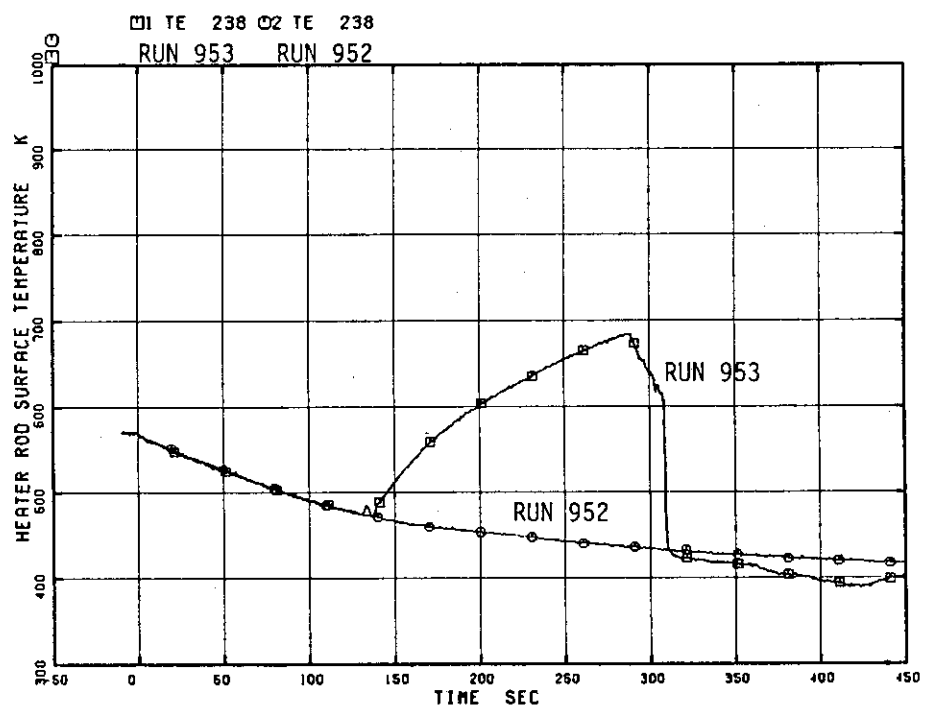


Fig. 7.10 Comparison of surface temperatures at position 6 of fuel rod A22

## RUN 953 AND RUN 952

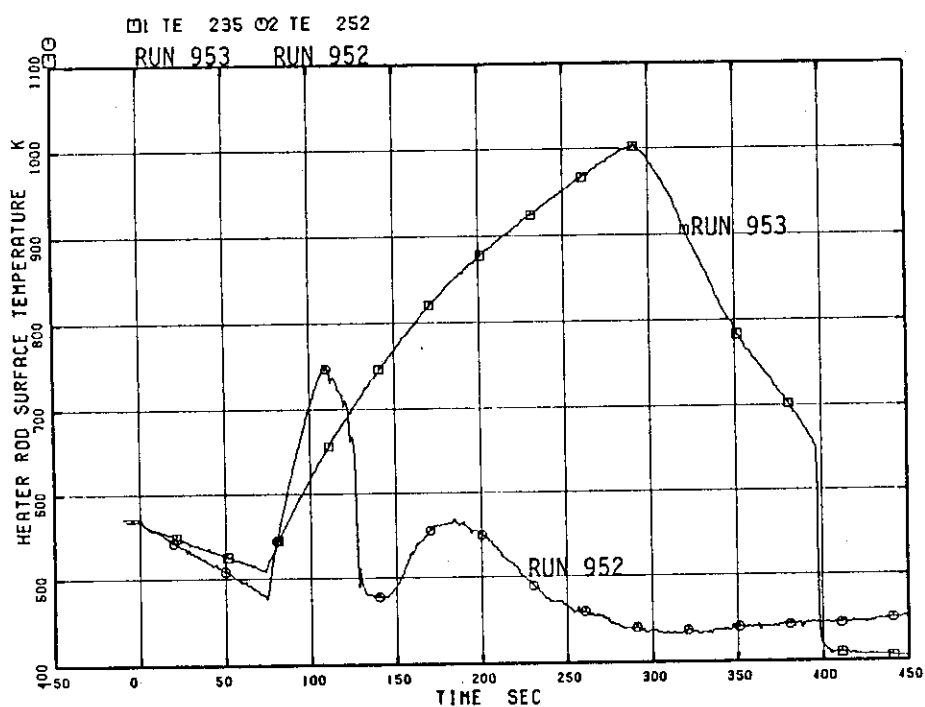


Fig. 7.11 Comparison of peak cladding temperatures

## 8. Concluding Remarks

RUN 953 is a 100% Main Steam Line (MSL) break test with an HPCS failure assumption conducted in a series of MSL break tests in the ROSA-III program. Most of the instrumentation performed satisfactorily. The following is a summary of the findings obtained through the examination of the present test results.

- (1) The system pressure decreased monotonously after the break initiation.

The rate of depressurization also decreased gradually with time. The steam discharge rate through the main steam line break decreased with time in response to the transient decay in the system pressure. Continuous depressurization led to the uncovering of the top of core starting at 29 s after break and the uncovering of the whole core at about 200 s after break. The PCT of 1004 K was reached at 292 s after break. The collapsed water level in the upper downcomer decreased to the L1 level at 245 s and LPCS and LPCI were actuated at 281 s after break. Following the LPCS and LPCI injection, reflooding of the core started and the entire core was quenched at 438 s after break. It must be remembered that the actuation of LPCS and LPCI by the liquid level signal in the downcomer, as in the present test, assumes a failure in the ECCS actuation by the containment pressure signal for an actual BWR.

- (2) In comparison with a reference MSL break test with full ECCS actuation logic, RUN 952, the results of the present MSL break test with an HPCS failure showed significant differences in the system response with regard to the core heatup and recovery. Although the system pressure decreased gradually at almost an equal rate in both tests, the core recovery was significantly delayed in RUN 953 due to a failure in HPCS actuation and a substantially higher PCT was obtained (1004 K in RUN

953 as compared to 752 K in RUN 952). The recovery of the core was achieved following the LPCS and LPCI actuation, and the long-term cooling of the core was satisfactory thereafter.

### Acknowledgment

The authors are grateful to H. Murata of the Ship Research Institute, Ministry of Transport, for the support work done on the data analysis. We are also grateful to M. Okazaki of the Institute of Nuclear Safety, Japan, Y. Koizumi of JAERI, and M. Iriko of Computer Services Co. for their contributions to the present test program. Finally, we wish to thank H. Asahi, T. Odaira, T. Takayasu, S. Sekiguchi, Y. Kitano and T. Numata of Nuclear Engineering Corporation for their assistance in conducting the experiment and H. Gotoh of Information System Laboratory Corporation for preparing the data plots.

### References

- (1) ANODA, Y., et al., "ROSA-III System Descripiton for Fuel Assembly No. 4", JAERI-M 9363 (1981).
- (2) SOBAJIMA, M., et al., "Instrumentation and Data Processing for ROSA-III Test" (in Japanese), JAERI-M 8499 (1979).
- (3) ABE, N., et al., "Electric Power Transient Curve for ROSA-III Tests", JAERI-M 8728 (1980).
- (4) "General Electric Standard Safety Analysis Report, BWR/6", DOCKET-STN-50531-22, General Electric Company.
- (5) "BWR Blowdown Emergency Core Cooling Program, Preliminary Facility Description Report for the BT/ECCIA Test Phase", GEAP-23592, NRC-2 (1977).
- (6) KAWAJI, M., et al., "A Main Steam Line Break Experiment at ROSA-III - RUN 952 (Standard Run with Full ECCS)", JAERI-M 84-229 (1984).

### Acknowledgment

The authors are grateful to H. Murata of the Ship Research Institute, Ministry of Transport, for the support work done on the data analysis. We are also grateful to M. Okazaki of the Institute of Nuclear Safety, Japan, Y. Koizumi of JAERI, and M. Iriko of Computer Services Co. for their contributions to the present test program. Finally, we wish to thank H. Asahi, T. Odaira, T. Takayasu, S. Sekiguchi, Y. Kitano and T. Numata of Nuclear Engineering Corporation for their assistance in conducting the experiment and H. Gotoh of Information System Laboratory Corporation for preparing the data plots.

### References

- (1) ANODA, Y., et al., "ROSA-III System Descripiton for Fuel Assembly No. 4", JAERI-M 9363 (1981).
- (2) SOBAJIMA, M., et al., "Instrumentation and Data Processing for ROSA-III Test" (in Japanese), JAERI-M 8499 (1979).
- (3) ABE, N., et al., "Electric Power Transient Curve for ROSA-III Tests", JAERI-M 8728 (1980).
- (4) "General Electric Standard Safety Analysis Report, BWR/6", DOCKET-STN-50531-22, General Electric Company.
- (5) "BWR Blowdown Emergency Core Cooling Program, Preliminary Facility Description Report for the BT/ECCIA Test Phase", GEAP-23592, NRC-2 (1977).
- (6) KAWAJI, M., et al., "A Main Steam Line Break Experiment at ROSA-III - RUN 952 (Standard Run with Full ECCS)", JAERI-M 84-229 (1984).